ACTA ORTHOPAEDICA SCANDINAVICA
SUPPLEMENTUM NO. 185

From the Laboratory for Experimental Orthopaedics, Department of Orthopaedics, University of Nijmegen; in collaboration with the Division of Applied Mechanics, Department of Mechanical Engineering, Eindhoven University of Technology; The Netherlands.

Some Fundamental Aspects of Human Joint Replacement

Analyses of stresses and heat conduction in bone-prosthesis structures

BY

RIK HUISKES

MUNKSGAARD COPENHAGEN

Some parts of the work described in this book have been presented at conferences previously.

With respect to section II:
- First European Conference on Evaluation of Biomaterials, Strasbourg, France, 1977 (Huiskes *et al*, 1977)*.
- European Society of Biomaterials Conference, Brussels, Belgium, 1978 (Huiskes and Slooff, 1978).
- 24th Annual Meeting Orthopedic Research Society, Dallas, Texas, 1978 (Huiskes and de Wijn, 1978).
- 25th Annual Meeting Orthopedic Research Society, San Francisco, California, 1979 (Huiskes, 1979).
- Third International Conference on Plastics in Medicine and Surgery, Enschede, the Netherlands, 1979 (Huiskes *et al*, 1979).

With respect to section III:
- 29th ACEMB, Boston, Massachusetts, 1976 (Huiskes *et al*, 1976).
- VIth International Congress of Biomechanics, Copenhagen, Denmark, 1977 (Huiskes *et al*, 1977).
- Deuxième Congrès de la Société de la Biomécanique, Liège, Belgium, 1977 (Huiskes and Slooff, 1977).
- 24th Annual Meeting Orthopedic Research Society, Dallas, Texas, 1978 (Huiskes and Slooff, 1978).
- First Conference of the European Society of Biomechanics, Brussels, Belgium, 1978 (Huiskes, 1978).
- Pauwels Symposium: Biomechanik in Orthopädie und Traumatologie, Berlin, BRD, 1979 (Huiskes and Slooff, 1979).
- Second Conference of the European Society of Biomechanics, Strasbourg, France, 1979 (Huiskes, 1979; Huiskes and de Wijn, 1979).
- VIIth International Congress of Biomechanics, Warshaw, Poland, 1979 (Huiskes and Slooff, 1979).

* Names and years in brackets refer to the lists of references at the end of the sections concerned.

ISBN 87-16-08695-3
ISSN 0300-8827

ACKNOWLEDGEMENTS

An engineer who tries to perform specialist work in 'orthopedic biomechanics' often feels like a novice on skis – each leg on a separate support and both not necessarily moving in the same direction. In such a position one often has to rely on help from others.
I gratefully acknowledge the help of all who contributed to the completion of this work.
The research work was conducted under the supervision of Prof.Dr.Ir. J.D. Janssen (Eindhoven University of Technology, Division of Applied Mechanics), Prof.Dr. T.J.J.H. Slooff and Prof.Dr. Th.J.G. van Rens (University of Nijmegen, Department of Orthopaedics). I am very grateful for the opportunities they provided, their fruitful ideas, support and reviewing of the manuscript.
My special thanks go out to the entire Department of Orthopaedics, University of Nijmegen, and to the members of the Division of Applied Mechanics, Department of Mechanical Engineering, Eindhoven University of Technology, for their positive attitude to my work and their invaluable support. In this last group I must single out Ir. Marcel Brekelmans and Dr.Ir. Frans Veldpaus who have so often advised me on matters of mechanics.
To Ir. Jos Banens (Computer Centre, Eindhoven University of Technology) who assisted me in the use of FEM computer systems, and to Ir. Joost de Wijn (Laboratory of Dental Materials Research, University of Nijmegen), on whose expertise on biomaterials I have often relied, I wish to express my heartfelt thanks.
Of great importance to the completion of the present work was the help of two engineering students, Jos van Heck and Ronald Schouten, who ran many computer programs for me, and medical student Frank Hoogbergen, who assisted me in reviewing the orthopedic literature.
I am much indebted to Miss Marlies Lutkie, who typed the many draft manuscripts with unfailing accuracy, speed and, above all, good humor. Gratitude, too, I wish to express to Ir. Ton de Lange for 'attending the shop' during the last months and for his help in the completion of the graphs.
I gratefully acknowledge the numerous useful suggestions of Mr. A. Smith-Hardy in dealing with the vagaries of English.

Voor Marianne en Sabine

en voor mijn ouders

"To a scientist a mathematical model is as a stethoscope to a physician or a trowel to a bricklayer. The model is an image of reality, an abstraction, which touches upon reality in such a manner as to render some if its characteristics visible. It is the expedient relating complex systems to more trivial and simple systems, which last then represent the former. The development of models enables us to compensate for the limits of our imagination and descriptive abilities; by refraining from details and concentrating on the essentials, the complex reality becomes surveyable, controllable and comprehensible".

J.P. Hooft (1979):
De onderzoeker aan de zoom van de praktijk;
De Ingenieur, no. 16, Jaargang 91, p.289 (translation).

CONTENTS

INTRODUCTION

Artificial-joint replacement, the fixation of an artificial device to substitute for the kinematic and dynamic function of human joints, has become a widely accepted treatment in orthopedic surgery against advanced joint arthritis and disabling effects of post-traumatic conditions and resective bone-tumor surgery. The performance of such a technical structure in the muscelo-skeletal system is quite complicated and has many biological and mechanical aspects. The long-term survival of the fixation is not trivial and it is the aim of those concerned with these treatments to create the optimal conditions both from the biological and mechanical points of view.
The need for better understanding of the complicated mechanical aspects of joints and joint replacements has given rise to collaboration between orthopedic surgeons and engineers in the fields of biomechanics and biomaterials. In orthopedic biomechanics, a field fairly recently evolved, the mechanical functions and structure of normal bones, joints and connective tissues as well as the mechanical interaction between bones and artificial implants are studied. The purpose of these investigations is to develop a better understanding, quantitatively, of the mechanical aspects of the muscelo-skeletal system and provide criteria on the mechanical aspects of diagnostic methods and surgical interventions; for example artificial-joint fixation. The investigations described in the following chapters are the results of such interdisciplinary ventures carried out in the Laboratory for Experimental Orthopaedics at the Department of Orthopedics of the University of Nijmegen, where an 'Orthopedic Biomechanics' section was set up about 5 years ago, in collaboration with the Applied Mechanics Division of the Department of Mechanical Engineering at the Eindhoven University of Technology. The studies were concerned with artificial-joint loosening problems. A more specific description of the objects of the studies will be given at the end of this introduction, where the contents and the sequence of the subjects presented will also be outlined.
Since this area of activities is rather new to engineering disciplines, especially in the Netherlands, pains have been taken to sketch out a general outline of artificial-joint replacement as an orthopedic treatment, its occurrence rate, its problems and the contributions that engineers can possibly make; part of this will be discussed in the remainder of this introduction.

Although not often recognized as such, arthritis is one of the major disabling diseases in our society. Some statistical data on arthritis in the U.S.A. were cited by Chao (1976): in 1973 an Arthritis Foundation study showed that approximately 20 million Americans of whom more than 75% are between 45 and 65 years of age, have symptoms of arthritis. In 1969, aged patients spent more than 70 million days in bed and employed people lost more than 14 million working days because of arthritis.
Although not a cause of high mortality, arthritis inflicts severe pain and functional disability. The economic consequences of this disease in terms of social security, manpower loss and health care are substantial.
Since the development of artificial joints made its dramatic breakthrough in the early sixties, many patients with severe arthritis were successfully operated and now function normally and free from pain. This development is illustrated in fig. 1 (Gschwend, 1976) giving the number of artificial hip replacements and other treatments of arthritis, as carried out in Swiss clinics.
Although the success of artificial-joint replacement dates back relatively few years, the development started a long time ago. Excellent reviews of the history in this respect have been given by Walker (1977) and Huggler and Schreiber (1978).

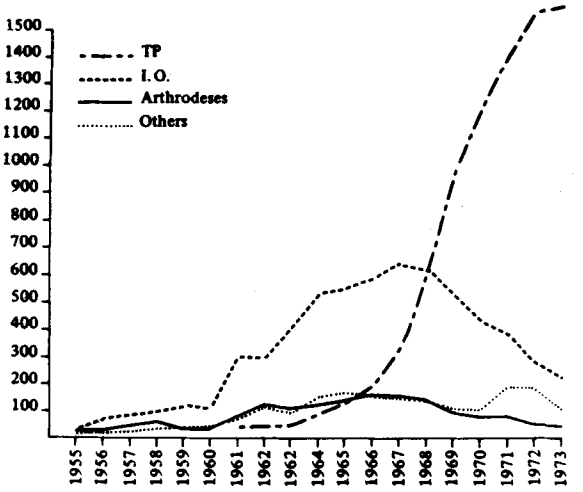

fig. 1: Number of hip operations for osteoarthritis in 9 Swiss orthopedic clinics, 1955-1973. TP: total hip replacement; IO: intertrochanteric osteotomy (where anatomical proportions of the joint are changed); arthrodeses: Stiffening of the joint (reproduced with permission of Gschwend, 1976).

Due to the important kinematic and load-bearing function of the hip and the high number of patients suffering from degenerative hip diseases, the first and main efforts in artificial joint replacement were focussed on this joint.
Starting early this century, many methods of treatment and materials were tried. More-or-less successful trials have been reported by Smith-Petersen (1939), Moore and Bohlman (1943) and Judet (1954) among others. In their different replacement concepts, only one bone component of the joint was replaced in function with the normal cartilage of the other component. Wiles (1957) reported on operations on patients using a total hip replacement, where both sides of the joint were replaced, by a femoral and an acetabular component respectively.
Although surgical procedures in general became more successful in the course of this century, thanks to better antiseptic measures and anesthetic procedures, the short and long-term results of the early joint replacement trials were relatively speaking rather poor, mainly because of the lack of an adequate fixation. These circumstances changed after Charnley (1960) introduced the use of acrylic cement as space-filling fixation material and his concept of 'low-friction' total hip arthroplasty, replacing the acetabular component of the joint with a plastic cup and the femoral component with a metal endoprosthesis.
Acrylic cement, or bone cement, is a 'cold-curing' plastic. It consists of a mixture of polymethylmethacrylate and monomethylmethacrylate and is inserted in the bone in a doughy phase, allowing the surgeon to mold it between the implant and the bone. After a few minutes it polymerizes to a solid substance. Although the acrylic cement sticks neither to the bone, nor to the implant, the space-filling capacities guarantee a smoothening of the load distribution and a firm placing of the implant. Fig. 2 shows a schematic illustration of a cemented Charnley hip prosthesis.
The results reported by Charnley (1972) were extraordinarily good and following this breakthrough total hip replacements have been carried out in ever growing numbers, making it one of the major surgical interventions in orthopedic clinics today.

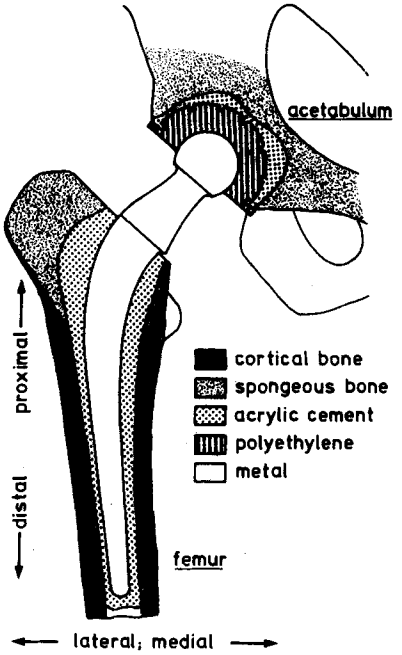

fig. 2: Schematic illustration of a Charnley total hip prosthesis (acetabular and femoral component) fixated in the bone with acrylic cement. Distal and proximal, medial and lateral directions are indicated.

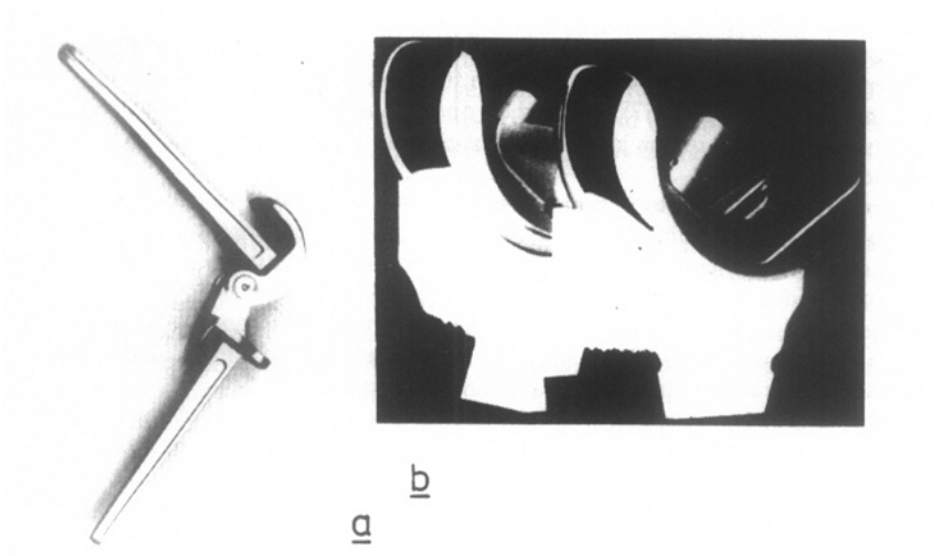

fig. 3: Artificial knee-joints are available in two principally different concepts, hinged and surface-types. Examples are (a) G.U.E.P.A.R. (hinged-type) and (b) Geomedic (surface-type).
(Reproduced with permission of v. Rens and Huiskes, 1976).

Although the hip joint still receives the most attention, developments have rapidly expanded to other joints. Artificial hinges for the knee-joint were already developed by Moeys (1954), Shiers (1954) and Walldius (1957), followed by numerous designs for knee-surface replacement and other hinged joints in the nineteen-seventies (fig. 3). Attention was given as early as the nineteen-fifties to the elbow, the shoulder and the finger joints, recently followed by the ankle and wrist. Several designs are now available for various joints and especially the hip and the knee are being replaced routinely in most orthopedic clinics.
In the Orthopedic Department of the University of Nijmegen in 1977 artificial-joint replacement was carried out in roughly 20% of all operative interventions and it accounted for approximately 30% of the total operation time; 75% of the replacements were in the hip and 23% in the knee-joint.
Using estimates from several sources, an assessment was made of the number of total joint replacements carried out annually in the U.S.A. by Hori *et al* (1978). In their questionnaire they not only investigated the number of replacements carried out, but also included the number of patients that were indicated for an artificial joint but did not receive one because, in the opinion of the surgeon no reliable design was available. A summary of their results is given in table I.

	1972	1973	1974	1975	1976	Total	1976
				implanted			indicated
Hip	55,000	75,000	77,500	80,000	80,000	367,500	89,600
Knee	4,000	10,000	20,000	32,500	40,000	106,500	52,800
Others	2,500	3,800	6,500	8,500	10,000	31,300	33,900
Total	61,500	88,800	104,000	121,000	130,000	505,300	176,300

table I: Estimated number of joint replacements carried out annually in the U.S.A. from 1972 to 1976 and indicated number of joint replacements in 1976 (after Hori et al, 1978).

Data with respect to the number of joint replacements carried out in the Netherlands were supplied by the Foundation for Medical Registration (table II).

Hip	: 7,277	Hand (wrist included)	: uncertain
Knee	: 643	Shoulder	: 29
Elbow	: 30	Ankle	: no data

table II: Number of arthroplasties (non-artificial included) carried out in 1977 in the Netherlands (source: Found. Med. Registration, Utrecht, the Netherlands).

It can be estimated that in the near future somewhere around 300,000 artificial-joint replacements will be performed annually in the world. If we assume an average life expectancy of the patients to be approximately 8 years (an arbitrary estimate), we find that on the average soms 2.4 million people with artificial joints will be alive.

Although widely applied, artificial-joint replacement is not without complications. Some of these are characteristic of all major operations, others are more specific. The most troublesome of these specific complications is loosening of the device, directly or indirectly caused by a variety of mechanical and biological phenomena. In patient reviews it was established that the incidence of loosening rises steeply with the amount of postoperative years. This has resulted in many revision- and salvage operations. Moreover, generally speaking, it limits the application of artificial joints to older people, the present criterion being about 55 years and over. Still, the need for joint replacement in young patients is anything but negligible. Presently, many efforts by scientists from medical and engineering disciplines are being put into the development of artificial joints and fixation procedures that will diminish the complications and guarantee longer service life.

The function of an artificial joint is purely mechanical, although of course the biological reactions of the bone and the soft tissues play important and complicating roles. The joint has to provide for a kinematic system that accords with the kinematic characteristics of the original joint; it has to be able to stand up to the physiological joint-loading and experience little wear and friction; the material should not induce undesirable tissue reactions and has to transfer the load to the bone in such a way that a rigid fixation remains intact for many years.
Until very recently artificial joints were being developed more or less by 'trial and error'. After a certain number of patients had received a specific design and a number of postoperative years had passed, the patients were reviewed. Based on the short and long-term findings, the design was often adapted or dropped altogether. Only seldom could a causative relation be established between the failures and the characteristics of the design. A good design may have been rejected merely because it was inadequately implanted and a bad design may have been widely accepted only because the surgeon-designer carried out the first operations exceptionally well; quite individual accomplishments, perhaps not reproducable by others. Also, quite good designs may have been rejected as a whole in the past, only because minor and easily changeable details had led to complications. As a result of this development, many types of prostheses are presently available for the different joints. These different types can be divided into a small number of categories; within each category the differences are only those of detail. If we count only the 'popular' types, about 48 different designs of knee prostheses are available, 10 different elbow prostheses, 4 different shoulder prostheses, 6 different ankle prostheses, around 10 different finger prostheses, a few wrist prostheses and the different designs of hip prostheses available far exceed a hundred. New designs, sometimes differing only slightly, are developed yearly. Few objective criteria are known for a justified choice between the different makes and, if a choice is made, the orthopedic surgeon usually never finds out whether failures are due to an inadequate surgical procedure, to individual properties of the patient or to the design features.

It is the object of the research work described in the following chapters to provide a more fundamental comprehension of some aspects of artificial joints and their performance in the body. Two subjects of investigation have been chosen, both regarding the incidence of implant loosening. First the cause of bone necrosis as usually seen directly after the operation in a small zone close to the acrylic cement, adjoining the bone, and more specifically, the possible effect in this phenomenon of the heat developed in the acrylic cement during the polymerization process. This part of the work is described in section II. Second, the stress distribution in the implant, the acrylic cement, the bone and on the contact regions of these materials, as results of the physiological joint-loading in relation to the strength of the components and possible mechanical failure. These stress analyses are confined to intramedullary fixation systems, prostheses that are fixated inside the medullar cavity of the

bones, using a stem, and although the methods that will be discussed and some of the results are valid for these systems in general, the analyses are principally focussed on the hip endoprosthesis. This part of the work is treated in section III.
Although results of experiments carried out in our own laboratories as well as those published in the literature will be used, the approach in both areas is mainly analytical. Principles of mechanics and heat conduction theory will be applied to evaluate the system behavior and the influences of the system parameters. This approach is not quite common in orthopedics and it is felt that, especially in this respect the (biomechanical) engineer can make a contribution to better fundamental understanding of the bone-implant structure and some of its problems.
It should be understood that such a contribution to a more fundamental understanding of some phenomena was the object of the work presented and that no new device or material is envisaged, although some objective quantitative guidelines for prosthesis designs and surgical procedures will result and moreover, a simple method will be proposed that can be used to predict the mechanical performance of specific endoprosthesis designs in patients and hence clear the way to a more 'custom fit' approach.
The two investigations described here are not the first ventures into the problem areas, nor will they be the last; part of the work has been devoted to an evaluation of studies published in the literature, a review of which is presented also in sections II and III, respectively. As the approach is uncommon in orthopedics and the methods used are of a quite complicated nature from a medical point of view, the possibilities and limitations of theoretical methods are discussed to a somewhat greater extent in section I and some relevant conclusions will be discussed in more general terms in section IV.
Section I also gives a more detailed characterization of artificial joints and artificial-joint replacement and describes some properties of the bone-implant system as far as they are relevant to the analyses presented. Complications of artificial-joint replacement, especially prosthesis loosening, will be discussed based on a review of the literature on this subject in section I too, after which the objects of the investigations presented in sections II and III will be defined in more detail.

REFERENCES

Chao, E.Y. (1976); The biomechanics of total joint replacement surgery; Geriatrics; March.

Charnley, J. (1972); The long-term results of low friction arthroplasty of the hip performed as a primary intervention; J. Bone Jt.Surg. 54 B:61.

Gschwend, N. (1976); Symposium on total postheses, clinical material and overall-results; In: Total hip prosthesis (Gschwend and Debrunner, eds.); Hans Huber Publ.; Bern, Stuttgart, Vienna.

Hori, R.Y., Lewis, J.L., Zimmerman, J.R. and Compere, C.L. (1978); The number of total joint replacements in the United States; Clin.Orthop. and Rel.Res.; No. 132, 46-52.

Huggler, A.H. und Schreiber, A. (1978); Alloarthroplastik des Hüftgelenkes; Georg Thieme Verlag, Stuttgart.

Judet, R. (1954); Experience of hip arthroplasties by acrylic prostheses since 1946; J. Bone Jt. Surg. 36-B, 691.

Moeys, E.Y. (1954); Metal alloplasty of the knee joint; J. Bone Jt. Surg. 36-A, 363.

Moore, A.T. and Bohlman, H.R. (1943); Metal hip joint – A case report; J. Bone Jt. Surg. 25:688.

Rens, Th.J.G. van and Huiskes, R. (1976); De operatieve behandeling van gonarthrosis; Ned. T. v. Geneesk. 20, nr. 31, p. 1322.

Shiers, L.P.G. (1954); Arthroplasty of the knee; J. Bone Jt. Surg. 36-B, 553.

Smith-Petersen, M.N. (1939); Arthroplasty of the hip. A new method; J. Bone Jt. Surg. 21:269.

Walker, P.S. (1977); Human joints and their artificial replacements; Charles C. Thomas, Publ., Springfield, I11.

Walldius, B. (1957); Arthroplasty of the knee, using an endoprosthesis; Acta Orthop. Scand. Suppl. 24:5.

Wiles, P. (1957); The surgery of the osteo-arthritis hip; Br. J. Surg., 45:488.

SECTION ONE

PROPERTIES AND COMPLICATIONS OF ARTIFICIAL-JOINT REPLACEMENT

CONTENTS

INTRODUCTION

In this section some general aspects of artificial-joint replacement are described as far as deemed relevant to an understanding of the objects and results of the studies discussed in sections II and III. Workers in medical as well as technical fields may encounter trivial information, because this section is meant to be an introduction for both. Properties of the bone-prosthesis system, relevant for the analyses, are described in chapter 1.
In chapter 2 a short review is given of literature data on complications of artificial-joint replacement, especially concerning prosthesis loosening. The objects and methods of the present studies are outlined in chapter 3.
Although some general aspects of artificial-joint replacement are discussed in this section, most are focussed on the hip joint.

CHAPTER ONE

CHARACTERIZATION AND PROPERTIES OF BONE-IMPLANT SYSTEMS

1.1. Surgical procedure

A division can be made into intramedullary-fixated implants (endoprostheses), where a prosthesis stem is fixed into the meduallary cavity, and surface replacement, where the implant is more or less fixated against the bone. Some prostheses, for instance tibial components of some knee prostheses, use a mixed form of fixation.
In both cases parts of the bones involved in the articulation are resected. When an intramedullary stem is used, the medullar cavity is cleaned and reamed to some extent. In this procedure a part of the vascularity system that nourishes the bone is, at least temporarily, disturbed, especially in the diaphyseal region. Presently, most of the artificial joints are fixated by means of acrylic cement. The two components of this cement are mixed by the surgeon during the operation. The curing process starts right after the mixing procedure and takes something in the order of 5 - 10 minutes. Still in a doughy state, the cement is inserted into the medullar cavity or positioned against the bone; the prosthesis is then pressed into the cement mass and held until the cement has cured to a solid mass.
Especially with intramedullary-fixated implants the surgeon has no complete control over the consistency and the thickness of the cement mantle. Often air, bone debris and blood are mixed in the cement and the distal part of the cement mass may be pushed downward into the medullar canal.
It has been recognized that a syringe should be used, to ensure a complete and homogeneous cement mantle (Slooff, 1969).
Recently the use of an intramedullary bone plug has been advocated to enable more pressure to be put on the cement mass during insertion and prevent the distal cement mass from

being pushed downward (Markolf and Amstutz, 1976; Oh *et al*, 1978; Krause *et al*, 1979; Weber and Stühmer, 1979). Pulsatile water lavage before cement insertion has been advised in order to clean the bony implant bed prior to fixation of all prostheses (Narten *et al*, 1977; Halawa *et al*, 1978; Miller *et al*, 1978).
A very important part of the operation is the positioning and alignment of the prosthesis. Usually this is done by visual judgement.
Some complications, called preoperative complications, may occur during the operation; these include: perforation of the implant through the bone, fracture of the bone, injury to arteries or veins, injury to nerves, anesthetic complications, embolies and several others.

1.2. Basic requirements for artificial joints

An artificial joint has to approximate as closely as possible the natural joint function for the full postoperative life span, without discomfort and complications. More specifically some practical requirements can be formulated that have to be taken into account when new designs or surgical procedures are being considered:

- The prosthesis and fixation materials should not induce undesirable tissue reactions, as bone necrosis or bone resorption; they should have acceptable friction and wear characteristics and not corrode.
- The surgical procedure should be relatively simple and fast, standardized and reproduceable, with minimal surgical trauma.
- The design of the prosthesis, the choice of materials, with reference to strength as well as stiffness properties, should be such as to guarantee adequate mechanical performance in such a way that stress concentrations are avoided and that implant, cement, bone and the relevant interfaces are not loaded beyond their strength or fatique limits.
- The implant should have a good salvage potential, meaning that if the system fails, another solution remains possible. Since the ultimate salvage solution is usually arthrodeses, for instance this means that as little bone as possible should have to be resected.
- Early mobilization, sterilization of the components and reasonable manufacturing costs of the implant should all be possible.

Obviously an adequate artificial-joint design will always be a trade-off between these different requirements. A mechanical compromise that usually has to be considered is the one between requirements of range of motion and degrees of freedom (or constraints) on the one hand, and of stability on the other. A low-constraint joint that has an extensive range of motion, in other words, is free to move in several directions in an extensive range, will on the one hand offer little stability, but on the other hand will have to transfer less loading to the fixation system, hence will give less rise to mechanical loosening than a highly constrained joint with a limited range of motion.

1.3. Implant shapes and materials

Artificial joints are available in a variety of types and shapes. Intramedullary stems are used in different designs for all joints but the ankle. The acetabular part of the hip prosthesis is a surface replacement; the femoral part usually has an intramedullary stem, although since recently surface replacement of the femoral head is also becoming popular (double cup prosthesis). The hinged knee prostheses are usually intramedullary-fixated; some of the knee

surface replacements also have intramedullary stems. Finger prostheses, elbow prostheses and shoulder prostheses use intramedullary-fixation in all cases. The artificial wrist joint is usually a surface replacement combined with a stem for both components.

The configuration of the artificial joint greatly depends on the kinematic function it has to perform and the stability it has to give. Three basic configurations are (e.g. Chao, 1976): the ball-and-socket design (hip, shoulder); the articulating-type with various degrees of freedom (knee, ankle, elbow, wrist); the hinged types (knee, finger, elbow). Combinations of these basic types are also used.
The designs may also vary greatly in shape and dimensions, even if functionally identical. A dimensional classification of about 20 popular hip-joint designs was given by Walker (1977): diameters of the prosthesis femoral head vary from 22 to 48 mm; neck lengths vary from 15 to 55 mm; stem lengths from 93 to 180 mm and a few exceptional stems from 240 to 370 mm. The stem may be strongly curved or rather straight, while different kinds of cross-sectional geometries are used (diamond-shaped, rectangular, rounded-off, triangular, oval). Some designs use a more or less pronounced collar on the proximal side of the stem, resting on the bone rim. The stem is usually tapered to a greater or lesser extent.

Many different implant materials have been used in the past. They must be strong, tough, resistent to fatigue and wear, tolerated by the body and processable at reasonable costs. Because of the favorable friction and wear properties, most designs presently use a metal component against a plastic component. The metal components usually consist of high-grade stainless steel, cobalt-chromium alloys or titanium alloys; the plastic components of high-density polyethylene (HDPE) or ultra-high molecular-weight polyethylene (UHMWP). Experiments are being carried out with ceramics, Delrin and composite materials.
Silastic is being used in finger prostheses. The femoral part of the total hip replacement is always fabricated in metal and the acetabular cup usually in plastic. An extensive review of materials used for human implantation and their properties has been published by Rostoker and Galante (1979).

1.4. Loading of the joint

By the joint-loading is meant the resulting force and moment that one joint component exerts on the other and vice versa, by means of their articulating contacts.
The kind of loading depends on the kind and intensity of the activity. The loading is caused by gravity forces, acceleration forces, muscle forces and forces due to ligament constraints. Investigations of human joint-loading belong to the first activities in biomechanics and date back many ages. Many studies on this subject have been published and many are still being carried out. A review of the relevant literature is given by Walker (1977). Since the joint forces cannot be measured directly they have to be estimated using equilibrium conditions and data from 'force-plate' studies (measuring the ground reaction force), EMG studies (electromyography, giving an indication at large of muscle activity), movement studies and anthropometric measurements. Promising new possibilities are those of computer simulation, modeling the complete skeletal system as a kinematic chain, taking the important muscle groups into account and solving the redundant problem using optimization criteria. A first effort in this direction was published by Seireg and Arvikar (1975).
Although reliable data, accurate in an absolute sense, is not available as yet, results of various studies indicate that the joint forces are much higher than sometimes assumed. Brewster *et al* (1974) have calculated from force-plate studies that the force in the ankle-joint

during normal walking can be as high as 4.5 to 5.5 times body weight. Forces in the knee-joint would reach about 3 times body weight and in the hip-joint about 4 times body weight during normal walking, according to Paul (1974). During stairs walking or sport activities these values will be even higher.
The loading on the artificial joint is not necessarily equal to the loading on the natural joint. Even if the same level of activity were assumed, differences may be due to the positioning of the joint relative to the bone, the constraints offered by the prosthesis in comparison to those of the natural joint, and the incidence of friction.
Valuable data on hip-joint loading was supplied by Rydell (1966) who implanted endo-prostheses instrumented with strain gauges in two patients and measured the hip-joint forces in several activities. An example of his results is shown in fig. 1.1. Magnitude and direction

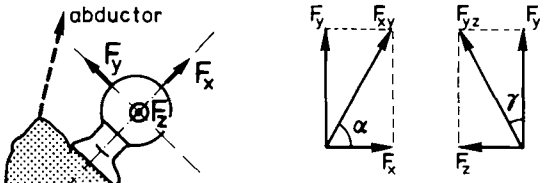

W = body weight; F = joint force;
F_{xy} = projection F on x-y-plane, etc.

walk-way moment	$-F/W$	$-F_x/W$	$-F_y/W$	$-F_z/W$	α	γ
1	1.8	1.3	1.2	0.5	45°	22°
2	1.1	0.8	0.8	0.2	44°	11°
3	1.8	1.2	1.2	0.3	44°	16°
4	0.8	0.6	0.5	0.2	42°	25°
5	0.8	0.5	0.6	0.2	45°	19°

fig. 1.1: Magnitudes, directions and points of application of hip-joint forces as measured by Rydell (1966), using an instrumented hip prosthesis implanted in a 51 yr-old male patient (right leg; weight: 75 kg), during level walking at 1.3 m/sec. Averages out of 12 measurements. Also shown is the resultant force of the important abductor muscle group on which magnitude and direction the joint force partly depends.

of the resultant joint forces varied considerably during the different activities and in the two patients. The maximal average force amounted to roughly 4.3 times body weight ($\alpha \approx 32°$ and $\gamma \approx 15°$) during running at 2.5 m/sec and was measured in patient no. 2 (56 yrs, female, 45 kg).

The loading that is transferred by the fixation system ultimately determines the stress distribution. This loading, in addition to the joint loading, depends on the geometry of the implant. In the case of the hip joint, the neck length and the varus-valgus angle of the neck are important parameters. Other forces, too, will influence the stress distribution in the bone-prosthesis structure as, for instance the abductor muscle forces (fig. 1.1).

1.5. Acrylic cement

Acrylic cement is a two-component material. The solid powder component consists principally of polymethylmethacrylate (PMMA) or polymer, the liquid component principally of monomethylmethacrylate (MMA) or monomer. Shortly after mixture of the two components

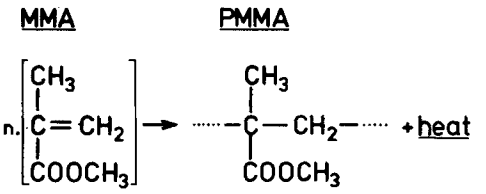

fig. 1.2: Description of the polymerization reaction in which monomethylmethacrylate molecules are connected to form polymer chains.

the polymerization process of the monomer starts (fig. 1.2), ultimately embedding the PMMA powder into a PMMA matrix, so that a solid substance remains. During the polymerization process heat is generated which has to be conducted through the adjoining materials, implant and bone. The total amount of generated heat is directly proportional to the mass of monomer used (Trommsdorf, 1963).
In more detail, the polymerization process of acrylic cement can be described as follows (Charnley, 1970; de Wijn, 1974; Oest *et al*, 1975; Debrunner *et al*, 1976): to the liquid component are added an inhibitor or stabilizer (hydroquinon) that prevents the monomer from polymerizing spontaneously, and also an initiator (benzoyl-peroxide). To the power component an accelerator is added (dimethyl-paratoluidine, DPT). After mixture of the components the initiator is decomposed by the accelerator into so-called radicals, molecule that trigger off the polymerization of the monomer. The compositions of the various commercial brands vary to some extent. The characteristics of the polymerization process are usually defined with reference to the temperature-time curve (fig. 1.3): the time from starting the mixture

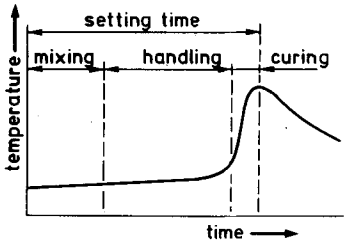

fig. 1.3: A typical temperature-time curve of curing acrylic cement. Terminology for phases in the polymerization process is shown (see also text).

until the peak temperature occurs is called the 'setting time', which is roughly 10 minutes; the first stage of this period, that takes about 3 to 4 minutes and in which the mixture tends to 'stick to the surgical glove', is called the 'mixing time' or 'dough time'; the second stage, that takes about 4 - 5 minutes and in which the mixture is still dough but no longer sticks to the glove, is called the 'handling time'. There appears to be no complete agreement on this terminology in the literature and, moreover, these stages are not uniquely defined, because the temperature-time curve depends not only on the cement properties, but also on the heat-conduction properties of the adjoining materials, hence on the specific circumstances.
The mixture reaches its ultimate hardness (sets) somewhat prior to the occurrence of the peak temperature. Hardness tests during the polymerization process were carried out by Debrunner *et al* (1976); an example of results is shown in fig. 1.4.

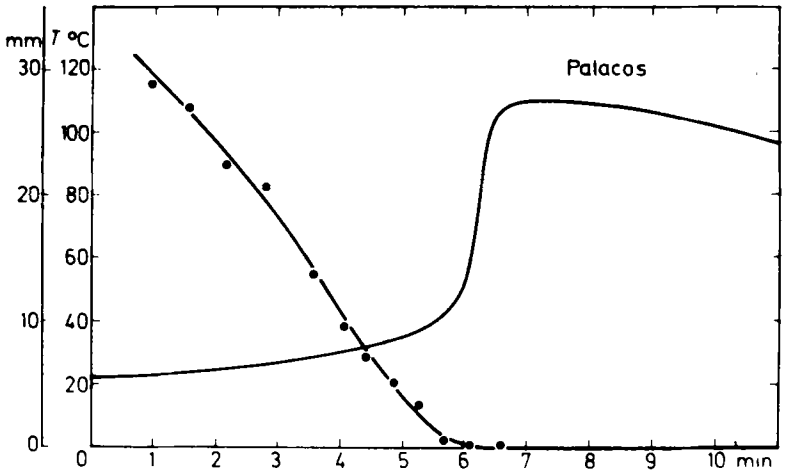

fig. 1.4: Temperature and hardness of curing acrylic cement, as function of time. Hardness was measured as penetration depth (mm) at constant force (reproduced with permission of Debrunner et al, 1976).

During the polymerization process the mixture undergoes dimensional changes due to volume contraction of the polymerizing component (density of PMMA: 1.18 kg/m^3; density of MMA: 0.94 kg/m^3), expansion of enclosed air and vaporized monomer bubbles and thermal shrinkage. The first two mechanisms are active during the setting phase, while the last-named occurs during the cooling phase. An overall expansion of 2 to 5 volume percent has been mentioned in the literature (de Wijn *et al*, 1975). These authors concluded that in fixating intramedullary stems the initial expansion will propably cause the mixture to flow in a longitudinal direction, while the cooling will cause the layer to shrink around the stem, leaving a gap between the bone and the cement mass (at the so-called 'cement-bone-interface') and locked-in stresses in the cement layer. Sometimes these stresses will cause the cement mantle to fracture during the operation (Miller *et al*, 1976; Chao, 1979).
The steep rise in temperature after the mixture has set is related to an acceleration of the polymerization process, called the 'Trommsdorf' or 'gel' effect.
The initial velocity of the polymerization process depends very much on the initial temperature, owing to the temperature sensitivity of the catalyser. The polymerization is never complete. It has been shown that there is 2 to 5% residual monomer in the cement and that 1 to 2% gradually enters into the tissue (e.g. Kutzner *et al*, 1974). This residual monomer may cause damage to the bone tissue adjoining the cement (e.g. Mohr, 1958).
Apart from the ones already mentioned, other components may have been added to the cement, like antibiotics or radiopaque fillers (barium sulfate, $BaSO_4$, or zirconium oxide, ZrO_2).

The mechanical properties of acrylic cement (e.g. strength and stiffness) as present in the patient are different from those of industrial PMMA. Differences are due to inhomogeneties caused by air entrainment and inclusion of blood and tissue debris during the mixing process, antibiotic and radiopaque additives and inhomogeneties caused by vaporized monomer during the polymerization process. The properties also change in the course of time due to temperature influences, moisture uptake and ageing. Extensive studies on mechanical properties of bone cement, preoperative as well as postoperative, have been published by Müller (1975,

Conditions	Young's modulus (N/mm^2)	Ultimate tensile strength (N/mm^2)	Elongation at fracture (%)
industrial PMMA;	2.8×10^3	74	8.4
acrylic cement, laboratory conditions;	2.6×10^3	43	2.0
10 months in the body simulated, tested at 37°C.	1.9×10^3	23	1.7

table 1.I: Approximative average value of five commercial brands for mechanical properties of acrylic cement, tested under different conditions, compared to properties of industrial PMMA (after Kusy, 1978).

1979), Lee *et al* (1978) and Kusy (1978). Kusy reports mechanical properties for five brands tested under different conditions (table 1.I). The acrylic cement is many times stronger in compression than in tension. Lautenschlager *et al* (1974) report 20.7 to 34.5 N/mm^2 ultimate compressive strength and 6.9 to 20.7 N/mm^2 ultimate tensile strength. It should be remarked that bone cement is somewhat viscoelastic, hence differences in strain rate may, apart from other circumstances, explain the variety in results to some extent. Lee *et al* (1978) investigated influences of several variables that may weaken the bone cement; a summary of their results is shown in table 1.II.

Variable	Possible % change in strength	
	UCS	UTS
Environmental temp. 37°C	- 10%	
Equilibrium moisture content	- 3%	
Ageing	- 10%	
Radiopaque fillers	- 5%	
Antibiotics	- 4%	
Inferior mixing technique	- 21%	
Insertion technique — delay	- 40%	- 54%
— pressure	+ 20%	
Inclusion of blood and tissue debris	- 16%	- 70%

table 1.II: Possible changes in compressive (UCS) and tensile (UTS) ultimate strength by different variables separately (after Lee et al, 1978).

Presently, many research efforts are devoted to the development of alternative intermediate materials that have the same favorable properties as PMMA, but lack the adverse side effects and give better fixation possibilities. Many of these efforts are concerned with porous

materials, allowing bone to grow in, as for instance porous acrylic cements (Feith, 1975; de Wijn *et al*, 1977, 1978; Ypma *et al*, 1978) and porous implant coatings (e.g. Ducheyne *et al*, 1977; Spector *et al*, 1978).

1.6. Bone reaction to joint replacement

Bone tissue can be divided into sponge-like trabecular bone and dense cortical bone. Trabecular or spongeous bone is for instance found in the proximal and distal parts of the long bones, near the joints (fig. 1.5.a). Hence the greater part of the bone to be resected for joint replacement will be spongeous bone (fig. 1.5.b).

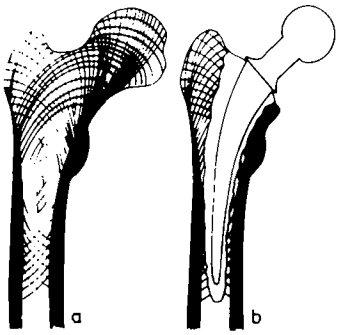

fig. 1.5: A schematic representation of bone structure, showing trabecular bone and cortical bone in the upper femur, before (a) and after (b) hip-joint replacement (reproduced with permission of Willert and Semlitsch, 1976).

Bone is a living material and is constantly being resorbed and appositioned, a process called bone remodeling. Due to this process the conditions in the biological part of the bone-prosthesis system gradually alter to a greater or lesser extent after the operation. Initially the bone remodeling process is usually restorative with respect to the surgical trauma. At a later stage progressive resorption caused by biochemical or mechanical factors may seriously endanger the service life span of the system.

A bone reaction that is of great importance for the functioning of the bone-prosthesis system is that of the bony implant bed, during and directly after the operation, but also at a later stage. The behavior of this 'bone-cement interface' will be discussed in paragraph 1.7. After intramedullary joint fixation, reactions occur that are typical for all intramedullary procedures. An extensive literature review with respect to these reactions is given by Feith (1975). The reactions, that are usually attributed to a disturbance of the intramedullar vascularity that nourishes the cortex, include necrosis of the inner part of the cortex, the appearance of large resorption lacunae in the middle third of the cortex ('spongiozation' of the cortex; Slooff, 1970) and subperiosteal bone apposition.
Another reaction often encountered is a phenomenon called 'disuse osteoporosis'; a process that may gradually occur postoperatively and in which the cortical bone becomes porous, thus affecting its mechanical properties such as strength and stiffness. A last significant reaction specific to hip-joint replacement is called 'calcar resorption', a process in which the bone rim in the calcar region resorbs to a greater or lesser extent (e.g. Charnley, 1978).

Fig. 1.6 shows an example of this phenomenon.

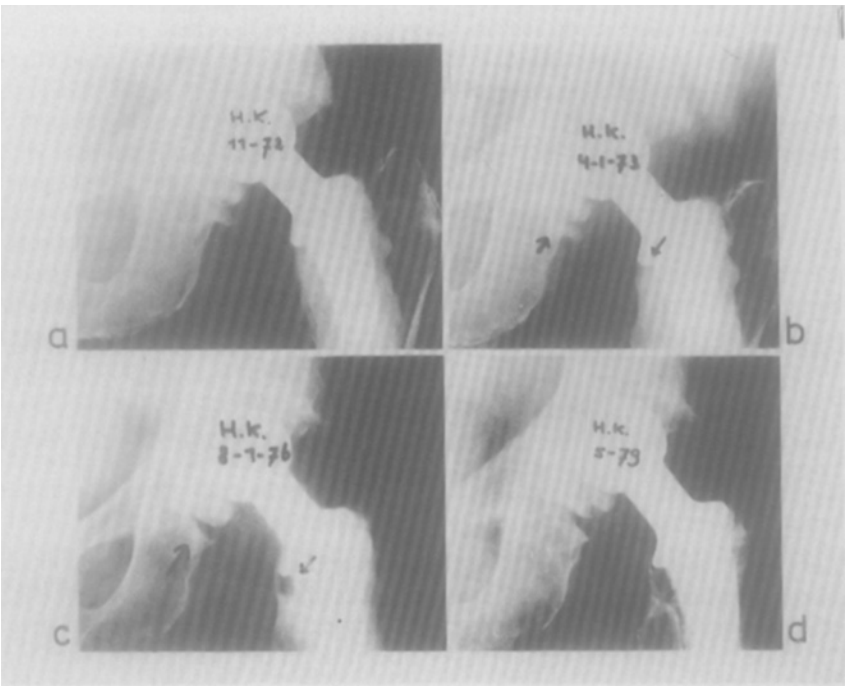

fig. 1.6: Roentgen series, showing calcar and acetabular (medial side of the cup) bone resorption (indicated by arrows) after total hip replacement; respectively directly (a), 2 months (b), 3 years (c) and 6.5 years (d) postoperative (patient material Department of Orthopedics, University of Nijmegen, the Netherlands).

Many investigations (cited in section III) have shown that the orientation and density distribution of trabecular and cortical bone coincide with optimal structural requirements to resist the stresses due to the loading of the bone. From these observations Wolff's law has been formulated (Koch, 1917), stating that bone growth is related to the stress (or strain!) pattern in the bone. It would, according to this law, not be illogical if at least part of the remodeling phenomena were caused by the effect of the greatly changed stress pattern in the bone, after the joint has been replaced. Especially disuse osteoporosis, as the name indicates, is attributed to this stress effect.

The process of calcar resorption is not yet fully understood. Its occurrence has been attributed to effects of vascular damage (e.g. Rhinelander, 1972, 1979) while some investigators support the opinion that it is initiated by 'foreign body' reactions to wear particles (e.g. Willert *et al*, 1976, 1978).
Another hypothesis often put forward is that of a stress-related effect. Especially in the calcar region the stress pattern is greatly changed after joint replacement. Upon joint-loading unphysiological radial and shear stress components will be present at the inner surface of the bone (fig. 1.7) and an unphysiological circumferential stress component will be present in the bone cortex. The axial normal stress in the cortex will be higher than in the natural case if a collar is applied on the prosthesis, but will be practically absent if no collar is used (fig. 1.7). Hence, resorption might occur due to overloading, but also to underloading.

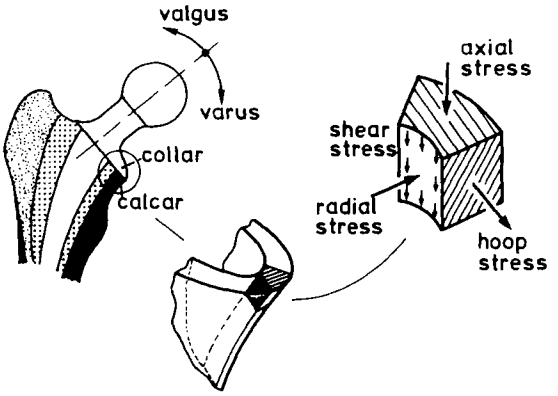

fig. 1.7: An example of a hip endoprosthesis with a collar, to rest on the calcar bone rim. Varus-valgus position as well as stress components in the calcar region are indicated: the axial stress component is a physiological one, the radial and shear stresses at the cement-bone interface and the circumferential (hoop)stresses in the bone, inflicted by the prosthesis, are quite unnatural.

Bocco *et al* (1977) and Griss *et al* (1978) found a significant reduction in the incidence of calcar resorption when the (collarless) prosthesis was placed in valgus position (fig. 1.7), compared to a fixation in varus position, thus changing the loading system relative to the fixation and also increasing the cement layer thickness on the medial side. Although most experimental and theoretical studies, as will be reviewed in section III, support the advantages of a collar, there appears to be no clinical evidence as to its benefit (e.g. Charnley, 1977, 1978; Lee *et al*, 1977; Müller and Niederer, 1977). Significant data was published by Diehl (1975) and by Griss *et al* (1978) indicating that due to usually minor bone resportion at the collar-calcar contact region and the formation of a soft intermediate tissue layer the collar will not be effective anyway.

1.7. The cement-bone interface

The cement-bone interface is the key region for success or failure of the artificial joint replacement; many complications find their origin at this junction of biological and technical material. Its initial shape depends on the bone structure: more or less smooth if cortical bone forms the implant bed and rather wild if the implant bed consists of trabecular bone. There is no chemical bond between the acrylic cement and the bone. Mechanical interlocking between the cement and the trabecular bone is possible to an extent depending on a number of factors: the viscosity of the cement mixture when inserted, the pressure applied to the cement mass, the cleanliness of the implant bed and dimensional changes of the cement.
As already mentioned in paragraph 1.1., it has recently been advocated to insert the mixture early during a more liquid phase and to press the cement into the trabecular spaces, using specially designed equipment and an intramedullary plug in the case of stem fixation (Markolf and Amstutz, 1976; Oh *et al*, 1978; Krause *et al*, 1979; Weber and Stühmer, 1979). It has also been advised to clean the implant bed after reaming, using pulsating pressurized water flow (Narten *et al*, 1977; Halawa *et al*, 1978; Miller *et al*, 1978).
An optimal mechanical interlocking between cement and bone will be advantageous for an

adequate performance of the bone-prosthesis system. However, due to the biological character of the bone, the structure of the interface will change postoperatively, both immediately and in the course of time. Histological studies on the short and long-term reaction of the bony implant bed were, for example published by Charnley (1970, 1978), Willert *et al* (1972, 1974, 1976, 1978) and Vernon-Roberts and Freeman (1976, 1977).
In the first instance, directly postoperatively, a layer of necrotic bone of a few mm thickness is usually found at the interface. Three factors may contribute to this phenomenon:
– the reaming of the implant bed and the disturbed vascularity;
– the thermal effects of the heat of polymerizing of the acrylic cement;
– the cytotoxic effect of the residual monomer.
Vernon-Roberts and Freeman (1976, 1977) believe that the first effect is the principal cause, because they found necrotic zones of bone in regions where neither heat nor monomer could have penetrated. According to Willert and Frech (1976), the amounts of residual monomer released into the bone tissue will certainly be capable of causing tissue necrosis. Several experimental temperature measurements in bone adjacent to polymerizing cement (as cited in section II) have not resulted in a conclusive opinion with respect to the thermal effect, owing to the wide spread of results.
A histological study concerning adverse side effects of bone cement in rabbits was published by Feith (1975). He concluded that reaming and residual monomer, especially an overdose, both cause bone necrosis at the interface, but that the principal causative factor is the heat of polymerizing. These experiments will be further discussed in section II.

Later, postoperatively, the layer of necrotic bone is resorbed and replaced by soft tissue in which new bone is formed. The structure of this new bone layer is not necessarily identical to that of the original layer. Vernon-Roberts and Freeman (1976) report that the initial trabecular-shaped interface, ensuring good mechanical interlocking between cement and bone, is often lost and replaced by a more or less smooth bone layer.
Also, the new bone is not in direct contact with the cement because a fibrous tissue layer always remains. This layer may be extremely thin and caused by a normal tissue reaction to the 'foreign body' (Charnley, 1970, 1978). Often, however, this layer is reported as quite thick and to appear on radiographs as a radioluscent demarcation line. Willert and Puls (1972) measured the layer to be usually 0.1 to 1.5 mm thick. Most authors believe that the occurrence of this thick layer is related to micromovements and stresses at the interface (e.g. Charnley, 1970; Willert and Puls, 1972; Willert *et al*, 1974; Vernon-Roberts and Freeman, 1977).
If a fibrous layer (radioluscent line) is abnormally thick or its thickness increases progressively, it is usually regarded as a sign of forthcoming prosthesis loosening (see chapter 2).
The 'strength' of the cement-bone interface depends on the amount of mechanical interlocking. Studies of the initial tensile and shear-strengths of cement-cancellous bone interfaces, using 'push-out' tests on cadaveric material, were carried out by Kölbel *et al* (1976). They report an average tensile strength of 1.9 ± 0.9 N/mm^2 and an average shear strength of 3.4 ± 0.6 N/mm^2. Halawa *et al* (1978) carried out comparable shear strength tests under different circumstances; they found an average increase of 100% in strength when a 2 - 3 mm cancellous bone layer was retained instead of a 5 mm layer, an average increase of 200% when the bone surface was cleaned before cementing, an average increase of 60% when the cement was inserted 3 min. instead of 6 min. after the beginning of mixing and an average increase of 100% when pressure (0.15 N/mm^2) was put to the curing cement.
These properties will, no doubt be seriously affected by interface remodeling and the formation of fibrous tissue layers, as discussed previously.

CHAPTER TWO

COMPLICATION OF ARTIFICIAL-JOINT REPLACEMENT

2.1. Introduction

Results and complications of artificial-joint replacement are usually studied in patient reviews. The results of these reviews, or follow-up studies, are becoming available in ever-increasing numbers. In the first studies published the number of postoperative follow-up years was usually rather small; recently studies on large series of late results (more than 5 yrs postoperatively) have been reported; especially on hip replacement.

The complications of artificial-joint replacement are usually divided into three categories (Müller, 1976; Schulitz and Dustmann, 1976): (1) pre-operative complications (mentioned in chapter 1.1), (2) early complication (up to four weeks postoperative, including dislocation of the joint, haematoma, thrombosis, allergic reactions, early infection and a few others) and (3) late complications (including infection, aseptic loosening, mechanical failure of the implant components, bone fracture, ectopic bone formation, migration of the implant and a number of others). An extensive follow-up study on 2256 patients who received total hip replacement was reported by Gschwend (1976). Postoperative complications were found in 10.68% of the cases, of which bone perforation (femur and acetabulum) accounted for approximately 8% and no other specific complication occurred in more than 1% of the cases. Early complications were found in 29.42% of the cases, of which 15.32% were local; the largest group consisted of haematoma (8%) and infection (1.5%).
All these complications do not in general cause failure of the joint replacement, as opposed to deep infection, aseptic loosening (loosening without infection) and mechanical failure of the implant. For deep infection, usually leading to re-operation, incidences of 0 to 11% are reported in the literature (e.g. Green, 1976; Hunter and Dandy, 1977).
Aseptic loosening and implant failure are subjects of the present investigation and will be treated in somewhat more detail.

2.2. Aseptic loosening

Aseptic loosening occurs when the implant loosens with respect to the bone by a cause other than infection. Usually patients feel pain on load bearing and the loosening can be established by clinical and radiological examination and by using scintigraphy (Feith *et al*, 1976), although not always with certainty. As a phenomenon it can either be fracture of the cement or a loosening of the cement-bone interface, leading to movement between the two materials. Sometimes prosthesis fracture is also accounted as loosening. Although a fractured component will usually be 'loose' and loosening of the implant may, on the other hand induce implant fracture, this complication is treated separately here.
Loosening of the implant most often results in a revision operation. The cause of the loosening is not always apparent, although its incidence is often found together with roentgenographically established cracks in the cement mantle, inadequate cementing (incomplete mantle), thick radioluscent lines, inadequate positioning, calcar resorption or a combination of these phenomena. During the re-operation fractioned cement or a thick layer of fibrous tissue are sometimes found.

Stühmer (1976) reports a loosening incidence of 4.3% in 2577 patients who received a total hip replacement, only 10.6% of the material could be qualified as late results (more than 5 yrs follow-up); 87.5% of the loosened cases occurred after 450 days postoperatively. The loosening incidences reported in comparable follow-up studies usually range between 0% and 7% with occasionally a higher number (e.g. Amstutz *et al*, 1970, 1978; Bergstroem *et al*, 1973; Charnley and Cupic 1973; Lazanksy, 1973; Weber and Charnley, 1975; Eftekar *et al*, 1976; Slooff *et al*, 1976; Stühmer, 1976; Witt and Hackenbroch, 1976, Rütt, 1977; Visuri *et al*, 1977).
Aseptic loosening occurs in all the various types of prostheses. Because of the large number of parameters involved (design used, materials used, surgical procedures, individual properties and level of activity of the patients) statistical analyses usually do not result in significant relations between the parameters and the incidence of loosening.
In many series aseptic loosening is the complication most occurring but, although undesirable, an incidence of 7% cannot be called alarming. However, in most patient reviews the number of postoperative years were relatively rather short and it is being shown in an increasing number of publications, that the number of artificial hip-joints that loosen aseptically rises sharply with the number of postoperative years, as opposed to septic loosening (due to infection). This was illustrated by an investigation of Witt and Hackenbroch (1976), who calculated average loosening incidences from publications concerning reviews on hip replacements carried out between 1963 and 1973 (table 2.I).

Postoperative period (years)	Average incidence of aseptic loosening	Average incidence of septic loosening
0.7 - 1.3	1.6%	2.4%
1.7 - 4.5	4 %	2.3%
5 - 9.5	8 %	3.3%

table 2.I: Average loosening percentages, septic as well as aseptic, calculated from various hip replacement reviews (after Witt and Hackenbroch, 1976).

Due to the progressively occurring incidence, aseptic loosening is considered as a very severe complication and many authors thus maintain that joint replacements should remain restricted to older patients (60 yrs. and over) (e.g. Müller, 1974; Stühmer, 1976).
Disturbing reports have been published recently on radiological reviews of patients who received a total hip replacement. Beckenbaugh and Ilstrup (1978) reviewed 333 Charnley hip arthroplasties after 4 to 7 postoperative years. They looked for roentgenographic evidence of loosening of the femoral component which they defined as significant subsidence of the prosthesis with respect to the bone. They found this evidence in 24% of the cases. Of the loosened cases 20% showed definite roentgenographic evidence of associated fracture in the cement. The overall clinical results of the loosened group was poor, although only 8% had required re-operation as yet. The authors ascribe the loosening principally to cement fracture, which will be progressive in their opinion, and ultimately require revision of all loosened hips.
A comparable investigation was reported by Gruen and Amstutz (1977); 398 total hip replacements after 0.5 to 6 postoperative years were reviewed radiographically. Radiographic evidence of loosening, which they defined as cement cracks and wide radioluscent lines at the cement-bone interface, was found in 19.5% of the cases. In 16.7% these signs

increased progressively. A radiographic analysis of 100 Charnley total hip replacements with a follow-up of 5 to 7 years was carried out by Salvati *et al* (1976). They established clear radioluscent lines at the cement-bone interface of the femoral component in 55% of the hips; 25% remained constant, 10% decreased and 21% gradually increased in thickness. They established radioluscent lines in the acetabular component in 93% of the hips; the line remained stable in 41%, decreased in 23% and gradually increased in 29% of the cases. Cement cracks they could only identify in 3% of the cases.

Loosening of acetabular components of artificial hip-joints is reported about as frequently as of femoral components; in some series its incidence is even higher (e.g. Dietschi *et al*, 1976).
A loosening incidence of approximately 20% of acetabular cups was reported by Visuri and Laurent (1977) in a series of 351 Charnley total hip replacements with 5 to 7 years follow-up; of the remaining 80%, 29% showed roentgenographic signs of loosening, this being a radioluscent zone of 1 to 12 mm at the cement-bone interface.
In a series of 95 total hip replacements after 4 to 7 postoperative years, Maier *et al* (1977) report 14.7% roentgenographically and clinically established cases of acetabular cup loosenings; in addition they found 4.9% of only roentgenographically established loosenings.

Much better results have been reported by Charnley (1978). In a series of 396 patients who received total hip replacement, with 12 to 15 years follow-up, 0.25% had to be re-operated due to loose femoral components and 1.26% due to loose acetabular components. For his total material of 10,000 total hip replacements he reports a revision percentage of 0.25% due to loose femoral or acetabular components. A summary of some roentgenographical data concerning this series, as established in several investigations cited by Charnley (1978), is shown in table 2.II.

Study No.	1	2	3	4	5	6	7	8	9
hip replacements	138	106	6,649	141	190	169	216	547	115
postoperative years	7-8	9-10	3-14	8-11	3-8	8-11	1.6-2.6	8	12-15
Femoral component									
subsidence	–	–	1.5%	–	–	–	12.6%	8.9%	8%
cement fracture	–	–	1.5%	–	–	–	23.3%	8.6%	–
calcar resorption	–	99.9%	–	–	37.2%	70%	23.1%	–	95%
Acetabular component									
migration	1.4%	1.4%	–	9.2%	–	–	–	–	11%
no radioluscent line	–	–	–	31.3%	–	–	–	–	41%
moderate radioluscent line	–	–	–	60.3%	–	–	–	53.7%	34%

table 2.II: Some results of radiographic reviews of total hip replacements (after Charnley, 1978).

In summarizing, it is found that the number of failed hip replacements increases late post-operatively due to aseptic loosening. Many patients, although still asymptomatic, show roentgenographic evidences of loosening such as cement fractures, subsidence of the prosthesis and progressive radioluscent demarcation lines at the cement-bone interface.

Although this is being contradicted by Charnley (1978), many investigators expect that the roentgenographic evidence indicates a forthcoming need for revision.

Considerably less literature is available on other than hip-joint replacements. For the knee-joint, loosening incidences have been reported of 4% to 30%, the higher numbers being representative of the hinged prostheses (Peterson, 1977; Freeman *et al*, 1978; Ducheyne *et al*, 1978; Lacey, 1978). Loosening incidences of 3% to 30% were reported for elbow prostheses, the high percentages certainly caused by the high torsional loading of the humeral component (Schlein, 1976; Nederpelt, 1978).

2.3. Implant failure and bone fracture

Mechanical failure of the artificial joint itself can either be due to fracture or plastic deformation of a component, while excessive wear may also be reckoned among the causes. Fracture of a component is frequently reported as occurring in femoral stems of hip prostheses. Martens *et al* (1974) reported six femoral stem fractures out of a series of 56 Charnley-Müller total hip replacements (10.7%). All fractures were located in the middle third of the stem and could be ascribed to fatigue. At least part of the fractures were preceded by fractures in the cement.
Ducheyne *et al* (1975) reported two stem fractures in a series of 90 Charnley total hip replacements. Both fractures occurred in the proximal part of the stem (at the curvature) and were preceded by plastic deformation. Galante *et al* (1975) reviewed 21 articles concerning follow-up studies of a total of 6,110 hip replacements and found that re-operation due to fractured stems was needed in only 0.15% of the cases. Charnley (1975) investigated 17 cases of fractured stems out of a series of approximately 6,500 total hip replacements (0.26%). He found that the incidence of stem fracture among patients over 76 kg in weight was 2.6% and for patients over 89 kg in weight even 6.1%. Besides weight he considers erosion or calcar resorption as the possible predominant factor in stem failure.
Collis (1977) reported 4 stem fractures out of 200 total hip replacements (2%); all in patients who weighed over 91 kg. The postoperative follow-up period was 4 to 6 years. All stem failures were preceded by cement fractures in the proximal-medial region.
Rostoker *et al* (1978) investigated 34 fractured stems. All fractures were found to be due to fatigue failure. In all the fractured cases the patient exhibited at least one of the 'risk factors', which they define as high body weight, malpositioning, lack of calcar support and roentgenographic signs of loosening. They also found metallurgical defects in 31 of the fractured stems. It should be remarked here that on detailed investigation no material will be found absolutely pure.
Dobbs (1977) investigated 29 cases of fractured stems, and on the basis of this review, developed a statistical model to predict the incidence of failure. Owing to uncertain parameter values, his model predictions are probably not very accurate, but when more accurate data become available on the relation between joint-loading and maximal stem stresses, taking the 'risk factors' into account, such models could conveniently be used in post-operative radiographic patient evaluation.

Fractures of acetabular components of total hip prostheses are not often reported in the literature. Fractures of elbow and knee prostheses stems have been reported occasionally, while finger-joint stems appear to fracture more frequently (Walker, 1977). Plastic deformation (cold creep) may occur in the plastic tibial components of artificial knee-joints (Walker, 1977; Lacy, 1978; Ducheyne *et al*, 1978).

Occasionally, plastic deformed metal intramedullary stems are also encountered.
Recently a case of thermal deformation of a polyethylene tibial component of an artificial knee-joint has been reported (Volz and Gradillas, 1978). The authors believe that such a deformation, caused by the polymerization heat of the acrylic cement, occurs more often and they found some evidence of it in several roentgenograms.

There is no doubt that prostheses components are subject to wear in the body, which does not necessarily have to present a problem. However, if the wear is excessive to an extent that it can no longer perform its function, it will result in failure. Much research has been and is being done on wear of various biomaterials (e.g. Charnley and Halley, 1975; Walker, 1977; Swansson and Freeman, 1977).
The wear rates of the materials presently used are such that the wear in itself appears to present no serious problems. This might be different, however, if younger patients received joint replacements.

Fracture of the bone, postoperatively, is not a complication often encountered after artificial-joint replacement. In a series of 5400 total hip arthroplasties McElfresh and Coventry (1974) reported 10 postoperative bone fractures, 6 of which were in the femur, 3 in the acetabulum and one in both. The acetabular fractures were not related to the hip replacement. In some of the femoral fractures defects of the cortex due to screw holes or misdirected reaming were apparent.
Scott *et al* (1975) also reported occasionally occurring femoral fractures, always related to cortical defects near the prosthesis stem tip.

A 'bone failure mode' with a higher incidence, already mentioned in chapter 2.2, is the gradual sinking of a component through the bone. Especially protrusion or migration of the artificial head or the cup of the hip-joint through the acetabulum (e.g. Hoogbergen *et al*, 1975; Charnley, 1978) and sinkage of the tibial knee-component in the tibia (e.g. Walker, 1977; Freeman *et al*, 1978) occur sometimes. The protrusion may be caused by interface bone remodeling, stress (fatigue) fractures of the subchrondal spongeous bone or a combination of both.

CHAPTER THREE

OBJECTS AND METHODS OF THE PRESENT STUDIES

3.1. Introduction

Clinical and roentgenographic follow-up studies, as discussed in the previous chapter, give valuable information on the adequacy of the treatment in general, the kinds and numbers of problems that may be encountered and the way in which complications manifest themselves. Usually no definite relation can be found between a complication and its cause, and when it is found, it is mostly statistical and not causative, due to the many uncertain parameters involved in a joint replacement. Especially with respect to such a treatment, however, a fundamental understanding of the relations between causes and effects of complications is of great importance. It has been mentioned previously that an artificial joint has to perform without complications for the full postoperative life span. This means that ten to fifteen years would have to pass before the data on the general adequacy of a specific design or procedure would be complete. This is not a good basis for 'trial and error' procedures and hence, in our opinion, all available means to predict the performance of a prosthetic device should be applied. However complicated the (biological) bone-prosthesis structure is, it is certainly possible to acquire fundamental knowledge on certain aspects. If, for example, a fundamental concept on the relation between the structural parameters and the purely mechanical performance of the prosthesis in the body can be developed, this might not lead to an immediate answer to the question of the optimal design features, since also other complicated aspects are involved, but it would at least provide a firm basis, or no basis, for a part of the arguments commonly used in solving this problem and it would at least extend the available means for a long-term performance prediction.

In orthopedic research, studies of animal or laboratory models are often applied. Another method, that is not very common, is the use of theoretical or mathematical models. For certain research objects, with respect to some problems of artificial-joint replacement, too, the use of these methods have many advantages (Huiskes and v. Heugten, 1974). In these methods the properties of the system to be investigated are described mathematically and, by using theories, are interrelated in formulas that describe the system behavior. One of the advantages of such theoretical analyses is the possibility to investigate influences of parameter changes and in this way acquiring a fundamental comprehension of relations between parameters and effects. In the following sections II and III, theoretical methods will be used in an effort to contribute to a more fundamental understanding of some aspects of artificial-joint replacement. These studies concern a stress analysis of intramedullary fixated prostheses, principally focussed on the hip-joint, and a heat-conduction analysis of acrylic cement in situ. Although the use of theoretical methods will certainly not be the ultimate answer to problems of artificial-joint replacement, it will hopefully be shown that these (engineering) methods deserve their rightful place next to follow-up studies, animal experiments and laboratory experiments in orthopedic research and that especially when used in interactive combination with these experiments an additional dimension in research possibilities evolves.

3.2. Heat-conduction analyses

As was discussed in paragraph 1.7, thermal damage due to the polymerization heat of acrylic cement is regarded as a possible factor contributing to necrosis of the bony implant bed. It was the object of the analysis presented in section II to establish whether the temperature values in the bone, during implant fixation, may be such as can cause thermal damage and, if so, what measures can be taken to reduce the chances of thermal damage.

Between cause (heat of polymerizing) and effect (bone temperature) there is a relation that depends on many parameters. The heat of polymerizing itself depends on the amount of monomer in the mixture and hence on its composition.
If the cement mass were completely isolated from its neighborhood, the temperature rise (ΔT) could easily be calculated from $Q = C\Delta T$, where Q denotes the total amount of polymerization heat and C the heat capacity. As the cement mass is in contact with its adjoining materials, implant and bone, heat conduction occurs during and after the polymerization process. Hence, on one hand the rate of heat generation in the cement mass depends on the polymerization rate, while on the other the rate of heat transport depends on the heat-conduction properties of the cement, the interface, the implant and the bone. By applying approximative mathematical descriptions of these properties and using heat-conduction theory, this process can be described in a mathematical (computer) model. With this model the temperature as a function of time can be calculated at any point of the structure, given the parameters that describe the following properties:
- the geometry of the implant, the cement mass and the bone,
- the heat capacities and the thermal conductivities of these materials,
- the cement-bone interface thermal conductivity,
- the bone surface heat loss,
- the polymerization rate,
- the cement composition.

In section II such a model will be used to predict the time- and location-dependent temperatures during fixation of artificial joints. The calculated temperature values are compared with thermal damage threshold levels in order to estimate the chances of bone necrosis occurring. By varying the system parameters, their influences on the temperature values are investigated from which quantitative guidelines for composition and application of the cement can be derived.

3.3. Stress analyses

The stress analyses, presented in section III, are confined to intramedullary fixated prostheses and focussed especially on the hip-joint; although some results are valid for these systems in general.
As was discussed in chapter 2, many complications of joint replacement are or may be related to stresses in the bone-prosthesis structure. Certainly stem, cement and bone fractures are caused by locally exceeding the (fatigue) strength of the materials. Although definite causes for interface bone remodeling, development of fibrous tissue layers, calcar bone resorption, implant migration and disuses osteoporosis are as yet unknown, there is some evidence that these phenomena are, at least to some extent, stress-related as well and thus it appears to be beneficial to provide a system in which the stress pattern is smooth and the stresses on and in bone are as 'natural' as possible.
For given joint-forces the stress distribution in the stem, in the bone, in the cement mantle

and at the interfaces depends on the geometry of the implant (for example stem length, thickness, taper, etc.), the geometry of the cement mantle (for example its thickness) and the geometry of the bone; on the mechanical properties of the materials (for example their modulus of elasticity) and on the mechanical interface conditions. By applying theories of continuum mechanics these properties can be described mathematically and interrelated in mathematical models. With such models the stress values in the system can be approximated for given joint-loading.

It was the object of the analysis described in section III to contribute to better understanding of the relations between the geometrical and materials properties of the system components on one hand and the stresses in the system that result from a specific joint-loading on the other. To accomplish this, simplified mathematical models of the intramedullary fixation structure were studied, using various methods. Also, relatively simple formulas were derived that roughly approximate to the most important stress values. As will be shown in section III, with these formulas a direct relation can be established between the most important design and material parameters and some aspects of the mechanical performance of the system.

REFERENCES

Amstutz, H.C. (1970); Complications of total hip replacement; Clin. Orthop. Rel. Res. 72: 123.

Amstutz, H.C., Green, R.A., Markolf, K.L. and McNeice, G.M. (1976); Loosening of total hip components; cause and preventions; **In**: The Hip, Proc. Hip Society, C.V. Mosby, St. Louis.

Beckenbaugh, R.D. and Ilstrup, D.M. (1978); Total hip arthroplasty, a review of three hundred and thirty-three cases with long follow-up; J. Bone Jt. Surg. 60-A, no. 3, 306.

Bergstroem, B., Lindberg, L., Persson, B.M. and Oennerfaelt, R. (1973); Complications after total hip arthroplasty according to Charnley in a Swedish series of cases; Clin. Orthop. Rel. Res. 95: 91.

Bocco, F., Langan, P. and Charnley, J. (1977); Changes in the calcar femoris in relation to cement technology in total hip replacement; Clin. Orthop. Rel. Res. 128, 287-295.

Brewster, R.C., Chao, E.Y. and Stauffer, R.N. (1974); Force analysis of the ankle joint during the stance phase of gait; 27th ACEMB, Philadelphia, p. 369 proceedings.

Chao, E.Y. (1976); The biomechanics of total joint replacement surgery; Geriatrics, March.

Chao, E.Y. (1979); private communication.

Charnley, J. (1970); Acrylic cement in orthopaedic surgery; E. and S. Livingstone; Edinburgh and London.

Charnley, J. and Cupic, Z. (1973); The nine and ten year results of the low-friction arthroplasty of the hip; Clin. Orthop. Rel. Res. 95: 9-25.

Charnley, J. (1975); Fracture of femoral prostheses in total hip replacement; Clin. Orthop. Rel. Res. 111: 105.

Charnley, J. and Halley, D.K. (1975); The rate of wear in total hip replacement; Clin. Orthop. Rel. Res. 112: 170.

Charnley, J. (1977); Prosthetic fixation and loosening; 3rd Annual Meeting Soc. for Biomaterials, New Orleans, La., April.

Charnley, J. (1978); Low-friction arthroplasty of the hip; Springer-Verlag, Berlin, Heidelberg, New York.

Collis, D.K. (1977); Femoral stem failure in total hip replacement; J. Bone Jt. Surg. 59-A, no. 2: 1033.

Debrunner, H.U., Wettstein, A. and Hofer, P. (1976); The polymerization of selfcuring acrylic cements and problems due to the cement anchorage of joint prostheses; **In**: Advances in Artificial Hip and Knee Joint Technolgy (Schaldach, M. and Hohmann, D., eds.): Springer-Verlag, Berlin, Heidelberg, New York.

Diehl, K. (1975); Knochenbeanspruchung und Knochenumbau bei der Alloplastik des coxalen Femurendes mit Zement-verankerung; Arch. Orthop. Unfall.-Chir. 83, 9-23.

Dietschi, C., Huggler, A. and Suezawa, Y. (1976); Problems of loosening; **In**: Total hip prosthesis (Gschwend and Debrunner, eds.): Hans Huber Publ.; Bern, Stuttgart, Vienna.

Dobbs (1977); A model to predict the incidence of fracture in femoral components; J. Bioeng. vol. 1, pp. 189-196.

Ducheyne, P., Meester, P. de, Aernoudt, E., Martens, M. and Mulier, J.C. (1975); Fatigue fractures of the femoral component of Charnley and Charnley-Müller type total hip prostheses; J. Biomed. Mat. Res. Symp. No. 6, pp. 199-219.

Ducheyne, P., Aernoudt, E., de Meester, P., Martens, M., Mulier, J.C. and van Leeuwen, D. (1977); Factors governing the mechanical behaviour of the implant porous coating trabecular bone interface; J. Biomech. Vol. 11, pp. 297-307.

Ducheyne, P., Kagan II, A., and Lacy, J.A. (1978); Failure of total knee arthroplasty due to loosening and deformation of the tibial component; J. Bone Jt. Surg. Vol. 60-A, pp. 384-391.
Eftekar, M.S., Kierman, H.A., jr., and Stinckfield, S.E. (1976); Systemic and local complications following low friction arthroplasty of the hip joint; Arch. of Surg. vol. 111, p. 150.
Feith, R. (1975); Side-effects of acrylic cement, implanted into bone; Acta Orthop. Scand. Suppl. nr. 161.
Feith, R., Slooff, T.J.J.H., Kazem, I. and van Rens, Th.J.G. (1976); Strontium 87m Sr bone scanning for the evaluation of total hip replacement; J. Bone Jt. Surg. 58-B, 79-83.
Freeman, M.A.R., Todd, R.C., Bamert, P. and Day, W.H. (1978); ICLH arthroplasty of the knee 1968-1977; J. Bone Jt. Surg. Vol. 60-B, no. 3, pp. 339-341.
Galante, J.O., Rostoker, W. and Doyle, J.M. (1975); Failed femoral stems in total hip prosthesis; J. Bone Jt. Surg. 57-A, no. 2, 230.
Green, D.L. (1976); Complications of total hip replacement; South. Med. J. 69, 1559.
Griss, P., Heimke, G., Werner, E., Bleicher, J. and Jentschwa, G. (1978); Was bedeutet die Resorption des Calcar Femoris nach der Totalendoprothesenoperation der Hüfte; Arch. Orthop. Traumat. Surg., 92, 225-232.
Gruen, T. and Amstutz, H.C. (1977); Mechanical "modes of failure" of femoral components – radiographic examination of total hip replacement; 22nd. National SAMPE Symp. vol. 22, Soc. for the Adv. of Mat. and Process. Eng.; San Diego, Cal, April.
Gschwend, N. (1976); Symposium on total prostheses, clinical material and over-all results. **In:** Total hip prosthesis (Gschwend and Debrunner,eds.); Hans Huber Publ.; Bern, Stuttgart, Vienna.
Halawa, M., Lee, A.J.C., Ling, R.S.M. and Vangala, S.S. (1978); The shear strength of trabecular bone from the femur and some factors affecting the shear strength of the cement-bone interface; Arch. Orthop. Traumatol. Surg. 92, pp. 19-30.
Hench, L.L., Pantano, C.G., Bussemi, P.J. and Greenspan, D.C. (1977); Analysis of bioglass fixation of hipprostheses; J. Biomed. Mat. Res. 11, 2: pp. 267-283.
Hoogbergen, T.J.M., van Rens, Th.J.G. and Huiskes, R. (1975); A long-term follow-up study of patients with hemiarthroplasty of the hip, with respect to protrusio of the prosthesis; **In:** Controversial opinions, selected proceedings IX Europ. Fed. Congr. of Surgeons (Greep *et al* eds.).
Huiskes, R. and van Heugten, P.C.M. (1974); A discussion of problem solving methods in biomechanical research; **In:** Proceedings of the Combined Meeting of the Dutch and Danish Orthopaedic Societies (Biermans *et al* eds.); Univ. of Nijmegen, The Netherlands.
Hunter, G.A. and Dandy, D. (1977); The natural history of the patient with an infected total hip replacement; J. Bone Jt. Surg. 59-B, 293.
Koch, J.C. (1917); The laws of bone architecture; Am. J. Anat. vol. 21.
Kölbel, R., Bergmann, G. and Boenick, U. (1976); Mechanical properties of the cement/bone bond; **In:** Advances in artificial hip and knee joint technology (M. Schaldach, D. Hohmann, eds.); Springer-Verlag, Berlin, Heidelberg, New York.
Krause, W.R., Miller, J.E. and Ng, W.W.P. (1979); Penetration of acrylic bone cement into cancellous bone; 25th Ann. ORS, San Francisco, Cal., February.
Kusy, R.P. (1978); Characterization of self-curing acrylic bone cements; J. Biomed. Mat. Res., Vol. 12, pp. 271-305.
Kutzner, F., Dittmann, E.C.H. and Ohnsorge, J. (1974); Restmonomerabgabe von abhärtenden Knochenzement. Experimentelle Untersuchungen; Arch. Orthop. Unfall.-Chir. 79, 247-253.
Lacey, J.A. (1978); A statistical review of 100 consecutive U.C.I. low-friction knee arthroplasties with analysis of results; Clin. Orthop. Rel. Res. 132: 163.

Lautenschlager, E.P., Moore, B.K. and Schoenfeld, C.M. (1974); Physical characteristics of setting acrylic bone cements; J. Biomed. Mat. Res. Symp. Vol. 8, no. 5, Part I, pp. 185-196.
Lazansky, M.G. (1973); Complications revisited; Clin. Orthop. Rel. Res., 95, 96-103.
Lee, A.J.C., Ling, R.S.M. and Vangala, S.S. (1977); The effect of implant design on fixation and performance; 3rd Annual Meeting Soc. for Biomaterials, New Orleans, La., April.
Lee, A.J.C., Ling, R.S.M. and Vangala, S.S. (1978); Some clinically relevant variables affecting the mechanical behaviour of bone cement; Arch. Orthop. Traumatol. Surg. 92, 1-18.
Maier, S., Griss, P., Rahmfeld, P. and Binkelacker, P. (1977); Nachuntersuchungsergebnisse der totalen Alloarthroplastiek der Hüfte unter besonderer Berücksichtigung der Spätkomplikationen; Z. f. Orthop. u. Grenzgebiete, Band 115, pp. 274-283.
Markolf, K.L. and Amstutz, H.C. (1976); In vitro measurements of bone-acrylic interface pressures during femoral prosthesis insertion; 22nd Annual ORS, New Orleans, Louisiana, January.
Martens, M., Aernoudt, E., de Meester, P., Ducheyne, P., Mulier, J.C., de Langh, R. and Kestelijn, P. (1974); Factors in the mechanical failure of the femoral component in total hip prosthesis; Acta Orthop. Scand. 45, 593-670.
McElfresh, E.C. and Coventry, M.B. (1974); Femoral and pelvic fractures after total hip arthroplasty; J. Bone Jt. Surg. 56-A, no. 3, 483.
Miller, J., Burke, D.L., Stachiewicz, J.W. and Kelebay, L. (1976); A study of the interface between polymethylmethacrylate and living cortical bone under conditions of load bearing; 22nd Ann. ORS, New Orleans, La., January.
Miller, J., Burke, D.L., Krause, W., Ahmed, A. and Kelebay, L.C. (1978); Blood and surgical debris on the surface of medullary canal bone as a factor in the loosening of hip arthroplasty components; 24th Annual ORS, Dallas, Texas, February.
Mohr, H.J. (1958); Pathologische Anatomie und kausale Genese der durch selbst-polymerisierendes Methacrylat hervorgerufenen Gewebsveränderungen; Z. ges. exp. Med. 130, 41-49.
Müller, K. (1975); Grundsätzliches Verhalten von Knochenzementen aus stoff-technischer Sicht; **In:** Die Knochenzemente (Oest *et al* eds.); Ferd. Enke Verlag, Stuttgart.
Müller, K. (1979); A practice-oriented study of the complex "Processing and Handling-Application-Resultant Properties" of autopolymerizing PMMA bone cements; Z. Werkstofftechn. 10, pp. 30-36.
Müller, M.E. (1974); **In:** Zeitschrift f. Orthop. 1977, band 115, p. 274-283.
Müller, M.E. (1976); Complications of total hip replacement. **In:** Total hip prosthesis (Gschwend and Debrunner eds.); Hand Huber Publ.; Bern, Stuttgart, Vienna.
Müller, M.E. and Niederer, P. (1977); Design, performance and fracture of femoral stem components; 3rd Annual Meeting Soc. for Biomaterials, New Orleans, La., April.
Narten, N.C., Larke, D., Greenwald, A.S. and Wilde, A.H. (1977); paper 32, 30th ACEMB, Los Angeles, Cal., Nov.
Nederpelt, K.J. (1978); private communication.
Oest, O., Müller, K. und Hupfauer, W. (1975); Die Knochenzemente; Ferd. Enke Verlag, Stuttgart.
Oh, J., Carlson, C.E., Tomford, W.W., and Harris, W.H. (1978); Improved fixation of the femoral component after total hip replacement using a methacrylate intramedullary plug; J. Bone Jt. Surg. vol. 60-A, no. 5, 608-613.
Paul, J.P. (1974); Force actions transmitted in the knee of normal subjects and by prosthetic joint replacement; Inst. Mech. Eng. Conf. on Total Knee Repl., London, Sept.
Peterson, L.S.A. (1977); Current status of total knee arthroplasties; Arch. Surg. vol. 112, pp. 1099-1104.

Rhinelander, F.W. (1972); Circulation in bone; **In:** The Bioschemistry and Physiology of bone (G.H. Bourne, ed.); 2nd ed. vol. II; Academic Press, New York.
Rhinelander, F.W. (1979); Personal communication; 5th. Ann. Meeting Soc. for Biomaterials, Clemson, So.Car., April-May.
Rostoker, W., Chao, E.Y.S. and Galante, J.O. (1978); Defects in failed stems of hip prostheses; J. Biomed. Mat. Res., vol. 12, 635-651.
Rostoker, W. and Galante, J.O. (1979); Materials for human implantation; ASME J. Biomech. Eng., vol. 101, Febr., pp. 2-14.
Rütt, A. (1977); Zur Aetiopathogenese der aseptischen Auslockerung von Hüftgelenktotalendoprothesen; Arch. Orthop.-Unfall.-Chir. 88: 139.
Rydell, N.W. (1966); Forces acting on the femoral head prosthesis; Acta Orthop. Scand. Suppl. 88, vol. 37.
Salvati, E.A., Chuem, Jm, V., Aglietti, P. and Wilson, P.D. (1976); Radiology of total hip replacements; Clin. Orthop. Rel. Res. 121, 74.
Schlein, A.P. (1976); Semi-constraint total elbow arthroplasty; Clin. Orthop. Rel. Res. No. 121, p. 222.
Schulitz, K.P. and Dustmann, H.O. (1976); Komplikationen der Totalendoprothese; Arch. Orthop. Unfall.-Chir., 85, 33-50.
Scott, R.D., Turner, R.H., Leitzes, S.M. and Aufranc, O.E. (1975); Femoral fractures in conjunction with total hip replacements; J. Bone Jt. Surg. 57-A, no. 4, 494.
Seireg, A. and Arvikar, R.J. (1975); The prediction of muscular load sharing and joint forces in the lower extremities during walking; J. Biomech. 8, 89.
Slooff, T.J.J.H. (1969); A cement syringe; Acta Orthop. Belg. 35, 1012-1014.
Slooff, T.J.J.H. (1970); De invloed van het acryl-cement bij de fixatie van de heupprothese. Dissertation, Univ. of Nijmegen, The Netherlands.
Slooff, T.J.J.H., Schaapsmeerders, F., v.d. Sandt, H.A. and van Rens, Th.J.G. (1976); Treatment of 40 loosened total hip replacements; Acta Orthop. Belg. 42, 492-500.
Spector, M., Michno, M.J., Smarook, W.H. and Kwiatkowski, G.T. (1978); A high-modulus polymer for porous orthopaedic implants; Biomechnical compatability of porous implants; J. Biomed. Mat. Res., vol. 12, 665-677.
Stühmer, G. (1976); Loosening of prostheses; **In:** Total hip prosthesis (Gschwend and Debrunner, eds.); Hans Huber, Publ.; Berlin, Stuttgart, Vienna.
Swansson, S.A.V. and Freeman, M.A.R. (1977); The scientific basis of joint replacement; Pitman Med. Publ. Comp., Tunbridge Wells.
Trommsdorf, E. (1963); Polymerisate der Acrylsäure, ihrer Homologe und Derivate; **In:** (Houwink, R. und Stavermann, A.J., eds.) Chemie und Technologie der Kunststoffe, Bd. II/1; Akad. Verlagsges. Leipzig, 541-599.
Vernon-Roberts, B. and Freeman, M.A.R. (1976); Morphological and analytical studies of the tissue adjacent to joint prostheses. **In:** Advances in artificial hip and knee joint technology (Schaldach and Hohmann, eds.); Springer-Verlag, Berlin, Heidelberg, New York.
Vernon-Roberts, B. and Freeman, M.A.R. (1977); The tissue response to total joint replacement prostheses; **In:** The scientific basis of joint replacement (S.A.V. Swansson and M.A.R. Freeman, eds.,); Pitman Med. Publ. Comp., Tunbridge Wells.
Visuri, T., Salenius, P. and Laurent, L.E. (1977); Total hip replacement by the Brunswick prosthesis; Acta Orthop. Scand. vol. 48, no. 1, pp. 197-203.
Visuri, T. and Laurent, L.E. (1977); Results of revision operations of loosened and infected total hip prosthesis; Acta Orthop. Scand. vol. 48, no. 1, p. 229.
Volz, R.G. and Gradillas, E.L. (1978); Thermal deformation of Polyethylene in a total knee prosthesis; J. Bone Jt. Surg. 60-A, no. 5, 662.

Walker, P.S. (1977); Human joints and their artificial replacements; Charles C. Thomas, Publ., Springfield, Ill.
Weber, F.A. and Charnley, J. (1975); A radiological study of fractures of acrylic cement in relation to the stem of a femoral head prosthesis; J. Bone Jt. Surg. 57-B, no. 3
Weber, B.G. and Stühmer, G. (1979); Improvements in total hip prosthesis implantation technique; Arch. Orthop. Traumatol. Surg. 93, pp. 185-189.
Willert, H.G. and Puls, P. (1972); Die Reaktion des Knochens auf Knochenzement bei der Allo-Arthroplastik der Hüfte; Arch. Orthop. Unfall.-Chir. 72, 33-71.
Willert, H.G., Ludwig, J. and Semlitsch, M. (1974); Reaction of bone to methacrylate after hip arthroplasty; J. Bone Jt. Surg. 56-A, 1368-1382.
Willert, H.G. and Frech, H.A. (1976); Tissue damage caused by bone cement; **In:** Advances in artificial hip and knee joint technology (N. Schaldach and D. Hohmann, eds.); Springer-Verlag; Berlin, Heidelberg, New York.
Willert, H.G. and Semlitsch, M. (1976); Problems associated with the cement anchorage of artificial joints; **In:** Advances in artificial hip and knee joint technology (N. Schaldach and D. Hohmann, eds.); Springer-Verlag; Berlin, Heidelberg, New York.
Willert, H.G., Semlitsch, M., Buchhorn, G. and Kriete, U. (1978); Materialverschleiss und Gewebereaktion bei künstlichen Gelenken; Orthopäde 7, 62-83.
Witt, A.N.N. and Hackenbroch, M.H. (1976); Therapeutische Möglichkeiten bei gelockerten Hüfttotalprothesen; Z. Orthop., 114, 330-341.
Wijn, de J.R. (1974); Reduction of maximum temperature in the polymerization of cold- and heat-curing acrylic resins; J. Biomed. Mat. Res., vol. 8, 421-434.
Wijn, de J.R., Driessens, F.C.M. and Slooff, T.J.J.H. (1975); Dimensional behaviour of curing bone cement masses; J. Biomed. Mat. Res. Symp. no. 6, 99-103.
Wijn, de J.R., Ypma, J., Huiskes, R., van Mullem, P.J. and Slooff, T.J.J.H. (1977); Stress relaxation and dynamic experiments with massive and porous bone cements; 1e Europ. Conf. on Evaluation of Biomaterials, Strasbourg, Sep.t
Wijn, de J.R., Mullem, P.J. van, Ypma, J., Huiskes, R. and Slooff, T.J.J.H. (1978); Development of polymethylmethacrylate-aqueous gel bone cement; parts I and II, Report Cement Group, Lab. Exp. Orthop. and Lab. Dent. Mat. Res., Univ. of Nijmegen, The Netherlands.
Ypma, J., Wijn, J.R. de, Huiskes, R. and Slooff, T.J.J.H. (1979); Strength and ingrowth aspects of porous acrylic bone cements; 5th Ann. Meeting Soc. of Biomaterials, So.Car., April-May.

SECTION TWO

HEAT-GENERATION AND CONDUCTION ANALYSES OF ACRYLIC BONE CEMENT IN SITU

CONTENTS

LIST OF SYMBOLS

General

t	sec	time
t_n, t_{n-1}, etc.	sec	times
Δt	sec	time step ($t_n - t_{n-1}$)
r, z	m	coordinates (cylindrical system)
x, z	m	coordinates (plane rectangular system)

Temperature

$T(r,z,t)$	°C	temperature
$T_n(r,z)$, $T_{n-1}(r,z)$, etc.	°C	temperature at time t_n, t_{n-1}, etc.
$T_a(r,z)$	°C	ambient temperature
$T_0(r,z)$	°C	initial temperature
T_{0j}	°C	initial temperature of material j (for possibilities of j see under 'indices')
$\Delta T(r,z,t)$	°C	temperature drop
$T_{max}(r,z)$	°C	maximal temperature
T_b	°C	maximal bone temperature
ΔT_b	°C	maximal bone-temperature increase ($T_b - 37°C$)
T_c	°C	maximal cement temperature
ΔT_c	°C	maximal cement-temperature increase ($T_c - T_{0c}$)
$\delta(t)$	mm	penetration depth (in the bone) of an isotherm
δ_m	mm	maximal penetration depth (in the bone) of the 50°C isotherm

Indices

The indices used for the parameters describing the materials properties and quantities (and some other parameters) refer to:

c – cement
i – implant
b – bone
p – polymer
m – the actually polymerizing monomer
rm – residual monomer
po – powder
li – liquid
ap – additives to the polymer
am – additives to the monomer
ac – additives to the cement mixture

Geometry and materials quantities

m	kg	mass
V	m^3	volume
ν	–	volume fraction (see paragraph 5.1)
P/L	gr/cc	powder-to-liquid ratio
r_u	m	outer bone radius
r_i	m	inner bone radius
s	m	cement layer thickness
r_s	m	implant stem radius
μ	–	weight ratio m_{ap}/m_p

Materials properties

λ	J/msec°C	thermal conductivity
C	J/m³°C	heat capacity
c	J/kg°C	specific heat
ρ	kg/m³	density

Heat generation

$\Phi(r,z,t)$	J/m³sec	heat source
$\Phi_n(r,z)$, $\Phi_{n-1}(r,z)$, etc.	J/m³sec	heat source at time t_n, t_{n-1}, etc.
Q	J/m³	heat generation per unit volume of acrylic cement
Q_t	J/kg	heat generation per unit mass of monomer
ρ_m	kg/m³	density of monomer
ν_m	–	volume fraction of actually polymerizing monomer in the cement mixture
$p(t)$	–	polymerized fraction of the monomer (polymerization function)
t_r	sec	retardation time (see paragraph 5.2.)
τ	sec	polymerization time (see paragraph 5.2.)
θ_p	sec^{-1}	maximal polymerization rate

Others

$q(r,z,t)$	J/m²	heat flow
α	J/m²sec°C	surface conduction and convection coefficient
β_{kl}	J/m²sec°C	thermal contact ('interface') conductivity from material k to material l
t_e	sec	time of exposure
$T_n(t_e)$	°C	threshold temperature for cell necrosis
$T_d(t_e)$	°C	threshold temperature for vascular damage

CHAPTER ONE

INTRODUCTION

In this section a mathematical (computer) model will be presented for the analysis of the heat generation and conduction process of self-curing acrylic cement in situ. The model will be used to simulate this process as it occurs during fixation of artificial joints, to predict time- and location-dependent temperature values in the bone-prosthesis system. The results will be compared with data on thermal damage threshold levels of bone tissue, as published in the literature, in order to assess the possibility of thermal necrosis. The second chapter contains a review of the literature on previous work. The third chapter treats possible threshold levels for thermal bone necrosis and in the fourth the model, its assumptions and the mathematical methods of solution will be discussed. In chapter five values for parameters describing the heat generation and conduction properties of the system, to be used in the model calculations, will be estimated on the basis of a thorough review of the literature. In order to evaluate the model and the method of analysis, two experiments described in the literature are simulated, as described in chapter six. In chapter seven the model is actually used to simulate the thermal behavior of the cement during fixation of intramedullary implants. To establish the influences of the system properties, a parametric analysis with respect to this bone-prosthesis system was carried out and will be described also in this chapter. Chapter eight discusses the use of the acrylic cement during acetabular cup fixation and in chapter nine various measures that can be taken to reduce the chances of thermal bone necrosis are evaluated as to their effectiveness.

CHAPTER TWO

A SHORT REVIEW OF THE LITERATURE ON EARLIER WORK

2.1. Temperature measurements in vivo

Several measurements of temperatures in the cement-bone contact region (the 'interface') in vivo have been reported in the literature, some of which are summarized in table 2.1. All investigators used thermocouples.
Although these results give some indication of the temperature values that might occur, there is some doubt as to their reliability. The heat-conduction process will certainly be affected by the thermocouples and, moreover, the cement-bone interface is a region rather than a well-defined location where a steep temperature gradient probably occurs. Hence, the 'cement-bone interface temperature' is a badly defined quantity and measurements in this region will be highly sensitive to the thermocouple locations. It is thus hard to draw

Authors	maximal cement-bone 'interface temperature'	conditions
Homsy *et al* (1972)	70 - 90°C	dog femurs, various bone cements
Meyer *et al* (1973)	70°C	human femurs, total hip replacement
Biehl *et al* (1974)	47°C	average value, human femur, total hip replacement
Labitzke and Paulus (1974)	45°C	average value, human femur, total hip replacement

table 2.1: Results of some temperature measurements in vivo at the cement-bone interface, as reported in the literature.

conclusions as to whether the reported temperatures are those of the cement or the bone.

Another kind of experiment in vivo was reported by d'Hollander *et al* (1976) who measured temperatures during total hip replacement at the outside surface of the femur and in the bloodstream of the ipsilateral iliac vein. The first quantity increased from an average of 31.5°C to one of 34.1°C; the latter remained practically stable at an average of 34.5°C.

2.2. Temperature measurements in vitro

Ohnsorge and Kroesen (1969) measured temperatures as a function of time, in the centre and at the surface of a ball of acrylic cement, curing in free air in the laboratory. They established maximal values of 122°C in the centre and 92°C at the surface. Comparable experiments carried out by Hupfauer and Ulatowski (1972) resulted in maximal temperature values of up to 134°C; it is not clear what causes the discrepancy between these results and those of Ohnsorge and Kroesen (1969). Hupfauer and Ulatowski (1972) in addition measured temperatures in plates of bone cement, using thermography. Although this method is not very accurate, the results clearly indicate that the temperature values were distributed rather inhomogeneously over the surface of the plate.
Ohnsorge and Goebel (1969, 1970) measured temperatures at different locations during fixation of a hip endoprosthesis in a cadaveric femur. An example of their results, which are rather illustrative, is shown in fig. 2.1. They repeated this experiment after pre-cooling the prosthesis to 0°C. The maximal 'interface temperature' in this case was about 20° less. However, due to pre-cooling, the setting time of the cement approximately doubled, which probably results in inferior mechanical properties (Oest *et al*, 1975).
Meyer *et al* (1973) measured temperatures in acrylic cement curing in a Teflon cup. They varied the quantities used, the powder-to-liquid ratio and the initial temperature. Their results will be used for an evaluation of the mathematical model applied here, as will be described in chapter 6.
Other temperature measurements, in various circumstances, were conducted by de Wijn (1974), Jefferiss *et al* (1975), Cameron *et al* (1975), Dipisa *et al* (1976), Debrunner *et al*

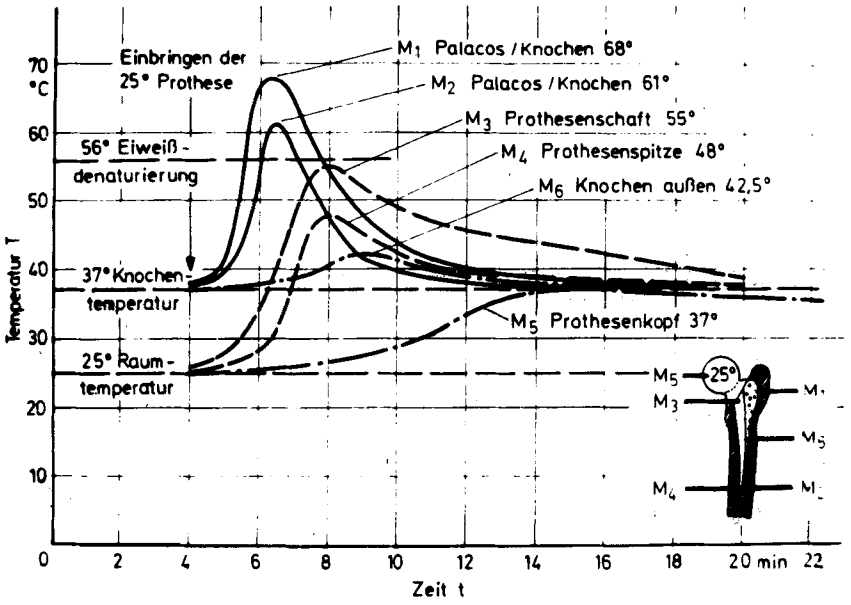

Fig. 2.1: Temperatures as a function of time at 6 locations in a cadaveric femur-prosthesis system during the polymerization of the acrylic cement (reproduced with permission of Ohnsorge and Goebel, 1969).

(1976), Lee and Turner (1977) and Seidel *et al* (1977). Varieties in commercial brands, influences of initial temperatures, 'heat sink' additives and the polymerization rate were studied in some of these experiments.

Experimental conditions were usually much better defined in these laboratory measurements compared to the experiments in vivo and useful information was obtained on the thermal behavior of the curing acrylic cement. Because of the empirical character of the experiments, however, it is often difficult to apply the results to the situation in vivo and derive general criteria for the use of the cement, as so little is known about the influences of the different geometrical and material parameters. Moreover, also in these laboratory experiments the 'interface temperatures' are unreliable, due to the thermocouple influence and the steep temperature gradient in this region.
It has become clear from these experiments that the properties and the geometry of the adjoining materials have a significant influence on the temperature values and that the heat-generation process can be affected by changing the composition of the cement mixture.
It was also found that the initial temperature of the cement greatly influences the setting time.

2.3. Theoretical studies

A theoretical study of the heat-conduction process in acrylic cement was carried out by Jefferiss *et al* (1975). Their model is very simple, assuming one-dimensional heat-flow and neglecting the time-dependent character of the heat generation process (a homogeneous initial temperature was assumend in the cement layer).

Such a simple model could be very valuable in roughly evaluating influences of some parameters, however, the parameter values they applied in their model for the heat capacity and conductivity properties of the materials were quite unrealistic.
D'Souza *et al* (1977) calculated transient temperatures in an axisymmetric slice consisting of a metal core and a 'bony' ring with acrylic cement in between. Few data were published but they claim a good agreement between the results and those of verification experiments.
A comparable analysis was carried out by Swenson *et al* (1976), who studied the influences of the cement-layer thickness on the maximal bone temperatures. In this case, too, few data were published.

CHAPTER THREE

THRESHOLD LEVELS FOR THERMAL BONE NECROSIS

After temperature values in bone have been measured or calculated, they have to be compared to a thermal damage criterion in order to estimate the chances of thermal necrosis; such a criterion is called the temperature threshold level for thermal damage (here denoted by $T_n(°C)$). In the literature on thermal behavior of acrylic cement, as discussed in the previous chapter, the threshold temperatures of collagen denaturation (56°C, Lehnartz (1959); 60°C, Viidik (1972); 70°C, Labitzke and Paulus (1974)) is usually taken as a criterion. It has been established, however, that collagen is more temperature-resistent than the protoplasm proteins (Lundskog, 1972). In this respect Leach *et al* (1943), on the basis of an extensive review, concluded that all endothelial cells die at a temperature of 47°C and over and also that temperatures between 42°C and 47°C, provided they are maintained long enough, may harm the cells. This was confirmed by Moritz (1947) and Sevitt (1957).
Not only the temperature, but also the time during which the tissue is exposed determines the threshold level for thermal damage; hence, this level will be time-dependent ($T_n = T_n(t_e)$ where t_e is the time of exposure). Investigations on time-dependent threshold curves for epithelial cells were carried out by Moritz and Henriques (1947). They established, for instance that a temperature of 70°C will kill the cells immediately, that a temperature of 55°C will do so after a 30 seconds, but that a temperature of 45°C would have to be maintained for more than 5 hours to harm the cell. Based on these results they constructed a temperature threshold curve ($T_n(t_e)$) for epithelial cells. Their results have been confirmed later by other investigators (as cited by Lundskog, 1972), for human as well as for porcine skin. Kuhl *et al* (1954) found a slightly lower threshold level for epidermal necrosis (52°C after 30 seconds) in mice experiments and ascribe the deviation to differences in the species.

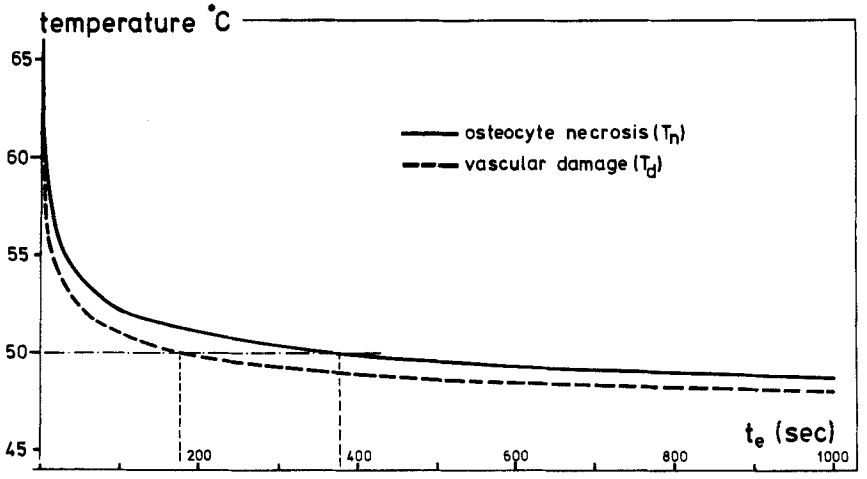

Fig. 3.1: The time-dependent threshold level for cell necrosis (T_n), as established for epithelial cells by Moritz and Henriques (1947) and also the time-dependent threshold level for vascular damage (T_d), as constructed on the basis of data from the same authors; t_e denotes the exposure time.

Lundskog (1972), in extensive histochemical studies on rabbits, roughly confirmed the threshold curve reported by Moritz and Henriques (1974) but established a lower threshold value for the bone cells, using heated implants (50°C after 30 seconds). He also indicated that much higher temperatures (up to 70°C) are needed before damage is done to the regenerative capacity of the bone tissue.
Due to the many parameters that are involved in experiments in vivo and also because of uncertainties as to the possible surgical trauma brought about by implants, the results of Lundskog cannot be considered as significantly different from those of Moritz and Henriques.
Because the threshold curve published by the last-named authors gives a good impression of both the temperature and the time aspects of thermal necrosis, it will be used here as a criterion for judging possible osteocyte necrosis.
Moritz and Henriques (1947) also reported that there is functional damage to the vascularity after exposure periods that are about 40 to 60% shorter compared to the necrosis level of epithelial cells. From this the vascular damage temperature threshold curve ($T_d(t_e)$) can be constructed. Graphs for both T_n and T_d are shown in fig. 3.1. It should be kept in mind, however, that cell necrosis has also been reported for lower temperatures (Lundskog, 1972).

CHAPTER FOUR

A THEORETICAL ANALYSIS OF HEAT GENERATION AND CONDUCTION

4.1. Assumptions and simplifications

To develop a mathematical model for simulating the process of heat generation and conduction, the relevant properties of the system must be described with parameters. In order to perform actual calculations these parameters must be given values. Relatively little is known about parameter values for heat-generation, heat-conduction and heat-capacity properties of the materials in the bone-prosthesis system. Hence, a very refined model can not actually be used. It is also open to question in view of complicated aspects (for instance the structure of bone, the vascularity, the geometry of the cement-bone interface and the consistency of the cement mantle, all of which vary considerably from patient to patient) whether a very refined model would be justified. Therefore a number of assumptions are made. In order to be able to analyse the thermal behavior of the cement using the classical heat-conduction theory it is assumed:

- no material transport takes place in the system, and the materials are incompressible,
- the local heat loss by conduction and convection at the boundary of the system (usually the outer bone surface) is proportional to the difference in the local boundary temperature and a constant local ambient temperature, or the boundary temperature is equal to this ambient temperature.

To simplify the analysis in view of the above-mentioned aspects of the complicated bone-prosthesis system, it is assumed that:

- the thermal properties of implant, cement and bone are isotropic,
- the cement mixture is homogeneous,
- the heat conduction and capacity properties of the materials are independent of the temperature,
- the heat generation as a function of time is independent of the temperature,
- the cement-bone interface is smooth and the local heat transport across the interface is proportional to the local difference in temperature between the two materials.

Obviously, the results of the model calculations can only predict the temperature values in the real system by approximation. Since influences of inaccuracies can be evaluated by parametric analyses, the model can still conveniently by used to obtain reliable approximative data, if gross effects are not neglected due to the assumptions. The most serious assumption in this respect, as follows from the experimental data discussed in paragraph 2.2. is neglecting the temperature influences on the time-dependent heat-generation, necessary because a mathematical description of this influence is not available. There are indications, however (Naylor and Billmeyer, 1953; Meyer *et al*, 1973; Debrunner *et al*, 1976), that this influence, which mainly affects the setting time of the cement, is relatively slight provided the initial temperature variance of the cement is kept within a small range.

The bone-prosthesis systems to be investigated are approximated by axisymmetric or plane geometry, which simplifies the solution procedures to a great extent and will, in most cases, give quite realistic results. It should be remarked here that the previously mentioned assumptions would not justify a true three-dimensional model, as a model requires a certain balance in the description of all aspects. Furthermore, if the aim is to perform extensive parametric analyses and evaluate the influences of the most important system parameters in

order to develop a fundamental concept of the heat-conduction process, the number of parameters in the model have to be kept restricted.

4.2. Mathematical formulation

In consequence of the previously mentioned assumptions, the process of heat generation and conduction can be described with the heat-conduction equation (Carlslaw and Jaeger, 1959) based on the conservation-of-energy principle and Fourier's law of heat conduction. Assuming an axisymmetric construction (fig. 4.1) consisting of (for example) three

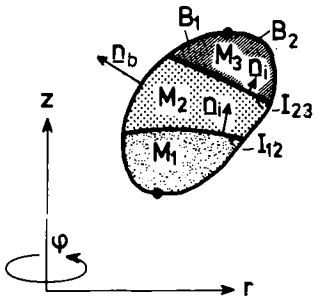

fig. 4.1: An arbitrary axisymmetric structure consisting of three materials (see text).

materials (M_1, M_2 and M_3) in contact at the interfaces (I_{12} and I_{23}) with boundaries B_1 and B_2, the time and location-dependent temperature $T(r,z,t)$ can be described by:

$$\frac{\partial}{\partial r}(\lambda r\frac{\partial T}{\partial r}) + \frac{\partial}{\partial z}(\lambda r\frac{\partial T}{\partial z}) - Cr\frac{\partial T}{\partial t} + r\Phi = 0 \qquad \text{in } M_1, M_2 \text{ and } M_3 \qquad (4.1)$$

$$\lambda\,(\underline{n},\text{grad}T) = -\alpha(T - T_a) \qquad \text{on } B_1 \qquad (4.2)$$

$$T = T_a \qquad \text{on } B_2 \qquad (4.3)$$

$$\lambda(\underline{n},\text{grad}T) = -\beta(T - T_{adj}) \qquad \text{on } I_{12} \text{ and } I_{23} \qquad (4.4)$$

where:

t	time	(sec)
r,z	coordinates	(m)
$T(r,z,t)$	temperature	(°C)
$\Phi(r,z,t)$	heat source	(J/m^3sec)
$\lambda(r,z)$	thermal conductivity	(J/msec°C)
$C(r,z)$	heat capacity	(J/m^3°C)
$\underline{n}(r,z)$	normal vector on boundary (b) or interface (i)	(-)
$\alpha(r,z)$	surface conduction and convection coefficient	(J/m^2sec°C)
$T_a(r,z)$	ambient temperature	(°C)

$\beta(r,z)$	interface conductivity	$(J/m^2 sec°C)$
$T_{adj}(r,z,t)$	temperature of the adjoining material	$(°C)$

with initial conditions: $T(r,z,0) = T_0(r,z)$ in M_1, M_2 and M_3 and on B_1, B_2, I_{12} and I_{23}.

For plane geometry (x-z plane), assuming no heat flow in the direction perpendicular to the x-z plane the differential equation transforms into

$$\frac{\partial}{\partial x}(\lambda\frac{\partial T}{\partial x}) + \frac{\partial}{\partial z}(\lambda\frac{\partial T}{\partial z}) - C\frac{\partial T}{\partial t} + \Phi = 0$$

while all other equations remain as they are, replacing r by x.

4.3. Method of solution

The differential equation presented in the previous paragraph can not be solved analytically in general. Hence, numerical (computer) methods have to be used. In order to be able to take arbitrary geometry into account, Finite Element Methods (FEM) offer the best options. Different solution procedures are available (e.g. Zienkiewicz, 1977) that can be divided into those that apply FE discretization in coordinates as well as in time, and those that apply FE discretization in geometry and a Finite Difference Method for discretization in time. Because a computer program for the solution of elliptical differential equations (such as the heat-conduction equation for steady state) in an arbitrary two-dimensional region based on FEM was available (Brekelmans, 1975), the latter method was chosen.
The temperature as a function of time is discretized according to:

$$\frac{\partial}{\partial t}T(t) \approx \frac{1}{\Delta t}\{T(t) - T(t-\Delta t)\} \qquad \text{(backward difference)}$$

where Δt denotes a time step.

By introducing the notation: $T_n(r,z) = T(r,z,t_n)$, $T_{n-1}(r,z) = T(r,z,t_{n-1})$, $\Phi_n(r,z) = \Phi(r,z,t_n)$, etc., where $\Delta t = t_n - t_{n-1}$, the equations (4.1) through (4.4) are approximated by respectively:

$$\frac{\partial}{\partial r}(\lambda r\frac{\partial T_n}{\partial r}) + \frac{\partial}{\partial z}(\lambda r\frac{\partial T_n}{\partial z}) - \frac{C}{\Delta t}rT_n + \frac{C}{\Delta t}rT_{n-1} + r\Phi_n = 0 \qquad \text{in } M_1, M_2, M_3 \qquad (4.5)$$

$$\lambda(\underline{n},\text{grad}T_n) = -\alpha(T_n - T_a) \qquad \text{on } B_1 \qquad (4.7)$$

$$T_n = T_a \qquad \text{on } B_2 \qquad (4.8)$$

$$\lambda(\underline{n},\text{grad}T_n) = -\beta(T_n - T_{adj,n}) \qquad \text{on } I_{12} \text{ and } I_{23} \qquad (4.9)$$

(4.5) is essentially an elliptical differential equation in T_n. The available computer program for the solution of such an equation and the appropriate boundary conditions (Brekelmans, 1975) was adapted to suit a step-by-step procedure in which for each step
$(\frac{C}{\Delta t}rT_{n-1} + r\Phi_n)$ is a given quantity calculated from the previous step (Huiskes, 1977).

This strategy could conveniently be followed by using the backward-difference formula for time discretization. The application of this formula results in an unconditionally stable procedure, according to Wilson *et al* (1966, 1974), while the accuracy depends on the time-step dimension. In the computer program the time step is taken as constant, because this greatly economizes the computer procedure. The solution procedure cannot be qualified as efficient and better methods in this respect may be found in the literature (e.g. Zienkiewicz, 1977). However, under the circumstances this choice has proved to be quite convenient and has given excellent results, provided the time-step dimension was small enough, as was established in a number of test problems with known solutions (Huiskes, 1977, 1979b).
The element used in the FEM procedure is triangular and has three nodal points. Within an element the temperature ($T_n(r,z)$) is assumed to be linear in r and z. The effects of the coarseness of the element mesh have also been studied in a number of tests (Huiskes, 1977).

CHAPTER FIVE

REVIEW OF THE LITERATURE ON THERMAL PROPERTIES

5.1. The composition of the acrylic cement

The acrylic cement mixture is composed of polymer powder (PMMA) and monomer liquid (MMA). The composition of the mixture is expressed in the P/L ratio (gr.polymer/cc monomer), which is usually around 2. An initiator is added to the powder and possibly radiopaque ($BaSO_4$ or ZrO_2) fillers or antibiotics. A stabilizer and a catalyzer are added to the liquid. The powder consists to approximately 99% of pure polymer, if no radiopaque or antibiotic additives are applied, and the liquid to approximately 97% of pure monomer. After polymerizing, about 2-5% residual monomer remains present in the cement (Charnley, 1970; de Wijn, 1974; Oest *et al*, 1975).
For convenience in later use, the following quantities are defined:

m_c = mass of the cement mixture (kg)

V_c = volume of the cement mixture (m^3)

ρ_c = apparent density of the cement mixture (kg/m^3)

and further:

m_i = mass of a component (kg)

V_i = volume of a component (m^3)

ρ_i = density of a component (kg/m^3)

ν_i = volume fraction of a component ($\nu_i = V_i/V_c$)

where i denotes: p (polymer), m (the part of the monomer that actually polymerizes), rm (residual monomer), ap (additives to the polymer powder), am (additives to the monomer liquid), ac (additives to the cement mixture), po (powder component), li (liquid component).

The fraction of the monomer that actually polymerizes in the mixture can be calculated from:

$$\nu_m = \frac{\rho_{po}}{\rho_{po} + P/L \times 10^3} + \nu_{rm} - \nu_{am} \qquad (5.1)$$

The density of the polymer is reported as $\rho_p = 1.18 \times 10^3 kg/m^3$ (Charnley, 1970) and $P/L \approx 2$; if it is assumed that the residual monomer and the additives to the liquid each comprise approximately 3% of the liquid component, it follows that $\nu_{rm} + \nu_{am} \approx 0.02$. The monomer fraction ν_m for given P/L ratio can be evaluated from fig. 5.1, for which formula (5.1) was used.
If a third component (ac) is added to the powder-liquid mixture, the monomer fraction in the three-component mixture can be calculated from:

$$\nu_m = \nu'_m (1 - \nu_{ac}) \qquad (5.2)$$

where ν'_m denotes the monomer fraction in the original two-component mixture.
This formula (5.2) will be used in chapter 9.

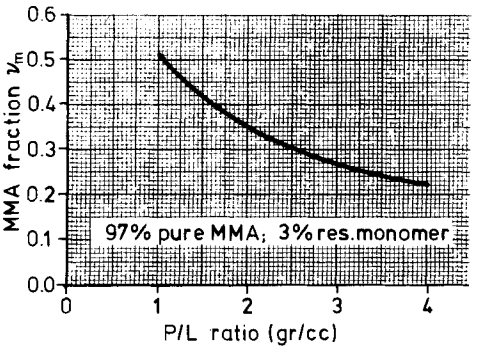

fig. 5.1: Graphical representation of the relation between the P/L ratio and the actually polymerizing monomer volume fraction ν_m.

5.2. Heat generation in acrylic cement

Heat is generated in the cement mass during the curing process, due to the exothermic polymerization reaction of the monomer. The total amount of heat generated per unit volume (Q) depends on the amount of monomer in the mixture and on the total amount of heat generated by the monomer per unit mass (Q_t).
It is obvious, that both quantities are related by:

$$Q = \nu_m \rho_m Q_t \qquad (J/m^3) \qquad (5.3)$$

It has been reported that $Q_t \approx 5.4 \times 10^5$ J/kg (e.g. Trommsdorf, 1963) and $\rho_m \approx 0.94 \times 10^3$ kg/m^3 (e.g. Charnley, 1970).

As the heat generated per unit time depends directly on the breakage of the double bond in the MMA molecules and hence on the amount of MMA molecules linked to PMMA per unit time, the heat source or heat generation function $\Phi(t)$ is proportional to the rate of polymerizing.
The polymerization process is, for our purpose, described by the polymerization function p(t) ($0 \leqq p \leqq 1$), giving the fraction of the monomer that has polymerized at a certain time. Hence it follows that

$$\Phi(t) = \nu_m \rho_m Q_t \frac{dp}{dt} \qquad (J/m^3 sec) \qquad (5.4)$$

The polymerization function can be measured by using light refraction methods (e.g. Naylor and Billmeyer, 1953) or by measuring the volumetric change of the mixture. The latter method was used by de Wijn (1977); fig. 5.2 shows an example of his results. The shape of this curve is very typical of these functions in general, although variations in setting time usually occur. For our purposes the 'polymerization time' τ (sec) is defined as the time from the beginning of the polymerization process until 75% of the monomer has polymerized. The beginning of the process is usually somewhat retarded by the stabilizer; this period is called the 'retardation time' (t_r(sec)). Usually $t_r \approx 100$ - 200 sec and $\tau \approx 200$ - 400 sec for bone cements.
It is assumed here that the curve shown in fig. 5.2 is in dimensionless form valid for all bone cements; this curve is described by $p_1 = p_1(t-t_r/\tau)$, $t \geqq t_r$, and is in this form only influenced by t_r and τ.

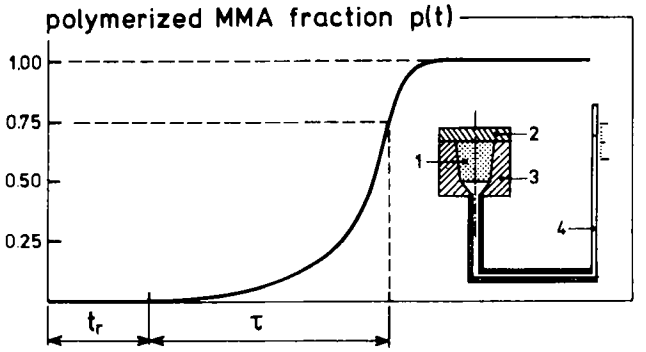

fig. 5.2: The polymerization function p(t) as measured by de Wijn (1977) in shrinkage tests using the apparatus shown in the inset; 1: cement mass; 2: Delrin lid; 3: Delrin cup; 4: glass tube filled with liquid to register the amount of shrinkage. In dimensionless form ($p_1 = p_1(t-t_r/\tau)$) this curve is assumed to be valid for acrylic cement in general.

It should be remarked here that slightly different curves (p_2 and p_3) will also be investigated later.

5.3. Heat capacity and conductivity properties

The heat capacity $C(J/m^3{}^\circ C)$ of a material can be calculated from $C = \rho c$, where c = specific heat ($J/kg^\circ C$), ρ = density (kg/m^3).
The thermal conductivity of a material is denoted by λ ($J/msec^\circ C$). These symbols are applied with indices; e.g. c_i, ρ_i, λ_i, where i denotes the material (c (cement mixture), b (bone), etc.).
In general c, ρ and λ may depend on the temperature and on phase transitions but, as discussed in chapter 4, these dependencies will be neglected in the analyses.

5.3.1. *Acrylic cement*

Kaye and Laby (1959) and Debrunner *et al* (1976) give for the specific heat of PMMA $c \approx 1.46 \times 10^3 J/kg^\circ C$. Hoffmann (cited by Oest *et al*, 1975) investigated the temperature dependency of c, with respect to PMMA as well as MMA; fig. 5.3 shows the results of this study. There appears to be little difference in the values for both materials. Both curves can be approximated by $c_m \approx c_p \approx 1.25 \times 10^3 + 6.50T$ $(0 \leq T \leq 100)$.
Values for the specific heat and the density of radiopaque additives, as given by Müller (1975), are shown in table 5.I.

The heat capacity of the cement mixture can be calculated from:

$$C_c = \nu_p C_p + \nu_m C_m + \nu_{ap} C_{ap} + \nu_{ac} C_{ac} + \nu_{am} C_{am} + \nu_{rm} C_{rm} \qquad (5.5)$$

the last two terms of which may be neglected.

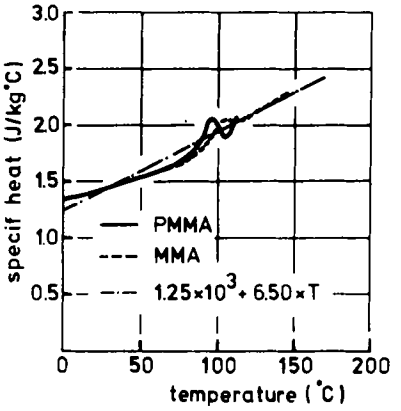

fig. 5.3: Temperature-dependent heat capacities of MMA and PMMA, as established by Hoffmann (in Oest et al, 1975) and linear approximation.

If $\nu_{ac} = 0$ it follows, assuming $C_p \approx C_m$, that

$$C_c \approx C_p + (1 - \nu_m)(C_{ap} - C_p)\frac{\mu}{\rho_{ap}/\rho_p + \mu} \tag{5.6}$$

where:

$\mu = m_{ap}/m_p$

If $\nu_{ap} = 0$, it follows that

$$C_c \approx C_p + \nu_{ac}(C_{ac} - C_p) \tag{5.7}$$

Formulas (5.6) and (5.7) will be used in chapter 9.

The heat capacity of the cement mixture C_c will, apart from a temperature dependency owing to c_p and c_m, also be affected by dimensional changes, due to the contraction of the monomer during the polymerization process.
Taking both effects into account, it follows that:

$$C_c(t) \approx \{1.25\times10^3 + 6.5T(t)\}\{\rho_p + \nu_m(1 - p(t))(\rho_m - \rho_p)\} \tag{5.8}$$

If the cement mixture polymerizes adiabatically (ideally isolated) the temperature T(t) in the mass is described by:

$$C_c \frac{dT}{dt} = Q\frac{dp}{dt} \tag{5.9}$$

By calculation of T(t), using the polymerization function $p_1(t)$ for a constant value of C_c as well as for C_c according to formula (5.8), it was shown that a good agreement between the two cases results if the (constant) heat capacity is taken as $C_c \approx 1.9\times10^6$ J/m^3°C (Huiskes, 1978). The estimated heat-capacity values are summarized in table 5.1.

	density kg/m^3	specific heat J/kg°C	heat capacity J/m^3°C
PMMA	1.19×10^3	1.6×10^3 (50°C)	1.9×10^6 (50°C)
MMA	0.94×10^3	1.6×10^3 (50°C)	1.5×10^6 (50°C)
$BaSO_4$	4.50×10^3	0.43×10^3	1.96×10^6
ZrO_2	5.60×10^3	0.70×10^3	3.91×10^6
Acrylic cement	1.1×10^3	1.7×10^3	1.9×10^6

table 5.I: Approximate values for heat-capacity parameters of bone cement and its possible components.

No investigations are known on the thermal conductivity of acrylic cement. For PMMA a value of approximately 0.17 J/msec°C has been reported (Barrett *et al*, 1953; Frados, 1966).

5.3.2. *Implant materials*

Heat capacity and conductivity properties of a few industrial materials, relevant for the analyses, are summarized in table 5.II.

	density kg/m^3	spec.heat J/kg°C	heat capacity J/m^3°C	therm. cond. J/msec°C	source
Cr-Ni-steel	7.8×10^3	0.46×10^3	3.6×10^6	14	Eckert and Drake (1972)
HDPE	0.96×10^3	2.22×10^3	2.06×10^6	0.29	Kaye and Laby (1959)
Teflon	2.2×10^3	1.04×10^3	2.29×10^6	0.23	Kaye and Laby (1959)

table 5.II: Thermal properties of some industrial materials.

5.3.3. *Bone*

Measurements of thermal properties of various soft tissues in the body have been carried out by several investigators (e.g. Balasubramanian *et al*, 1977); data on bone are scarce, however and the values available show a considerable scatter.
No doubt the properties greatly depend on the macroscopic structure, either trabecular (spongeous) or cortical (compact), the microscopic structure, for example orientation and coarseness of the bone matrix, the fat content, the water content, and the macroscopic and microscopic vascularity. Hence great individual differences probably occur, while properties in vivo, too, may differ from those of cadaveric material.
Values for the heat-capacity properties, as reported in the literature, are summarized in table 5.III.

Author	ρ_b (kg/m^3)	c_b(J/kg°C)	C_b(J/m^3°C)	test object
Henschel (1943)	2.1x10^3	1.26x10^3	2.65x10^6	Fresh cortical bone (human)
Lundskog (1972)	--	1.26x10^3	–	Fresh cortical bone (human)
Clattenburg *et al* (1975) (1)	2.1-2.3x10^3	1.15-1.73x10^3	2.64-3.64x10^6	Fresh spongeous bone (calf)
Kummer (1972)	2.2-2.9x10^3	–	–	Fresh cortical bone (human)
Saulgozis *et al* (1974)	1.86-1.93x10^3	–	–	Fresh cortical bone (human)

table 5.III: Heat capacity of cortical and spongeous bone, as reported in the literature. (1) Only C_b originally published, values of ρ_b supplied by Cohen (1978).

Values for the thermal conductivity have been measured in different circumstances; a summary of literature data is shown in table 5.IV.

Source	λ_b(J/msec°C)		test object
Chato (1965)	0.38		Fresh cortical bone (human)
Vachon *et al* (1967)	2.3	(1)	In vivo cortical bone (bovine); 37°C
Vachon *et al* (1967)	0.6	(1)	Fresh cortical bone (bovine)
Lundskog (1972)	19	(2)	Fresh cortical bone (various mammals)
Lundskog (1972)	4	(2)	Dried cortical bone (various mammals)
Graf and Stein (1957)	0.36-0.60		In vivo spongeous bone (human); 37°C
Graf and Stein (1957)	0.29-0.43		Fresh spongeous bone (human); 37°C
Sundén (1967)	0.53		In vivo spongeous bone (rabbit); 37°C
Clattenburg *et al* (1975)	0.26-0.33	(3)	Fresh spongeous bone (calf); 25°C
Bowman *et al* (1979)	0.39		Fresh spongeous bone (human); 37°C

table 5.IV: Values of λ_b as reported in the literature. (1) Measurements on the outside bone surface; (2) unreliable technique, gross effects of evaporation; (3) isotropic properties established, at 60°C about 15% higher values.

With regard to the thermal conductivity, apparently the greatest range in values is found for cortical bone, but the experiments of Lundskog (1972) can be qualified as definitely unreliable and the measurements of Vachon *et al* (1967) as possibly unreliable, because of the rough technique and influences of the sub-periosteal vascularity at the outside surface of the bone. Altogether it appears that, presently, λ_b for wet cortical bone should be

assumed as approximately 0.4 J/msec°C, for spongeous bone in vivo from 0.36 to 0.60 J/msec°C. Since the experiments by Graf and Stein (1957) were carried out in vivo and in vitro in the same kind of bone (sternum) using the same technique, the differences reflect the influence of the vascularity.
As regards the influence of the vascularity on the heat-conduction properties of the bone structure, three aspects can be distinguished: (1) the influence of the microcirculation on the heat-conduction properties of the bone material, (2) the influences of large blood vessels and (3) the heat transport at the bone surface in the highly vascularized periosteum. As to the first effect, it can probably be assumed that the continuum model of the bone material still applies, but that λ_b should be adapted (Graf and Stein, 1957). The second effect will probably greatly disturb the heat flow, but is a quite local phenomenon that will be neglected here. The third effect will be discussed in paragraph 5.4.
With regard to long bones it has been shown (Rhinelander, 1972) that the greater part of the cortex thickness ($> 2/3$) is vascularized from within the medullar system and only the superficial part by the periosteal system. In the diaphyseal region, the intramedullar vascularity is, at least temporarily, disturbed prior to fixation of endoprostheses and hence the greater part of the cortex will be without circulation until the periosteal system takes over the function of the intramedullar system (Rhinelander, 1972). It is therefore assumed as probable, that the vascularity will exert no influence on the thermal conductivity in the diaphyseal cortex during the polymerization process.
As regards the metaphyseal and epiphyseal regions of the bone, where the implant is fixated against spongeous bone, the function of the vascularity during surgery is uncertain; at least part of the circulation will be temporarily disturbed.
Possible influences of the microcirculation can be evaluated by variation of λ_b, guided by the results of Graf and Stein (1957), as shown in table 5.IV.

5.3.4. *The cement-bone interface*

It is a well known phenomenon that when heat flows across a contact region between two materials, the temperatures in the two materials at the contact surfaces are not equal: the contact region has a certain heat-flow resistance (e.g. Jacobs and Starr, 1939; Fried, 1969). The heat resistance depends mainly on the roughness of the materials and the kind of intermediate medium (gas, liquid).
This contact heat-resistance phenomenon can, in the simplest form, be described by:

$$q = \beta \Delta T \qquad (5.10)$$

where q is the specific heat flow through the contact region ($J/m^2 sec$),
ΔT the temperature drop over the interface (°C),
β the interface conductivity ($J/m^2 sec°C$).
This mathematical model is illustrated in fig. 5.4. Owing to the (in this case steady) heat flow (q) there is a certain temperature profile in materials 1 and 2. At the contact region or interface which is assumed to be infinitely thin, a discontinuity (ΔT) in the temperature profile is present, due to the heat-flow resistance; the conductivity of the interface is described by β. In reality, as illustrated in fig. 5.4, the interface has a certain thickness (s_i), over which the temperature decreases more-or-less continuously.
The conductivity of the cement-bone interface will depend on the structure and the preparation of the bony implant bed, the consistency of the cement and the pressure applied to it when inserted, the presence of blood, water or bone debris and probably the dimensional behavior of the cement mass. Owing to these random influences and the small dimensions,

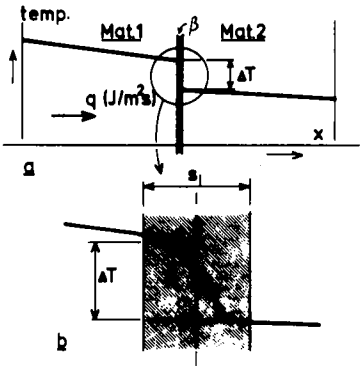

fig. 5.4: Illustration of a simplified model of an interface heat resistance (a), showing the temperature profile in the two materials and the discontinuous temperature drop at the interface, assumed as infinitely thin; in reality (b) the interface has a certain thickness and the temperature drop is more-or-less continuous.

too, the interface conductivity, provided the linear model applies to this complicated structure, will be very difficult to measure. Hence the strategy will be to vary the interface conductivity β in a 'possible' range in the analyses and to evaluate its influence on the heat-conduction process.

In order to obtain a rough impression of the value of β, the steady state heat conduction in a plane model of an arbitrarily shaped bone-cement interface was analysed, using the methods described in chapter 4. The model is shown in fig. 5.5; the interface is assumed to

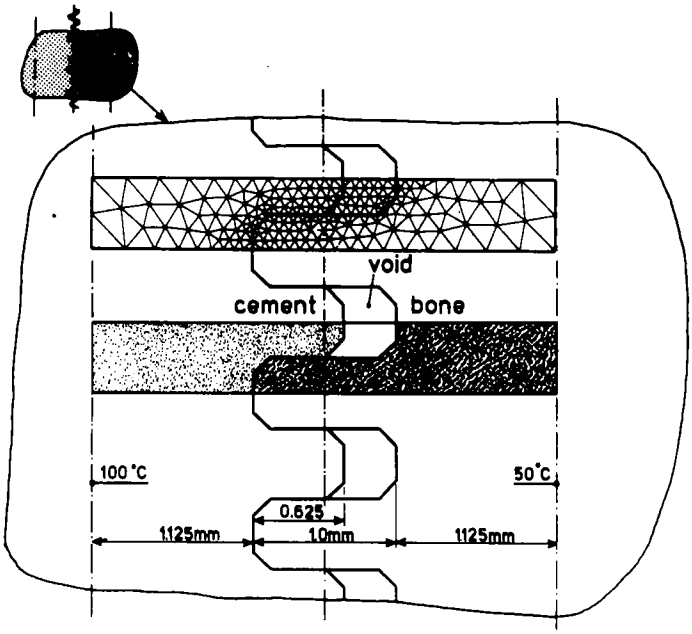

fig. 5.5: A simplified plane model of an arbitrary cement-bone interface. In the trabecular voids a nonconductive material is assumed; the element mesh for the simulation of the (steady state) heat conduction through the interface is shown.

be 1-mm-thick and consists of bone 'trabeculae', partly in contact with acrylic cement, leaving intratrabecular gaps filled with a nonconductive medium. For reasons of symmetry only a part of the model has to be regarded; the element mesh is shown in fig. 5.5 (generated by computer; Schoofs *et al*, 1978). Parameter values were taken as: $C_c = 1.8 \times 10^6$ J/m^3°C; $C_b = 2.9 \times 10^6$ J/m^3°C; $\lambda_c = 0.17$ J/msec°C; $\lambda_b = 0.4$ J/msec°C. Fig. 5.6 shows the temperature profile on two lines in the materials, as calculated in the computer simulation.

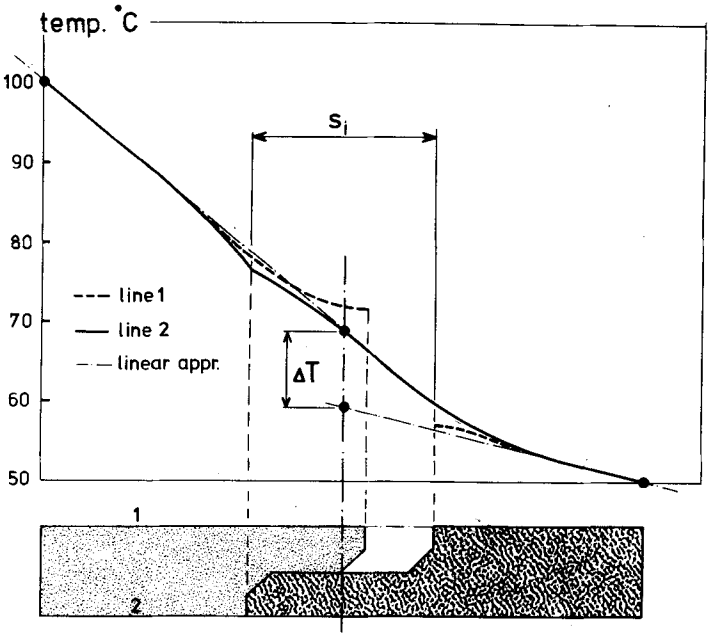

fig. 5.6: Temperature profiles in the interface model on two lines as calculated in the FEM simulation and a linear approximation of these profiles in each material, which results in an apparent discontinuous temperature drop ΔT.

Linear approximations of the temperature profiles were fitted to these graphs, resulting in a discontinuous temperature drop (ΔT) over an assumed infinitely thin 'interface' located in the middle of the real interface. In this simplified description the specific heat flow can be calculated from:

$$q = -\lambda_b \frac{dT_b}{dx} = -\lambda_c \frac{dT_c}{dx},$$

where $T_b(x)$ = temperature in bone (linear approximation);
$T_c(x)$ = temperature in cement (linear approximation).

The interface conductivity β can then be calculated from (5.10), which gives $\beta = 375$ J/m^{2}sec°C in this case.
Isotherms, as calculated with the FEM model, are shown in fig. 5.7, indicating that the tips of the trabeculae, surrounded by cement, will reach high temperatures even if the temperatures in the rest of the bone are not very high.

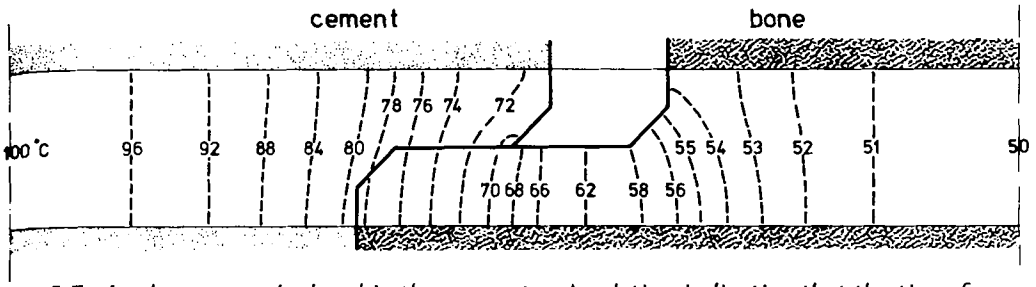

fig. 5.7: Isotherms as calculated in the computer simulation indicating that the tips of trabeculae, surrounded by cement, may reach quite high temperature values.

At the rather smooth cement-implant interface the heat resistance will be low. A value of β_{ci} = 1,000-10,000 J/m^{2}sec°C should be appropriate (Fried, 1969).

5.4. Boundary heat transport

Heat loss at the boundary of the model, which will usually be the bone surface, depends on a surface conduction and convection coefficient (α), as discussed in chapter 4, and on the ambient temperature (T_a).
When the bone surface is the boundary of tne model, the coefficient α depends on the heat exchange mechanism between the superficial bone and the periosteal circulation, although no doubt conduction through the soft tissue also occurs. Nothing appears to be known about these phenomena.
For technical surfaces in different media, values for α were reported by Gröber *et al* (1961), as shown in table 5.V.

Medium (free convection)	α (J/m^{2}sec°C)	Medium (forced convection)	α (J/m^{2}sec°C)
gas	3 - 24	gas	11 - 117
water	116 - 698	viscous liquids	58 - 582
bubbling water	1,163 - 23,260	water	581 - 10,630

table 5.V: Values of α with respect to technological surfaces in different media (after Gröber et al, 1961).

Blood and soft tissues consist mainly of water and it has been shown that the thermal conductivity of soft tissues is only slightly less than water (water: $\lambda \approx 0.6$ J/msec°C (20°C), Eckert and Drake (1972); muscle: $\lambda \approx 0.5$ J/msec°C (21°C), Balasubramanian *et al* (1977)). In view of the values given in table 5.V it is then quite probable that $\alpha > 500$ J/m^{2}sec°C and remotely possible that $100 < \alpha < 500$ J/m^{2}sec°C. The probability that there is an adequate heat transport at the bone surface was confirmed by d'Hollander *et al* (1976), who measured a temperature increase of only 3°C at the outside surface of the femur during hip replacement; the temperature dropped after reaching this peak value.

5.5. Initial and ambient temperatures

The temperatures in the components of the bone-prosthesis system, prior to insertion of the implant, depend on the circumstances. Implants and bone cement will be approximately at 'room temperature' although both components may have been slightly warmed up by manual handling and the onset of the polymerization process. The initial temperature of the bone (T_{0b}) is probably equal to the ambient temperature (T_a), which will not be higher than 37°C, but probably somewhat lower; for instance d'Hollander *et al* (1976) have measured values between 32 and 35°C (see paragraph 2.1.).

5.6. Conclusions

Based on a thorough review of the relevant literature, estimates for the thermal properties of bone-prosthesis systems have been discussed in this chapter.
The geometry of the system has not been discussed, as it depends so much on the joint component which is under consideration and can better be treated in the chapters concerned.
A summary of probable and possible values is shown in table 5.VI. It should be borne in mind that in some cases the values and value ranges shown are only 'educated guesses', especially where the 'possible range' is concerned. Sometimes (as for example for λ_c) only one value is shown in the 'probable value or range' column simple because only one value has been published; the 'possible range' column then reflects uncertainty about this value. The ranges in these columns will be used later as lower and upper boundaries in the parametric analyses. Some parameters are adjustable, for instance ν_m (by the P/L ratio) and C_c (by additives), the probable ranges of adjustability are then shown in the relevant column.

As can be concluded from table 5.VI many properties might well come in for more thorough experimental investigations. For such investigations it is of importance to know how sensitive the process of heat generation and conduction is for the parameter values, so as to establish which parameters are the most important and the accuracy with which each parameter would have to be measured. Analyses such as those presented in the following chapters, where the influences of the parameters on the process are evaluated, can provide guidelines for such experiments.

parameter	unit	probable value	adjustable range	possible range
Heat generation:				
ρ_m	kg/m^3	0.94×10^3	–	–
Q_t	J/kg	5.4×10^5	–	–
ν_m	–	0.35	0.27 - 0.42	–
Q	J/m^3	1.8×10^8	$1.4 - 2.1 \times 10^8$	–
p(t)	–	$p_1(t)$	$p_2(t)$, $p_3(t)$	–
t_r	sec	150	–	–
τ	sec	200 - 400	–	–
Heat capacity and conductivity:				
Acrylic cement:				
C_c	$J/m^3°C$	$1.8 - 2.0 \times 10^6$	–	$1.7 - 2.1 \times 10^6$
λ_c	J/msec°C	0.17	–	0.14 - 0.20
Cortical bone:				
C_b	$J/m^3°C$	$2.2 - 3.2 \times 10^6$	–	$1.8 - 4.1 \times 10^6$
λ_b	J/msec°C	0.3 - 0.5	–	0.2 - 0.6
Spongeous bone:				
C_b	$J/m^3°C$	$2.8 - 3.4 \times 10^6$	–	$2.6 - 3.6 \times 10^6$
λ_b	J/msec°C	0.5	–	0.4 - 0.6
Interface conductivity:				
β_{ci}	$J/m^2sec°C$	1,000 - 10,000	–	500 - ∞
β_{cb}	$J/m^2sec°C$	100 - 1,000	–	50 - ∞
Bone surface heat loss:				
α	$J/m^2sec°C$	500 - 10,000	–	100 - ∞
Initial and ambient temperatures:				
$T_a = T_{0b}$	°C	32 - 35	–	30 - 37
T_{0c}	°C	20 - 25	–	–
T_{0i}	°C	20 - 25	–	–

table 5.VI: Probable and possible values of the relevant thermal parameters. Implant property values were shown in table 5.II.

CHAPTER SIX

EVALUATION OF THE MODEL

In order to evaluate the model as to its suitability for the curing cement and judge the parameter-value estimates, two experiments published in the literature were simulated. As not all the parameters that have to be given a value in the model calculations were measured in the experiments and the reliability of the experimental results is sometimes doubtful, this simulation process cannot be regarded as a true verification procedure, but merely as a rough evaluation.

6.1. A ball of curing acrylic cement

Ohnsorge and Kroesen (1969) measured temperatures as a function of time in the centre and at the surface of a ball of acrylic cement curing in free air. Parameter-values that can be derived from their publication are given in table 6.I.

commercial brand	: Palacos	initial temperature	: $T_{0c} = 25°C$
P/L ratio	: 2.1 gr/cc	ball radius	: $R = 2.2 \times 10^{-2}$ m
ambient temperature	: $T_a = 25°C$	ball mass	: $m_c = 52.2 \times 10^{-3}$ kg

table 6.I: Data from Ohnsorge and Kroesen (1969).

The monomer fraction in the mixture can be evaluated using fig. 5.1 and the given P/L ratio, from which it follows that $\nu_m \approx 0.34$. Hence, using the data presented in paragraph 5.2, $Q \approx 1.7 \times 10^8$ J/m^3. For cooling in free air, $\alpha \approx 3$ - 24 J/m^2 sec°C (table 5.V).
Owing to symmetry of the ball, only a section has to be taken into account in the analysis. Fig. 6.1 shows the element mesh for the axisymmetric model. At the boundaries r = 0 and z = 0, α is taken as zero to simulate the spherical geometry. Of course, a spherical model would be more appropriate here from a theoretical point of view; however, the computer program is only suited for plane and cylindrical models.
The time step Δt in the solution procedure was taken as 10 sec; 100 steps were taken into account. The polymerization function $p_1(t)$ was used, with $t_r = 0$ and $\tau = 240$ sec (a value that will be motivated at the end of this paragraph).
Fig. 6.2 shows an example of calculated results: the temperature in the ball as a function of r, for three different values of α, at time t = 350 sec. It is found even for rather high values of α, that the heat flow from the centre (which is proportional to $\frac{dT}{dr}$) is practically zero. Hence the process in the centre is practically adiabatic. Since in that case (near the centre)

$$C_c \frac{dT}{dt} = Q \frac{dp}{dt}, \text{ hence } T(t) = \frac{Q}{C_c} p + T_{0c},$$

it follows that:

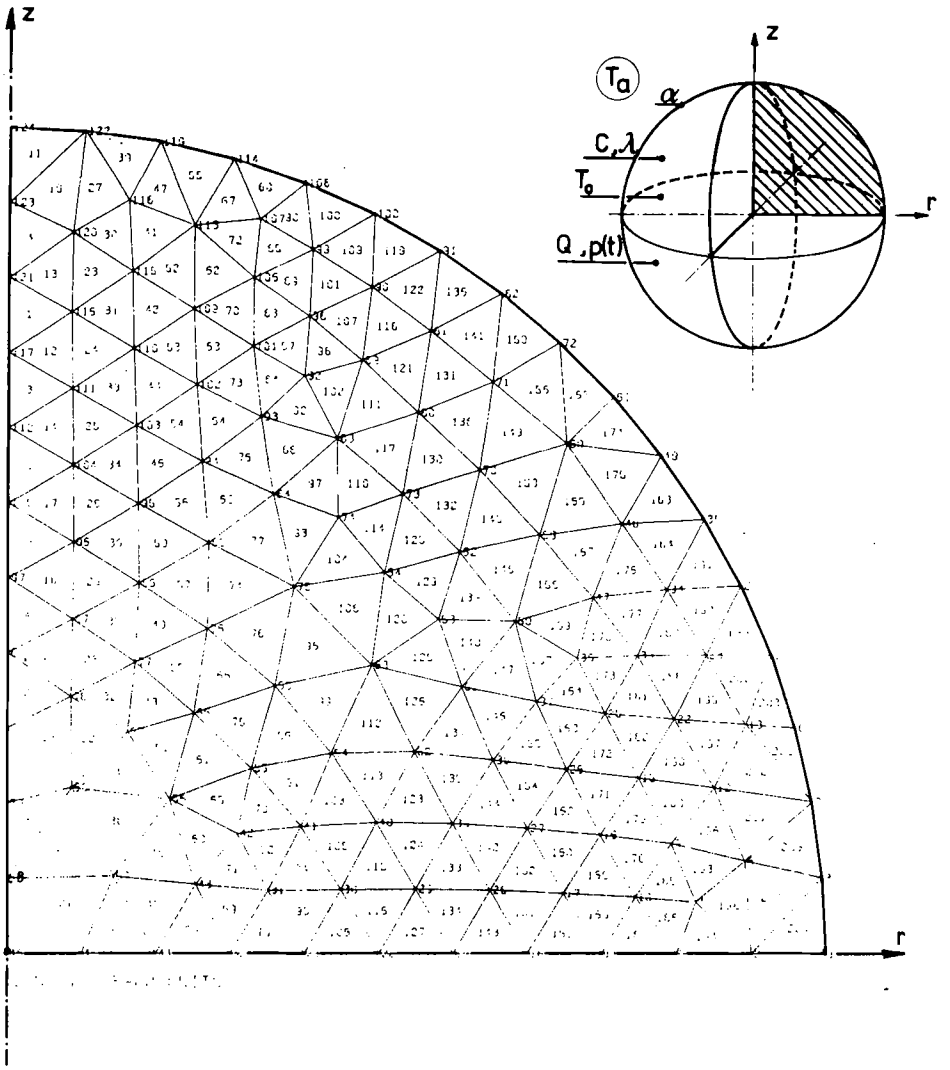

fig. 6.1: Element mesh for the computer simulation of the heat generation and conduction process in a curing ball of acrylic cement; the model is axisymmetric. The parameters on which the process of heat generation and conduction depend are also shown.

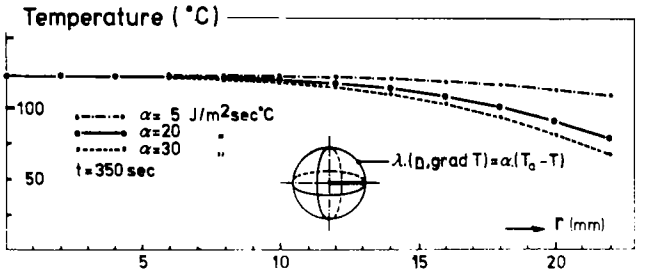

fig. 6.2: The temperature in the cement ball as a function of the radius r at time t = 350 sec, as calculated for three different values of α.

- the temperature in the centre is proportional to the polymerization function, which gives the option of evaluating this function by measuring the temperature in a comparable experimental set-up;
- when the maximal temperature in the centre is denoted by T_c, then

$$T_c - T_{0c} = \frac{Q}{C_c}$$

thus the value of $\frac{Q}{C_c}$ can be evaluated directly from the experiment.

For the experiment it was reported that $T_c = 122°C$, hence $\frac{Q}{C_c} = 97°C$.

Assuming $Q = 1.7 \times 10^8 J/m^3$, it follows that $C_c = 1.75 \times 10^6 J/m^3 °C$, which is somewhat lower than estimated in chapter 5, but quite realistic. The difference could easily be explained by experimental inaccuracies, incomplete polymerization or a slightly different P/L ratio.

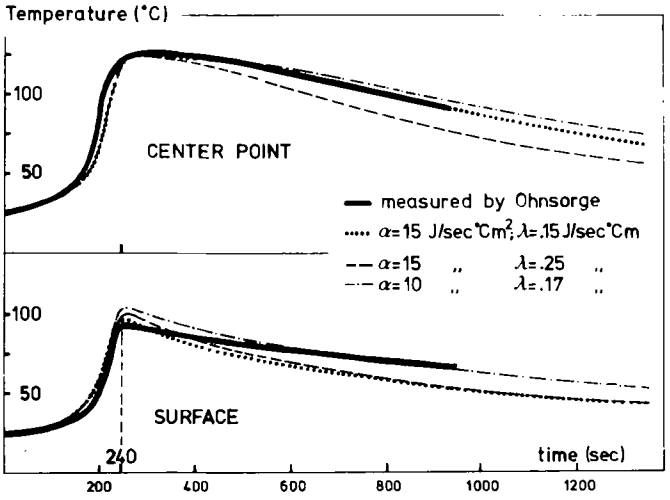

fig. 6.3: Temperatures as a function of time in the centre and at the surface of the ball, as measured and as calculated using different values for α and λ.

Fig. 6.3 shows the centre and surface temperatures as a function of time as calculated for different values of λ and α, compared to the experimental results. Obviously the value of λ exerts more influence on the centre temperature, while α exerts more influence on the surface temperature. The curve for $\lambda = 0.17$ J/msec°C and $\alpha = 10$ J/m²sec°C shows the best agreement with the experimental curves.
The polymerization time τ was chosen in such a way that the time at which the surface temperature reached its peak in the model coincided with the experimental finding.
It is remarkable that in using the polymerization function $p_1(t)$ both experimental curves are approximated reasonably well. This gives confidence in the applicability of the general shape of this polymerization function.
In the experiment the surface temperature was slightly higher than in the simulation.
This is probably caused by monomer evaporation at the surface.

6.2. Acrylic cement curing in a Teflon cup

Meyer *et al* (1973) measured temperatures as a function of time at eight locations in acrylic cement, curing in a Teflon cup. The cup (and the cement slice) were axisymmetric. Initial temperatures, height of the cement slice and P/L ratio were varied. The cup is shown together with the element mesh for the simulation in fig. 6.4. Only the experiments entailing a cement slice height of 10 mm were simulated. Measuring points were numbered 1, 3, 5 and 7 (in the middle of the cement slice) and 2, 4, 6 and 8 (near to the Teflon), all located in an axial section.

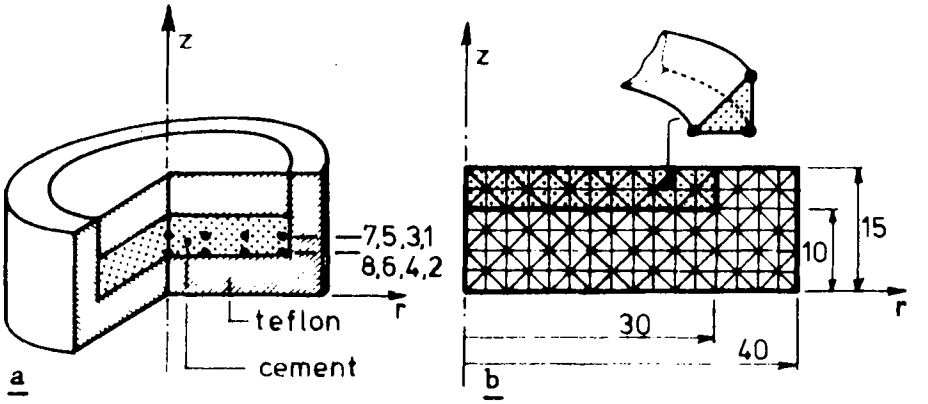

fig. 6.4: (a) The Teflon cup with the cement mass as used for experiments by Meyer et al (1973); temperature measuring points are shown, 7 and 8 on the symmetry axis; 7, 5, 3 and 1 in the middle of the mass; 8, 6, 4 and 2 near the Teflon. (b) Dimensions and element mesh for the computer simulation.

commercial brand	:	Simplex-p
P/L ratio	:	1.5; 2; 2.5 and 3 gr/cc (ν_m: 0.42; 0.35; 0.30 and 0.27; fig. 5.1)
initial temperature	:	4; 15; 20; 30 and 37°C
ambient temperature	:	equal to initial temperature
retardation time	:	$t_r \approx 150$ sec

table 6.II: Data supplied by Meyer et al (1973).

Table 6.II shows some values for parameters that can be derived from the publications of Meyer *et al*. Parameter values for Teflon were taken in accordance with table 5.II. The polymerization time was chosen in such a way that the time at which the center point temperature (point 7) reached its peak coincided in simulation and experiment (τ = 350 sec for P/L = 2 gr/cc and $T_a = T_{0c} = 25°C$); the polymerization curve $p_1(t)$ was again used. In the solution procedure the time step (Δt) was chosen as 10 sec; 100 steps were taken into account; a time step of 1 sec with 1000 steps did not give significantly different results (Huiskes, 1977). Values for cement parameters were taken in accordance with those mentioned in paragraph 5.6., except for C_c. By taking $C_c = 1.75 \times 10^6$ J/m^3°C a good agreement resulted for the measured and calculated maximal center point temperatures, which is the same value for C_c as evolved from the previous simulation.

It was established that a variation of α in the range from zero to infinite exerted no significant influence on the maximal cement temperatures. Likewise a variation of the Teflon properties within a realistic range, and a variation of λ_c within a realistic range exerted little influence.
To be able to obtain a reasonable approximation of the temperatures in all measured points the conductivity at the cement-Teflon interface had to be taken as $\beta = 50$ J/m^{2}sec°C.

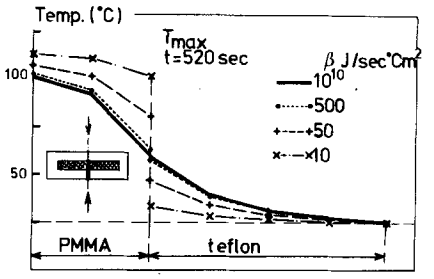

fig. 6.5: Temperatures as a function of the axial coordinate (z) in the cement and in the Teflon, at time t = 520 sec, as calculated for different values of the interface conductivity β.

Fig. 6.5 shows the influence of β on the temperature profiles in cement and Teflon along the axis of the structure. The fact that such a rather low value of β has to be assumed to approximate the temperature values measured close to the cement-Teflon interface, is probably caused by steep temperature gradients in reality near the interface, which cannot be simulated due to the coarseness of the element mesh.

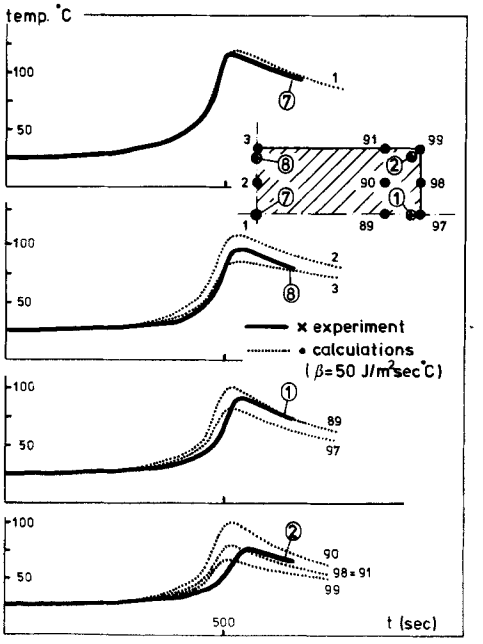

fig. 6.6: Temperatures as a function of time, as measured at 4 points in the cement mass by Meyer et al (1973), and as calculated at different points close to the measuring points indicated in the figure.

It should be remarked that, due to the steep temperature gradient, the temperature measurements at the interface are somewhat unreliable. Moreover, the exact position of the interface thermocouples is not mentioned in the publication.
Fig. 6.6 shows a comparison of temperatures as a function of time as measured and as calculated, where $\beta = 50\ J/m^2 sec^\circ C$, at four of the measuring points. Since the location of measuring points 1, 2 and 8 is not exactly known, calculated results for points in the neighborhood are shown in the graphs. Results of measuring points 3 and 5 were practically equal to those of point 7 and those of points 4 and 6 were practically equal to those of point 8.
Again the use of the polymerization function $p_1(t)$ results in quite reasonable approximations of the experimental curves, except for a small shift in the polymerization time at the 'cooler points'.

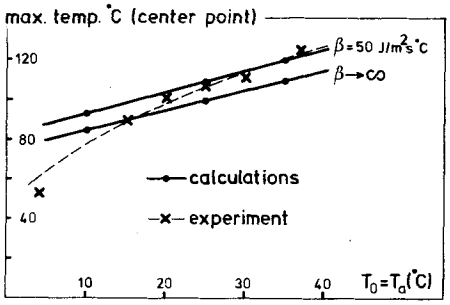

fig. 6.7: Maximal cement temperature as a function of the initial temperatures as measured by Meyer et al (1973) and as calculated in the model.

Fig. 6.7 shows the influence of the initial temperature on the maximal temperature value at the center point as calculated and as measured. Evidently a reliable prediction results from the model so long as the range of variation is not too extended. In the experiment an increase in the polymerization time results for low values of T_{0c}, not taken into account in the model.

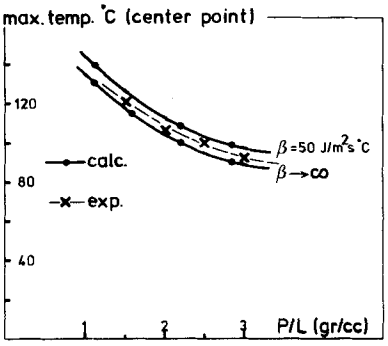

fig. 6.8: The maximal cement temperature as a function of the P/L ratio as measured by Meyer et al (1973) and as calculated in the model.

Fig. 6.8 shows the influence of the P/L ratio on the maximal temperature value at the center point, as calculated and as measured. Again, it is apparently possible, using the model, to predict this influence with quite good accuracy.

6.3. Conclusions

By simulation of two experiments presented in the literature it was shown that the process of heat generation and conduction in curing acrylic cement can be simulated with acceptable accuracy and that the estimates for (cement) parameter values discussed in chapter 5 are quite reasonable. The general shape of the measured polymerization function is found to be realistic. Although the polymerization function is not independent of the temperature, it is found that in reality its influence only results in a relatively small shift of the curves, especially in the initial part of the polymerization process. The value of β exerts a considerable influence on temperature values near the interface of the cement and the adjoining material. In the bone-prosthesis system this is precisely the location where the temperature values are of interest. As has been discussed previously, results of temperature measurements in this region are unreliable. But, due to the fact that so little is known about the value of β, the same is true for calculated temperature values in this region. By conducting parametric analyses, however, a good impression can be obtained on the possible temperature values and the influences of the important parameters on these values. In this respect the model gives much more information than experiments possibly could.

CHAPTER SEVEN

PARAMETRIC ANALYSES WITH RESPECT TO INTRAMEDULLARY FIXATED IMPLANTS

7.1. Description of the model

In this chapter the influences of the relevant parameters on the process of heat generation and conduction in a realistic system will be evaluated by means of parametric analyses. In order to maintain insight into the effect of parametric changes, the system to be analysed should be as simple as possible. Therefore a both simple and realistic model was chosen.

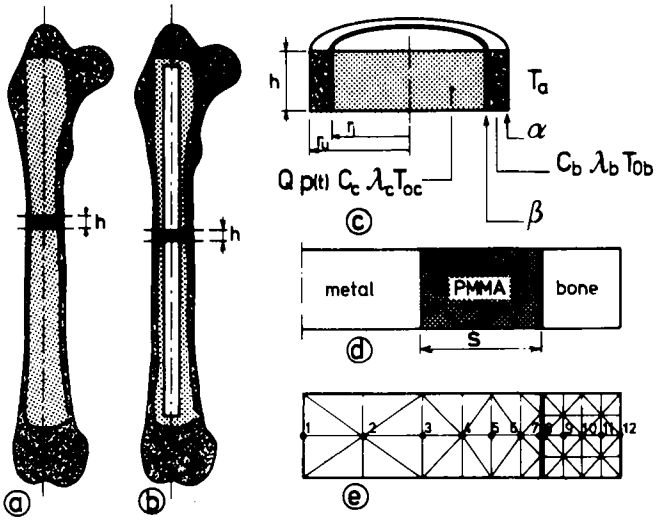

fig. 7.1: An arbitrary long bone filled with acrylic cement (a), which may also contain an implant (stem) (b). The axisymmetric model of the diaphysis region is shown (c); giving the parameters that influence the heat generation and conduction process also. The dimension of the implant may vary (d); the cement layer thickness is denoted by s. The element mesh used in the computer simulation is also shown (e).

The model consists of a slice from the diaphysis of an arbitrary long bone (fig. 7.1), the medullary canal of which is filled with curing acrylic cement (fig. 7.1.a) and may also contain a metal stem (fig. 7.1.b). The cortex of the bone is assumed to be axisymmetric and heat flow in the axial direction is assumed to be zero. The model and the model parameters, in the event that no stem is present, are shown in fig. 7.1.c. When a stem is present, the cement layer thickness is denoted by s (mm) (fig. 7.1.d). The element mesh for the model is shown in fig. 7.1.e; mesh refinement is applied close to the cement-bone interface so as to be able to describe a steep temperature gradient in this region adequately.

The parameters were varied with respect to a reference value. The set of reference values is shown in table 7.I. In the reference case no implant is present, as it will no doubt be the

parameter	unit	reference value	parameter	unit	reference value
Geometry (no implant present)			**Cement**		
r_u	m	16×10^{-3}	C_c	$J/m^3°C$	1.75×10^6
r_i	m	12×10^{-3}	λ_c	J/msec°C	0.17
s (1)	m	12×10^{-3}	T_{0c}	°C	20
Heat-generation			**Bone (cortical)**		
Q	J/m^3	1.7×10^8	C_b	$J/m^3°C$	2.9×10^6
p(t)	–	$p_1(t)$	λ_b	J/msec°C	0.4
t_r	sec	0	T_{0b}	°C	37
τ	sec	350			
Cement-bone interface			**Bone surface**		
β_{cb}	J/m^2 sec°C	1,000	α	J/m^2 sec°C	500
			T_a	°C	37

table 7.I: Reference values for parameters in the diaphysis model; (1) In the reference case no implant is present, hence: $s = r_i$.

'worst case' for the bone temperature values. The reference values were chosen as more-or-less probable average values, as summarized in table 5.VI; if there were serious uncertainty about a parameter (as, for instance in the case of β), a more-or-less 'worst case' value was chosen. In table 5.VI, $Q = 1.8 \times 10^8 J/m^3$ and $C_c = 1.9 \times 10^6 J/m^3°C$ were given as probable values. Based on the results of the simulations described in the previous chapter, $Q = 1.7 \times 10^8 J/m^3$ and $C_c = 1.75 \times 10^6 J/m^3°C$ have been chosen as probable values in the forthcoming analyses.
For the calculations where a (metal) implant is assumed to be present, values for the parameters are taken in accordance with table 5.II (Cr-Ni-steel; $C_i = 3.6 \times 10^6 J/m^3°C$; $\lambda_i = 14$ J/msec°C).
Parameters will be varied in what is expected to be a realistic range, which is determined either by uncertainty about the parameter value (see table 5.VI), or by a range in which the parameter may vary in reality, due to circumstances or cement composition. Since the solution procedure is numerical, the parametric analysis is carried out by calculating for each parameter separately the temperatures for several values, and interpolating between separate results. In some calculations, values different than those shown in table 7.I were taken for other than the varied parameter; where this is the case, the deviating value will be mentioned.

Fig. 7.2.a shows temperatures as a function of time in the cement and the bone and fig. 7.2.b temperatures as a function of the radius r at three different times. The middle of the cement mass (point 1) reaches approximately 121°C (T_c), the bone at the bone-cement interface approximately 59°C (T_b).
In order to judge the possibilities of thermal damage of the bone tissue, the temperature values in the bone have to be taken into account, but also the exposure time. These data have to be compared to the threshold levels shown in fig. 3.1.
To simplify this procedure, the penetration depths of the 50°C and 55°C isotherms into the bone as function of time ($\delta(t)$) were calculated (fig. 7.3). The maximal penetration depth of the 50°C isotherm is denoted as δ_m.

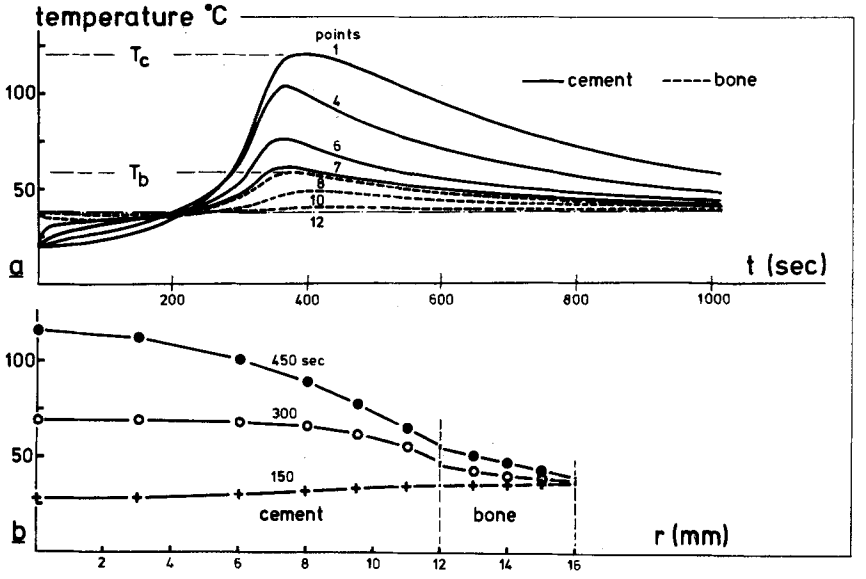

fig. 7.2: (a) Temperatures as a function of time at the 12 points indicated in fig. 7.1.e; T_c and T_b are the maximal temperatures in cement and bone respectively. (b) Temperatures as a function of the radius r, at three different times (both calculations of the reference case).

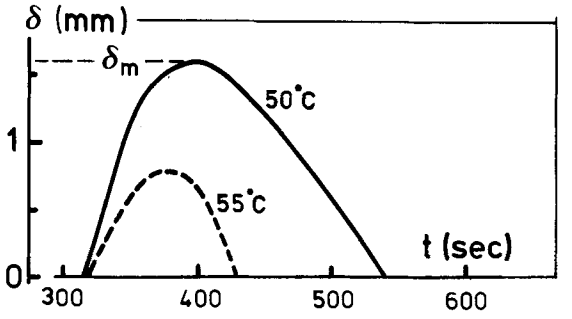

fig. 7.3: The penetration depths of the 50°C and the 55°C isotherms into the bone cortex as functions of time; δ_m is the maximal penetration depth of the 50°C isotherm.

If this graph is compared to fig. 3.1 it is found that about 0,5 mm of the bone would be liable to bone-cell necrosis and about 1 mm to vascular damage.

To evaluate the influences of parametric changes, three variables that are representative of the temperature distribution will be regarded: the maximal cement temperature (T_c as shown in fig. 7.2.a or ΔT_c, defined as T_c -20°C), the maximal bone temperature at the interface (T_b (fig. 7.2.a) or ΔT_b, defined as T_b -37°C) and the maximal penetration depth of the 50°C isotherm (δ_m, fig. 7.3).

7.2. Heat transport at the bone surface

The heat loss at the outside surface of the bone depends on α (J/m^2 sec°C) and T_a (°C). Theoretically speaking, α may vary between zero (bone surface temperature equal to T_a) and infinite (bone completely isolated). Temperatures at the cement and bone points as a function of time for both these upper and lower boundary values are shown in fig. 7.4. In the event of complete isolation, the whole system warms up to around 73°C, a value that can easily be verified using data for total heat-generation and heat-capacity properties.

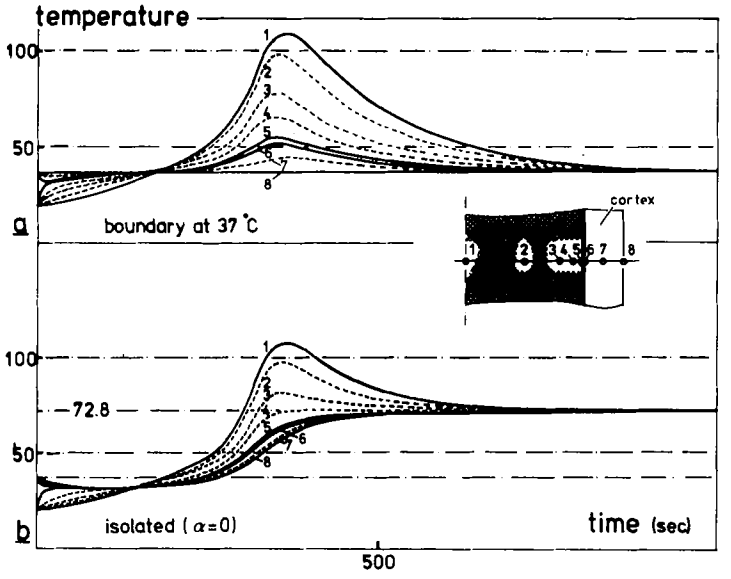

fig. 7.4: Temperatures as a function of time at 8 points in the cement and the bone as calculated in the event of an idealized heat transport (a) and of an idealized isolation at the bone surface (b).

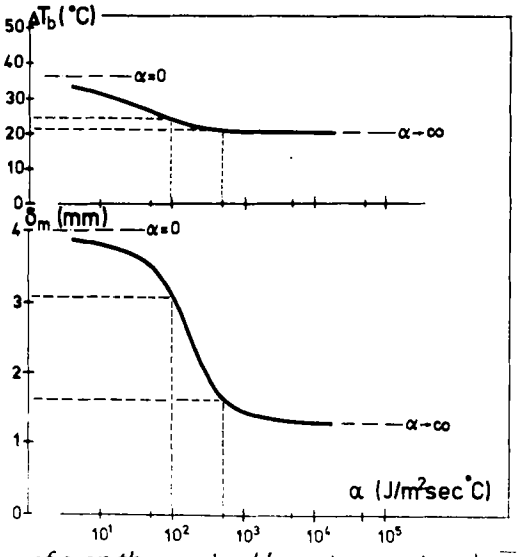

fig. 7.5: The influence of α on the maximal bone temperature increase ΔT_b and on the maximal penetration depth of the 50°C isotherm δ_m (logarithmic scale for α).

As follows from fig. 7.4 the value of α has no significant influence on T_c. The influence of α on ΔT_b is shown in fig. 7.5. It is found that α has little influence when $\alpha > 100$. The influence of α on δ_m, too, is shown in fig. 7.5; for α to have little influence in this case it would have to be over 500; for $\alpha < 500$ the influence is pronounced.

7.3. Cement-bone interface conductivity

The influence of β (J/m^{2}sec°C) on ΔT_b and δ_m is shown in fig. 7.6; β has a marked influence for $\beta < 1000$. A value of 1000, as used in the reference case, or higher, more-or-less simulates 'worst case' conditions for the bone.

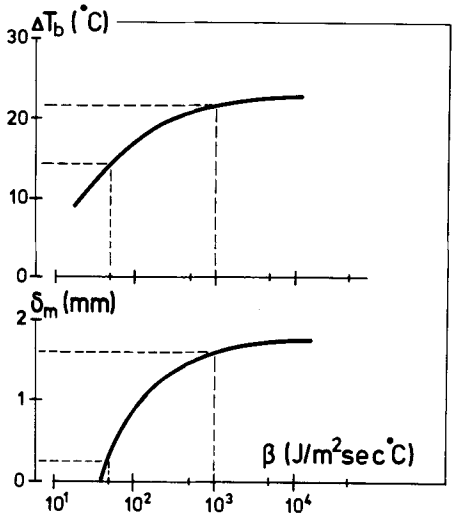

fig. 7.6: The influence of β on ΔT_b and on δ_m (logarithmic scale for β).

7.4. Bone and implant dimensions

When a metal implant is present in the cement, it functions as a 'heat sink', due to its superior heat capacity and conductivity properties. An example of temperature values as calculated, assuming an axisymmetric stem of 12 mm thickness in the cement, is shown in fig. 7.7. Values taken for the parameters in this case were equal to those in the reference case with the exceptions β_{cb} = 500 J/m^{2}sec°C and $T_{0c} = T_{0i}$ = 25°C; β_{ci} was taken as infinite. As follows from fig. 7.7, T_c reaches only approximately 80°C, and T_b reaches approximately 54°C. The maximal penetration depth of the 50°C isotherm $\delta_m \approx 1.3$ mm (fig. 7.7.c). The bone at the cement-bone interface is maintained at a temperature of more than 50°C for only 110 sec which, according to the threshold curve in fig. 3.1, is not enough to cause vascular damage or bone cell necrosis. As can be concluded from the temperature as a function of time in the stem (fig. 7.7.a), the stem takes up the heat initially and later returns it to the rest of the system. In a real prosthesis stem heat will also flow in the axial direction, which will reduce the temperatures even further.

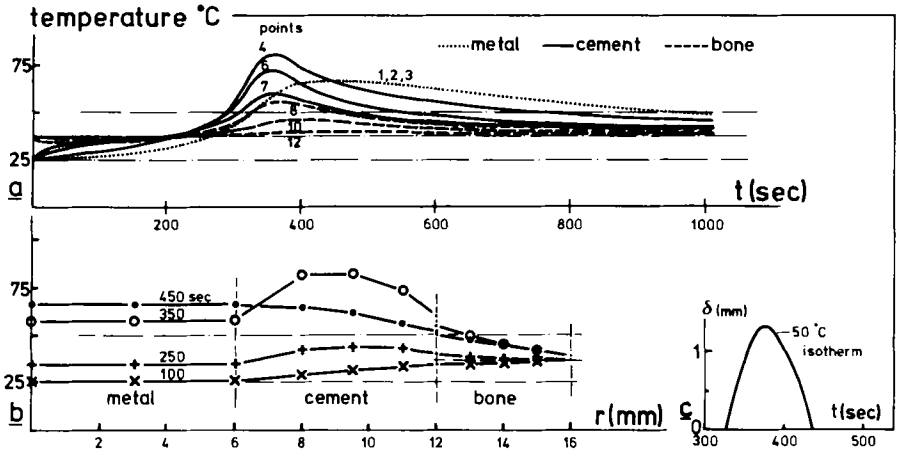

fig. 7.7: (a) Temperatures as a function of time in implant, cement and bone, at 12 points (indicated in fig. 7.1.e); (b) temperatures as function of the radius r in the three materials at three different times; (c) penetration depth of the 50°C isotherm into the bone cortex as function of time.

By varying the bone dimensions, the influence of individual differences can be evaluated, and the possibilities can be judged of using animal models in experimental heat-conduction studies in vivo.
In first-order approximation, the relation between heat generation and heat conduction in a system can be estimated by comparing the heat-producing volume to the heat-transporting surface. In the medullary canal, assuming axisymmetry, the ratio between these two parameters (volume/surface) is proportional to the inner bone radius r_i. Hence it should be expected that the temperature values measured in bones of small animals are not representative of humans, as r_i greatly differs in the various animals. This follows also from regarding the steady state heat-conduction resistance of the cortex and the bone surface (R_c(msec°C/J)) which is found from (e.g. Eckert and Drake, 1972)

$$R_c = \frac{\ln(r_u/r_i)}{\lambda_b} + \frac{1}{\alpha r_u} \qquad (7.1)$$

From (7.1) it follows that α exerts its greatest influence on the smaller bone. When $\alpha \to \infty$, R_c depends on $\ln(r_u/r_i)/\lambda_b$ only and if r_u/r_i and λ_b were constant in different animals, deviations in the bone temperatures would be due to differences in the heat generation-conduction relation only. When $\alpha = 0$, the heat resistance is infinite and in this case the end-temperature of the system depends on the total heat generation in the cement and the heat capacity of the cement and the bone, hence on the ratio volume-cement/volume-cement-and-bone; in the event that r_u/r_i is constant in different animals this ratio, and hence the maximal temperature, is equal.

To investigate the differences further, the model was analyzed for different dimensions (see table 7.II); in all three cases $r_u/r_i = 1.33$ was assumed.
Fig. 7.8 shows the influence of α on the maximal bone temperature increase ΔT_b for the three different dimensions. As was previously predicted, for low α and for high values of α it has no influence on the differences in ΔT_b, while for low values there is no difference.

	r_i (mm)	r_u (mm)	simulated bone
Reference calculation	12	16	human femur
Variation 1	7.5	10	dog femur
Variation 2	3.75	5	rabbit femur

table 7.II: Variations in bone dimension.

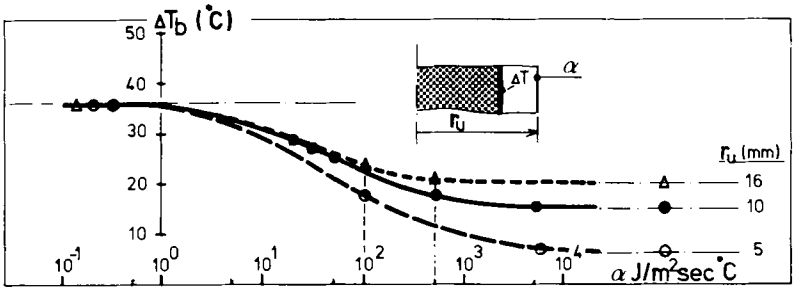

fig. 7.8: The influence of α on ΔT_b for three different bone dimensions (logarithmic scale for α).

For $\alpha \approx 100$ the difference between the dog bone and the human bone will have practically vanished and for $\alpha \approx 10$ the difference between the rabbit bone and the human bone. As discussed previously, probably $\alpha > 500$, hence results of animal experiments in this respect cannot simply be translated into human circumstances.

When animals have to be used as models in this respect, a method of scaling could be introduced. When the differential equation that describes the process of heat-generation and conduction (chapter 4) is written in dimensionless form it follows that, if the dimensionless numbers

$$\frac{\tau\lambda_c}{C_c r_i^2} \text{ and } \frac{\tau\lambda_b}{C_b(r_u-r_i)^2} \qquad \text{(Fourier number)},$$

$$\frac{\beta r_i}{\lambda_c}, \frac{\beta(r_u-r_i)}{\lambda_b} \text{ and } \frac{\alpha(r_u-r_i)}{\lambda_b} \qquad \text{(Biot number)},$$

$$\frac{Q}{C_c T_a} \text{ and } r_u/r_i,$$

are equal in the human and the animal model, the results will be equal in both cases. For the Fourier numbers this could be accomplished by adapting the polymerization time (τ) and the heat capacity of the cement (C_c) in the animal case; then also Q would have to be adapted for the source number (Q/C_cT_a).

Little can be done to satisfy the requirements for the Biot numbers, so scaling would only be possible if $\alpha \rightarrow \infty$ and $\beta \rightarrow \infty$.

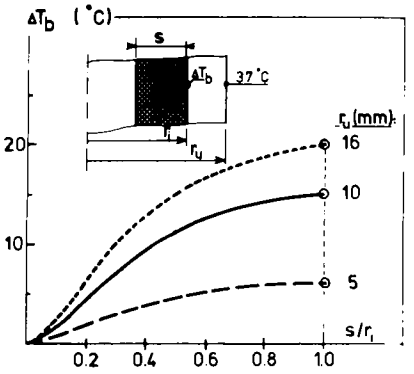

fig. 7.9: Maximal bone-temperature increase (ΔT_b) as a function of the relative cement layer thickness (s/r_i), for three different bone dimensions (r_u/r_i constant).

Fig. 7.9 shows the maximal temperature increase of the bone (ΔT_b) in the event that an implant is present as a function of the ratio between the thickness of the cement layer and the inner radius of the bone (s/r_i), for the three bone dimensions. In the calculations on which these results are based, α was taken as infinite. For $s/r_i = 1$, no implant is present in the cement and the medullary canal is completely filled with acrylic cement. As follows from these graphs, besides the bone dimension the thickness of the cement layer (the thickness of the implant) has a marked influence on the maximal bone temperature.

As to influences of individual differences in bone dimension, these can also be estimated using formula (7.1). When the differences are such that r_u/r_i remains constant, the previously discussed influences apply in the same way.
When the cortex thickness varies, assuming equal r_i, only the heat-conduction properties change. It can be calculated from formula (7.1) that, with respect to the (human) reference case (α = 500 J/m^{2}sec°C), a variation in cortex thickness from 3 to 5 mm has the same influence as a variation in α from about 3250 to 222 J/m^{2}sec°C, a variation that hardly affects ΔT_b, but has a significant influence on δ_m (fig. 7.5).

7.5. Heat generation parameters

The heat generation in the cement depends on Q and on p(t). The influence of Q on ΔT_c, ΔT_b and δ_m is shown in fig. 7.10. Q has a marked influence on all temperature values.

Apart from the polymerization function $p_1(t)$ two other curves were applied, $p_2(t)$, a slower curve and $p_3(t)$, a faster curve, respectively (fig. 7.11). These curves were different especially in their auto-acceleration aspect; the best way to characterize these differences is by their maximal polymerization rate (θ_p = max(dp/dt)) rather then by their polymerization time ($\theta_{p1} = 11\times10^{-3}\,sec^{-1}$; $\theta_{p2} = 4.4\times10^{-3}\,sec^{-1}$; $\theta_{p3} = 28\times10^{-3}\,sec^{-1}$). The resulting cement and bone temperatures as a function of time for these three curves are shown in fig. 7.11.

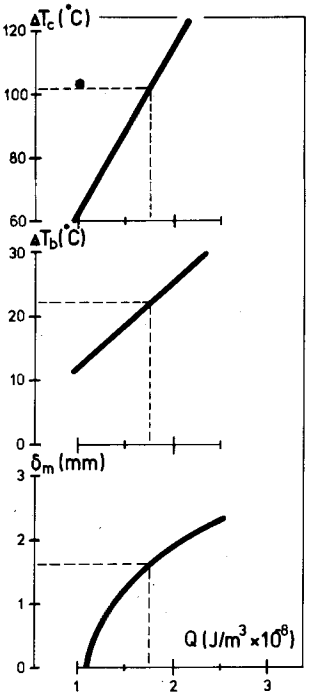

fig. 7.10: The influence of Q on ΔT_c, ΔT_b and δ_m.

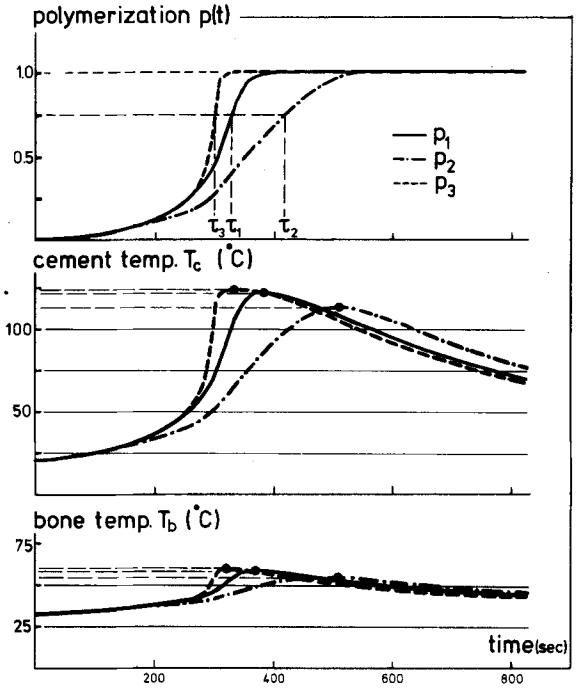

fig. 7.11: From top downwards: the three polymerization functions applied ($p_1(t)$, $p_2(t)$, $p_3(t)$), the cement temperature (center point) and the bone temperature (interface) that result from these functions.

The results for curve $p_3(t)$ are practically equal to those of an idealized 'snap-curing' cement, which is as fast as possible. Application of curve $p_2(t)$ gives a reduction of about 4°C in the maximal interface bone temperature T_b, as compared to curve $p_1(t)$, and a reduction of about 0.5 mm in δ_m. Between the results of curves $p_1(t)$ and $p_3(t)$ there is only a slight difference.

7.6. Heat capacity and conductivity parameters

The influence of the heat capacity of the bone is but slight over a wide range.
For $2x10^6 \leq C_b \leq 4x10^6$ J/m³°C, the influence on T_c is insignificant, T_b varies between 60°C and 57°C and δ_m varies between 1.8 mm and 1.3 mm.

The conductivity of the bone, λ_b, has a greater influence on both T_b and δ_m, especially for low values. Fig. 7.12 shows the influence on ΔT_b, for $0.2 \leq \lambda_b \leq 2.0$ J/msec°C and different values for α. It should be remarked that such a wide range for λ_b is not realistic.

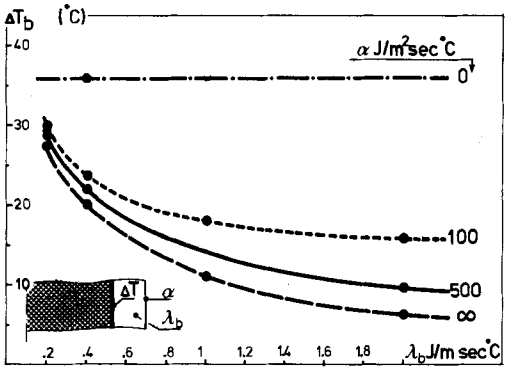

fig. 7.12: The maximal bone-temperature increase (ΔT_b) as a function of λ_b, for different values of α.

The value of λ_c has no significant influence on T_c. For $0.14 \leq \lambda_c \leq 0.20$ J/msec°C, which is a rather wide range, T_b varies between 57°C and 60°C, and δ_m varies between 1.3 mm and 1.7 mm.
The heat capacity of the cement, C_c, has a marked influence on T_c, T_b and δ_m in a range of $1.5x10^6 \leq C_c \leq 2.5x10^6$ J/m³°C, as is shown in fig. 7.13. C_c is one of the parameters that can be adjusted by adding material of a higher heat capacity to the cement, as will be discussed in chapter 9.

7.7. Initial and ambient temperatures

The influence of the cement initial temperature on T_c, T_b and δ_m in a range of $15 \leq T_{0c} \leq 25$°C is quite insignificant. A greater range is not realistic, at least not in the model, because the initial temperature will probably significantly affect the polymerization process, an influence that is not taken into account in the model.

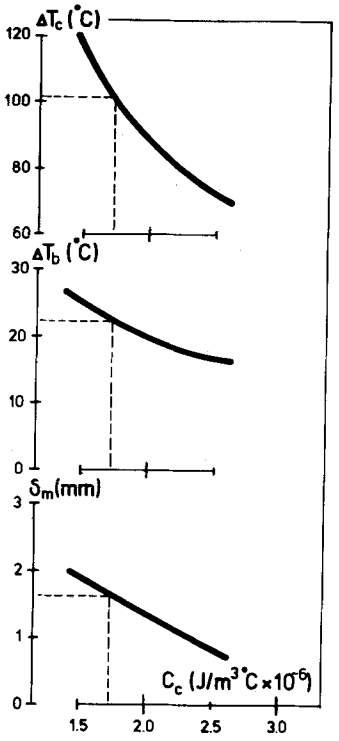

fig. 7.13: The influence of C_c on ΔT_c, ΔT_b and δ_m.

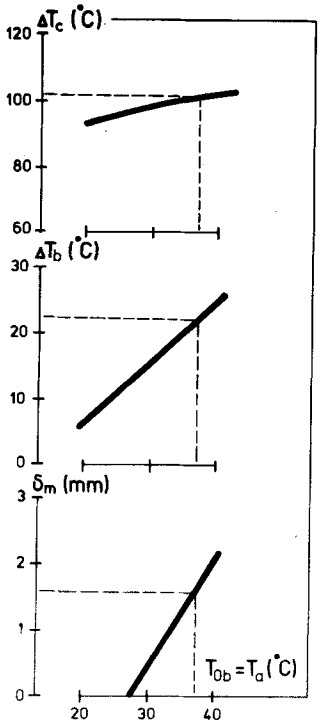

fig. 7.14: The influence of $T_{0b} = T_a$ on ΔT_c, ΔT_b and δ_m.

Both T_b and δ_m are greatly influenced by the initial bone temperature T_{0b} and the ambient (periosteal blood) temperature T_a, as shown in fig. 7.14. T_{0b} and T_a are taken as equal, because both represent the local temperature of the biological system.

The implant initial temperature, in the event that an implant is present, was not varied. As follows from a first-order approximative consideration of the 'heat-sink' capacity of the implant, reducing the initial temperature by 10°C will have about the same influence as increasing the stem radius by 1 mm (for a radius of approximately 6 mm).

7.8. Conclusions

The influence of α ($J/m^2 sec°C$) on the temperature values is slight if $\alpha > 500$. If $\alpha < 500$, however, the influence especially on δ_m is quite pronounced; a lower value of α would then make a greater part of the cortex liable to necrosis. As discussed in paragraph 5.4. it is quite probable that $\alpha > 500$.
The influence of the interface conductivity is pronounced if $\beta < 1000$ $J/m^2 sec°C$. This might well be so and in that case the temperatures in the bone may be much lower, although it should be borne in mind that in single trabeculae surrounded by cement the bone may still reach high maximal temperature values, as discussed in paragraph 5.3.4.
The influence of the polymerization curve p(t) on T_c and T_b is not very outspoken in a realistic range of polymerization rates. If the 'Trommsdorf effect' (the auto-acceleration phase of the process) were significantly surpressed, as in curve no. 2, some temperature reduction would be evident, but probably less than sometimes expected (de Wijn, 1974; Huiskes *et al*, 1977). The reduction of the penetration depth δ_m, however, is quite pronounced for a slow curve.
Also the presence of a metal stem in the cement (as, for instance in intramedullary fixated implants) has a marked effect on the temperatures. The influence of the stem thickness is great, owing to a combined effect of a greater 'heat sink' capacity of the implant and a lesser cement layer thickness.

The influences of the other parameters on T_c, T_b and δ_m can be linearized in the neighbourhood (usually over a fairly wide range) of their reference values.
The linearized influences are summarized in table 7.III as percentage increase in T_c, T_b and δ_m per percentage increase in the parameter value.
It is remarkable that Q, C_c and $T_{0b} = T_a$ exert the greatest influences. These parameters belong to the ones that can be influenced by the surgeon or the cement manufacturer, as will be discussed in chapter 9.

It was shown in the reference calculation that the bone reached a maximal temperature of approximately 59°C, while the inner cortex up to 1.6 mm from the interface reached temperature of 50°C and over. Where there was a (metal) implant of 12 mm in thickness the bone reached a maximal temperature of 54°C, while 1.3 mm of the inner cortex reached a temperature of 50°C or over. As these temperatures were maintained for only a short time, the cortex tissue in the latter case would not be liable to tissue necrosis, applying the threshold curve of fig. 3.1.
Due to uncertainties in the parameter values, these quantities should not be regarded in too absolute a sense. A valid impression of the influences exerted by the probable and possible ranges of parameter values on the bone-temperature rise (ΔT_b) and the penetration depth (δ_m) is given by the diagram in fig. 7.15. The ranges for the parameters are shown in table 7.IV as

parameter	% increase T_c / % increase par.	% increase T_b / % increase par.	% increase δ_m / % increase par.
r_i (1)	–	0.15	–
Q	0.74	0.37	1.43
λ_b	- 0.02	- 0.12	- 0.37
C_b	- 0.02	- 0.07	- 0.45
λ_c	- 0.06	0.06	0.32
C_c	- 0.55	- 0.21	- 1.20
T_{0c}	0.08	0.04	0.19
$T_{0b} = T_a$	0.12	0.56	3.70

table 7.III: 'Sensitivity' factors of T_c, T_b and δ_m for changes in the parameters. The numbers give the percentage increase per percentage increase of the parameters; (1) it is assumed that r_u changes accordingly relative to r_i; in this case the influences on T_c and δ_m were not calculated.

parameter	unit	probable value or range	possible range
r_i	mm	11 - 13	12 - 14
α	$J/m^2 sec°C$	500 - 10,000	100 - ∞
β	$J/m^2 sec°C$	100 - 1,000	50 - ∞
Q	J/m^3	$1.7x10^8$	$1.65 - 1.75x10^8$
p(t)	–	p_1	p_2 - p_3
λ_b	J/msec°C	0.3 - 0.5	0.2 - 0.6
C_b	$J/m^3°C$	$2.2 - 3.2x10^6$	$1.8 - 4.1x10^6$
λ_c	J/msec°C	0.17	0.16 - 0.18
C_c	$J/m^3°C$	$1.75x10^8$	$1.7 - 1.8x10^8$
T_{0c}	°C	20	18 - 25
T_a	°C	32 - 25	30 - 37

table 7.IV: Estimated ranges of the parameter values.

based on the literature review (discussed in chapter 5), the experiment simulations (discussed in chapter 6) and, in some cases, on an 'educated guess'. The diagram in fig. 7.15 shows the approximative factors by which ΔT_b and δ_m will deviate from their reference values for parameter values within their ranges. If it is assumed that the influences of all parameters are independent, a first-order approximation of the probable ranges in ΔT_b and δ_m can be calculated by multiplication of separate influences (for example: if f_1 and f_2 are upper or lower boundary factors of two parameters in fig. 7.15, the combined influence factor would, in first-order approximation

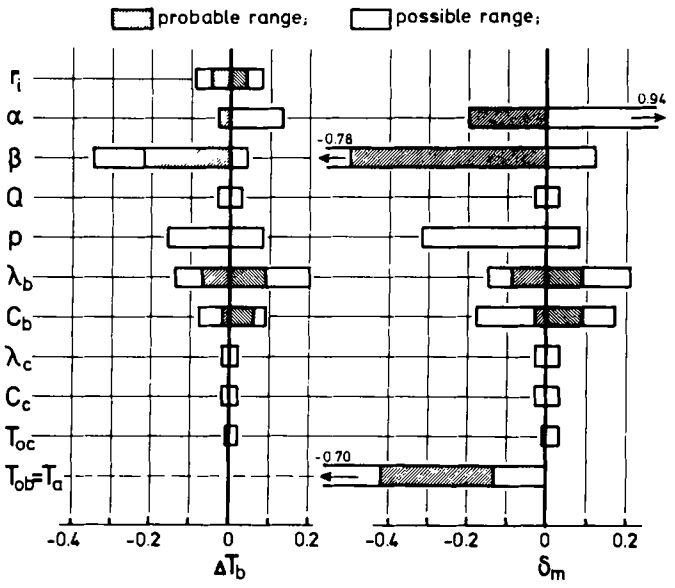

fig. 7.15: The influences of the probable and possible ranges of parameter values on ΔT_b and δ_m. The influences are given as maximal negative and positive deviations from the reference values.

case	reference value		probable range	
	T_b (°C)	δ_m (mm)	T_b (°C)	δ_m (mm)
reference calculation (no implant)	59	1.6	51-62	0-1.9
implant present (thickness 12 mm)	54	1.3	48-57	0-1.5
rabbit femur (no implant)	48	0	44-50	0

table 7.V: Probable ranges of T_b and δ_m in three cases, as calculated using the combined effects of the probable ranges in the parameter values, as shown in fig. 7.15, except $T_{0b} = T_a$ (see also text).

be $\{1 - (1 + f_1)(1 + f_2)\}$). Results of applications for a few cases are shown in table 7.V. In this table the influence of $T_{0b} = T_a$ is not taken into account. In the reference case $T_{0b} = T_a = 37°C$; however, the local bone and blood temperatures during an operation are probably lower (d'Hollander *et al*, 1976).
Using the factors for the possible parameter ranges in fig. 7.15, a 'possible' range in T_b and δ_m could be calculated also. However, it is improbable, although possible, that an individual parameter has a value outside its probable range, but it is quite improbable that all parameters exceed their probable upper and lower boundaries simultaneously. Moreover, since the combined influences were assumed to be independent in this calculation, it is doubtful whether, for such large deviations of the parameters from their reference values, such a calculation still has any realistic significance.
Based on the data shown in table 7.V and the threshold curve in fig. 3.1 the cautions conclusion can be drawn that, during fixation of intramedullary stems, tissue necrosis of the

cortex in a very small zone near the interface is just possible. If the influence of the initial bone temperature, probably less than 37°C, is taken into account, necrosis would be improbable. Also, it can be concluded that, in the case of the rabbit femur, where the whole medullar canal is filled with acrylic cement, tissue necrosis is quite improbable. One should be cautious with such conclusions in an analysis of this kind that is in essence meant to evaluate influences and tendencies rather than to find absolute data. However, it appears very unlikely that the bone tissue necrosis found by Feith (1975) in his rabbit experiments would be principally caused by the heat of polymerizing, as will be further discussed in paragraph 7.9.
At this point it should be remarked that although the thermal damage threshold curves in fig. 3.1 were introduced as convenient criteria for judging the possibilities for thermal damage, Lundskog (1972) reported osteocyte necrosis for cells that were exposed to a temperature of 50°C for only 30 seconds. If this criterion is used it is apparent, looking at the data presented in table 7.V, that in the case of intramedullary stem fixation, osteocyte necrosis within a region of 0 - 1.5 mm of the cortex is a distinct possibility. In the case of the rabbit femur necrosis would still be improbable.
However uncertain these conclusions are in an absolute sense, it is clear that bone-prosthesis systems are not 'designed' within their safety limit where thermal damage is concerned. An overall conclusion with respect to intramedullary fixation of implants can be, that the temperature in the bone could reach values that might well give rise to bone necrosis.
More certainty can be had by narrowing the possible ranges of parameter values by means of experiment. Theoretical analyses as presented here provide guidelines for such experiments. From the results of the parametric analyses it is evident that the following properties should then be specially evaluated with greater accuracy:
- the thermal conductivity of the cement-bone interface,
- the bone and local blood temperature prior to insertion of the cement,
- the heat transport mechanism at the bone surface,
- the thermal conductivity of cortical bone.

7.9. A hypothesis on thermal tissue damage by acrylic cements

An extensive histological study concerning adverse side effects of acrylic cement was conducted by Feith (1975). He treated different groups of rabbits with (1) suction and reaming of the femoral intramedullary canal (RS), (2) RS and a pre-polymerized rod of acrylic cement (residual monomer and no heat), (3) RS and a commercial cement mixture to polymerize in situ (residual monomer and heat), (4) RS and a cement mixture without catalyser (overdose monomer and no heat) and (5) RS and a mixture of an experimental aqueous gel-cement to polymerize in situ (residual monomer and minor heat). He concluded that reaming and residual monomer, especially an overdose, cause bone necrosis at the interface, but that the principal causative factor is the heat of polymerizing.
By simulating the case in which a medullar cavity of a rabbit bone is filled with acrylic cement it was shown in this chapter that results of such experiments cannot simply be applied to human circumstances owing to the different dimensions. These results indicated that it is very unlikely that in the rabbits of Feith (1975) the thermal effect was the principal causative factor in bone necrosis. In his different groups he did not isolate the thermal effect, but the heat was always present together with residual monomer. The results of his different groups, on which he based his conclusions, are schematically summarized in fig. 7.16, only as regards necrosis of the inner cortex (Feith studied other effects as well).
Also shown in fig. 7.16 is an extrapolation of the results obtained here, presented as a

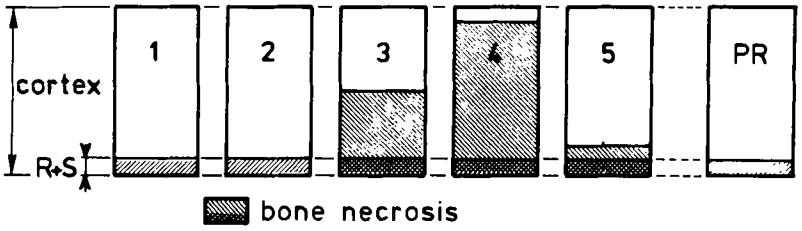

fig. 7.16: Schematic summary of results reported by Feith (1 through 5) and an extrapolation of results of the present work (PR), with respect to inner cortical necrosis of rabbit femurs after filling of the medular cavity with acrylic cement. Parameters are: reaming and suction (RS), residual monomer (M) and heat of polymerizing (H). 1: RS only; 2: RS + M; 3: RS + M + H; 4: RS + M (overdose); 5: RS + M + H (little heat); PR: RS + H.

hypothetical sixth group where reaming and suction and heat of polymerizing would be applied and in which, as was predicted by the rabbit model calculations, the amount of bone necrosis would be the same as in reaming and suction only.
As there appears to be no reason to doubt the findings of Feith and because the present analysis has shown that the heat of polymerizing alone (a case that he did not investigate) would most probably not induce tissue necrosis in the rabbit, the hypothesis can be put forward, following directly from fig. 7.16, that the necrotic effect of the residual monomer would be more pronounced at higher temperatures, so that the temperature has an indirect effect rather than a direct effect.

CHAPTER EIGHT

TEMPERATURE VALUES DURING ACETABULAR CUP FIXATION

In this chapter a heat generation and conduction analysis of acrylic cement during acetabular cup fixation will be presented. A schematic cross-section of the bone-prosthesis system concerned is shown in fig. 8.1. In the model used for the analysis the (plastic) cup, the cement layer and a part of the (spongeous) acetabular bone (as shown in fig. 8.1) are taken into account. Heat loss from the bone in the model to the adjoining bone or soft tissues is described by the boundary conduction and convection coefficient α. The model is axi-symmetric and although this does not give a very accurate geometrical description of the real system as far as the bone is concerned, it will at least give a more-or-less accurate description of the heat-conduction process in the frontal plane.

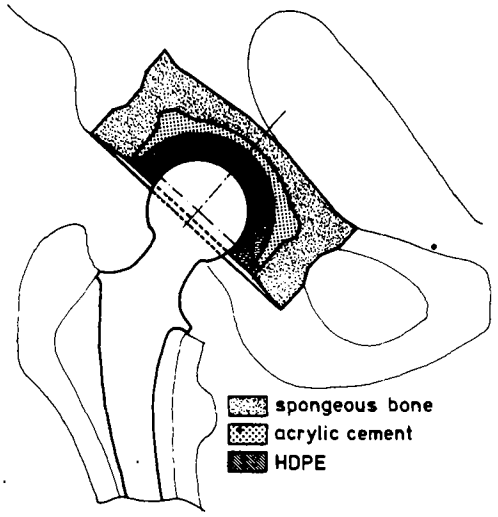

fig. 8.1: Schematic frontal section of an acetabular cup fixation system, indicating the part of the acetabulum that is taken into account in the model.

The model and its parameters are shown in fig. 8.2; the parameter values used in the analysis are summarized in table 8.I.
Fig. 8.3 shows the element mesh for the model, as generated by computer program (Schoofs *et al*, 1978). Time-dependent temperatures were calculated, as described in chapter 4, for all nodal points. The nodal points, the results of which will be considered, are shown in fig. 8.4. These points are located more-or-less on three 'lines' (1, 2 and 3). The points on 'line' 2 are numbered as shown.
Temperatures as a function of time as calculated for these points are shown in fig. 8.5. The temperature in the middle of the cement mass (point 7) reaches a maximal value of approximately 110°C, the bone at the cement-bone interface (point 10) a value of approximately 57°C and the HDPE at the cement-implant interface (point 4) approximately 69°C.

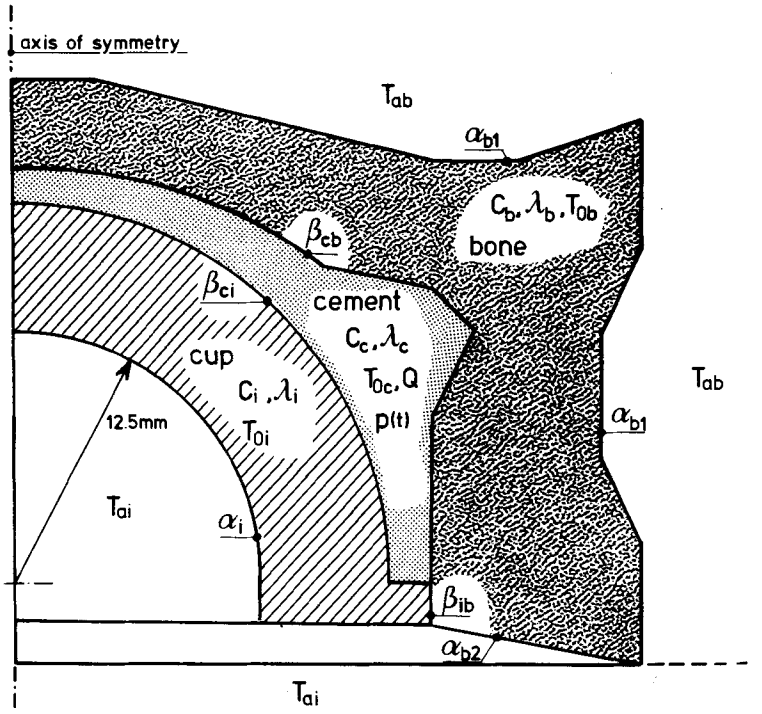

fig. 8.2: The (axisymmetric) model giving the parameters of the process of heat generation and conduction.

parameter	unit	value	parameter	unit	value
heat generation			**cement**		
Q	J/m^3	1.7×10^8	C_c	$J/m^3°C$	1.75×10^6
p(t)	–	$p_1(t)$	λ_c	J/msec°C	0.17
t_r	sec	0	T_{0c}	°C	25
τ	sec	350			
interface conditions			**bone (spongeous)**		
β_{ci}	$J/m^2sec°C$	500	C_b	$J/m^3°C$	3.0×10^6
β_{cb}	$J/m^2sec°C$	500	λ_b	J/msec°C	0.4
β_{ib}	$J/m^2sec°C$	500	T_{0b}	°C	37
boundary conditions			**cup (HDPE)**		
α_i	$J/m^2sec°C$	10	C_i	$J/m^3°C$	2.2×10^6
α_{b1}	$J/m^2sec°C$	10	λ_i	J/msec°C	0.29
α_{b2}	$J/m^2sec°C$	500	T_{0i}	°C	25
T_{ai}	°C	25			
T_{ab}	°C	37			

table 8.1: Values as used for parameters in the acetabular cup model.

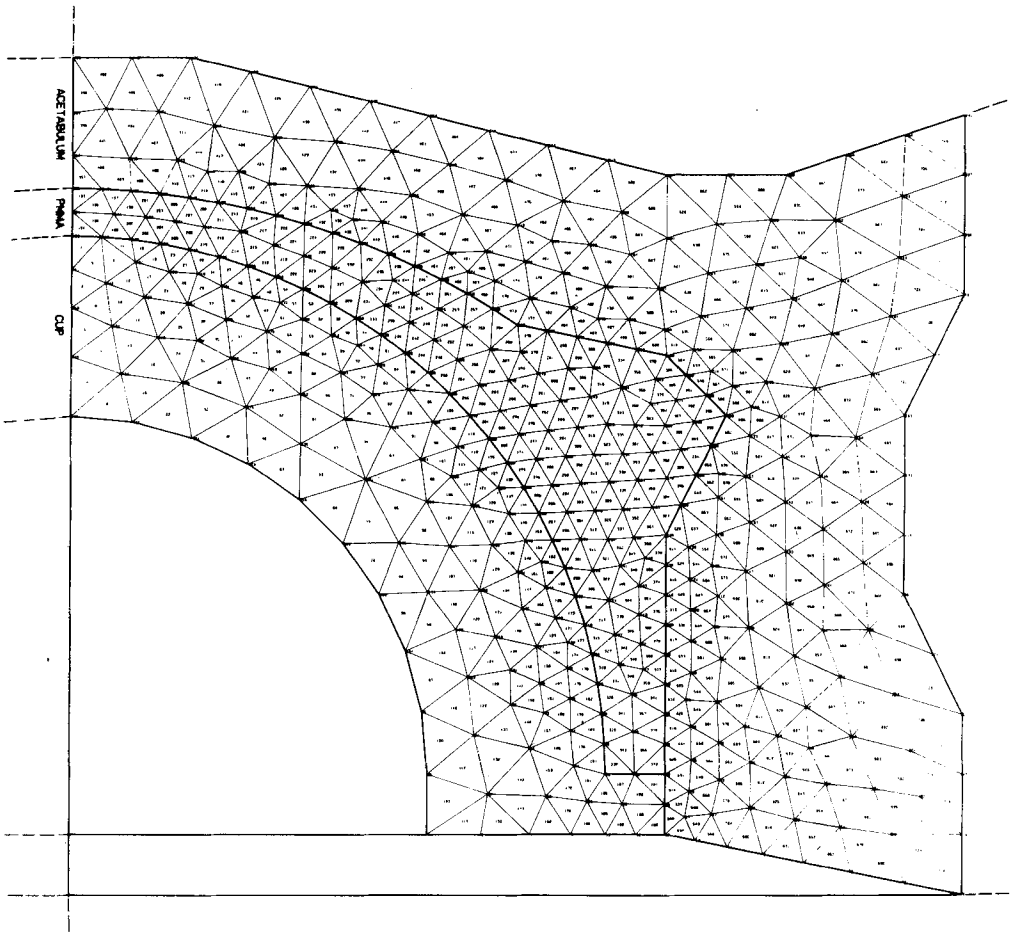

fig. 8.3: The element mesh used in the computer simulation.

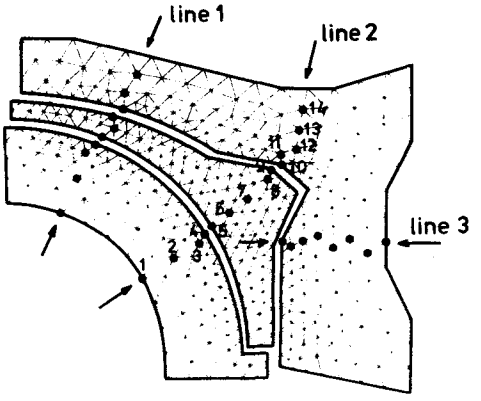

fig. 8.4: Points roughly located on three 'lines' of which those on 'line' 2 are numbered; the temperatures as calculated at these points are discussed in the text.

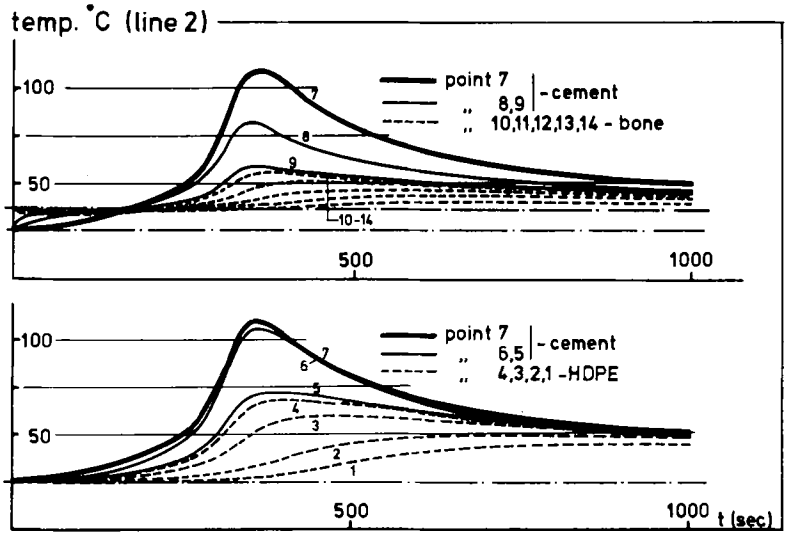

fig. 8.5: Temperature as a function of time at the 14 points indicated in fig. 8.4, as calculated in the computer simulation (top graph: cement and bone; bottom graph: cement and cup; the temperature of point 7 (in the middle of the cement mass) is drawn in both graphs).

The temperatures in the HDPE are higher than those in the bone, due to the superior heat-capacity and conductivity properties of the latter material, but also to the smaller area of the cup-cement interface compared to the cement-bone interface.
For the three 'lines' shown in fig. 8.4, time-dependent penetration depths of the 45, 50, 55 and 60°C isotherms into the bone ($\delta(t)$) have been calculated, as shown in fig. 8.6.
On 'line' 3 especially, a relatively large part of the bone will be liable to tissue necrosis, as can be concluded on comparing these graphs with the time-dependent threshold level in fig. 3.1. The high temperature values at 'line' 3 are caused by the circumstance that the bone is somewhat surrounded by cement here. The lowest maximal temperature values are reached at 'line' 1, due to the relatively thin cement mantle in this region.

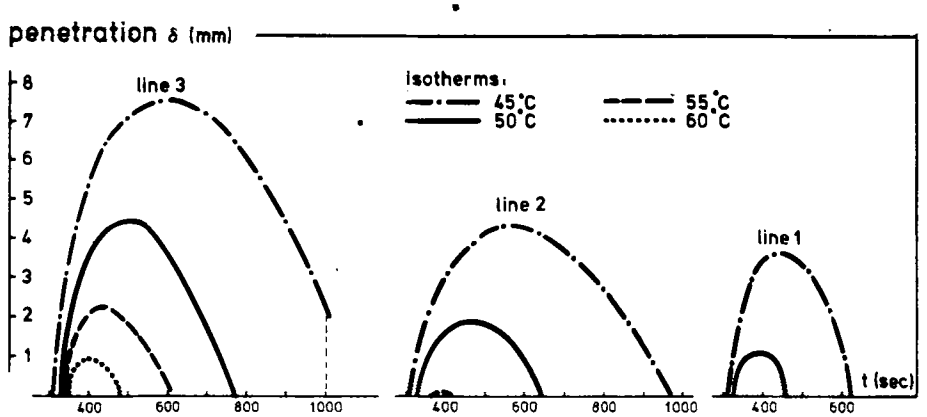

fig. 8.6: Penetration depths of the 45, 50, 55 and 60°C isotherms into the bone on 'lines' 1, 2 and 3 as functions of time.

From the calculated time-dependent temperatures the liability of the bone to vascular damage or bone cell necrosis was estimated using the threshold level curves of fig. 3.1, taking temperature values as well as the exposure times into account. From this evaluation a 'necrosis map' as shown in fig. 8.7 evolves; also shown on this 'map' is the region in the cement that reaches over 100°C and would therefore be liable to monomer evaporation. This 'necrosis map' gives an indication of the region most probably damaged and should not be regarded in too absolute a sense, since some parameter values are somewhat uncertain and the thermal damage threshold curves of fig. 3.1 also have uncertain aspects. If the data presented by Lundskog (1972) were taken as a threshold criterion (cell necrosis after exposure for 30 seconds to 50°C) a much larger part of the bone would be liable to necrosis, as indicated in fig. 8.7.

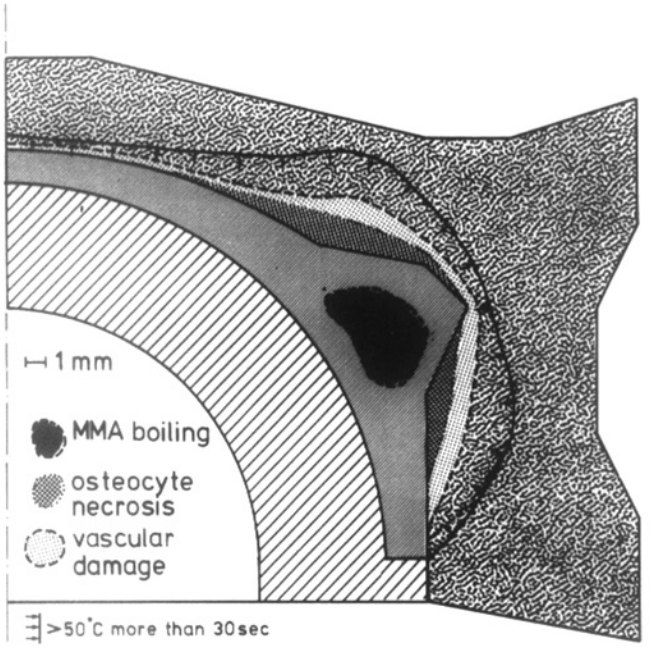

fig. 8.7: A 'necrosis map' as constructed from the calculated results, giving a rough impression of parts of the bone liable to osteocyte necrosis and vascular damage, using the time-dependent threshold levels in fig. 3.1 as criteria; also indicated is the part of the bone that would be liable to osteocyte necrosis if the data of Lundskog (1972) were used as a criterion (necrosis after 30 sec at 50°C).

This model is not so well suited for extensive parametric analyses as the model discussed in the previous chapter, owing to its greater geometrical complexity. It has been shown, however, that the values of α have little influence on the maximal temperatures of cement and bone. The parameters that exert a significant influence on the bone temperatures, and whose values are somewhat uncertain, are β_{cb}, λ_b, C_b and T_{0b}. The values of T_{0b} and T_a will probably be higher than in the system previously analysed, owing to the fact that the system is enclosed by much soft tissue and highly vascularized spongeous bone. Thanks to the many and more dependable results published on the properties of spongeous bone,

compared to cortical bone, greater confidence can be given to the values of λ_b and C_b than in the previous model (see also table 5.VI). Inaccuracies in the predicted temperature values would thus for the greater part be due to uncertainty in the value of β. Of course, it should not be forgotten that the geometry chosen for the model is a more-or-less general representation of the many possible ones in reality and that individual differences in maximal temperature values might thus occur to a greater or lesser extent.
Due to variations in β only, the probable temperature increase in the bone could vary from approximately 0.8 to 1.0 times the calculated values. Due to the fact that the cement is fixated to spongeous bone, somewhat lower values for β may be expected compared to those in the previous model.

In conclusion it can be said that owing to geometrical circumstances, but also to a higher initial bone temperature and the inferior thermal properties of HDPE compared to metal, there will be a greater chance for thermal damage during acetabular cup fixation than during fixation of intramedullary (metal) implants. If such damage occurs, a zone of about 1 - 2 mm will be affected, but in specific regions a larger zone (4 - 5 mm) may be liable to damage. The chance of thermal necrosis can be reduced in this case, apart from the measures to be discussed in the next chapter, by smoothening the (macro) geometry of the bony implant bed and by avoiding the application of large cement masses.

CHAPTER NINE

MEASURES FOR DIMINISHING THE CHANCES OF THERMAL TISSUE DAMAGE

As was shown in chapter 7, some options are available to reduce the maximal temperatures in the system, because the process of heat generation and conduction is quite sensitive to some of the parameters that can be influenced, either by the surgeon or by the cement manufacturer. Experiments with a number of the possible measures have been published in the literature, for instance the addition of such 'heat sinks' as radiopaque fillers, titanium dioxide (Homsy *et al*, 1972), crystalline monomers (Lee and Turner, 1977) or aqueous gels (de Wijn *et al*, 1978); retardation of the polymerization curve (de Wijn, 1974) and pre-cooling of the cement or the implant (Ohnsorge and Goebel, 1970; Meyer *et al*, 1973; Dipisa *et al*, 1976).
Some of the possible measures will be evaluated as to their effect on the maximal temperature values in the bone-prosthesis system, on the basis of the parametric analysis discussed in chapter 7.

9.1. Adding 'heat sinks' to the powder

When a 'heat sink' is added to the powder, in other words, when a material with superior heat-capacity properties is substituted for a part of the polymer powder, both the heat capacity and the thermal conductivity of the mixture are affected.
If the weight ratio additive/powder is denoted by μ, the heat capacity C_c of the mixture can be calculated using formula (5.6) (paragraph 5.3.). The influences of the changed value of C_c on the temperature increases (ΔT_c, ΔT_b) and the penetration depth of the 50°C isotherm (δ_m) in the model described in paragraph 7.1 can be evaluated using fig. 7.13. For added barium sulfate ($\rho = 4.5 \times 10^3$ kg/m^3, $C = 1.96 \times 10^6$ J/m^3°C) and zirconium oxide ($\rho = 5.6 \times 10^3$ kg/m^3, $C = 3.91 \times 10^6$ J/m^3°C) this evaluation was carried out neglecting the influence on the thermal conductivity and assuming a constant value of ν_m (0.35).

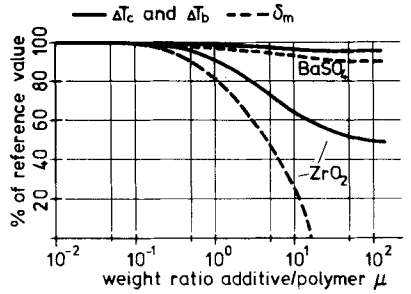

fig. 9.1: Approximative influence of the amounts of barium sulfate and zirconium oxide added to the powder on the maximal temperature increase of the cement (ΔT_c), of the bone (ΔT_b) and on the penetration depth of the 50°isotherm, as percentages of the reference values (reference case ΔT_c = 101°C, ΔT_b = 22°C and δ_m = 1.6 mm); (100% = no additives).

For these two additives fig. 9.1 shows the influence of the weight ratio μ on the cement-temperature increase (ΔT_c), the bone(-interface) temperature increase (ΔT_b) and the penetration depth (δ_m), expressed as percentages of their reference values, as evaluated in chapter 7. Evidently the addition of $BaSo_4$ has only a minor influence; adding ZrO_2 has considerably more effect. However, for $\mu = 1$, the decrease in ΔT_c and ΔT_b is only about 10% and the decrease in δ_m about 20%.

9.2. Adding an aqueous gel to the mixture

If an aqueous gel is added to the cement, in other words, is substituted for a part of the cement, a porous cement will result when used for implantation (e.g. de Wijn *et al*, 1978). In this case the amount of heat generated per unit volume of mixture, the heat capacity of the mixture and the thermal conductivity are affected. If it is assumed that the volume ratio between the polymer and the monomer remains constant, ν_m can be calculated for a given volume fraction of gel (ν_{ac}) by using formula (5.2) (paragraph 5.1.) and C_c can be calculated using formula (5.7) (paragraph 5.3.). For the thermal conductivity it is assumed that $\lambda_c = \lambda'_c + \nu_{ac}(\lambda_{ac} - \lambda'_c)$, where λ'_c is the conductivity of only the acrylic part of the mixture. Assuming that the influence of the changes in the three parameters are exerted independently, the effect of the changes combined can be approximated using the results described in chapter 7. This was carried out taking the thermal properties of the gel as those of water. Fig. 9.2 shows the influence of the volume fraction of gel in the mixture on the temperature increases ΔT_c and ΔT_b and the penetration depth δ_m, as percentage changes with respect to their reference value. Apparently this measure has a marked influence on the temperatures.

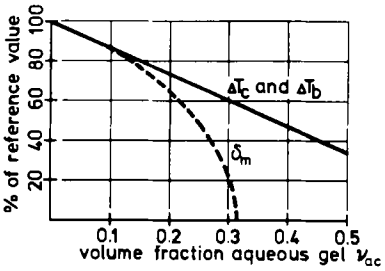

fig. 9.2: Approximative influence of the amount of aqueous gel added to the cement mixture on ΔT_c, ΔT_b and δ_m as percentages of the reference values (100% = no gel added).

9.3. Increasing the P/L ratio

If the P/L ratio is increased, ν_m and hence Q are decreased. The influence of this measure, that can be evaluated directly from figs. 5.1 and 7.10, is shown in fig. 9.3.

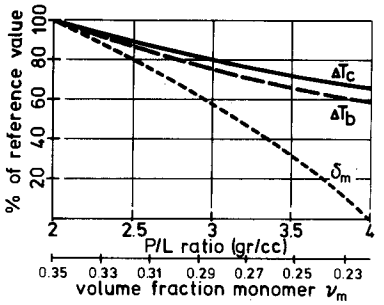

fig. 9.3: Approximative influence of the P/L ratio on ΔT_c, ΔT_b and δ_m as percentages of the reference values (100% = 2 gr/cc).

9.4. Retarding the polymerization process

The polymerization function, especially the auto-acceleration effect, can be retarded with chemical additives (de Wijn, 1974). The auto-acceleration effect is characterized by the maximal polymerization rate (θ_p = max(dp/dt)). The influence of retardation, as evaluated by using the polymerization functions p_1, p_2 and p_3 in chapter 7, on ΔT_c, ΔT_b and δ_m is shown in fig. 9.4, where $1/\theta_p$ is chosen for the variable and 100% is taken for idealized 'snap-curing' cement. For interpretation of these graphs it is convenient to note that when $1/\theta_p$ = 200 sec the auto-acceleration period would be approximately twice as long compared to $1/\theta_p$ = 100 sec.

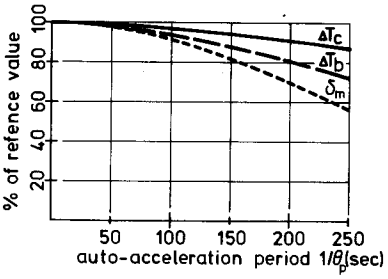

fig. 9.4: Approximative influence of the rate of polymerization (the auto-acceleration effect) on ΔT_c, ΔT_b and δ_m; the variable on the horizontal axis is the inverse of the maximal polymerization rate (100% = 'snap-curing').

9.5. Pre-cooling the operation region

As was shown in chapter 7, the bone temperature prior to insertion of the cement and the ambient (local blood) temperature exert a marked influence on the maximal temperatures in the bone. It would be possible to cool the local operation region, prior to insertion, with a

physiological water solution. Fig. 9.5 once more shows the effect of this measure on ΔT_c, ΔT_b and δ_m.

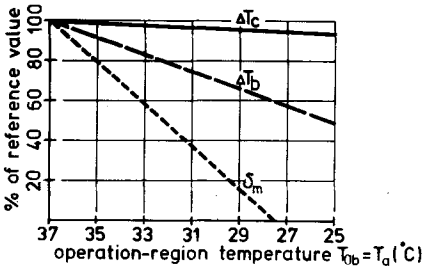

fig. 9.5: Approximative influence of the bone and the local blood temperatures prior to the polymerization process on ΔT_c, ΔT_b and δ_m (100% = local bone and blood temperatures of 37°C).

9.6. Conclusions

Other measures than those discussed in this chapter would be possible, as for instance pre-cooling of the cement and the implant. Although this would certainly reduce the temperature values, it was shown in chapter 7 that, for instance pre-cooling of the cement to 15°C has only a minor influence on the bone temperature; it was also shown in the literature (e.g. Ohnsorge and Goebel, 1970; Dipisa *et al*, 1976) that more drastic pre-cooling seriously prejudices the polymerization process.
Another possibility would be, at least in theory, to protect the bone by increasing the heat-flow resistance at the cement-bone interface; in other words, by decreasing β. How this could be done in reality is not clear at the moment; some thin protective layer with low thermal conductivity would be the answer. In this respect it can also be concluded that a thorough cleansing of the bony implant bed prior to cement insertion is not advantageous and would, at least locally, increase the chances of thermal bone necrosis. An effective measure that could be taken by the surgeon, as has been illustrated in chapters 7 and 8, is to avoid large cement masses and restrict the thickness of the cement layers. Fig. 9.6 once more shows the influences of the (metal) implant thickness (hence: the cement mantle thickness) on ΔT_c, ΔT_b and δ_m in intramedullary stem fixation.

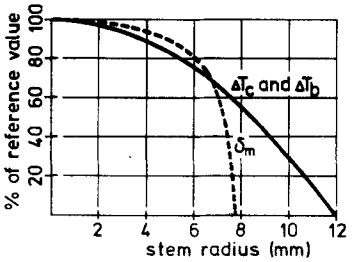

fig. 9.6: Approximative influence of the (metal) stem thickness (hence also the cement layer thickness s) on ΔT_c, ΔT_b and δ_m (100% = no implant present).

Another possibility would be, where large cement masses are required, to use prefabricated plastic, for instance in coated stems.
It should be noted that some of the possible measures affect the quality (strength) of the cement (see section I); for instance 'heat sink' additives to the powder, drastic increase of the P/L ratio and the addition of aqueous gels. So they should not be applied over the full range of their possibilities.
However, good results can be expected if some of the measures were taken in combination. If 10 volume % aqueous gel were added to the mixture, the P/L ratio would be increased from 2 gr/cc to 2.25 gr/cc, the auto-acceleration effect would be retarded by 100 sec and the operation region would be cooled to 30°C, prior to and during the polymerization, the maximal rise of the bone temperature would decrease by about 50%, thus in most cases banishing the chances of thermal bone necrosis completely.

CHAPTER TEN

DISCUSSION

In this section the process of heat generation and conduction of acrylic cement in situ has been analysed. By making certain assumptions as to the properties of the cement and the bone material, and by approximating the geometry of the bone-prosthesis system by axi-symmetry, the heat generation and conduction process was mathematically described on the basis of the conservation-of-energy principle and Fourier's law. The equations have been solved using a computer program applying FEM and backward time discretization. Based on a literature review, values for parameters used in the models were estimated. Relatively little was found to be known about these parameters; hence, in some cases only a range of probable values could be established. This range will, no doubt, also reflect the individual differences where biological material is concerned and random compositional differences where acrylic cement is concerned. Due to the uncertainties as regards parameter values, the use of more refined mathematical models would, in this respect, not be justified as yet. Unfortunately, the influence of the temperature on the polymerization process itself could not be taken into account, owing to lack of knowledge about this relation; in the mathematical model and the solution procedure chosen here this influence can easily be accounted for. By simulation of two experiments published in the literature, the applicability of the model and the appropriateness of the chosen parameter values have been evaluated to some extent and it was shown that the method can in fact be used to predict the time-dependent temperature values by approximation. Based on a literature review, threshold levels for thermal tissue damage were evaluated. As was to be expected here, too, no exact value for this level evolved. Taking the upper and lower boundaries of all dependable published data, one could say that for a bone temperature above 60°C bone necrosis is probable and for a temperature below 48°C it is improbable. Between 48 and 60°C it depends on the exposure time; for a temperature of 50°C the threshold exposure time may be between 30 sec (Lundskog, 1972) and 400 sec (Moritz and Henriques, 1947) as regards cell necrosis.
In analyzing a number of situations in which bone cement is used for fixation of implants, it was found that the maximal bone-temperature values to be expected are precisely within this range. Because of this, no definite answer can be given to the question whether thermal damage occurs or not; the possibilities certainly exist and much will depend on the specific circumstances. No doubt this is also the reason for the variety in results of animal and laboratory experiments, published on this problem.

It was shown that in surface fixation using plastic implants, for instance the acetabular cup, there is a higher chance of bone necrosis than in intramedullary fixation, using metal implants. Nevertheless in the first case, too, the maximal bone temperature will probably not be higher than 60°C. The higher temperatures that have been reported in the literature were probably measured in the cement part of the cement-bone interface. Very high temperatures will only occur locally, in the tips of trabeculae surrounded by cement.
More definite data could be obtained in using the methods described here if certain properties of the bone-prosthesis system were established with better accuracy by experiment. Guidelines for such experiments, as followed from the analyses, have been discussed in chapter 7. Due to individual differences and random influences, however, a considerable scatter in the data will always remain. It is, for instance, frequently mentioned in the literature that the results of Moritz and Henriques (1947), Kuhl *et al* (1954) and Lundskog (1972)

with respect to the thermal threshold levels for cell necrosis are not significantly different (e.g. Kuhl *et al*, 1954; Lundskog, 1972; Feith, 1975). As was shown here, however, the differences in their levels more-or-less coincide with the upper and lower boundaries of the probable bone temperature values. Hence, narrowing of this probable range would give no better answer. More progress could be expected from applying more detailed theoretical analyses of the cement-bone interface region, using the approximative results presented here as boundary conditions and combining the theoretical studies with experimental histological data.

It was established that results of animal experiments are not representative of humans as far as heat generation and conduction aspects are concerned, owing to the differences in dimensions.
By simulating the rabbit experiments of Feith (1975) and combining the theoretical and experimental results, the hypothesis evolved that the temperature has an indirect effect, by means of the influences on the monomer reactions, rather than a direct effect on the tissue necrosis. Whether this is true or not, it would in any case be better to reduce the temperatures as much as possible. This can certainly be accomplished by taking certain precautions. In the literature some possible ones have been investigated; the measures proposed were mostly partial and drastic, most often resulting in a cement of inferior quality. It could be established here that certain quite simple and effective measures can be taken that will not prejudice the cement quality and that very good results can be expected if a number of slight measures are combined.
The most remarkable influence is exerted by the local bone and blood temperature prior to cement insertion. It should be quite possible to cool this region to 30°C or even 25°C, which will drastically decrease the maximal bone temperatures. Also, the cement layer dimensions could be restricted as far as possible and the geometry of the implant bed could be made smooth and concave in the macroscopic sense.
The in situ curing cement is in essence only needed to adapt the smooth implant to the irregular bone. Hence the thickness of this cement layer would not necessarily have to be more than dictated by the dimensions of the irregularities. Where only fillings are required, pre-polymerized materials could be used as well.

REFERENCES

Balasubramanian, T.A., Bowman, H.F., Woods, M. and Judge, A. (1977); Thermal transport properties of selected human tissues; paper no. 125; 3th Ann. Meeting of the Soc. for Biomaterials, New Orleans, Louisiana.

Barrett, E.P., Jonnard, A. and Missmer, J.H. (1953); Some physical properties of bone char. and synthad.; Indust. Eng. Chem. 45, 1524-1526.

Biehl, G., Harms, J. and Hauser, U. (1974); Experimentelle Untersuchungen über die Wärmeentwicklung im Knochen bei der Polymerisation von Knochenzement; Arch. Orthop. Unfall. Chir. 78, 62-69.

Bowman, H.F., Murphy, K.G., Balasubramanian, M. and Judge, A. (1979); Thermal conductivity of selected human tissue; 5th Ann. Meeting Soc. Biomaterials, Clemson, So.Car., April-May.

Brekelmans, W.A.M. (1975); Een werkwijze voor het numeriek oplossen van een bepaald type elliptische differentiaalvergelijkingen; Report WE-75-03, Dept. Applied Mech., Mech. Eng., Eindhoven Univ. of Technology.

Cameron, H.U., Jacob, R., McNab, I. and Pilliar, R.M. (1975); Use of polymethylmethacrylate to enhance screw fixation in bone; J. Bone Jt. Surg. 57-A, no. 5, 655-656.

Carlslaw, H.S. and Jaeger, J.C. (1959); Conduction of heat in solids; Oxford Univ. Press.

Charnley, J. (1970); Acrylic cement in orthopaedic surgery; E. and S. Livingstone; Edinburgh and London.

Chato, J.C. (1965); A survey of thermal conductivity and diffusivity data on biological materials; 5th. Conf. on Thermal Conductivity; Vol. 2, sessions IV-VI, Denver, Col.

Clattenburg, R., Cohen, J., Conners, S. and Cook, N. (1975); Thermal properties of cancellous bone; J. Biomed. Mat. Res., vol. 9, 169-182.

Cohen, J. (1978); Private communication.

Debrunner, H.U., Wettstein, A. and Hofer, P. (1976); The polymerization of selfcuring acrylic cements and problems due to the cement anchorage of joint prostheses; **In:** Advances in Artificial Hip and Knee Joint Technology; (Schaldach, M. and Hohmann, D., eds.); Springer-Verlag, Berlin, Heidelberg, New York.

Dipisa, J.A., Sih, G.S. and Berman, A.T. (1976); The temperature problem at the bone-acrylic cement interface of the total hip replacement; Clin. Orthop. and Rel. Res. 121, 95-98.

D'Souza, N., Stachiewicz, J.W., Miller, J., Ahmed, A.M. and Burke, D.L. (1977); Thermal analysis of axisymmetric bone implants using selfcuring polymethylmethacrylate; paper no. 57, 3rd Ann. Meeting of the Soc. for Biomaterials; New Orleans, Louis.

Eckert, E.R.G. and Drake, R.M.Jr. (1972); Analysis of heat and mass transfer; McGraw Hill, Kogakusha, Tokyo.

Feith, R. (1975); Side-effects of acrylic cement, implanted into bone; Suppl. nr. 161, Acta Orthop. Scand.

Frados, J. (ed.) (1966); Modern Plastics Encyclopedia 1967; Modern Plastics vol. 44, p. 41.

Fried, E. (1969); Thermal conduction contribution to heat transfer at contacts; **In:** Thermal conductivity; (Tye, R.P., ed.); Acad. press, London and New York.

Graf, K. und Stein, E. (1957); Fortlaufende Registrierung der Knochenmarkdurchblutung des Menschen mit der Wärmeleitsonde; Zeitschrift f. die gesamte exp. Medizin, Bd. 129, s. 1-14.

Gröber, Erk und Grigull (1961); Wärmeübertragung; Springer-Verlag, Berlin.

Henschel, C.J. (1943); Heat impact of revolving instruments on vital dentin tubules; J. Dent. Res. no. 22, p. 323.

d'Hollander, A., Burny, F., Monteny, E. and Donkerwolcke, M. (1976); Extra-osseous variations of temperature during polymerization of acrylic cement in hip arthroplasties; Acta Orthop. Scand. 47, pp. 186-188.
Homsy, C.A., Tullos, H.S., Anderson, M.S., Differante, N.M. and King, J.W. (1972); Some physiological aspects of prosthesis stabilization with acrylic polymer; Clin. Orthop. and Rel. Res.,, 83, pp. 317-328.
Huiskes, R. (1977); Warmte-afvoer van zelfhardend botcement; Report no. RH-77-02, Lab. Exp. Orthop., Dept. Orthop., Univ. of Nijmegen, The Netherlands.
Huiskes, R., de Wijn, J.R., Slooff, T.J.J.H. and van Rens, Th.J.G. (1977); Thermodynamic FEM analysis of self-curing bone cements (PMMA); 1st Eur. Conf. on Evaluation of Biomaterials; Strasbourg, September (acc. for publication in Advances in Biomaterials, Winter and Leray, eds.).
Huiskes, R. (1978); Warming-up of acrylic cement, assuming non-linear heat capacity properties; unpublished data.
Huiskes, R., and Slooff, T.J.J.H. (1978); Temperature values in bone tissue during implantation of self-curing PMMA; Eur. Soc. of Biomaterials, Brussels, May.
Huiskes, R., and de Wijn, J.R. (1978); Heat conduction in acrylic bone cement, a thermodynamic analysis; 24th Ann. Meeting Orthop. Res. Soc., Dallas, Tex., Febr. (publ. Transactions J. Bone Jt. Surg. vol. 2, no. 1).
Huiskes, R. (1979a); Thermal tissue damage by acrylic cements; 25th Ann. Meeting Orthop. Res. Soc., San Francisco, Cal., February (to be published in Transactions J. Bone Jt. Surg. 1979).
Huiskes, R. (1979b); Solution of the diffusion-convection equation, using FEM; Report ORa-79-05; Lab. Exp. Orthop., Dept. Orthop., Univ. of Nijmegen, The Netherlands.
Huiskes, R., de Wijn, J.R. and Slooff, T.J.J.H. (1979); Heat analysis of self-curing PMMA as used in bone cements; 3rd Int. Conf. Plastics in Med. and Surg.; Enschede, Netherlands, June.
Hupfauer, W. und Ulatowski, L. (1972); Die Temperaturenentwicklung verschiedener Knochenzemente während des Abhärtungsvorganges; Arch. Orthop. Unfall.-Chir. 72, 174-184.
Jacobs, R.B. and Starr, C. (1939); Thermal conductance of metallic contacts; Rev. Scient. Instrum. 10, 140.
Jefferiss, C.D., Lee, A.J.C. and Ling, R.S.M. (1975); Thermal aspects of self-curing polymethylmethacrylate; J. Bone Jt. Surg. 57-B, no. 4, pp. 511-518.
Kaye, G.W.C. and Laby, T.H. (1959); Tables of physical and chemical constants and some mathematical functions; Longmann, London.
Kuhl, P.R., Sheline, G.E. and Alpen, E.L. (1954); Blister formation and tissue temperature in radiant energy and contact burns; Amer. J. Pathol. 30, p. 695.
Kummer, B.K.F. (1972); Biomechanics of bone; In: Biomechanics, its foundation and objectives (Y.C. Fung, ed.); Englewood Cliffe, N.J.; Prentice Hall.
Labitzke Paulus, M. (1974); Intraoperative Temperaturmessungen in der Hüftchirurgie während der Polymerisation des Knochenzementes Palacos; Arch. Orthop. Unfall.-Chir. 79, 341-346.
Leach, E.H., Peters, R.A. and Rossiter, R.J. (1943); Experimental thermal burns, especially the moderate temperature burn; Quart. J. Exp. Physiol. 32, 67.
Lee, H.B. and Turner, D.T. (1977); Temperature control of a bone cement by addition of crystalline monomer; J. Biomed. Mat. Res., 11, 671-676.
Lehnartz, E. (1959); Chemische Physiologie; Springer-Verlag, Berlin, Göttingen, Heidelberg.
Lundskog, J. (1972); Heat and bone tissue; Scand. J. of Plastics and Reconstr. Surg.; suppl. 9.
Meyer, J.R., Lautenschlager, E.P. and Moore, E.K. (1973); On the setting properties of acrylic bone cement; J. Bone Jt. Surg. 55-A, 149-156.

Moritz, A.R. and Henriques, F.C.Jr. (1947); Studies of thermal injury II; Am. J. Path. 23, 695.
Moritz, A.R. (1947); Studies of thermal injury III; Am. J. Path. 23, 915.
Müller, K. (1975); Verhalten von Knochenzementen unter Körperähnlichen Umgebungs Bedingungen; **In:** Die Knochenzemente (Oest *et al* eds.); Ferdinand Enke Verlag, Stuttgart.
Naylor, M.A. and Billmeyer, F.W. (1953); A new apparatus for rate studies applied to the photopolymerization of methylmethacrylate; J. Am. Chem. Soc., 75, 2181-2184.
Oest, O., Müller, K. und Hupfauer, W. (1975); Die Knochenzemente; Ferd. Enke Verlag, Stuttgart.
Ohnsorge, J. und Goebel, G. (1969); Oberflächentemperaturen des abhärtenden Knochenzementes Palacos beim Verankern von Metallendoprothesen im Oberschenkelmarkraum; Arch. Orthop. Unfall.-Chir. 67, 89-100.
Ohnsorge, J. und Kroesen, A. (1969); Thermoelektrische Temperaturmessungen des abhärtender Knochenzementes "Palacos"; Z. Orthop. 106, 476-482.
Ohnsorge, J. und Goebel, G. (1970); Die Verwendung unterkühlter Metallendoprothesen in der Hüftchirurgie; Z. Orthop. 107, 683-696.
Rhinelander, F.W. (1972); Circulation in bone; **In:** The biochemistry and physiology of bone (Bourne, G.H., ed.); 2nd ed. vol. II; Academic Press, New York.
Saulgozis, Y., Slutskii, L.I., Knets, I.V. and Yanson, Kh.A. (1974); Investigation of the relations between the various mechanical properties and the biochemical composition of human bone tissue; Polymer Mechanics 9/1, 119-125.
Schoofs, A.J.G., van Beukering, L.H.Th.M. en Sluiter, M.L.C. (1978); Triquamesh; Progel-report PRGL-1/O-R 78/1; Report No. WE-78-01, Dept. Applied Mech., Mech. Eng., Eindhoven Univ. of Technology, The Netherlands.
Seidel, H., Eggert, A. und Piettsch, H. (1977); Intraoperative Temperaturmessungen an der Zementknochengrenze bei TEP-Implantation; Arch. Orthop. Unfall.-Chir. 90, pp. 251-257.
Sevitt, S. (1957); Burns, pathology and therapeutic applications; Butterworth Cie, London.
Sundén, G. (1967); Some aspects of longitudinal bone growth; Acta Orthop. Scand. Suppl. No. 103.
Swenson, L.W., Jr., Schurman, D.J. and Piziali, R. (1976); Thermal analysis of total hip replacements using PMMA bone cement; 22nd Ann. Meeting Orthop. Res. Soc., San Franciso, Cal., February.
Trommsdorf, E. (1963); Polymerisate der Acrylsaüre, ihrer Homologe und Derivate; **In:** Chemie und Technologie der Kunststoffe (Houwelink, R. und Staverman, A.J., eds.), Bd. II/I; Akad. Verlagsges. Leipzig, 541-599.
Vachon, R.I., Walker, F.J., Walker, D.F. and Nix, G.H. (1967); In vivo determination of thermal conductivity of bone using the thermal comparator technique; 7th. Int. Conf. on Med. and Biol. Eng., Stockholm; session 37.
Viidik, A. (1972); Functional properties of collagenous tissues; Int. Rev. of Conn. Tissue Res., Vol. VI (Hall, D.A. and Jackson, D.S., eds.); Academic Press, New York.
Wilson, E.L. and Nickell, R.E. (1966); Application of the FEM to heat conduction analyses; Nucl. Eng. and Des., 4, pp. 276-288.
Wilson, E.L., Bathe, K.J. and Peterson, F.E. (1974); Finite element analysis of linear and nonlinear heat transfer; Nucl. Eng. and Des., 29, 110-124.
Wijn, de J.R. (1974); Reduction of maximum temperature in the polymerization of cold- and heat-curing acrylic resins; J. Biomed. Mat. Res. vol. 8, 421-434.
Wijn, de J.R. (1977); Private communication.
Wijn, de J.R., Mullem, P.J. van, Ypma, J., Huiskes, R. and Slooff, T.J.J.H. (1978); Development of polymethylmethacrylate-aqueous gel bone cements; parts I and II; Report Cement Group, Lab. Exp. Orthop. and Lab. Dent. Mat. Res., Univ. of Nijmegen, the Netherlands.
Zienkiewicz, O.C. (1977); The Finite Element Methods; 3rd ed.; McGraw-Hill, Ltd. London.

SECTION THREE

STRESS ANALYSES OF INTRAMEDULLARY FIXATION SYSTEMS

CONTENTS

LIST OF SYMBOLS

In the following list of symbols, where i or j occur as indices, they either denote b (for bone), c (for cement) or s (for stem).

geometrical parameters

L_b	mm	bone length
L	mm	fixated stem length
L_f	mm	free stem length
r_s	mm	stem radius
d_s	mm	stem diameter
r_b	mm	inner bone radius
d_b	mm	inner bone diameter
r_o	mm	outer bone radius
d_o	mm	outer bone diameter
ρ	mm	ratio r_s/r_b
γ_s	mm	outer circumference of the stem
γ_b	mm	inner circumference of the bone
d	mm	stem thickness in y-direction (plane model), see paragraph 5.5.

reference systems

x, y, z	mm	rectangular coordinate system
r, φ, z	mm	cylindrical coordinate system
ξ	mm	coordinate in negative z-direction ($\xi = L - z$), see paragraph 5.3.

materials properties

E_i	N/mm^2	Young's modulus
ν_i	-	Poissons's ratio

loading parameters

X	N	force on the proximal end of the free stem region in negative x-direction (see fig. 3.1)
Z	N	force on the proximal end of the free stem region in negative z-direction (see fig. 3.1)
M	Nmm	bending moment on the proximal end of the free stem region around the y-axis (see fig. 3.1)
$M_i(z)$	Nmm	bending moment in bone, layer or stem

$M(z)$	Nmm	total bending moment in cross-section ($M = M_b + M_s + M_c$)
M_L	Nmm	bending moment in the stem, at $z = L$ (fig. 5.8)
M_0	Nmm	bending moment in the bone, at $z = 0$ (fig. 5.8)
$N_i(z)$	N	normal (axial) force in bone, layer or stem (positive z-direction)
$N(z)$	N	total normal force in cross-section ($N = N_b + N_s + N_c$)
N_L	N	normal force in the stem at $z = L$ (see fig. 5.11)
N_0	N	normal force in the bone, at $z = 0$ (fig. 5.11)
$T_i(z)$	N	transverse force in bone, layer or stem (positive z-direction)
$T(z)$	N	total transverse force in cross-section ($T = T_b + T_s + T_c$)
T_L	N	transverse force in the stem, at $z = L$ (see fig. 5.8)
T_0	N	transverse force in the bone, at $z = 0$ (see fig. 5.8)
$p_s(z)$	N/mm	continuously distributed transverse load exerted by the cement layer on the stem (fig. 5.9)
$p_b(z)$	N/mm	continuously distributed transverse load exerted by the cement layer on the bone (fig. 5.9)
$p(z)$	N/mm	as p_s and p_b, if both are assumed equal
$q_s(z)$	N/mm	continuously distributed shearing load exerted by the cement layer on the stem (fig. 5.11)
$q_b(z)$	N/mm	continuously distributed shearing load exerted by the cement layer on the bone (fig. 5.11)
$q(z)$	N/mm	as q_s and q_b, if both are assumed equal

displacements

$u_s(z)$	mm	deflection of the stem neutral axis in x-direction
$u_b(z)$	mm	deflection of the bone neutral axis in x-direction
$w_s(z)$	mm	displacement of the stem in z-direction
$w_b(z)$	mm	displacement of the bone in z-direction

cross-sectional parameters

A_i	mm^2	cross-sectional area
W_i	mm^3	moment of resistance
I_i	mm^4	second moment of inertia
P_i	N	compressional stiffness ($P_i = E_i A_i$)
F_i	Nmm^2	flexural stiffness ($F_i = E_i I_i$)
C_a	N/mm^2	stiffness of the cement layer against axial loading (shear)
C_t	N/mm^2	stiffness of the cement layer against transverse loading
λ_a	mm^{-1}	coefficient for axial loading
λ_t	mm^{-1}	coefficient for transverse loading

stress parameters

$\sigma_r, \sigma_t, \sigma_z$	N/mm^2	direct stresses (table 3.III)
$\tau_{rt}, \tau_{rz}, \tau_{tz}$	N/mm^2	shear stresses (table 3.III)
$\hat{\sigma}, \hat{\tau}$	N/mm^2	stress 'amplitudes' (paragraph 5.1)
σ_1, σ_2	N/mm^2	principal stresses
σ_{eq}	N/mm^2	equivalent stress (chapter 3)
$s_{zi}(z)$	N/mm^2	maximal axial stress (σ_z) in a cross-section
$\bar{s}_{ri}(z)$	N/mm^2	average normal stress in transverse direction at the stem-cement interface (s) or at the cement-bone interface (b) (paragraph 5.2.1.)
$t_i(z)$	N/mm^2	axial shear stress at the stem-cement interface (s) or at the cement-bone interface (b) (paragraph 5.2.2.)

others

$g(\nu_c)$	–	expression in ν_c (appendix B)
c_1, c_2	–	constants (appendix B)
α, β, ϵ	–	factors (paragraph 7.1.)

CHAPTER ONE

INTRODUCTION

The question as to whether a specific structure will fail or not depends on two different sets of properties. First, the strength of the structure, in this case of the implant, the cement layer, the bone and the connection between these components; second, the loading of the structure in a local sense; in other words, the stress distribution. This last depends solely on: the loading of the structure (the joint loading), the geometry of the structure, the constitutive properties of the materials (for instance their elasticity) and the conditions at the connections of the components (the interfaces).
The strength characteristics of the components can be evaluated by applying laboratory materials testing, the stress distribution by applying stress analyses, either experimental or theoretical. Theoretical analyses may either be analytical, in which case the stress components are directly expressed in formulas that contain the loading, geometrical and materials parameters (closed-form solutions), or numerical, in which case the solution is not available in closed form, but obtained by applying numerical (computer) procedures. Regarding experimental stress analyses, different methods are available (Durelli, 1977) of which only a few are suitable to be used for bone-prosthesis structures (e.g. strain gauges, stress coating, photo-elastic techniques).
It should be the aim of a stress analysis not only to evaluate the stress distribution in specific circumstances, but also to obtain general, fundamental concepts on the relation between the stresses and the loading, geometrical and materials properties or, in other words, to find the characteristic parameters of the structure and evaluate their influences on the mechanical behavior. This aim is best fulfilled by using analytical methods, since in that case the characteristic parameters and variables are directly related in formulas. However, closed-form solutions can usually only be obtained for simple structures, so that often numerical methods will have to be used. By applying parametric analyses in this case, the influences of the structural parameters on the stresses can be evaluated empirically.
Experimental methods are empirical in essence and usually have only few possibilities for parametric analyses, they thus offer only limited options for acquiring fundamental and general data (Huiskes and v. Heugten, 1974).

To conduct a theoretical stress analysis, analytical or numerical, a mathematical model of the structure has to be developed which describes its mechanical behavior to an adequate degree of accuracy. In the case of intramedullary bone-prosthesis structures such a model is far from trivial. In the first place the structure is difficult to describe mathematically, owing to:

- the irregular geometry of the bone;
- the nonhomogeneous, anisotropic and viscoelastic properties of the bone tissue;
- the dynamic character of the joint loading;
- locked-in stresses in the cement mantle, caused by dimensional changes during the polymerization-process;
- the complicated mechanical conditions of the cement-stem and cement-bone contact regions, the 'interfaces', where loosening-upon-tension and slip may occur.

Even if a model taking these complicated properties into account can be set up, it will be difficult to establish the values of the parameters that have to be used in the calculations.

Moreover, the relations between such a refined model and the real structure will be badly defined, because:

- bone geometry, bone material properties and loading characteristics vary considerably from patient to patient;
- the mechanical characteristics of the bone-prosthesis structure depend on the surgical procedure, which may vary to a great extent;
- the bone geometry, the bone-material properties and the interface conditions may undergo gradual postoperative change due to bone remodeling.

Altogether, a detailed accurate theoretical analysis of the mechanical behavior of specific bone-prosthesis structures is an unrealistic goal as yet. However, general, fundamental concepts of the influences of the essential characteristics of such a structure can be obtained and tendencies can be studied by analyzing simplified models using both analytical and numerical methods, as will be shown in this section.

A survey of the literature on previous work is given in the following chapter.

In the third chapter a simplified (general) model of intramedullary fixation systems is introduced. This model is analyzed using different methods, as described in chapter 5. The analyses provide the essential characteristics of the bone-prosthesis structure and a number of simple formulas to approximate the most important stress values in the stem, the cement and the bone. A simple and rapid numerical evaluation method for specific stem designs and their expected mechanical performance in a given bone will also be developed.

Results of an experimental stress analysis, that serve as references for the theoretical results, will be briefly discussed in the fourth chapter.

The theoretical model is an abstraction of the real system, of which many complicated aspects are neglected. The possible influences of these aspects are discussed in chapter 6.

In the last chapters some guidelines will be given for implant designs and implantation procedures, as derived from the analyses. Due to the fact that the hip joint is by far the one most often replaced and that most data available concern the proximal femur, the following analyses are focussed on hip endoprostheses. It should be kept in mind, however, that the methods and some of the results can be generalized to apply to other intramedullary-fixated artificial joints as well.

CHAPTER TWO

REVIEW OF LITERATURE ON RELEVANT THEORETICAL STRESS ANALYSES

Scientists have long been interested in stresses and strains in human bones. The first sophisticated stress analysis of a human bone, the proximal femur, was published by Meyer in 1867. This work was repeated and extended by Wolff (1870) and resulted in the well known hypothesis on the functional stress-related adaption of the bone structure. Koch (1917) confirmed this hypothesis after analyzing a cadaveric femur with beam theory and promoted it to 'Wolff's law'. Beam theory was later used for stress analyses of the human femur by Toridis (1969), this time taking three-dimensional loading and geometry into account, by Rybicki *et al* (1972), who compared the results with more sophisticated stress analyses methods (Finite Elements), and by Scholten (1975), who took three-dimensional geometry and non-homogeneous material properties into account and also applied Finite Element Methods. Although frequently used, it has not been verified whether the assumptions of linear elastic beam theory apply to the mechanical behavior of the femur, a problem investigated in our group and which will be discussed briefly in chapter 4.

As in other areas of solid mechanics, biomechanics research has greatly benifited from the introduction of Finite Element Methods (FEM), a computer-oriented method for stress analyses, eminently suitable for arbitrarily shaped structures with arbitrary loading and materials properties (e.g. Zienkiewicz, 1977). This method was introduced into the orthopedic biomechanics field as an expedient for structural analyses of bone, by Brekelmans *et al* (1972) and Rybicki *et al* (1972) simultaneously. Both presented relatively simple plane-stress models of the femur. FEM models developed in later years by other investigators became more refined, especially in their geometrical aspects. With few exceptions, all concerned the femur.

Wood *et al* (1973, 1975) presented a plane-stress model of the proximal femur, taking non-uniform thickness into account. Olofsson (1975, 1976) analyzed a truly three-dimensional FEM model of the intact femur. The problems of data manipulation, interpretation and representation that are still connected with such complex models, are reflected in his work. His calculations took up huge amounts of computer time, leaving few possibilities for parametric analyses.

Quite refined and accurate two-dimensional and three-dimensional FEM models of the proximal femur were developed by Scholten (1975). Geometry and elastic properties (non-homogeneous) were exclusively measured for these calculations. The results were compared with beam models, an example of which is shown in fig. 2.1.

A somewhat less refined three-dimensional model was reported by Valliapan *et al* (1977). They varied the joint loading and compared the results with a two-dimensional analysis, a beam analysis and an experimental strain analysis. Agreement was good in the relative sense, but poor in the absolute sense, especially in the proximal-medial region, which they attributed to discrepancies between the modeled and real bone-geometrical and material properties. A three-dimensional anisotropic FEM analysis of the femur was carried out by Vichnin and Batterman (1977), who used geometrical data measured by Laaper (1973a).

Harris *et al* (1978), too, analyzed a three-dimensional model of the proximal femur and compared the results with a two-dimensional and a beam model; agreements appear to be reasonable.

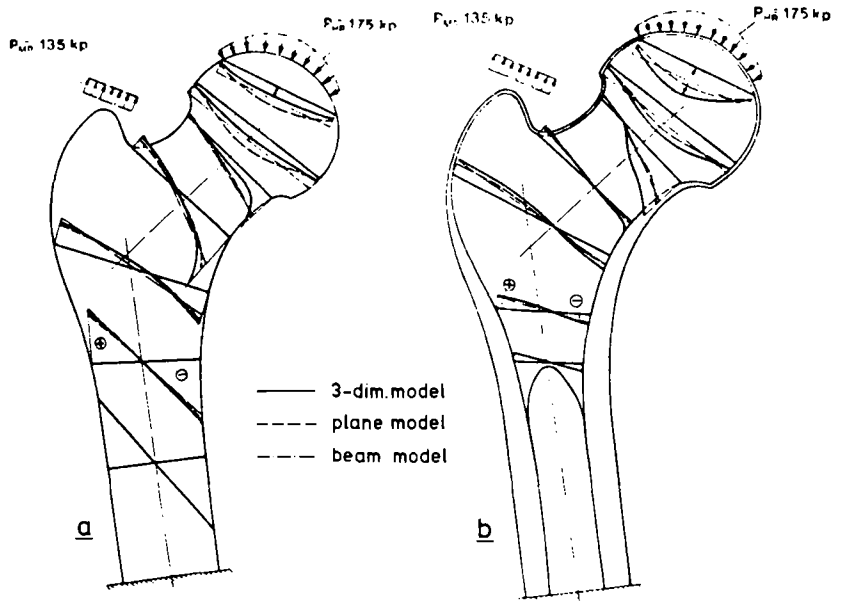

fig. 2.1: Comparison of a three-dimensional FEM model, a two-dimensional FEM model and a beam model of the proximal femur. Axial direct stresses in the cortex (a) and in the spongeous bone (b) are shown. The plane shown is a plane of symmetry in the three models. Up to the neck region the agreement is rather good (reproduced with permission of Scholten, 1975).

With the object of verifying certain assumptions in the process of modeling, Rohlmann *et al* (1977, 1978) analyzed a longitudinal slice of the femur, using FEM and strain gauges. They also analyzed a three-dimensional model with FEM (Rohlmann *et al*, 1979), the results of which they compared with those of strain-gauge experiments on a cadaveric femur. They found poor agreement in the absolute sense and concluded that in a FEM model a quite refined element mesh should be used, the boundaries between spongeous and cortical bone should be accurately evaluated and modeled and the exact ratio of stiffness properties should be taken into account.
Apart from the femur, the tibia has received some attention in structural analysis. Chand *et al* (1976) published a two-dimensional FEM analysis of the knee joint and Hayes *et al* (1978) reported a three-dimensional analysis of an axisymmetric model of the proximal tibia. The full tibia was analyzed by Piziali *et al* (1976) and by Minns *et al* (1977).

In the meantime theoretical stress analyses of bone-prosthesis structures were published, again usually on the femoral part of the hip joint. A plane-stress FEM model of the proximal femur with three different types of prostheses was reported by McNeice *et al* (1975) and McNeice and Amstutz (1976). Based on their studies they defined 4 different failure modes for cement fracture, which they later used to evaluate results of total hip replacements radiographically (McNeice and Gruen, 1976; Gruen and Amstutz, 1977). Their model will be discussed further in paragraph 5.5.
Forte (1975) carried out a FEM beam analysis of a prosthesis stem with the object of optimizing its shape; a quite unrealistic model, since the important mechanical interaction with the bone was completely ignored.

A simplified axisymmetric model of an intramedullary fixation system using three-dimensional FEM and composite beam theory was analyzed by Bartel and Ulsoy (1975), Bartel and Samehyek (1976), Bartel and Desormeaux (1976a, 1976b). Thanks to a reduction in the number of geometrical parameters, these studies resulted in a more general comprehension of the mechanical behavior than did other, more complicated studies.
Andriacchi *et al* (1975) used a plane-stress FEM analysis to study the proximal femur with different kinds of prostheses implanted in neutral, varus and valgus positions. Since in their model there was no connection between the medial and the lateral cortex, they in fact analyzed a kind of sandwich construction that can hardly be expected to be a reliable representation of the real system, as will be discussed in paragraph 5.5.
The same method was applied by Kwak *et al* (1979), who studied the influences of the cement layer thickness in a two-dimensional FEM model of the proximal femur with an implanted Charnley prosthesis.
A better method was presented by Hampton *et al* (1976) who analyzed a comparable plane-stress model, but took the full stiffness properties of the femur into account by modeling a side plate or 'spanning-element' layer between the medial and the lateral cortex. They also developed a three-dimensional FEM model of the same structure.
Svensson *et al* (1977) presented a two-dimensional FEM model, taking three-dimensional geometry into account and also using 'spanning-element' layers to model the medial-lateral bone connection. They found a reasonable qualitative agreement between the calculated stresses at the bone surface and results of stress-coating experiments carried out by Brockhurst (1975). They simulated different stem designs and elastic layer properties and concluded that, by using a thick stem, most of the critical stresses will be reduced. They were the first to investigate the influences of the interface conditions. In one calculation they assumed the stem-cement connection as allowing slip and no tension and found a completely different stress distribution at the interfaces compared to the results of calculations in which the materials were assumed to be rigidly connected.

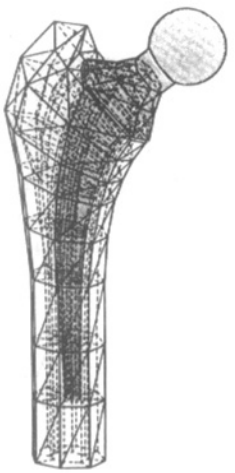

fig. 2.2: Element mesh of a three-dimensional FEM model of the proximal femur with implanted hip prosthesis. This and comparable models, analyzed by Röhrle et al (1977, 1979) and Scholten et al (1978) are the most detailed ones in the present literature with respect to geometrical and material representation (reproduced with permission of Röhrle et al, 1979).

Probably the most detailed FEM analyses of the proximal femur with implanted prostheses were carried out by Röhrle *et al* (1977, 1979) and Scholten *et al* (1978). Their models were truly three-dimensional, using adequately refined element meshes (fig. 2.2); non-homogeneous bone properties were taken into account as well as three-dimensional loading. Interfaces were modeled as either allowing or not allowing slip and otherwise rigidly connected. These models were used in comparative studies to evaluate specific designs and to answer specific questions with respect to design features as, for instance the influences of calcar support or the stiffness of the intermediate layer.
Another three-dimensional FEM analysis of the proximal femur with an implanted hip prosthesis was reported by Crowninshield *et al* (1979), who had earlier analyzed the influences of cross-sectional stem shapes (Crowninshield and Branch, 1978). They carried out parametric analyses, varying Young's moduli of stem and cement, stem thickness and stem length. Based on their results they advocate a decrease of cement stiffness and an increase of stem length, thickness and stiffness in order to decrease the cement stresses. Their calculations were compared to simple strain-gauge experiments, resulting in qualitatively reasonable agreement for femoral surface stresses. In their model the different materials were assumed to be rigidly connected at the interfaces.
A detailed three-dimensional FEM analysis was reported by Tarr *et al* (1979). In a model using a rather coarse element mesh, a cobalt-chromium and a more flexible titanium alloy stem were simulated. They found that stresses in the stem and in the distal cement layer were lower with the titanium alloy, while stresses in the proximal cement layer were higher. Comparison of results with a simple strain-gauge experiment on a cadaveric femur gave poor absolute, but reasonable qualitative agreement.

An interesting venture was undertaken by Rohlmann *et al* (1979), who analyzed a model of a hip endoprosthesis cemented into a brass tube, using three-dimensional FEM (a model with 1600 degrees of freedom) and also strain-gauge experiments. They found rather poor continuity of stresses at the interfaces in the calculations and only moderate agreement between experimental and theoretical results, both of which they ascribed to the coarseness of the element mesh, indicating that in the three-dimensional FEM models quite a high level of mesh refinement is needed.
Another approach to structural analysis of intramedullary fixation systems was followed by an Italian group (Calderale *et al*, 1977; Barberi *et al*, 1978; Gola and Gugliotta, 1979), who modeled the femur and the prosthesis stem as cantilever beams, coupled by an elastic (cement) layer. The model was analyzed numerically, using minimal potential energy.criteria. The model can be applied for transverse loading only. The stiffness of the elastic layer was evaluated experimentally. Although the information resulting from analyses of this kind is limited, they are quite simple and can conveniently be used for a first-order rapid evaluation of stem designs.

Where intramedullary fixation is concerned, few efforts have been put into sophisticated theoretical analyses of other than hip endoprostheses. Van Campen *et al* (1978, 1979) reported two- and three-dimensional FEM analyses of the tibial stem fixation of a hinged artificial knee joint, comparing the results with strain-gauge experiments. A three-dimensional FEM analysis of a new intramedullary fixation system for artificial finger joints was carried out in our group (Huiskes and v. Heck, 1978; Huiskes *et al*, 1979).
Theoretical stress analyses of other than intramedullary fixated prostheses, at least not mainly fixated in this manner, have been carried out for tibial components of artificial knee joints (Chao *et al*, 1977; Lewis, 1977; Askew *et al*, 1978, 1979; Hayes, 1978) and for the hip-surface replacement (v. Heck and Huiskes, 1979).

Because of the many complicated features of bone-prosthesis structures and the usually uncertain numerical values of parameters, one cannot expect to be able to develop a mathematical model that will predict the stress distribution in the real structure in an absolute sense. This fact is recognized by most of the authors previously cited and it is often remarked that, because of the possibilities for parametric analyses in the models, they can still contribute to a better comprehension of the mechanical behavior. Although this is true in general, the overall picture of the work previously discussed is rather confusing. This is due to the fact that many of the complex models used are rather specific and little is known about the influences of simplifying assumptions; this often places the analysis procedures in a frame of 'numerical empiricism' (Oden and Bathe, 1978) and results in anything but general concepts. Hence, the results of the analyses are sometimes in conflict and are usually quite specific. To acquire more general data a model should be relatively simple, with options for either extensive parametric analysis or closed-form solutions. Therefore, detailed three-dimensional FEM models are not very suitable to fulfil this aim due to their complexity and also, at least contemporarily, to the excessive computer time and data manipulation efforts needed, thus limiting the possibilities for extensive parameter variation. Moreover, it appears to be rather illogical to use a model that is quite refined in its geometrical aspects, while rough in the other aspects, such as those summarized in chapter 1.

In short, it is evident that although many significant contributions to insight in the mechanical behavior of intramedullary bone-prosthesis structures have been presented in the literature, there is a need for more general and fundamental concepts on the relations between structural parameters and mechanical performance. It was the object of the work presented in this section to find the essential characteristics of the structure and to provide such concepts.

CHAPTER THREE

A SIMPLIFIED MODEL OF INTRAMEDULLARY FIXATION STRUCTURES

The model is shown in fig. 3.1. It consists of an axisymmetric 'bone' with an axisymmetric intramedullary stem. Both the stem and the bone have constant cross-sectional properties.

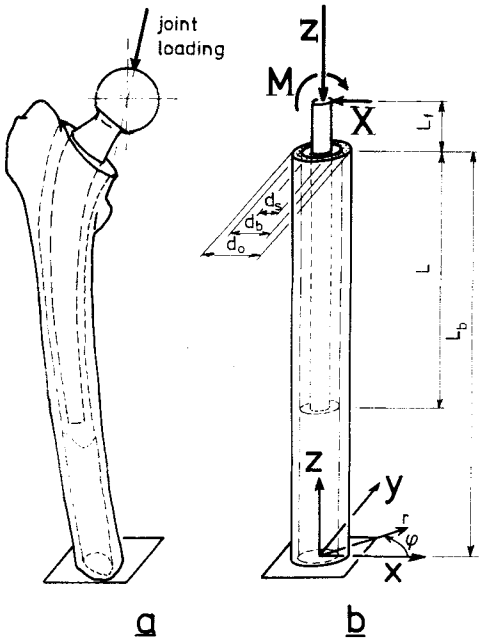

fig. 3.1: The axisymmetric model (b) of an implanted hip endoprosthesis (a); geometrical parameters, coordinate systems and loading are shown.

Between the stem and the bone a layer of acrylic cement, rigidly connected to both the stem and the bone, is assumed. Although the model can be regarded as a general one for any intramedullary fixation structure, the dimensions were chosen according to the hip endoprosthesis, as more-or-less average as reported in the literature (Kempf *et al*, 1976; Laaper, 1973a; Huiskes and Slooff, 1979b). Although dimensions will be varied in the calculations, a set of what will be referred to as 'reference values' is shown in table 3.I.
The stem, layer and bone materials are assumed as behaving linear elastic, isotropic and homogeneous. Values for Young's moduli and Poisson's ratios were chosen as more-or-less average values of those presented in the literature (table 3.II; see also section I).
A three-dimensional state of loading on the stem is assumed, represented by an axial force (Z), a transverse force (X) and a bending moment (M). The stress analyses are carried out for each of these loading cases separately. Since the stresses and deformations in the structure, because of the linear assumptions, are proportional to the load magnitudes, these were chosen arbitrarily as 1,000 N, 100 N and 10,000 Nmm, respectively.

parameter	symbol	unit	value	parameter	symbol	unit	value
bone length	L_b	mm	205	stem cross-sectional area	A_s	mm^2	78.5
cemented stem length	L	mm	80	stem second moment of inertia	I_s	mm^4	490.1
free stem length	L_f	mm	25	bone cross-sectional area	A_b	mm^2	392.7
stem radius	r_s	mm	5	bone second moment of inertia	I_b	mm^4	31,906.8
inner bone radius	r_b	mm	10				
outer bone radius	r_o	mm	15				

table 3.I: Reference values for geometrical and some mechanical parameters in the axi-symmetric (constant cross-section) model.

parameter	symbol (1)	unit	bone (cortical) (2)	stem (steel)	cement
Young's modulus	E	N/mm^2	$2x10^4$	$2x10^5$	$2x10^3$
Poisson's ratio	ν	–	0.33	0.33	0.33

table 3.II: Reference values for the materials properties; (1) subscripts b, s and c refer to bone, stem and cement, respectively; (2) e.g. Evans (1973).

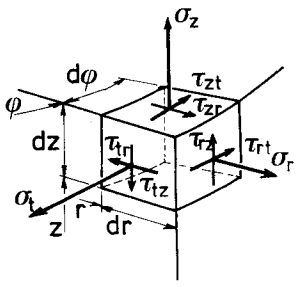

fig. 3.2: The nine components of the stress tensor in a cylindrical coordinate system (r, φ, z).

The state of stress at a point of the structure is described by the three-dimensional stress tensor in a cylindrical coordinate system (r, φ, z) as shown in fig. 3.2. The stress components are described in table 3.III. Due to the action = reaction law, some stress components have to be continuous across the stem-cement and cement-bone interfaces; in this model these components are: σ_r, τ_{rt} and τ_{rz}.
Due to compatibility requirements and differences in elastic moduli of the materials, the other stress components have to be discontinuous across the interfaces. In order to be able to judge the stress state at a point of the structure or simply to reduce the amount of data describing the stress state, an equivalent stress based on a certain failure criterion can be

stress component	names used	stress component	names used
σ_r	radial stress, transverse stress	$\tau_{rt} = \tau_{tr}$	tangential shear stress, circumferential shear stress
σ_t	tangential stress, circumferential stress, hoop stress	$\tau_{rz} = \tau_{zr}$	axial shear stress, longitudinal shear stress
σ_z	axial stress, bending stress	$\tau_{zt} = \tau_{tz}$	transverse shear stress

table 3.III: The six independent stress components of the stress tensor and their terminology.

calculated from the six independent stress components. Here the maximal deformational energy criterion is used, according to Maxwell-Hüber-Hencky-Von Mises:

$$\sigma_{eq} = \sqrt{[\{(\sigma_r-\sigma_t)^2 + (\sigma_r-\sigma_z)^2 + (\sigma_t-\sigma_z)^2\}/2 + 3(\tau_{rt}^2 + \tau_{rz}^2 + \tau_{tz}^2)]}$$

It should be remarked here, that his equivalent stress has proven its value as a yield criterion for such materials as stainless steel. Although it will probably give an indication of the stress state in cement or bone, its value as a yield criterion for these materials is uncertain.

The model presented here will be analyzed using different analytical as well as numerical methods (FEM), as described in chapter 5.
It cannot be expected that with such a simplified model the stress distribution in the real structure can be predicted accurately in an absolute sense, which is obviously not the object of the investigation. It is expected, on the other hand, that the structure is described by the model in a qualitative sense. In order to roughly verify this expectation, the calculated results are compared to results of strain-gauge experiments that will be discussed briefly in the next chapter. In chapter 6 the influences of system parameters that are neglected in this simplified model (thermal stresses, interface loosening, nonconstant cross-sectional properties of the structure, the occurrence of torsional loading and a few others) will be evaluated or at least discussed.

CHAPTER FOUR

AN EXPERIMENTAL STRESS ANALYSIS OF A CADAVERIC FEMUR WITH IMPLANTS

Apart from theoretical stress analyses, as reviewed in chapter 2, also experimental stress and strain analyses of bones, both intact and provided with implants, have been reported. Brittle-coating, photo-elastic, optical and strain-gauge techniques have been used. Many strain-gauge experiments concerning intramedullary fixation structures have been reported recently, devoted, with few exceptions (e.g. v. Campen *et al*, 1978, 1979) to the proximal femur with hip endoprostheses.
The first experiments of this kind were carried out in our group (Slooff, 1970, 1971; Brekelmans en Poort, 1973; v. Heugten, 1974; Huiskes *et al*, 1976; Huiskes, 1978; Huiskes and Slooff, 1979b). Strains were measured on the outside surface of the loaded femur, intact as well as provided with implants. Comparable experiments were conducted by Oh and Harris (1978) who applied only a few strain gauges, but carried out measurements on different bones with different prostheses, by Huggler *et al* (1978) who also attached strain gauges to the prosthesis stem, and by McBeath *et al* (1979). As discussed in chapter 2, more of these experiments have been carried out specifically to verify theoretical results.

The experiments conducted by our group concerned the cadaveric femur of a 52 yr-old man. To the femur, kept in formaline, 112 rosette strain gauges were attached (fig. 4.1.a). Forces on the head in 3 perpendicular directions and couples in 3 planes were applied separately in turn (fig. 4.1.b).
To calculate the measured strain values (three for each strain gauge) to principal stresses, linear elasticity, homogeneity and isotropy was assumed; the bone Young's modulus was taken as 20,000 N/mm^2 and its Poisson's ratio as 0.37.
Equivalent stresses were calculated using the maximal deformational energy criterion of Maxwell-Hüber-Hencky-Von Mises. It should be noted that with such an experimental method the complete strain distribution in the structure can not be measured, but only the strain state at the outside surface. The stresses, calculated from the experimental data, were compared to the corresponding values of stresses as calculated for the model, in this case σ_t, σ_z and $\tau_{zt} = \tau_{tz}$ at the outside surface of the bone.
It was found that in loading by pure couples (up to 12,500 Nmm) the bone showed linear elastic behavior; loading by axial force (up to 1,000 N) resulted in nonlinear behavior. This indicates material linearity and geometrical nonlinearity, which means that due to the bending of the bone, an additional couple is introduced, that increases with the applied load. Some viscoelastic behavior occurred; however, after $3\frac{1}{2}$ min. of constant loading the strains stabilized to constant values. The reproduceability of the strain measurements was better than 5%, even after $2\frac{1}{2}$ years.

The measurements were repeated for the same femur applied with prostheses: Küntscher-nails of three different diameters, hip endoprostheses, fixated with and without cement, with short and long stems and osteosynthesis plates, screwed to the bone. For the present study only the results referring to the intact femur and the femur applied with a short and a long cemented Mueller prosthesis (fig. 4.1.c) are relevant. An example of these results is shown in fig. 4.2. It is evident that the stress state at the outside surface of the proximal femur is influenced by the presence of the stem; the stresses are considerably lower if a

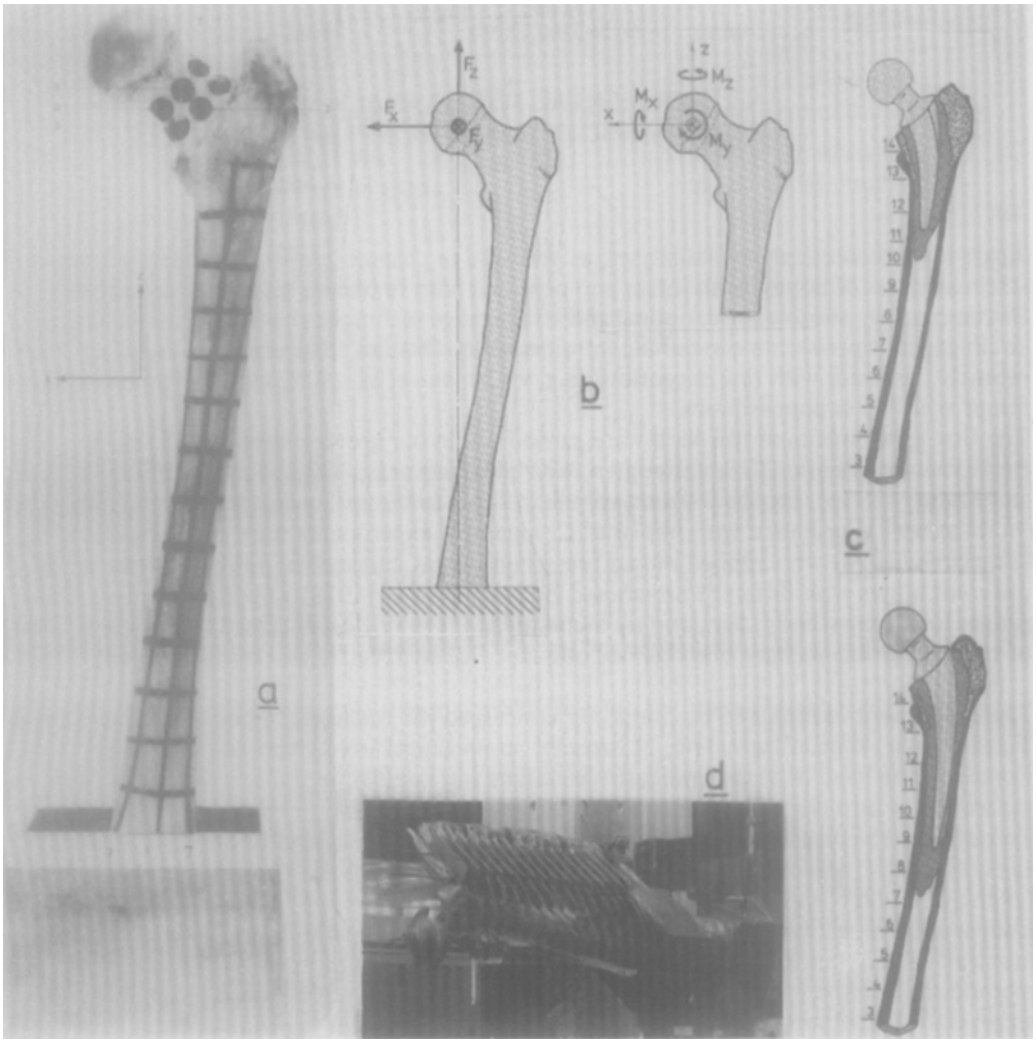

fig. 4.1: Experimental stress analysis of a cadaveric femur. Strain gauges were attached at the crossings of the black lines (a); forces in 3 directions and moments in 3 planes were applied to the head (b); measurements were performed on the intact femur as well as on the femur applied with hip prostheses (c); (d) shows the laboratory setting.

prosthesis stem is present because part of the loading is taken up by the stem. According to Saint Venant's principle there is no influence on the distal side of the bone, hence the strains should be practically equal for the three cases in this region. The graphs in fig. 4.2 will later be compared with results of the model calculations.

The experiments were carried out on the left femur of the cadaver; the right femur was used for detailed measurements of the cross-sectional geometry (Laaper, 1973a).

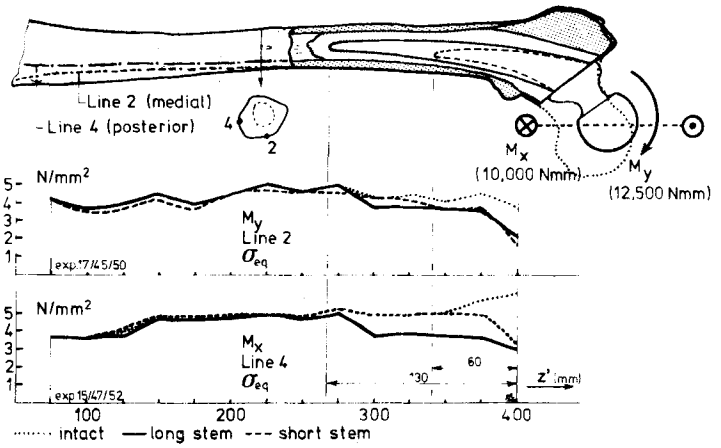

fig. 4.2: Equivalent stresses at the outside surface of the femur, intact and with two endoprostheses of different lengths, loaded with two bending couples in different planes, respectively. Top graph: σ_{eq} on line 2 on loading with M_y; bottom graph: σ_{eq} on line 4 on loading with M_x. The stresses were calculated from the measured strains, assuming homogeneity, isotropy and linear elasticity ($E = 20{,}000\ N/mm^2$, $\nu = 0.37$).

The data from these measurements were used for a three-dimensional beam-theory analysis of the femur (Laaper, 1973b; v. Heugten, 1975; Huiskes and Slooff, 1979b). A comparison of beam-theory results and strain-gauge results, principal stresses at different locations on loading with a couple in the frontal plane, is shown in fig. 4.3.
These results indicate that at least the intact femur behaves approximately in accordance with linear beam theory (which was also found by Scholten (1975) on comparing a beam analysis with a three-dimensional FEM analysis (fig. 2.1)), apart from the mentioned geometrical nonlinearity on loading with forces, especially in the z-direction.
It should be remarked here that the Young's modulus is only used to calculate measured strains to stresses. The agreement with the beam analysis thus indicates a good choice of the value of this parameter.
It is remarkable, regarding figs. 4.2 and 4.3, that although the femur is wider on the proximal side, the strain values over the length of the bone are, roughly speaking, more-or-less constant. This indicates that the flexural stiffness of the bone would be fairly constant, due to the higher flexibility of the bone material (spongeous bone) at the proximal side.

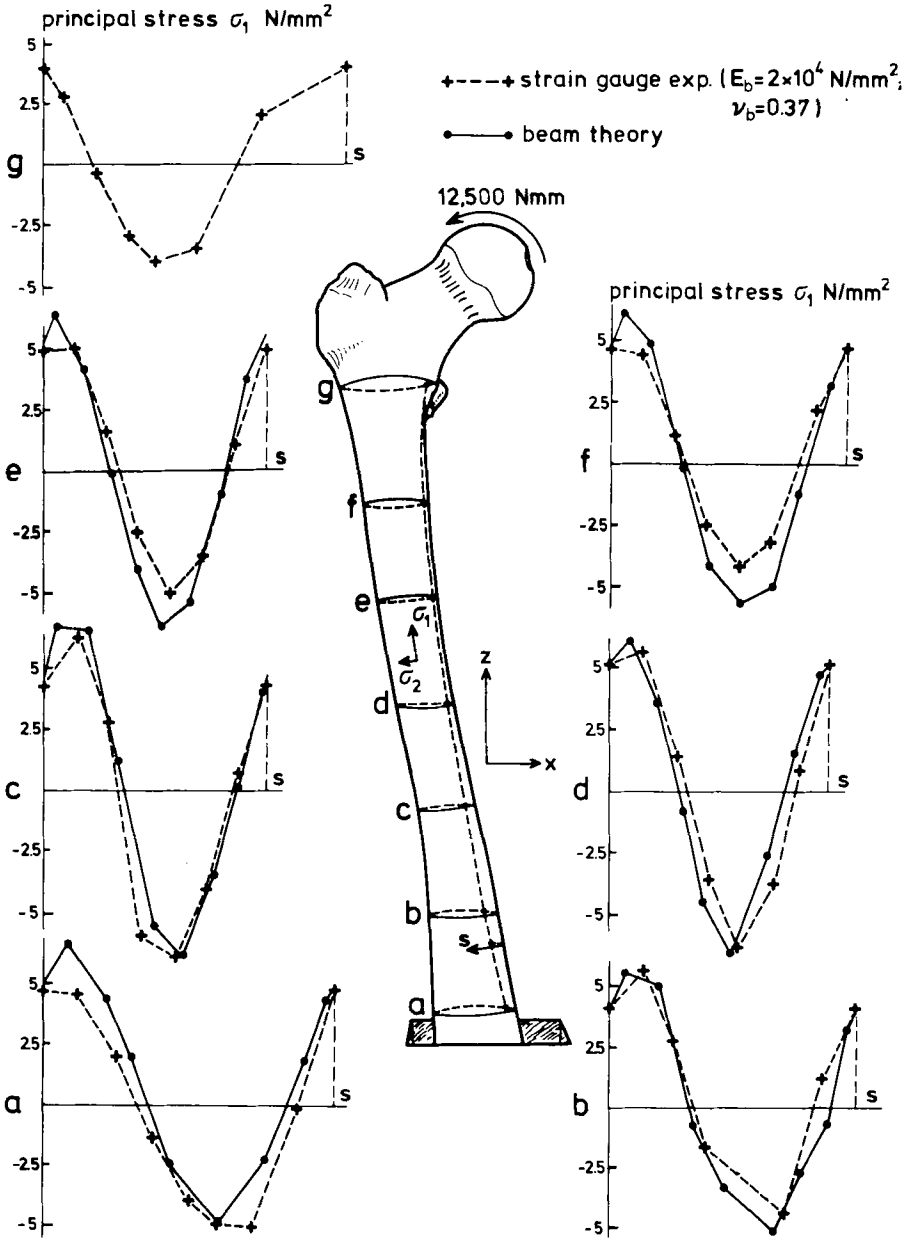

fig. 4.3: Principal stresses (σ_1) on the outside of the femur, as calculated from strain-gauge measurements (left cadaveric femur) and as calculated with beam theory, using cross-sectional geometry data. The beam analysis did not extend further proximally than location f. The principal stress direction is, with good approximation, in that of the femoral axis. For the calculation of principal stresses from principal strains in the strain-gauge experiments, homogeneity, isotropy and linear elasticity was assumed. Loading with a couple of M_y = -12,500 Nmm resulted in strain values apposite in sign but practically equal in the absolute sense.

CHAPTER FIVE

THEORETICAL STRESS ANALYSES

In this chapter a three-dimensional FEM analysis of the model presented in chapter 3 will be discussed. The results of this analysis serve as references for the development of more simplified, analytical descriptions of the model that are better suited to characterize its mechanical behavior in principle.
In paragraph 5.4. a FEM beam model of the structure will be presented. This last model and the analytical models, too, are based on beams-on-elastic-foundation-theory, in which it is assumed that the stem and the bone separately behave in accordance with linear beam theory, while the cement mantle serves as an elastic layer. This in contradiction to composite beam theory, sometimes applied in the literature, in which it is assumed that the structure as an entity behaves according to beam theory.
In the last paragraph of this chapter the possibilities and limitations of plane FEM analyses will be discussed.

5.1. Three-dimensional FEM analysis

For the FEM analysis of the model an axisymmetric ring element is used, that can take nonaxisymmetric loading into account by expansion of loads, displacements, strains and stresses into Fourier series (Fourier element). The complete solution can be obtained as a superposition of the term-by-term solutions (Wilson, 1965; v. Campen, 1970; Zienkiewicz, 1977). The structure is divided into approximately 750 ring elements (1900 nodal points, 5700 degrees of freedom) as shown in fig. 5.1. Also other elements and element meshes were applied, as discussed in Huiskes *et al* (1977).

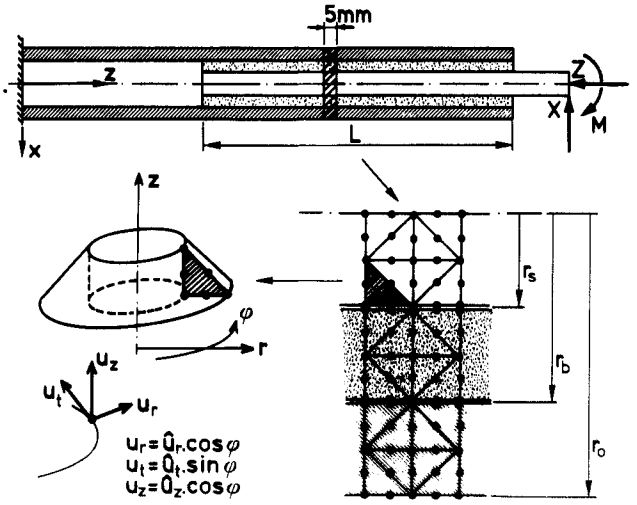

fig. 5.1: Element mesh and ring element used in the three-dimensional FEM calculations.

The loads (Z, X and M) are expanded into Fourier series, but only the first term of each series is used. Hence, the loads are assumed to be distributed along a nodal ring (fig. 5.2) and Z, X and M are the respective resultants of these distributions. This greatly economizes the solution procedure, while the effects of the assumed loading on the structure are equal to those of concentrated loading, thanks to the relatively large free-stem length to which Saint Venant's principle applies.

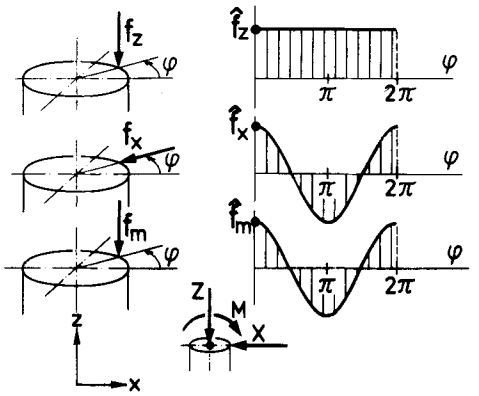

fig. 5.2: The forces and the moment on the stem are assumed to be distributed along a nodal ring, either as constant or as sine or cosine functions in φ: $f_Z = \hat{f}_Z$, $f_X = \hat{f}_X \cos\varphi$ and $f_M = \hat{f}_M \cos\varphi$, the resultants of which are Z, X and M, respectively.

In consequence of this method the stresses, strains and displacements that result from the axial loading (Z) are constant in φ and those that result from the transverse loading (X and M) are sine or cosine functions in φ. For the stresses these functions are summarized in table 5.1.
The quantities $\hat{\sigma}_r$, $\hat{\sigma}_t$, $\hat{\tau}_{rt}$ etc. will be referred to as stress 'amplitudes'; it should be borne in mind that the term in this case does not refer to dynamic loading. It is evident that the stress amplitude values are equal to the maximum stress values on a nodal ring, for τ_{rt} and τ_{tz} at $\varphi = \pi/2$, for the other components at $\varphi = 0$.

stress component		axial loading (Z)	transverse loading (X, M)
radial stress	σ_r	$\hat{\sigma}_r(r,z)$	$\hat{\sigma}_r(r,z)\cos\varphi$
hoop stress	σ_t	$\hat{\sigma}_t(r,z)$	$\hat{\sigma}_t(r,z)\cos\varphi$
axial stress	σ_z	$\hat{\sigma}_z(r,z)$	$\hat{\sigma}_z(r,z)\cos\varphi$
circumferential shear stress	τ_{rt}	0	$\hat{\tau}_{rt}(r,z)\sin\varphi$
longitudinal shear stress	τ_{rz}	$\hat{\tau}_{rz}(r,z)$	$\hat{\tau}_{rz}(r,z)\cos\varphi$
transverse shear stress	τ_{tz}	0	$\hat{\tau}_{tz}(r,z)\sin\varphi$

table 5.1: Expressions for the six stress components in axial and in transverse loading.

The element used is triangular in cross-section and has 6 nodal points. In each element the stress amplitudes are linear in r and z.
The calculations have been carried out using the FEM computer system FEMSYS (Banens, 1977). The accuracy of the results has been checked using analytical considerations (Huiskes, 1977).

Results:

All stress component amplitudes at all nodal points were calculated for the three loading cases. From these amplitudes the stresses for any value of φ can be evaluated using the expressions shown in table 5.1 and the equivalent stress can be calculated using the formula presented in chapter 3. In the present work the stress distribution as a function of φ and r (presented in Huiskes, 1977, and Huiskes *et al*, 1977) will not be discussed. As a rule, stress amplitudes as a function of z on four different lines will be presented: in the stem (line 1) and in the cement (line 2) at the stem-cement interface ($r = r_s$) and in the cement (line 3) and in the bone (line 4) at the cement-bone interface ($r = r_b$).

Fig. 5.3 gives an example of stress (σ_{eq}) as a function of z on the four lines just mentioned, resulting from the transverse force X. A set of all relevant results for loading cases Z and X is shown in appendix A.

When the results of the FEM calculations are compared with those of the experimental stress analysis of the cadaveric femur with implants, discussed in chapter 4, no detailed agreement can be expected owing to the simplified character of the model.

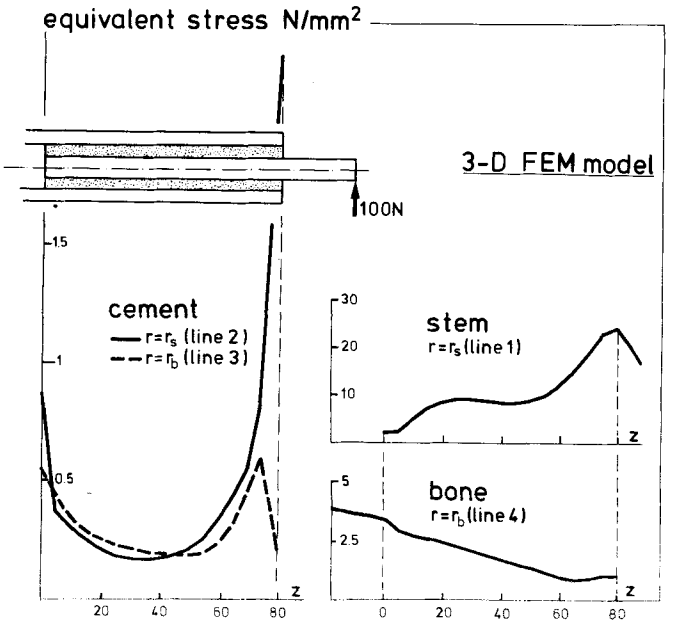

fig. 5.3: Equivalent stresses in the stem (at line 1), the bone (at line 4) and the cement (at lines 2 and 3) as functions of z, for a transverse force of 100 N on the stem.

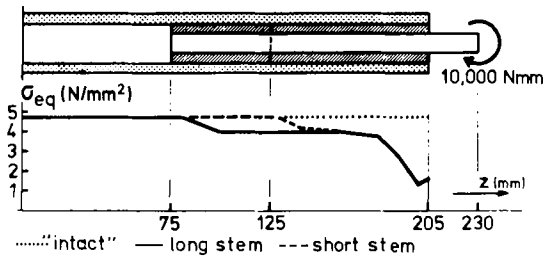

fig. 5.4: Equivalent stresses at the outside surface of the bone cylinder, for two different stem lengths (80 and 130 mm) and the bone without stem, on loading with a pure couple. To be compared with experimental results shown in fig. 4.2.

A qualitative agreement was clearly established, however, as is illustrated in fig. 5.4, showing equivalent stresses on the outside surface of the bone cylinder as calculated for the 'intact' case and with implants of two different lengths on loading with a bending moment. Comparison of these graphs with fig. 4.2 makes it apparent that the model results and the experimental results agree in the qualitative sense.

As regards the calculated stress distribution in general the following conclusions can be reached:

- Relative to the axial stress (σ_z) all other stress components in the stem have insignificant values for all loads. Hence, the equivalent stress is practically equal to the axial stress. This indicates also that the stem behaves in accordance with beam theory, which is hardly surprising.
- This is also true, although to a lesser extent, for the bone. On the proximal side stress components other than the axial one have significant values also. This means that, apart from the proximal side, the equivalent stress is almost equal to σ_z, as shown in fig. 5.5.

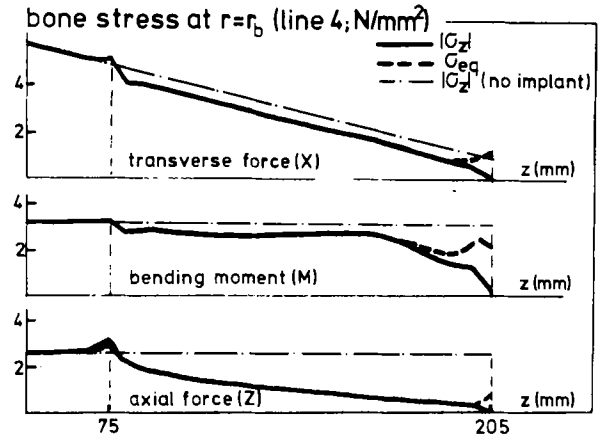

fig. 5.5: Axial stress ($\hat{\sigma}_z$) and equivalent stress (σ_{eq}) in the bone at line 4 ($r = r_b$) as functions of z, for three loading cases. Only on the proximal side do they differ. The 'natural' axial stress for the bone without implant is also shown. Especially the axial force results in low stress values as compared with the intact bone (stem length: 130 mm).

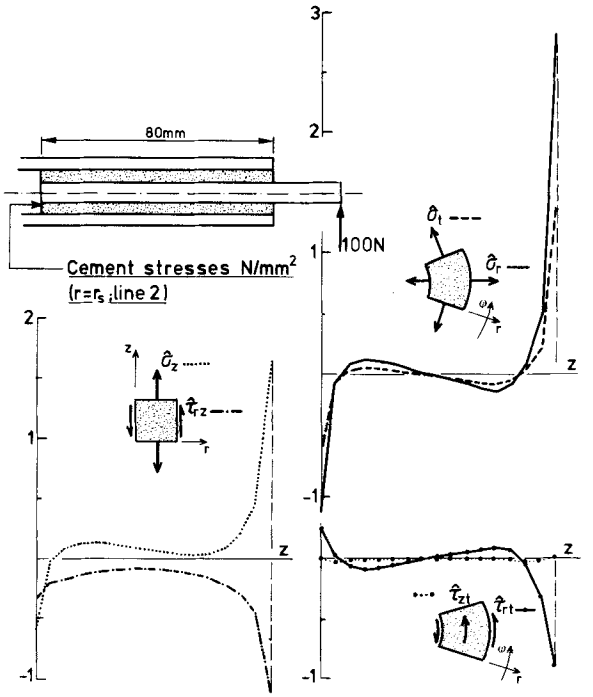

fig. 5.6: Stresses in the cement at the stem-cement interface on loading with a transverse force. Apart from $\hat{\tau}_{zt}$ the components are of comparable magnitude, indicating that the stress state in the cement is truly three-dimensional; $\hat{\sigma}_r$ shows the highest value.

- The stress state in the cement is truly three-dimensional, which means that the stress components have comparable magnitudes (fig. 5.6). The highest stresses in the cement occur near the stem-cement interface, on the proximal and distal sides, for all stress components and for all loading cases. Of the six components, σ_r shows the highest values at these locations.
  If σ_{eq} is used as a criterion for the stress state, then σ_r gives a good indication of its maximum value and τ_{rz} gives a good indication of its course as a function of z.
- Although the stress distributions differ for the transverse force and the bending moment, the results in principle give the same kind of information; hence, for a principle characterization it would be sufficient to consider only one of these loading cases. Here the transverse force was chosen as the representative loading case.
- As mentioned in chapter 3, the stress components σ_r, τ_{rt} and τ_{rz} have to be continuous across the interface due to the action = reaction law. In the calculated results this requirement was fulfilled with quite reasonable accuracy (Huiskes, 1977).
- As is shown, for instance in fig. 5.6, the cement stress components show high stress concentrations at both ends. Where τ_{rz} is concerned, the stress should, after a steep rise, decrease sharply to zero at the ends. That this is not described by the model is due to an inadequately refined element mesh in these regions.
  To describe this end-effect (that also occurs in so-called 'shear-lag' problems, e.g. Timoshenko and Goodier, 1970) a very refined mesh would be needed.
  The stress values found for τ_{rz} at the ends are assumed to be reasonable representations

of the maximal values that will in reality occur somewhat away from the ends. In this respect shear stress measurements were carried out by Stern (1977) in an axisymmetric structure consisting of an aluminium tube and a steel rod with acrylic cement in between, under axial loading, using optic stress films. He found the same kind of curves as calculated with the model.

It is apparent when looking at the stress distribution in the structure (figs. 5.3 through 5.6 and appendix A), that the fixation system can be divided into three regions (fig. 5.7): a middle region, where the structure behaves as a composite beam, which means that the stem and the bone each take a part of the total load depending on the ratio of their flexural and compressional stiffness; a proximal region, where the load is passed from the stem to the bone, and a distal region where, looking from the other side, the load is passed from the bone to the stem. As will be shown in paragraph 5.3, these regions can be treated separately and approximative formulas can be derived to describe the most important stress components in these regions as functions of the structural parameters. These approximations are based on beams-on-elastic-foundation theory, that will be discussed in paragraph 5.2.

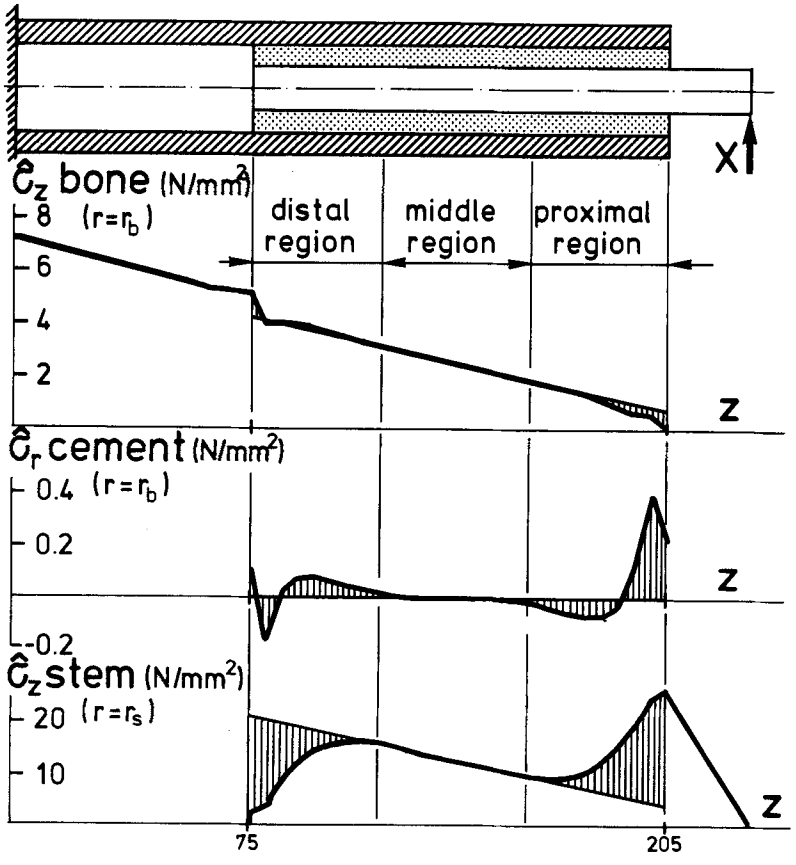

fig. 5.7: With respect to its mechanical behavior, the intramedullary fixation system can be divided into three regions. The middle region behaves in accordance with composite beam theory. Deviations from composite beam theory in the proximal and distal regions are shown with respect to axial stresses in the bone and the stem, and to radial stresses in the cement (stem length: 130 mm).

5.2. Beams-on-elastic-foundation theory

As will be shown in this paragraph, the mechanical behavior of the model can be approximated by applying beams-on-elastic-foundation theory, for transverse as well as for axial loading. Both cases will be treated separately.

5.2.1. *Transverse loading*

The theory of beams-on-elastic-foundation has been described in depth by Hetényi (1946). The difference in this case from the usual one, is caused by the circumstance that both beams (the stem and the bone) make a contribution to each other's elastic foundation. It is assumed that both the stem and the bone behave in accordance with beam theory. The resistance of the intermediate layer (the cement mantle) to shear- and axial loading is neglected in this case and its transverse stiffness is taken into account by assuming a continuous set of linear springs (Winkler hypothesis; Hetényi, 1946).

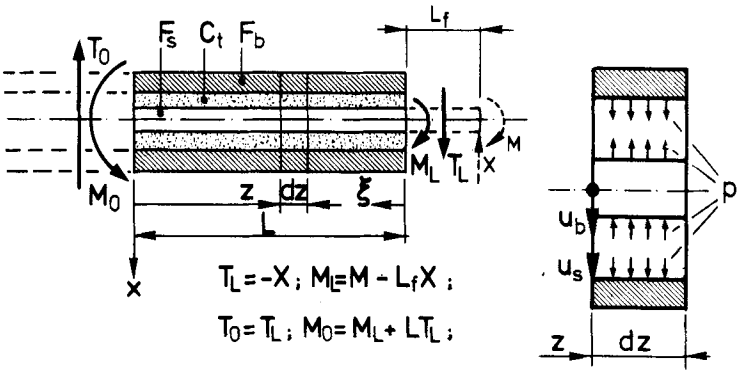

fig. 5.8: Parameters and variables of the beams-on-elastic-foundation model for transverse loading. The external loads in this model can easily be calculated from the previously defined loading system (M and X), as shown in the figure.

The parameters of the model are shown in fig. 5.8. The transverse stiffness of the elastic layer C_t (N/mm^2) is defined by

$$p = C_t(u_s - u_b) \tag{5.1}$$

where $u_s(z)$ and $u_b(z)$ are the deflections of the stem and the bone neutral axes, respectively, and $p(z)$ (N/mm) is the continuously distributed transverse load that the cement exerts on the stem and vice versa and that the cement exerts on the bone and vice versa.
As follows directly from beam theory

$$F_s \frac{d^4 u_s}{dz^4} + p = 0 \quad \text{and} \quad F_b \frac{d^4 u_b}{dz^4} - p = 0 \tag{5.2}$$

where F_s and F_b denote the flexural stiffness of the stem and the bone, respectively ($F = EI$).

Equations (5.1) and (5.2) can be solved to give:

$$u_s(z) = e^{\lambda_t z} D_1(z) + e^{-\lambda_t z} D_2(z) + \sum_{i=0}^{3} a_i z^i \tag{5.3}$$

$$u_b(z) = -\frac{F_s}{F_b} e^{\lambda_t z} D_1(z) + \frac{F_s}{F_b} e^{-\lambda_t z} D_2(z) + \sum_{i=0}^{3} a_i z^i \tag{5.4}$$

$$p(z) = C_t\left(1 + \frac{F_s}{F_b}\right)\left(e^{\lambda_t z} D_1(z) + e^{-\lambda_t z} D_2(z)\right) \tag{5.5}$$

where

$$D_1 = A_1 \cos\lambda_t z + A_2 \sin\lambda_t z$$

$$D_2 = A_3 \cos\lambda_t z + A_4 \sin\lambda_t z$$

$$\lambda_t = \sqrt[4]{\left\{\frac{C_t}{4}\left(\frac{1}{F_s} + \frac{1}{F_b}\right)\right\}}$$

by using the boundary conditions

$$u_b(0) = 0; \quad \frac{du_b}{dz}(0) = 0; \quad \frac{d^2u_b}{dz^2}(L) = 0; \quad \frac{d^3u_b}{dz^3}(L) = 0; \quad \frac{d^2u_s}{dz^2}(0) = 0; \quad \frac{d^3u_s}{dz^3}(0) = 0;$$

$$\frac{d^2u_s}{dz^2}(L) = \frac{M_L}{F_s}; \quad \frac{d^3u_s}{dz^3}(L) = -\frac{T_L}{F_s},$$

the constants A_1 through A_4 and a_0 through a_3 can be calculated which gives u_s, u_b and p. The bending moments in the stem and bone follow from

$$M_s(z) = F_s \frac{d^2u_s}{dz^2} \quad \text{and} \quad M_b(z) = F_b \frac{d^2u_b}{dz^2} \tag{5.6}$$

For these calculations a computer program was set up.

The parameters that determine the mechanical behavior of the structure described by $M_s(z)$, $M_b(z)$ and $p(z)$, are C_t, F_s, F_b and L. The formulas presented above are valid for arbitrary (constant) cross-sectional geometry of the stem and the bone, where C_t can be approximated by the formulas given in appendix B.
As follows from formulas (5.3), (5.4) and (5.5) the mechanical behavior of the structure is principally characterized by the parameter λ_t.

Since

$$\lambda_t = \sqrt[4]{\{\frac{C_t}{4F_s}(1 + \frac{F_s}{F_b})\}}$$

it follows that when $F_s \ll F_b$, the bone can be assumed to be rigid.

If circular geometry is assumed, as in the model described in chapter 3, it follows (see also appendix B), that

$$F_s = \frac{\pi}{4}E_s r_s^4, \quad F_b = \frac{\pi}{4}E_b(r_o^4 - r_b^4), \quad C_t = c_1 E_c g(\nu_c)\,(c_2 + \frac{\rho}{1-\rho});$$

where c_1, c_2 : constants depending on the interface conditions and
$g(\nu_c)$: expression in ν_c, to be evaluated graphically;
$\rho = r_s/r_b$

In this case the continuously distributed transverse load p(z) is the resultant of the stress components σ_r and τ_{rt}, as shown in fig. 5.9.

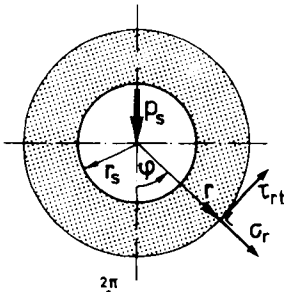

$$p(r,z) := -\int_0^{2\pi} [\sigma_r \cos\varphi - \tau_{rt}\sin\varphi] r\, d\varphi$$

fig. 5.9: Definition of the continuously distributed transverse load p(r,z) in a circular cross-section; $p_s(z) = p(r_s,z)$ and $p_b(z) = p(r_b,z)$. In the beams-on-elastic-foundation theory $p(r,z) = p(z)$, hence $p_s = p_b = p$.

A comparison of results (M_s, M_b and p as functions of z) as calculated with the FEM model and with the method presented in this paragraph, is shown in fig. 5.10. The agreement in M_s and M_b is good, the agreement in p is reasonable.

The variables $M_s(z)$ and $M_b(z)$ can be calculated directly to axial stem and bone stresses (σ_z) the maximal values of which are denoted by $s_{zs}(z)$ and $s_{zb}(z)$, respectively, as

$$s_{zs} = \frac{M_s}{W_s} \quad \text{and} \quad s_{zb} = \frac{M_b}{W_b} \tag{5.7}$$

The transverse load p(z) cannot be calculated to stresses, since it depends on both σ_r and τ_{rt} (fig. 5.9). Representative average stress variables $\bar{s}_{rs}(z)$ and $\bar{s}_{rb}(z)$ are introduced as

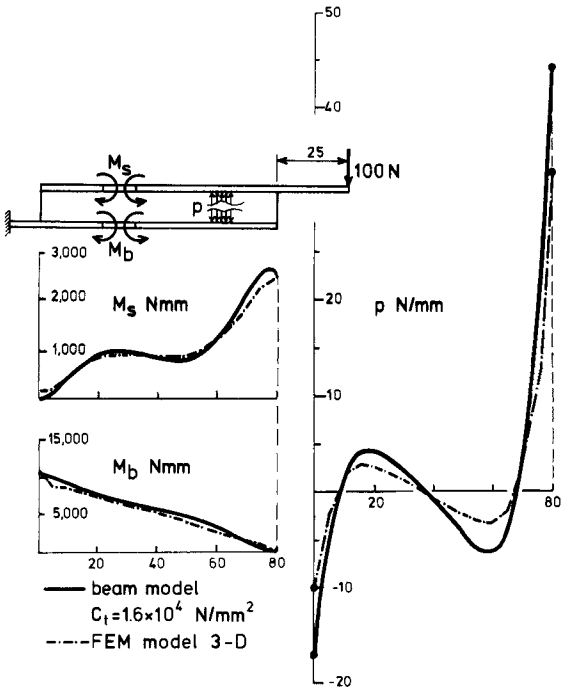

fig. 5.10: Comparison of the bending moments in the stem (M_s) and the bone (M_b), and the continuously distributed transverse load (p), as calculated with the FEM model and with the beams-on-elastic-foundation theory. The curve for p(z) in the case of the FEM model is taken as $p = (p_s + p_b) / 2$; in the analytical model $p_s = p_b = p$.

$$\bar{s}_{rs} = \frac{p}{2r_s} \quad \text{and} \quad \bar{s}_{rb} = \frac{p}{2r_b} \tag{5.8}$$

5.2.2. *Axial loading*

For axial loading the same strategy is followed as for transverse loading. It is again assumed that both the stem and the bone behave in accordance with beam theory. The resistance of the cement mantle to transverse loading and axial loading is neglected in this case and its axial shearing stiffness is represented by a continuous set of linear springs.
The parameters of the model are shown in fig. 5.11.
The shearing stiffness of the cement layer C_a (N/mm²) for axial loading is defined as

$$q = C_a(w_b - w_s) \tag{5.9}$$

where $w_b(z)$ and $w_s(z)$ are the displacements in the axial direction of the bone and the stem, respectively, and $q(z)$ (N/mm) is the continuously distributed axial shearing load that the cement exerts on the stem and the bone and vice-versa.

As follows directly from beam theory (or bar theory),

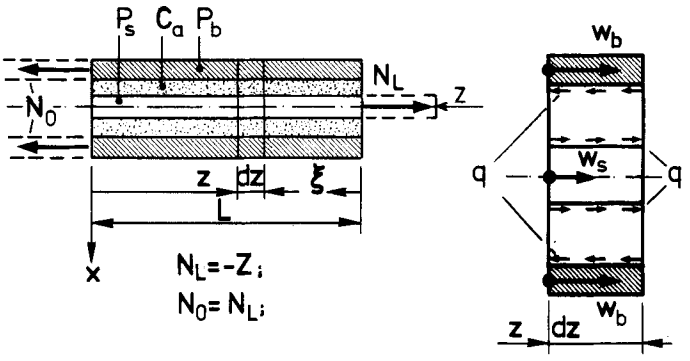

fig. 5.11: Parameters and variables of the beams-on-elastic-foundation model for transverse loading. The axial load N_L is directed opposite to the previously defined load Z.

$$P_s\frac{d^2w_s}{dz^2} + q = 0 \quad \text{and} \quad P_b\frac{d^2w_b}{dz^2} - q = 0 \tag{5.10}$$

where P_s and P_b are the compressional stiffness of stem and bone respectively ($P = EA$).

Equations (5.9) and (5.10) can be solved to give

$$w_s(z) = A_1e^{\lambda_a z} + A_2e^{-\lambda_a z} + A_3 + A_4z \tag{5.11}$$

$$w_b(z) = -\frac{P_s}{P_b}A_1e^{\lambda_a z} - \frac{P_s}{P_b}A_2e^{-\lambda_a z} + A_3 + A_4z \tag{5.12}$$

$$q(z) = -C_a(1 + \frac{P_s}{P_b})(A_1e^{\lambda_a z} + A_2e^{-\lambda_a z}) \tag{5.13}$$

where

$$\lambda_a = \sqrt{\{C_a(\frac{1}{P_s} + \frac{1}{P_b})\}}$$

Using the boundary conditions:

$$w_b(0) = 0; \quad \frac{dw_b}{dz}(L) = 0; \quad \frac{dw_s}{dz}(0) = 0; \quad \frac{dw_s}{dz}(L) = \frac{N_L}{P_s},$$

the constants A_1 through A_4 can be calculated, which gives w_s, w_b and q.

The axial loads in stem and bone follow from

$$N_s(z) = P_s \frac{dw_s}{dz} \quad \text{and} \quad N_b(z) = P_b \frac{dw_b}{dz} \tag{5.14}$$

The parameters that determine the mechanical behavior of the structure described by $N_s(z)$, $N_b(z)$ and q(z), are C_a, P_s, P_b and L, and the formulas presented are again valid for arbitrary (constant) cross-sectional geometry of the stem and the bone, where C_a can be approximated by the formulas given in appendix B. In the axial loading case, too, it follows since

$$\lambda_a = \sqrt{\{\frac{C_a}{P_s}(1 + \frac{P_s}{P_b})\}}$$

that if $P_s \ll P_b$, the bone can be assumed to be rigid.

For circular geometry, as in the model described in chapter 3, it follows (see also appendix B), that

$$P_s = \pi E_s r_s^2; \quad P_b = \pi E_b(r_o^2 - r_b^2); \quad C_a = -\frac{\pi E_c}{(1 + \nu_c)\ln\rho}$$

In this case the continuously distributed axial shearing load q(z) is the resultant of the axial shear stress τ_{rz}. In general

$$q(r,z) = \int_0^{2\pi} \tau_{rz}(r,z) r d\varphi; \tag{5.15}$$

if we define $t_s(z) = \tau_{rz}(r_s,z)$ and $t_b(z) = \tau_{rz}(r_b,z)$, it follows that

$$q_s(z) = t_s \gamma_s \quad \text{and} \quad q_b(z) = t_b \gamma_b, \tag{5.16}$$

where γ_s and γ_b (mm) are the outer stem and the inner bone circumferences, respectively. Due to the assumptions in the beams-on-elastic-foundation theory, $q_s = q_b = q$.

The axial stress in the stem and the bone denoted by $s_{zs}(z)$ and $s_{zb}(z)$, respectively, follow from

$$s_{zs} = \frac{N_s}{A_s} \quad \text{and} \quad s_{zb} = \frac{N_b}{A_b} \tag{5.17}$$

Fig. 5.12 shows a comparison of bone, stem and interface shear stresses as calculated with the FEM model and as calculated using the formulas presented in this paragraph. The agreement is good.

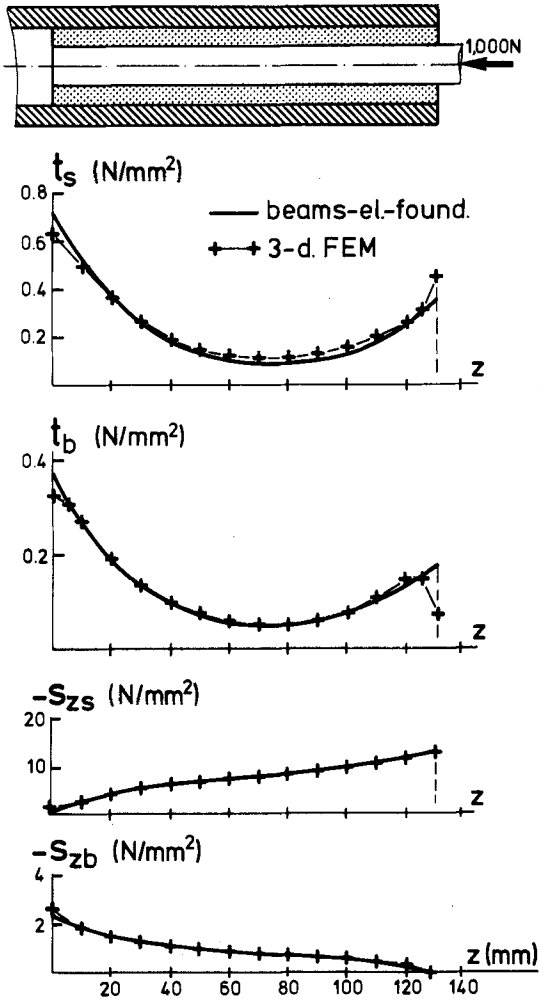

fig. 5.12: Comparison of axial stem stress (s_{zs}), bone stress (s_{zb}), stem-cement interface shear stress (t_s) and bone-cement interface shear stress (t_b) upon axial loading (N_L = -1000N) as calculated with the FEM model and as calculated with the beams-on-elastic-foundation model.

As already discussed in paragraph 5.1 the shear stress at the interfaces at both ends, after the steep rise, should decrease sharply to zero. In this case, too, the model does not describe this phenomenon. The calculated values for t_s and t_b at the ends should be regarded as representing maximal values that occur a little distance away from these ends in reality.

5.3. Approximative formulas

As we have seen in paragraph 5.1, the fixation system can be divided into three regions where its mechanical behavior is concerned. This can easily be understood if the structure is assumed to be of semi-infinite length (fig. 5.13).

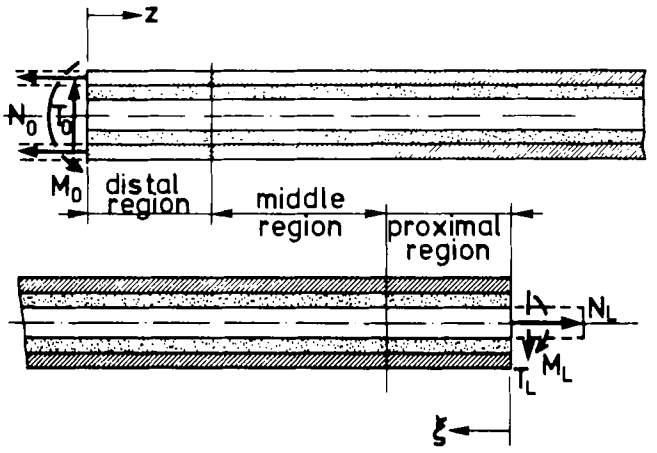

fig. 5.13: On assuming the structure to be of semi-infinite length, the proximal and distal regions are treated separately. The loading systems for these two cases are shown.

The solutions of the differential equations for axial and transverse loading, (5.3) through (5.5) and (5.11) through (5.13), are again valid; also the boundary conditions for z = 0 remain unchanged, but the boundary conditions for z = L have to be replaced by requirements of vanishing initial effects for $z \to \infty$; hence $D_1 = 0$ in formulas (5.3) through (5.5) and $A_1 = 0$ in formulas (5.11) through (5.13). After establishing the constants, using the remaining boundary conditions at z = 0, it follows for transverse loading at the distal side that:

$$M_s(z) = \frac{F_s}{F_s+F_b}\left\{M_0 - T_0 z - e^{-\lambda_t z}\left(M_0 \cos\lambda_t z + \left(M_0 - \frac{T_0}{\lambda_t}\right)\sin\lambda_t z\right)\right\} \tag{5.18}$$

$$M_b(z) = \frac{F_s}{F_s+F_b}\left\{\frac{F_b}{F_s}M_0 - \frac{F_b}{F_s}T_0 z + e^{-\lambda_t z}\left(M_0 \cos\lambda_t z + \left(M_0 - \frac{T_0}{\lambda_t}\right)\sin\lambda_t z\right)\right\} \tag{5.19}$$

$$p(z) = \frac{1}{2}\frac{C_t}{\lambda_t^2 F_b} e^{-\lambda_t z}\left(M_0 \sin\lambda_t z - \left(M_0 - \frac{T_0}{\lambda_t}\right)\cos\lambda_t z\right) \tag{5.20}$$

and for axial loading that

$$N_s(z) = \frac{P_s}{P_s+P_b} N_0\left(1 - e^{-\lambda_a z}\right); \quad N_b(z) = \frac{P_b}{P_s+P_b} N_0\left(1 + \frac{P_s}{P_b} e^{-\lambda_a z}\right); \tag{5.21}$$

$$q(z) = -\frac{\lambda_a P_s}{P_s+P_b} N_0 e^{-\lambda_a z} \qquad (5.22)$$

The same kind of formulas can be established for the other (proximal) side, replacing z by ξ, F_s by F_b, P_s by P_b, M_0 by M_L, T_0 by $-T_L$ and N_0 by N_L.
On both sides separately the system has a force introduction region the length of which is determined by $e^{-\lambda_t z}$ and $e^{-\lambda_a z}$, hence by λ_t and λ_a. For higher z the expressions for the loading variables reduce to:

$$M_s(z) = \frac{F_s}{F_s+F_b}(M_0-T_0 z); \quad M_b(z) = \frac{F_b}{F_s+F_b}(M_0-T_0 z); \quad p(z) = 0; \qquad (5.23)$$

$$N_s(z) = \frac{P_s}{P_s+P_b} N_0; \quad N_b(z) = \frac{P_b}{P_s+P_b} N_0; \quad q(z) = 0 \qquad (5.24)$$

the well known formulas for composite beam theory, applying to an infinitely long composite structure (e.g. Muskhelshvili, 1963; Bartel and Desormeaux, 1976a). In this case the flexural and compressional stiffness of the cement layer is neglected, allowed since $F_c \ll F_s+F_b$ and $P_c \ll P_s+P_b$.
Whether or not these formulas apply to the middle region or, in other words, whether or not there is a middle region, depends on the stem length and the values of λ_a and λ_t. For transverse loading the traditional criterion for beams-on-elastic-foundation theory can be used (Hetenyi, 1946):

$\lambda_t L \leqq \frac{\pi}{4}$: short beam; both the stem and the bone can be assumed as rigid to find a good approximation of p(z).

$\frac{\pi}{4} < \lambda_t L < \pi$: intermediate beam length; both sides of the system influence each other; the full theory has to be used; composite beam theory is not appropriate for any section.

$\lambda_t L \geqq \pi$: long beam, the behavior of the proximal and distal ends are independent by approximation and the structure can be analyzed by analyzing the proximal region, the middle region and the distal region separately.

This is illustrated in fig. 5.14, where the expression $e^{-\lambda_t z}\cos\lambda_t z$, that principally determines the behavior of p(z), is shown graphically for a stem length of 80 mm and different values of λ_t.
When the same criterion is used for axial loading, for λ_a, it follows for $\lambda_a L = \pi$, $e^{-\lambda_a L/2} \approx 0.2$; hence 80% of the initial effect would have vanished at half the stem length, so there would still be a significant interaction between both sides. For $\lambda_a L \approx 4.6$, 90% of the effect would have vanished and 95% for $\lambda_a L \approx 6.0$.

Fig. 5.15 shows a comparison of results for p(z) and q(z) as calculated using the beams-on-elastic-foundation theory presented in paragraph 5.2. and using the semi-infinite approximation for both sides (formulas (5.20), (5.22) and their equivalents for the proximal side). The semi-infinite approximation is quite good where p(z) is concerned. In the case of axial loading both ends apparently still influence each other, which was to be expected since $\lambda_a L \approx 2.9$ in this case. However, even for this low value the approximation of q(z) is not bad.

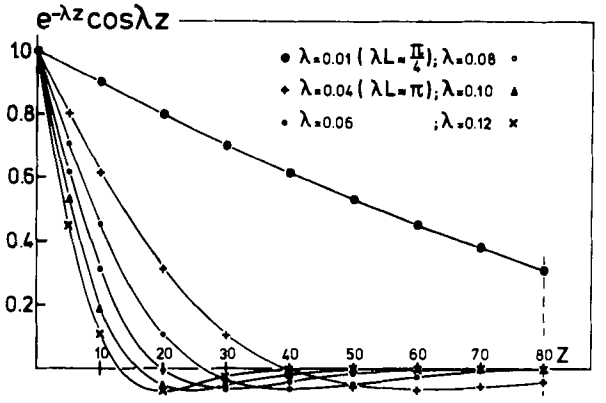

fig. 5.14: The function $e^{-\lambda z}\cos\lambda z$ for different (realistic) values of λ. When $\lambda L \leq \frac{\pi}{4}$ the function is practically linear.

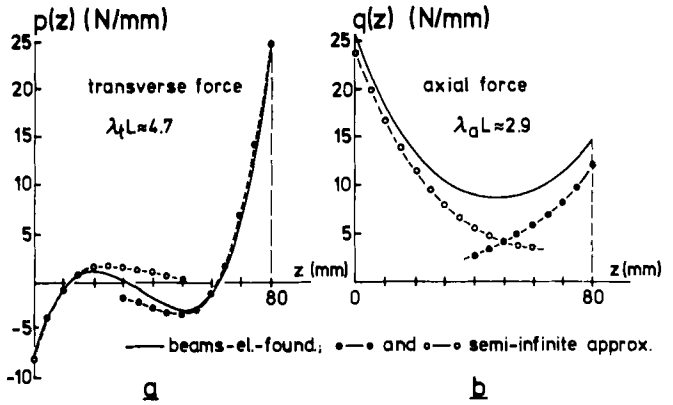

fig. 5.15: A comparison of results for p(z) (a) and q(z) (b) as calculated for a structure of finite length and as calculated assuming semi-infinite length on both sides, respectively.

Summarizing, it can be said that the application of the approximative semi-infinite beams-on-elastic-foundation theory gives excellent opportunities to characterize the mechanical behavior of the intramedullary bone-prosthesis structure and to develop a fundamental, general concept on the relations between stresses and the most important structural parameters.
A first characterization follows from the quantities $\lambda_t L$ and $\lambda_a L$, where

$$\lambda_t = \sqrt[4]{\left\{\frac{C_t}{4}\left(\frac{1}{F_s} + \frac{1}{F_b}\right)\right\}} \quad \text{and} \quad \lambda_a = \sqrt{\left\{C_a\left(\frac{1}{P_s} + \frac{1}{P_b}\right)\right\}},$$

and C_t and C_a can be evaluated using the formulas presented in appendix B.

When $\lambda_t L \geqq \pi$ and $\lambda_a L \geqq \pi$ the structure can be divided into a proximal, a middle and a distal region, in which the most important stress components can be calculated using simple formulas, as summarized in table 5.II. From these formulas, the stresses in the stem and the bone (s_{zs} and s_{zb}) and the normal and shear stresses at the interfaces (s_{rs}, s_{rb}, t_s and t_b) can be calculated for given geometry.

	Transverse loading (M_L and T_L)	Axial loading (N_L)
proximal region		
stem:	$M_s(L) = M_L$	
cement/interfaces:	$p(L) = \frac{1}{2}\frac{C_t}{\lambda_t^2 F_s}\left(M_L + \frac{T_L}{\lambda_t}\right)$	$q(L) = -\frac{\lambda_a P_b}{P_s + P_b} N_L$
middle region		
stem:	$M_s(\xi) = \frac{F_s}{F_s + F_b}(M_L + T_L \xi)$	$N_s(\xi) = \frac{P_s}{P_s + P_b} N_L$
bone:	$M_b(\xi) = \frac{F_b}{F_s + F_b}(M_L + T_L \xi)$	$N_b(\xi) = \frac{P_b}{P_s + P_b} N_L$
distal region		
bone:	$M_b(0) = M_L + T_L$	$N_b(0) = N_L$
cement/interfaces:	$p(0) = -\frac{1}{2}\frac{C_t}{\lambda_t^2 F_b}\left(M_L + T_L L - \frac{T_L}{\lambda_t}\right)$	$q(0) = -\frac{\lambda_a P_s}{P_s + P_b} N_L$

table 5.II: Approximative formulas describing the most important loading variables in the stem (M_s and N_s), the bone (M_b and N_b), in the cement layer and at the interfaces (p and q) in the proximal, middle and distal regions respectively (see also fig. 5.13).

It should be remarked here that the axial stress in the cement layer can also be approximated in the middle region, using composite beam theory. However, as was found in paragraph 5.1. (fig. 5.6) the value of this stress component in the cement in the middle region is quite low in comparison to stresses in the proximal and the distal regions.

5.4. FEM beam analysis

The model described in paragraph 5.2., where stem and bone separately are assumed to behave in accordance with beam theory and where the intermediate layer is assumed to react as a continuous set of linear springs, can also be simulated using simple FEM beam analysis. The reason for developing such a model is the possibility of taking nonconstant cross-sectional geometries of the stem and the bone into account and, likewise, of modeling

variations in the elastic moduli of the three materials in order to investigate influences of incomplete cement mantles and bone resorption. Spongeous bone layers of varying thickness, too, can be taken into account in such a model.
In this model the stem and the bone are represented by a number of beam elements and the cement mantle by special spring elements that simulate the stiffness of the layer in the axial and transverse directions (C_a and C_t), as shown in fig. 5.16. In the model, the quantities $M_s(z)$, $M_b(z)$, $N_s(z)$, $N_b(z)$, $q(z)$, $p(z)$, $s_{zs}(z)$, $s_{zb}(z)$, $\bar{s}_{rs}(z)$, $\bar{s}_{rb}(z)$, $t_s(z)$ and $t_b(z)$ are calculated, just as with the model described in paragraph 5.2. On comparison of results from both models, the agreement was found to be excellent.

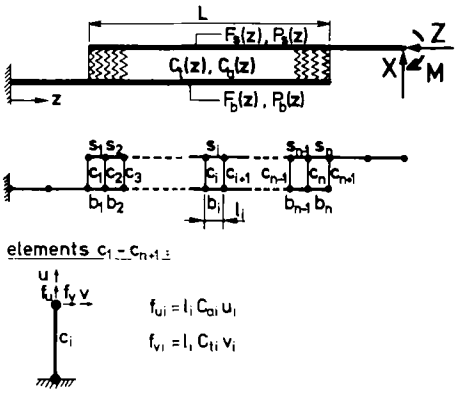

fig. 5.16: Characterization of the FEM beam model; the elements s_i and b_i are beam elements representing the stem and the bone, respectively. The cement mantle is represented by 'spring elements' (c_i), with certain stiffness characteristics in axial and transverse directions.

This model can easily be extended to three-dimensional geometry and a more sophisticated (three-dimensional) representation of the cement mantle. The restriction of this model is the requirement that the bone and the stem separately should behave in accordance with beam theory.

5.5. Two-dimensional (plane) FEM analysis

It is the object of this paragraph to discuss the possibilities and limitations of two-dimensional FEM analyses rather than present results of such a model. Although a two-dimensional FEM analysis of the simplified model presented in chapter 3 was carried out and will be used in chapter 6, it was apparent that the relation between the results of the three-dimensional model and those of the two-dimensional model was rather confusing. Many two-dimensional models have been presented in the literature, as discussed in chapter 2, and it appears to be worth while to evaluate these models, which can be done by using the previously developed concepts.

Obviously, the modeling has to be carried out in such a way that the essential characteristics of the structure are represented in the model. As was shown in the previous paragraphs, the essential parameters of the intramedullary bone-prosthesis structure are λ_t, λ_a, F_s, F_b, P_b, P_s,

C_a, C_t and L. Apart from these, there are other important parameters, for example the flexural and compressional stiffness of the cement mantle (F_c and P_c) and the outer stem and the inner bone circumferences (γ_s and γ_b) which do not influence the mechanical behavior so much in general, but do influence the local stress values. These parameters, too, should be represented adequately in the model.

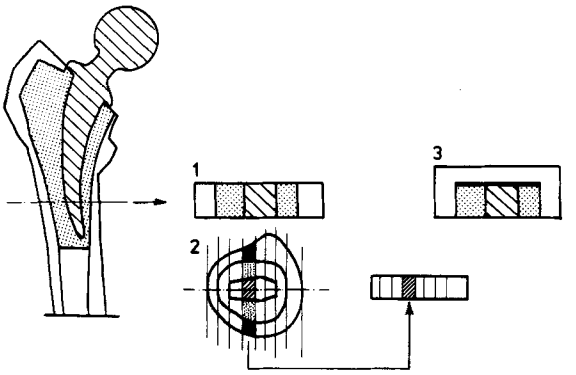

fig. 5.17: Three different methods of representing the hip endoprosthesis fixation system in a plane model: 1. as it appears in a longitudinal section; 2. using composite materials theory to take the out-of-plane material stiffness into account (see also fig. 5.18); 3. using side plates (a 'spanning-element' layer) to take the medial-lateral cortex connection into account.

Three different methods of modeling in two dimensions have been reported in the literature (fig. 5.17). The simplest method is the one in which a longitudinal-plane mid-section of the structure is modeled as it appears, for instance on an X-ray (fig. 5.17.1; e.g. Andriacchi *et al*, 1975; Kwak *et al*, 1979). In this case no connection exists in the model between the lateral and the medial cortex. Hence, apart from the question whether this model can take the correct parameter values of the system into account, the model in essence consists of three beams connected by two elastic layers. Since the elastic lines (or neutral axes) of these beams do not coincide, a sandwich construction results, in which the stiffness is to a great extent determined by shear at the cement-bone interfaces (e.g. Girkman, 1963) which is a quite unrealistic representation of the structure.
A second method is the one in which the theory of composite materials is used (fig. 5.17.2; McNeice *et al*, 1975, 1976). In this case the system is modeled as in the previous case but the stiffness of the 'out-of-plane' material is taken into account by calculating a combination of an effective thickness (t_e) and Young's modulus (E_e) for every plane element, as shown in fig. 5.18.

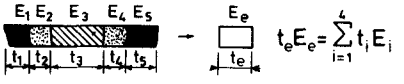

fig. 5.18: In using the composite materials theory, the out-of-plane stiffness of the structure consisting, in this case, of three materials, is represented by a plane element whose stiffness characteristics are calculated from the three original materials, taking into account their thickness and Young's moduli.

Apart from the fact that in this case, too, a sandwich construction results, the essential characteristics of the structure are not modeled correctly, because those elements that represent the stem also incorporate the stiffness of a piece of cement and a piece of bone and those elements that represent the cement incorporate part of the bone. What is modeled correctly in using this method is the overall stiffness of the full cross-section. McNeice *et al* (1975) show in their results that the stresses in the stem increase by a factor of three if loosening occurs at the stem-cement interface. This is exactly what would happen in a sandwich construction, as they in fact analyzed, but not in the real structure, where the lateral and medial cortex are connected, as will be shown in the next chapter.
A third method of modeling is the one in which the connection between the lateral and medial cortex of the bone is taken into account by applying a side plate or a 'spanning-element' layer in the model (fig. 5.17.3; e.g. Hampton *et al*, 1976; Svensson *et al*, 1977). This method is the only one that gives the option of modeling the system as a two-beam structure in a plane and hence the only one that is suitable. However, it is questionable whether even in using this method the essential parameters mentioned previously can be adequately represented.

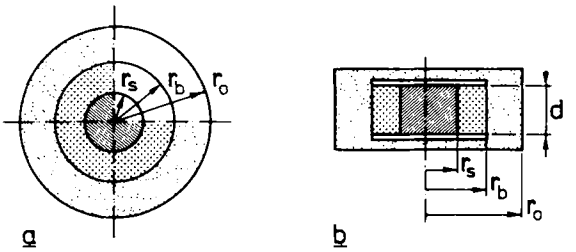

fig. 5.19: A plane representation (b) of a structure with axisymmetric cross-section (a), applying side plates.

As an example, a system with circular cross-section is assumed (fig. 5.19.a). This structure has to be represented in a plane model, taking a 'spanning-element' layer into account (fig. 5.19.b). The 'real' values of the essential parameters and those in the two-dimensional representation can then be compared as shown in table 5.III.
On comparing these quantities it follows (when E_c, E_s, r_s and r_b are equal in both models), that

$$\frac{\lambda_a \text{ (circ. geom.)}}{\lambda_a \text{ (plane geom.)}} \approx \sqrt{-\frac{2(1-\rho)}{\rho \ln \rho}} \quad \text{and} \quad \frac{\lambda_t \text{ (circ. geom.)}}{\lambda_t \text{ (plane geom.)}} \approx \sqrt[4]{\frac{16}{3\pi}} \approx 1.15$$

For $\rho = 0.5$, $\lambda_a(\text{circ})/\lambda_a(\text{plane}) \approx 1.7$ and for $\rho = 0.8$, $\lambda_a(\text{circ})/\lambda_a(\text{plane}) \approx 1.5$.
Apparently the ratios of λ_a and λ_t are independent of d and hence, since only d can be freely adjusted in the model, the ratios are more or less fixed.
Hence, for axial loading especially, the most crucial parameter of the circular structure is badly modeled in the plane representation. As follows from table 5.III also, d can never be chosen in such a way that all other requirements are fulfilled. If $r_s = 5$ mm and $r_b = 10$ mm, then $-\pi/\ln\rho \approx 4.5$ and $4\rho/(1-\rho) = 4$, hence, in order to satisfy requirements for equal C_a, d should be equal to 22.65 and to satisfy requirements for C_t, d should be equal to 10.
The requirements for P_s and F_s could be satisfied by assuming non-uniform thickness of the stem in the plane model. If d has been chosen to satisfy requirements for C_a or C_t, nothing more can be done to satisfy requirements for F_c, P_c, γ_s and γ_b.

parameter		circular geometry	rectangular geometry
P_b		$\pi E_b(r_o^2 - r_b^2)$	depending on side-plate dimensions
F_b		$\frac{\pi}{4}E_b(r_o^4 - r_b^4)$	
γ_b		$2\pi r_b$	$2d$
P_s		$\pi E_s r_s^2$	$2E_s d r_s$
F_s		$\frac{\pi}{4}E_s r_s^4$	$\frac{2}{3}E_s d r_s^3$
γ_s		$2\pi r_s$	$2d$
P_c		$\pi E_c(r_b^2 - r_s^2)$	$2d(r_b - r_s)$
F_c		$\frac{\pi}{4}E_c(r_b^4 - r_s^4)$	$\frac{1}{6}d(r_b - r_s)^3$
C_a	(1)	$-\frac{\pi E_c}{(1+\nu_c)\ln\rho}$	$\frac{dE_c}{(1+\nu_c)(r_b-r_s)}$
C_t	(1)	$\frac{4\rho E_c(1-\nu_c)}{(1-\rho)(1+\nu_c)(1-2\nu_c)}$	$\frac{2dE_c(1-\nu_c)}{(r_b-r_s)(1+\nu_c)(1-2\nu_c)}$
λ_a^2	(2)	$-\frac{E_c}{E_s}\frac{1}{(1+\nu_c)\ln\rho}\frac{1}{r_s^2}$	$\frac{E_c}{E_s}\frac{1}{2r_s(r_b-r_s)(1+\nu_c)}$
λ_t^4	(2)	$\frac{E_c}{E_s}\frac{4\rho(1-\nu_c)}{(1-\rho)(1+\nu_c)(1-2\nu_c)}\frac{1}{\pi r_s^4}$	$\frac{3}{4}\frac{E_c}{E_s}\frac{1-\nu_c}{(r_b-r_s)(1+\nu_c)(1-2\nu_c)}\cdot\frac{1}{r_s^3}$

table 5.III: Formulas describing the characteristic parameters in an axisymmetric structure and in a two-dimensional (plane) model (see fig. 5.19); (1) rough approximation, see appendix B; (2) to make a 'first-order' general comparison possible $\lambda_a^2 \approx C_a/P_s$ and $\lambda_t^4 \approx C_t/4F_s$ are taken.

In conclusion, it is evident that, unless axial and transverse loading are investigated with two different models and a method of scaling is introduced, the relation between the mechanical behavior of an intramedullary bone-prosthesis structure and that of a two-dimensional model is not very well defined. This does not imply that two-dimensional FEM models are worthless in this case; when side plates are applied and care is taken to choose the dimensions in such a way as to meet the above-mentioned requirements as fully as possible, tendencies could certainly be investigated in a relative sense. But these two-dimensional models certainly do not have the accuracy that the visual apparent agreements between the models and the real structure suggest. Furthermore, a comparison of results of different two-dimensional models is difficult.

It is evident, looking at these results, that for detailed investigations truly three-dimensional models should be used. FEM beam models as presented in paragraph 5.4. are more dependable, though less refined than two-dimensional models.

5.6. Conclusions

A simplified axisymmetric model of intramedullary bone-prosthesis structures was analyzed, using various methods. A three-dimensional FEM model was developed which gives detailed information on the stress distribution in the structure.
By comparison of some results with those of strain-gauge experiments on a cadaveric femur with hip endoprostheses, a qualitative agreement was apparent.
By making some additional simplifying assumptions, an analytical solution for the most important stress components in the structure could be found by applying beams-on-elastic-foundation theory. The most important parameters that characterize the mechanical performance of the structure were thus established.
It was found that the structure can be divided into three regions that can be analyzed separately, using quite simple formulas to calculate the most important stress components.
The theory, applied here for the analytical solutions, can be extended towards non-constant cross-sectional geometry, for example using minimal potential energy principles (Raleigh - Ritz) to find a solution. Such a solution, however, would not be in closed form, so that numerical methods would have to be applied.
A method of this kind was used by Calderale *et al* (1977), for transverse loading.
In the present study a FEM beam model was chosen for an extension towards a more realistic geometrical description, because this method offers excellent options for model refinement and is quite cheap and practical in use.
By applying the concepts developed in this chapter, two-dimensional FEM models could be evaluated and it was found that an intramedullary bone-prosthesis structure is not very well suited for such representation and that, moreover, many pitfalls are evident in the modeling process.

It is felt that the models presented here will give reasonable 'first-order' approximations of the intramedullary fixation system mechanical behavior, which implies that the most important parameters of the structure are adequately represented in the models. It will be shown in chapters 7 and 8 that the models can conveniently be used to develop quantitative guidelines for implant design and implantation procedures.
In the following chapter the influences of properties of the structure that were neglected in the models will be discussed.

CHAPTER SIX

INFLUENCES OF NEGLECTED ASPECTS OF THE STRUCTURE

In this chapter some properties of the intramedullary bone-prosthesis structure that have been neglected in the previously discussed models and that may influence the mechanical behavior of the system will be discussed. These properties are the possible presence of locked-in cement stresses, more complicated mechanical conditions at the interfaces, a non-constant cross-sectional geometry of the stem and a few others.

6.1. Locked-in thermal stresses

Due to the cooling of the acrylic cement, immediately after the polymerization process, the cement layer will shrink around the stem (see also section I).
This will result in locked-in stresses that may influence the mechanical behavior of the structure. On these (initial) stresses, the stresses resulting from the joint loading will have to be superimposed and, moreover, they may influence the mechanical condition of the stem-cement interface that will behave as rigidly connected so long as compression is present.
When the temperature distribution in the cement right after the polymerization process is known, the shrinkage stresses in an axisymmetric model consisting of bone cement around a (rigid) stem can be calculated (Timoshenko and Goodier, 1970). Using data on temperature distributions as discussed in section II, these calculations were carried out for different stem dimensions and cement properties (Huiskes and de Wijn, 1979). Fig. 6.1 shows an example of results.

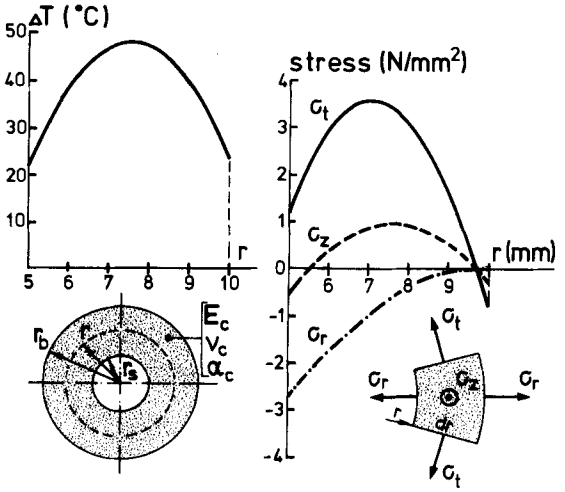

fig. 6.1: Locked-in thermal stresses in a model of a slice of bone cement. The initial temperature distribution ΔT (according to fig. 7.7, section II) and the radial (σ_r), axial (σ_z) and circumferential (σ_t) stress components are shown. Parameter values: E_c = 2,000 N/mm²; ν_c = 0.33; coefficient of linear expansion $\alpha_c = 5x10^{-5}\ °C^{-1}$ (according to Ahmed et al, 1977). In the model the properties are taken as independent of the temperature; plane strain state is assumed.

The radial (compressional) stress at the stem-cement interface reaches a value of approximately 2.5 N/mm^2 and the hoop stress in the middle of the cement mass 3.5 N/mm^2. Comparable results were reported by Ahmed *et al* (1977), who have studied the same kind of model. These values are quite sensitive to the thickness of the stem. For a stem 15 mm in diameter the stress values approximately double if the same initial temperature is assumed. However, as was shown in section II, in a thin cement layer the temperature will be much less. The hoop stress and the axial stress are also quite sensitive to Poisson's ratio of the cement, while all three stress components are proportional to Young's modulus.
The calculated stress values are of the same order of magnitude as the values that have been found to result from the joint loading (appendix A) and thus would certainly interfere with the mechanical behavior of the structure.
However, acrylic cement is known to creep, especially under conditions as in the body (see also section I). In a relaxation test of a rod of acrylic cement in water at 37°C, initially under a tensile stress of 4 N/mm^2, it was found that the stress decreased by 75% in approximately 170 hrs (7 days), as is shown in fig. 6.2 (Huiskes and de Wijn, 1979). Extrapolating this data, it can be assumed that after approximately 70 days the stress would have decreased by 90% and after a year would have practically vanished.

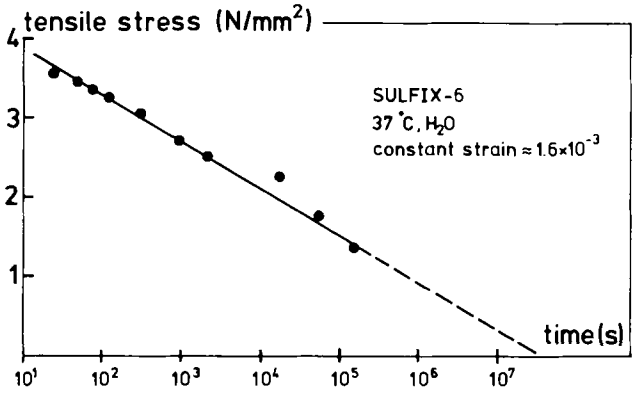

fig. 6.2: Stress relaxation in a test-bar of acrylic cement in tension.

6.2. Mechanical conditions at the interfaces

As mentioned in section I, there is no chemical bond between the stem and the cement, nor between the bone and the cement. Due to mechanical interlocking of cement and (spongeous) bone, the cement-bone interface may be able to transfer tensile stresses to some extent, although even this is doubtful when a soft fibrous tissue layer is present. The stem-cement interface will certainly disconnect on tension, while the shear resistance depends solely on friction. Friction, at the stem-cement interface as well as at the cement-bone interface depends on the roughness of the contact surfaces and on the compressional stress, hence also on initial locked-in stresses.
It is rather difficult to take the interface conditions into account in a stress analysis, since not enough accurate data is available for an adequate description. Moreover, the conditions will vary considerably and change in the course of time. The object of this paragraph is to roughly evaluate how the interface conditions affect the stress distribution in the intramedullary fixation system. In the first part it will be shown that loosening upon tension and

slip at the stem-cement interface significantly affect the stress distribution in the cement, using a two-dimensional FEM model that can take these phenomena into account. In the second and third parts the problem will be approached in a more fundamental fashion, using the concepts developed in paragraph 5.2.
The influence of a loose stem will only be evaluated for transverse loading. For axial loading, the interface conditions would very much depend on friction and on the tapering of the stem. When the stem is not held by the friction forces it will simply subside until it again finds support. If the stem is held by the friction forces, the interfaces can be assumed to be rigidly connected. From a mechanical point of view this problem is further complicated because the friction forces might be exceeded locally.

6.2.1. *Numerical evaluation*

The FEM programs as used here offer options to define conditions at contact regions. The condition that no tensile stress occurs between two materials can also be taken into account, by applying an iterative procedure (Banens, 1977). This method was used for the stem-cement interface in a two-dimensional model. The model and its parameters are described in fig. 6.3. A 'spanning-element' layer was used to model the medial-lateral cortex connection, as discussed in paragraph 5.5. Material properties, loading and dimensions in the x-z plane were chosen in accordance with the axisymmetric model described in chapter 3.

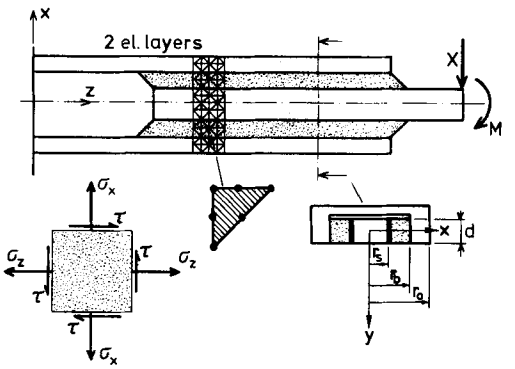

fig. 6.3: A two-dimensional FEM model of the simplified intramedullary fixation structure. A 'spanning-element' layer (or side plate) is applied; dimensions and stress components are given. An element with triangular geometry and 6 nodal points was used; the displacement field in the element is quadratic. Note that the x-coordinate is defined as positive, opposite to the three-dimensional FEM model (chapter 3).

Dimensions in the x-y plane were chosen in such a way that the flexural and compressional stiffness of stem and bone (F_s, F_b, P_s and P_b) were equal to those in the axisymmetric model. As discussed in paragraph 5.5., these measures are not sufficient to obtain equivalent results.
Calculations were carried out for two cases: A rigidly connected stem-cement interface and slip-and-no-tension at the interface. Fig. 6.4. shows a comparison of stresses at the stem-cement interfaces, as calculated for the two cases; apparently the stress distribution in the cement is greatly influenced when a loose stem is assumed.
The stresses in the cement at the cement-bone interface also differ, as is shown for σ_x in

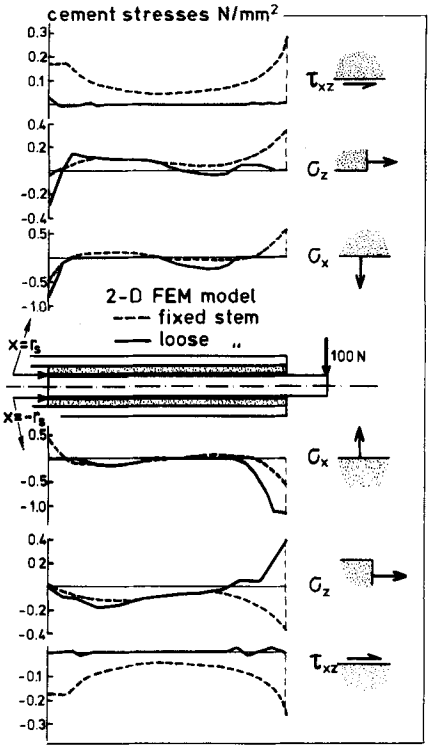

fig. 6.4: Stress components in the cement at the stem-cement interface on both sides of the stem, calculated for a rigidly fixed interface and as calculated simulating slip and loosening-upon-tension. The 'noise' in the courses of τ_{xy} for the latter case is due to inaccuracies in the solution procedure.

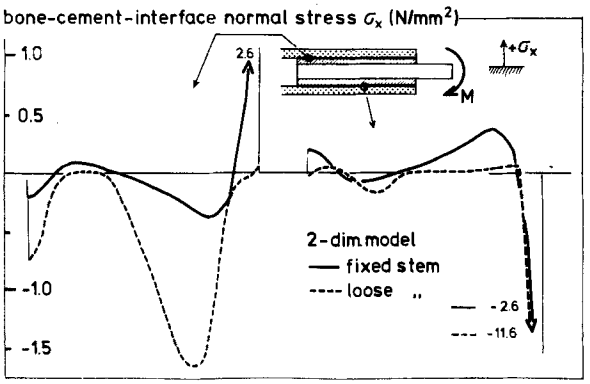

fig. 6.5: Transverse stresses at the cement-bone interface as calculated for a rigidly connected stem-cement interface and as calculated simulating slip and loosening-upon-tension at this interface. Apparently the latter phenomenon results in the effect that at the cement-bone interface also, hardly any tensile stress is present. The same effect was found for the shear stresses.

fig. 6.5. Apparently only very slight tensile stresses occur at this interface in the loose stem case. Shear stresses, too, were found to be very low at this interface. Hence, little difference would be found for the stress distribution in the cement if the cement-bone interface were also assumed as loose in addition to the stem-cement interface. The stem stresses were found to be slightly different, as shown in fig. 6.6. It should be noted that the stem stresses do not increase very much in the loose-stem case, as would be found for a sandwich construction as discussed in paragraph 5.5., where no side plates are applied in the model. The (axial) stresses in the bone do not change significantly for a loose stem.

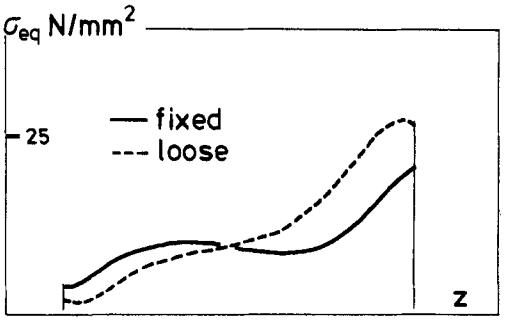

fig. 6.6: A comparison of stem (equivalent) stresses as calculated simulating a rigidly connected stem-cement interface and simulating slip and loosening-upon-tension at this interface.

From the stresses normal to the interface (σ_x) as calculated in the model, the continuously distributed transverse load p(z), as defined in paragraph 5.2, can be derived simply by superposition of the stresses on either side of the stem, multiplied by the stem thickness in y-direction (d). It then follows (fig. 6.7) that the difference between the results for the two cases is not very outspoken. It thus appears that the interface condition has a general effect by which, for instance p(z) is affected and $M_s(z)$ and $M_b(z)$ will also be affected, and a local effect, by which the local stress values, as for instance is apparent in fig. 6.4, are affected. Both effects will be evaluated separately in the remainder of this paragraph.

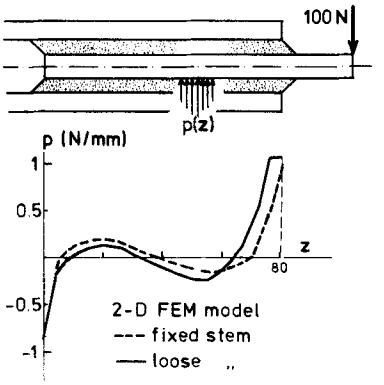

fig. 6.7: A comparison of the continuously distributed transverse loads p(z) on the stem as calculated from the FEM results concerning a fixed and a loose stem-cement interface.

6.2.2. *The general effect*

It was shown in paragraph 5.2. that, upon transverse loading, the mechanical behavior of the structure is principally determined by the parameters λ_t, F_s, F_b, C_t and L. For a loose stem only C_t is affected and, through C_t, also λ_t. If we assume circular geometry (axisymmetric model) the value of C_t can be approximated by (appendix B)

$C_t \approx 6.2E_c(0.24 + \frac{\rho}{1-\rho})$ for a rigidly connected interface and

$C_t \approx 2.1E_c(0.24 + \frac{\rho}{1-\rho})$ for a loose interface.

It then follows that

C_t(loose stem)/C_t(fixed stem) ≈ 0.34
λ_t(loose stem)/λ_t(fixed stem) ≈ 0.76

The stem will thus 'feel' a more flexible layer in the loose case and the force-introduction regions at the proximal and the distal sides will be more extended.
Also, the maximal values of p(z) at the proximal and distal sides will be lower in the loose case, since both depend on C_t/λ_t^2 and C_t/λ_t^3 (table 5.II).
In fig. 6.8 it is shown, for example how this change in C_t affects $M_s(z)$, $M_b(z)$ and p(z), as calculated with the beams-on-elastic-foundation model described in paragraph 5.2.

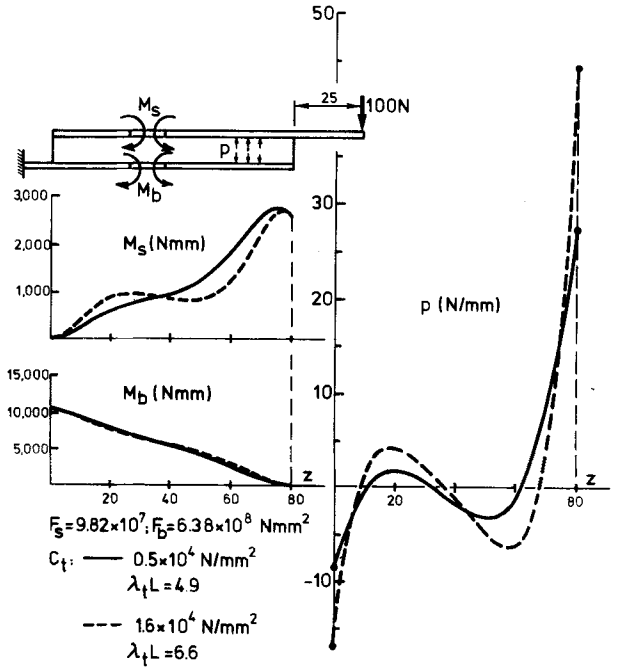

fig. 6.8: Bending moments in stem and bone ($M_s(z)$ and $M_b(z)$) and distributed transverse load p(z) calculated using the beams-on-elastic-foundation model, for two different values of C_t, simulating a fixed stem ($C_t = 1.6x10^4 N/mm^2$) and a loose stem ($C_t = 0.5x10^4 N/mm^2$).

6.2.3. *The local effect*

The local effect is caused by the circumstance that in the loose case only approximately half of the stem circumference is available to transfer loading. As was shown in paragraph 5.2. (fig. 5.9), for a fixed stem $p_s(z)$ is found from

$$p_s(z) = -\int_0^{2\pi} (\sigma_r \cos\varphi - \tau_{rt}\sin\varphi) r_s d\varphi$$

Because $\sigma_r = \hat{\sigma}_r \cos\varphi$, $\tau_{rt} = \hat{\tau}_{rt}\sin\varphi$ and $\hat{\tau}_{rt}$ is always opposite in sign as compared to $\hat{\sigma}_r$, it follows that

$$|p_s(z)| = \pi r_s(|\hat{\sigma}_r| + |\hat{\tau}_{rt}|), \text{ for a fixed stem} \qquad (6.1)$$

For the case of the loose stem (assuming $\tau_{rt} = 0$) σ_r can be approximated by assuming it to be distributed along half of the stem circumference (fig. 6.9) as a cosine function in φ: $\sigma_r = \hat{\sigma}_r \cos\varphi$, $-\frac{\pi}{2} \leq \varphi \leq \frac{\pi}{2}$, so that

$$|p_s(z)| = \frac{\pi}{2} r_s |\hat{\sigma}_r|, \text{ for a loose stem} \qquad (6.2)$$

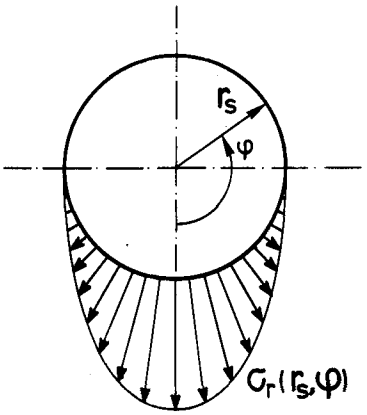

fig. 6.9: Radial stress distribution at the stem-cement interface, in the case of a loose stem, assumed as a cosine function along half the circumference.

It thus follows for $p_s(z)$ with the same local value that $\hat{\sigma}_r$ is at least twice as high in the loose case compared to the fixed case.
The local influence of a loose stem for a given local value of p(z) was evaluated using a FEM model of a slice of the (axisymmetric) intramedullary fixation system, assuming the previously mentioned expression for σ_r (Huiskes and Schouten, 1979), an example of which calculations is given in fig. 6.10. It is evident that for given p(z) the radial stress as well as the hoop stress will be much higher in the loose case. In these calculations it was again found that at the cement-bone interface the radial stress was distributed only along half the circumference, hence it would make very little difference if this interface were

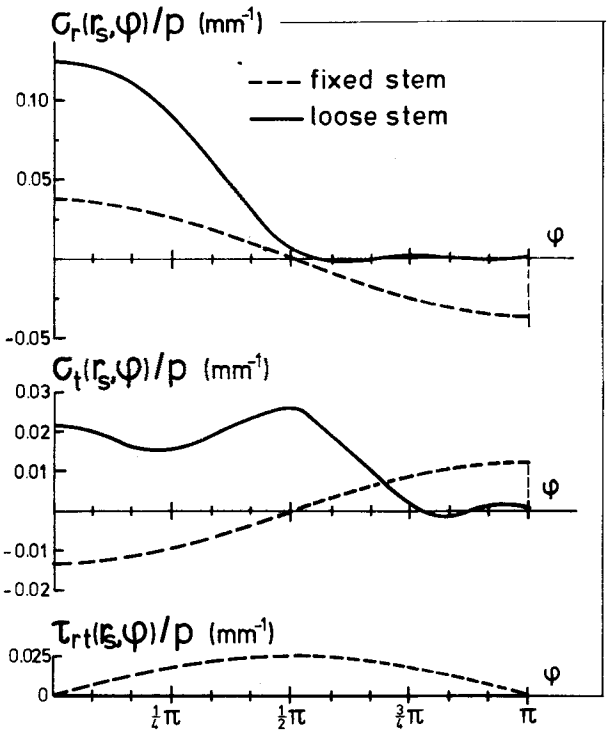

fig. 6.10: Radial, circumferential and shear stress distribution on half the circumference of the stem-cement interface, as calculated using FEM in a slice of the structure, for a loose stem and a fixed stem (Huiskes and Schouten, 1979). The stress components are given as relative to the local value of the transverse load p(z). The 'noise' in the curves of the stresses in the case of a loose stem is caused by the solution procedure (Fourier expansion).

assumed to be loose in addition, which could be concluded also from the results discussed in paragraph 6.2.1.

6.2.4. *Conclusions*

In reality the interface conditions will be more complicated. Friction will most certainly occur and locked-in stresses may also be present, at least directly postoperatively. Even in the idealized axisymmetric model discussed here, the interface behavior is nonlinear, because in principle the contact area changes with the load. For a loose stem, no initial locked-in stresses, assuming a contact area over half the stem circumference results in a reasonable approximation of the stress distribution (Schoofs, 1979). In the case that locked-in stresses are present, the non-linear effect will be more pronounced. In this case, that will occur during the initial postoperative period, a C_t value in accordance with a fixed stem is an upper boundary and one in accordance with a loose stem a lower boundary for the apparent cement layer stiffness.

It was shown that the loosening-upon-tension aspect of the stem-cement interface has a moderate general effect on the mechanical behavior of the structure and an outspoken local effect, mainly on the cement and interface stresses. The general effect can be taken into account by adjusting the value of C_t and the local effect by interpreting the continuously distributed transverse load p(z) as working on half the stem circumference only. If it is the object to evaluate the stress distribution in the cement layer and at the interfaces in detailed three-dimensional FEM models, the slip and loosening-upon-tension aspects should be taken into account. Once this is done for the stem-cement interface, the conditions at the cement-bone interface will not have much influence anymore.

6.3. Nonconstant cross-sectional properties of the stem

For the analyses discussed in chapter 5, it was assumed that the cross-sectional properties of the stem (F_s and P_s) were constant. The stem may be tapered to some extent and since Young's modulus is constant, F_s and P_s will be functions of z, as well as C_t and C_a. It can be anticipated that for a slight taper the formulas derived in chapter 5 will still apply by approximation; for a more pronounced taper this may not be so.
When the dependencies of z in C_a and C_t are neglected in this case (neglecting dC_a/dz, d^2C_a/dz^2, dC_t/dz and d^2C_t/dz^2), the differential equations as in paragraph 5.2. can be formulated in the bending moments (M_s and M_b) and the axial forces (N_s and N_b), respectively, so that the coefficients λ_t and λ_a still have significance; this time, however, as functions of z.
A first-order evaluation of the taper influence can be established by regarding the influences on $\lambda_t(z)$ and $\lambda_a(z)$. Three different stem shapes are assumed (fig. 6.11) in an example (axisymmetric structure). For λ_t and λ_a it can be found (taking C_t and C_a according to appendix B) that

$$\lambda_t = A_1 \sqrt[4]{\left\{\frac{\rho}{1-\rho}\left(\frac{F_b}{F_s}+1\right)\right\}} \quad \text{and} \quad \lambda_a = A_2 \sqrt{\left\{\frac{-1}{\ln\rho}\left(\frac{P_b}{P_s}+1\right)\right\}}$$

where $\rho = r_s/r_b$ and A_1 and A_2 are constants depending on E_c, ν_c, E_b, the bone dimensions and the interface conditions.

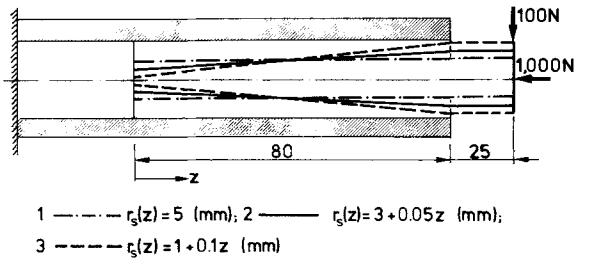

fig. 6.11: The three different stem shapes investigated with the FEM beam model.

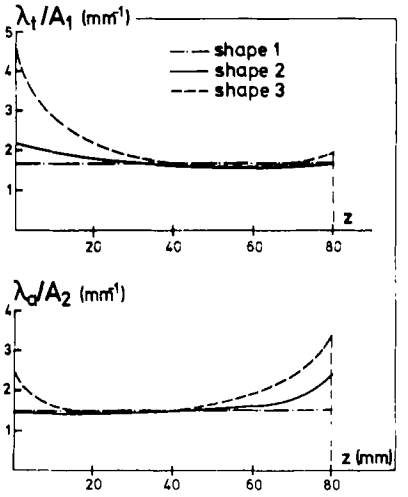

fig. 6.12: The coefficients λ_t and λ_a as functions of z for the three stem shapes (for the constants A_1 and A_2 see text).

For the tapers shown in fig. 6.11 the courses of λ_t/A_1 and λ_a/A_2 as functions of z were evaluated, as shown in fig. 6.12. It can be anticipated, looking at these graphs, that in transverse loading there will be little difference in the mechanical behavior of the structure on the proximal side, but a significant difference on the distal side, especially where the pronounced taper is concerned. In axial loading there should be little difference for the moderate taper compared to the constant cross-sectional shape on the distal side and some difference on the proximal side; there should be a marked difference for the pronounced taper compared to the constant shape.
Nonconstant cross-sectional properties of the structure can be taken into account in the FEM beam model, as described in paragraph 5.4. This model was used to calculate p(z), q(z), $M_s(z)$, $M_b(z)$, $N_s(z)$ and $N_b(z)$ for the examples shown in fig. 6.11. Results are shown in fig. 6.13. It follows from these graphs, on consideration of the courses of p(z) and q(z), that the predictions expressed previously are fulfilled. Nevertheless the difference in q(z) at the distal side for the moderate taper shape compared to the constant shape is somewhat more outspoken than anticipated. Since in the case of the straight stem $\lambda_t L \approx 5.0$ and $\lambda_a L \approx 2.9$, this non-predicted difference is probably caused by a significant influence from the proximal side on the distal side in axial loading (as discussed in paragraph 5.3., π/λ_a determines the length of the load-introduction regions for axial loading).
It is also found that the maximal values of p(z) and q(z) on the distal side can be predicted by approximation with the formulas presented in table 5.11 using the local value of r_s (respectively r_s = 5,3 and 2 mm). For transverse loading especially this approximation is excellent, as shown in fig. 6.13. At the proximal side such an approximation does not succeed, probably owing to a stronger dependency of the stress variables on F_s and P_s (see table 5.11), and a higher sensitivity of C_t and C_a for the (varying) ratio ρ in this region, because of the small thickness of the cement layer.

Since the stem thickness varies, $M_s(z)$, $N_s(z)$, p(z) and q(z) are no longer proportional to the stem, cement and cement-stem interface stresses. Representative of these stresses are the average transverse stress at the interface $\bar{s}_{rs} = p/2r_s$ and the maximal axial stem stress $s_{zs} = M_s/W_s$, in transverse loading, and the interface shear stress $t_s = q/\gamma_s$ and the maximal

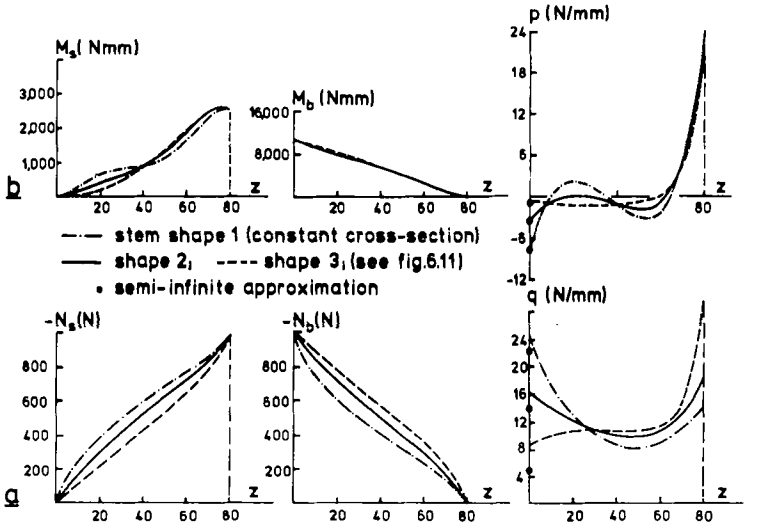

fig. 6.13: Continuously distributed shearing load q(z), stem and bone axial forces $N_s(z)$ and $N_b(z)$ on axial loading (a) and continuously distributed transverse load p(z), stem and bone bending moments $M_s(z)$ and $M_b(z)$ on transverse loading (b), as calculated using the FEM beam model for the three stem shapes. Also indicated are the values for q(0) and p(0) (distal side), as calculated with the semi-infinite approximation, using the local stem radius in the formulas.

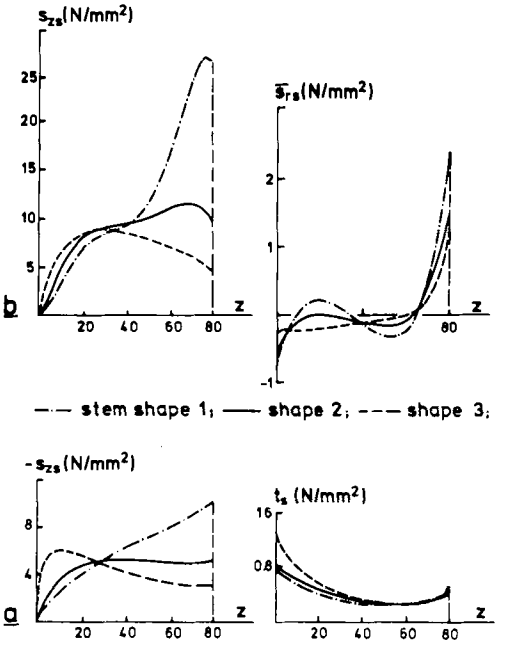

fig. 6.14: Stem and cement stresses on axial loading (a) and on transverse loading (b), as calculated for the three stem shapes.

axial stem stress $s_{zs} = N_s/A_s$ in axial loading, as defined in paragraph 5.2. These stress quantities are shown in fig. 6.14 for the three different stem shapes. The courses of $s_{zs}(z)$ for the tapered stems are very much like the stem stresses that were measured by Huggler *et al* (1978) in strain-gauge experiments on hip prostheses in cadaveric femurs, and the courses of $s_{zs}(z)$, $\bar{s}_{rs}(z)$ and $t_s(z)$ are comparable to results of three-dimensional FEM models (e.g. Scholten *et al*, 1978). It should be noted that the stresses in the bone ($s_{zb}(z)$) and at the cement-bone interface ($\bar{s}_{rb}(z)$ and $t_b(z)$) are directly proportional to $M_b(z)$ and $N_b(z)$, $p(z)$ and $q(z)$, respectively, since r_b remains constant. Regarding figs. 6.13 and 6.14 it is evident that the use of a tapered stem benefits the system performance. In transverse loading the pronounced taper shows the best results, in axial loading the moderate taper. In chapter 8 the stem shape will be further discussed.

In the literature, composite beam theory is often used to evaluate the stresses in the stem (e.g. Bartel and Desormeaux, 1976a; Walker, 1977; Swanson and Freeman, 1977). As we have seen in paragraph 5.3., this approximation is valid for the middle region of structures with constant cross-section, if $\lambda_t L$ and $\lambda_a L$ are sufficiently large. For tapered stems the approximation may be rather poor, as is illustrated in fig. 6.15 for the moderately tapered stem.

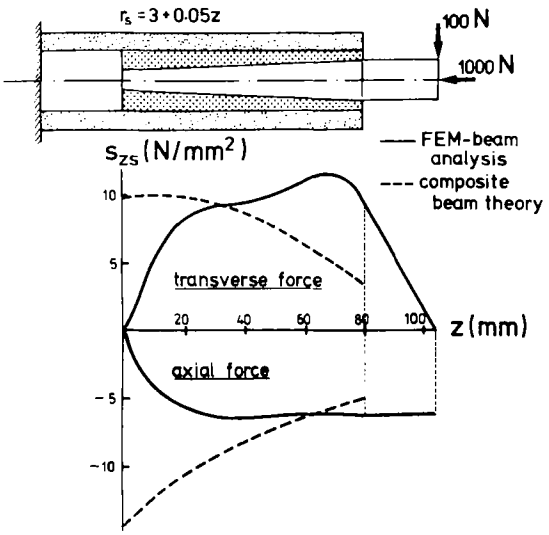

fig. 6.15: A comparison of stem stresses on axial and transverse loading, as calculated for stem shape no. 2, using the FEM beam model and composite beam theory; the latter method is in this case not very accurate.

6.4. Other aspects

The cross-sectional properties of the bone will vary, too, as functions of z. In the femur the outside dimensions increase from the diaphysis region to the proximal side. Likewise, the width of the medullar canal increases, while more trabecular bone is present in the metaphysis (with a lower Young's modulus) compared to the diaphysis region. The varieties in the geometrical and material stiffness, however, work in opposite directions, as was discussed

in chapter 4, so that the varieties in F_b and P_b are probably not very pronounced. Since the stem and the bone play analogue but inverse roles with respect to the proximal and distal sides, the same kind of reasoning as for the nonconstant stem shape applies. Also in this case the influences of arbitrary variations in z can be evaluated by using the FEM beam model.

It is not known whether, due to the trabecular bone in the epiphyseal regions of the bones, deviations from beam theory might occur. It is to be expected, because, as was shown in paragraph 5.1., in the schematized 'bone' with homogeneous properties assumed, deviations from beam theory already occurred (fig. 5.5).
In, for instance the proximal tibia, this effect will be more pronounced than in the proximal femur, since in the latter case cortical bone is present in the calcar region (on the medial side) where the greater part of the (transverse) load is introduced, due to the loosening-upon-tension aspect of the stem-cement interface.
Due also to the epiphyseal spongeous bone, which serves as an elastic layer, the peak values in p(z) and q(z) could be lower and the load introduction somewhat smoother (smaller λ_t and λ_a) as indeed is apparent in the results from the three-dimensional models of Scholten *et al* (1978), where non-homogeneous bone properties are taken into account. These effects can also be investigated by means of the FEM beam model.
Apart from the inhomogeneous properties of the bone, anisotropy was also neglected in the models, as well as the slight curvatures of the stem and the bone. It is expected that these phenomena will not affect the qualitative aspects of the model results.

It has been shown in paragraph 5.2. that the formulas derived for the characterization of the mechanical behavior of the structure are valid for arbitrary cross-sections of the stem and the bone, while for circular geometry examples were evaluated. This means that the local influences of different stem cross-section geometries can be studied perfectly by modeling local sections, as was done by Crowninshield and Branch (1978). For such studies the local loading can be derived from more general beams-on-elastic-foundation or FEM beam analyses, as discussed here.

Effects that likewise were not taken into account here are those that may follow from the implantation procedure, for instance incomplete cement mantles, or from bone remodeling, for example proximal bone resorption. The influences of these effects could be roughly evaluated by applying the FEM beam model.
Furthermore the effect of a collar on the proximal side of the hip-endoprosthesis stem (collar-calcar contact, see section I) has not been taken into account. In all stress analyses reported in the literature this collar-calcar contact is considered as beneficial, which is hardly surprising, since the loads (especially the axial load) will be introduced more directly to the cortex, in a more natural way. As follows directly from the analysis presented in paragraph 5.3. this will only influence the stresses in the proximal load introduction region and not in the middle and the distal regions, as was also found by Crowninshield *et al* (1979) in their three-dimensional FEM model. There appears to be enough evidence that collar-calcar contact, although present directly after surgery, disappears upon load bearing post-operatively, due to (although mostly minor) bone resorption (see section I). Hence a collar has no significance for the long-term performance of the bone-prosthesis structure.
When looking at the time factor in this respect, it is evident (see also section I) that several effects tend to change the mechanical characteristics of the intramedullary fixation structure.
For example:
early postoperative:
- collar-calcar contact (if a collar is present);

– thermal locked-in stresses (initial stresses, no loosening upon tension at the cement-stem interface);

later postoperative:

– no collar-calcar contact;
– no thermal locked-in stresses (loosening upon tension, hence a lower C_t value for the cement mantle, decreased λ_t; less friction);
– osteoporosis (decreasing F_b and P_b, hence increasing λ_t and λ_a);

late postoperative:

– calcar resorption (increased free stem length, reduced fixation length);
– further osteoporosis (decreasing F_b and P_b, increasing λ_t and λ_a, especially at the proximal side);
– cement ageing (reduced E_c, reducing C_a and C_t, λ_a and λ_t);
– fibrous tissue layer at the cement-bone interface.

An interesting investigation would be to follow such processes and roughly quantify the effects of the changes on the stress distribution in the structure. For such a study the analytical concepts and the FEM beam model developed here can be used, combined with radiographical or (in animal studies) histological data.

Another aspect that has been neglected here, and indeed has received little attention in orthopedic biomechanics literature, is the incidence of torsion on the stem. Torsion will occur in the artificial-hip joint, as was shown for instance by Rydell (1966) (see section I), and will even be the most important loading case in the elbow joint. For a first-order evaluation of the effect of torsional loading the axisymmetric model can again be used. Also in this case the Winkler hypothesis can be applied to the cement layer. Its stiffness is then represented by a continuous set of linear torsional springs. The mechanical behavior of the structure in torsion is described by torsional moments in the stem and the bone and by a continuously distributed shearing moment at the interfaces (Nmm/mm), as functions of z. Here, too, the stiffness of the cement mantle can be approximated by a stiffness factor comparable to C_a in axial loading. If the differential equations are formulated in the tangential displacements of the outer stem and the inner bone circumferences, they are found to be completely analogous with those of the axial loading case, boundary conditions included. Hence the solutions are identical, except for the expressions of the stiffness factors.
A comparison of stem, bone and cement stiffness factors is shown in table 6.I.

	axial loading		torsional loading		
cement mantle (C_a in axial loading)	$-\frac{\pi E_c}{(1+\nu_c)\ln\rho}$	(N/mm²)	$\frac{\pi\rho E_c r_b}{(1-\rho)(1+\nu_c)}$	(1)	(N/mm)
stem (P_s in axial loading)	$\pi r_s^2 E_s$	(N)	$\frac{\pi E_s r_s^3}{4(1+\nu_s)}$		(Nmm)
bone (P_b in axial loading)	$\pi E_b(r_o^2 - r_b^2)$	(N)	$\frac{\pi E_b(r_o^4 - r_b^4)}{4r_b(1+\nu_b)}$		(Nmm)

table 6.I: Structural stiffness factors of the stem, the bone and the cement mantle (axisymmetric model) in torsional loading compared to those for axial loading; (1) reasonable approximation when ρ is sufficiently close to 1.

Likewise the coefficient λ_w in torsion, that determines the lengths of the proximal and distal regions has the same form as λ_a in axial loading. For $\rho = 0.5$ it follows (assuming the reference values as discussed in chapter 3 for the other parameters) that $\lambda_a \approx 0.04\ mm^{-1}$ and $\lambda_w \approx 0.06\ mm^{-1}$; for $\rho = 0{,}8$, $\lambda_a \approx 0.05\ mm^{-1}$ and $\lambda_w \approx 0.08\ mm^{-1}$.
In conclusion, the proximal and distal regions will be shorter in torsional loading compared to axial loading and, qualitatively speaking, the same tendencies that are found for axial loading apply to torsional loading.
It should be remarked here that one should be rather careful with these formulas for torsional loading, since they have not been verified in a FEM analysis.
Furthermore, especially for non-circular geometries the mechanical behavior of the structure may be quite complicated in torsion.

CHAPTER SEVEN

THE INFLUENCES OF THE ESSENTIAL PARAMETERS

7.1. Premises

The influences of the essential parameters on the mechanical behavior of the bone-prosthesis structure can be evaluated with the formulas derived in paragraph 5.3. (see table 5.II) and by applying parametric analysis, using the other models discussed in chapter 5.
For reasons of convenience, the factors in the formulas of table 5.II are denoted as follows:

proximal region : $\alpha_m = \frac{1}{2}\frac{C_t}{\lambda_t^2 F_s}$; $\alpha_t = \frac{1}{2}\frac{C_t}{\lambda_t^3 F_s}$; $\alpha_n = \frac{\lambda_a P_b}{P_s + P_b}$;

distal region : $\beta_m = \frac{1}{2}\frac{C_t}{\lambda_t^2 F_b}$; $\beta_t = \frac{1}{2}\frac{C_t}{\lambda_t^3 F_b}$; $\beta_n = \frac{\lambda_a P_s}{P_s + P_b}$;

middle region : $\epsilon_m = \frac{F_s}{F_s + F_b}$; $\epsilon_n = \frac{P_s}{P_s + P_b}$;

where λ_t and λ_a can be evaluated from

$$\lambda_t = \sqrt[4]{\left\{\frac{C_t}{4}\left(\frac{1}{F_s} + \frac{1}{F_b}\right)\right\}} \quad \text{and} \quad \lambda_a = \sqrt{\left\{C_a\left(\frac{1}{P_s} + \frac{1}{P_b}\right)\right\}}$$

Using these two expressions, the factors α_m through ϵ_n can be rewritten as functions of C_t, C_a, F_s, F_b, P_s and P_b only.
These forms are valid for arbitrary cross-sectional geometry; C_a and C_t can be approximated using the formulas presented in appendix B.
Using the factors defined above, the stress variables for the proximal, distal and middle regions, as defined in paragraph 5.3., can be expressed as shown in table 7.I; these stresses are once more illustrated in fig. 7.1. By considering these formulas and the expressions for the factors α_m through ϵ_n (taking the expressions for λ_t and λ_a into account) the influences of the structural parameters on the most important stresses can be directly evaluated.
In table 7.II these influences are given qualitatively.

In the following paragraphs the parameter influences are discussed separately, mainly using the formulas but also as follows from parametric analyses with the other models.

7.2. The stem length

The length of the stem, together with the values of λ_t and λ_a, determine whether the proximal and distal stresses influence each other and whether there is a middle region that behaves approximately in accordance with composite beam theory.

stress component	proximal region (z = L)	distal region (z = 0)
$s_{zs} = \frac{M_s}{W_s} + \frac{N_s}{A_s}$	$\frac{M_L}{W_s} + \frac{N_L}{A_s}$	0
$\bar{s}_{rs} = \frac{p}{2r_s}$	$\frac{\alpha_m}{2r_s} M_L + \frac{\alpha_t}{2r_s} T_L$	$-\frac{\beta_m}{2r_s}(M_L + T_L L) + \frac{\beta_t}{2r_s} T_L$
$\bar{s}_{rb} = \frac{p}{2r_b}$	$\frac{\alpha_m}{2r_b} M_L + \frac{\alpha_t}{2r_b}$	$-\frac{\beta_m}{2r_b}(M_L + T_L L) + \frac{\beta_t}{2r_b} T_L$
$t_s = \frac{q}{\gamma_s}$	$-\frac{\alpha_n}{2\pi r_s} N_L$	$-\frac{\beta_n}{2\pi r_s} N_L$
$t_b = \frac{q}{\gamma_b}$	$-\frac{\alpha_n}{2\pi r_b} N_L$	$-\frac{\beta_n}{2\pi r_b} N_L$
middle region: $s_{zs} = \frac{M_s}{W_s} + \frac{N_s}{A_s} = \frac{\epsilon_m}{W_s}(M_L + T_L(L-z)) + \frac{\epsilon_n}{A_s} N_L$		

table 7.I: Approximative formulas describing the most important stress variables in the stem, the bone, in the cement layer and at the interfaces in the proximal, middle and distal regions respectively (see also table 5.II and fig. 7.1).

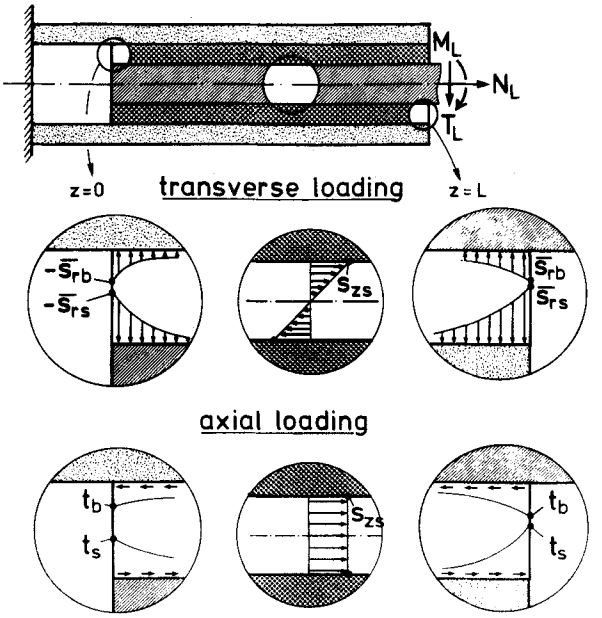

fig. 7.1: An illustration of the stress components in the stem, the bone, the cement and at the interfaces, on transverse and axial loading, as described by the approximative formulas.

	C_t	F_s	F_b	C_a	P_s	P_b
proximal:						
α_m	+	—	+	o	o	o
α_t	+	—	+	o	o	o
α_n	o	o	o	+	—	+
distal:						
β_m	+	+	—	o	o	o
β_t	+	+	—	o	o	o
β_n	o	o	o	+	+	—
middle:						
ϵ_m	o	+	—	o	o	o
ϵ_n	o	o	o	o	+	—

table 7.II: Qualitative influences of the single characteristic structural parameters on the factors α, β and ε; for (+) the factor increases with increasing parameter value, for (—) it decreases, for (o) there is no influence.

It should be kept in mind that, generally speaking, the stresses at the proximal and distal sides are lower when they do not influence each other and that the middle region serves no purpose in the prosthesis-bone load transmission.
For values of approximately $\lambda_t L \geqq \pi$ and $\lambda_a L \geqq \pi$ there is little influence from the distal on the proximal side and vice versa. This means also, that when the stem length is extended beyond $L \approx \pi/\lambda_t$ and $L \approx \pi/\lambda_a$, this has very little influence on the stresses in the structure resulting from the respective loading cases. However, there is one exception: as shown in tables 5.II and 7.I, L appears in the formulas for the distal stresses ($p(0)$, $\bar{s}_{rs}(0)$ and $\bar{s}_{rb}(0)$) and the stem stresses in the middle region ($s_{zs}(z)$), as a coefficient of T_L, the transverse force. Hence, for this loading case it is of importance to keep the length restricted; a more-or-less 'optimal' value would then be $L \approx \pi/\lambda_t$.

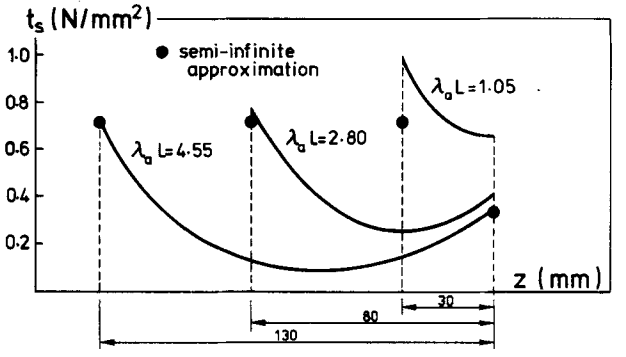

fig. 7.2: Shear stress at the stem-cement interface on axial loading as calculated using the beams-on-elastic-foundation theory, for three different lengths of the stem. Also indicated are the values for q(0) and q(L) as calculated using the semi-infinite approximation, which is appropriate when $\lambda_a L$ is sufficiently high.

Fig. 7.2 gives an example of $t_s(z)$ upon axial loading as calculated for three different stem lengths, using the beams-on-elastic-foundation theory described in paragraph 5.2.2.; the values that result from the semi-infinite theory,using the formulas of table 7.I, are also shown. It is evident that for $L > 80$ mm, extending the length has little effect on the maximal stress values. As follows again from fig. 7.2, the semi-infinite approximation is better for the longer stems.
Fig. 7.3 shows an example of the courses of $M_s(z)$, $M_b(z)$ and $p(z)$ upon transverse loading for three different stem lengths, as calculated with the theory described in paragraph 5.2.1. It should be noted that a dimensionless coordinate (z/L) is used on the horizontal axis. Extending the length from 80 to 130 mm has no effect on the proximal stresses and a negative effect on the distal cement stresses and the stem stresses, due to the previously described influence of T_L. In this case, too, the semi-infinite approximations of p(0) and p(L) are indicated in the figure.

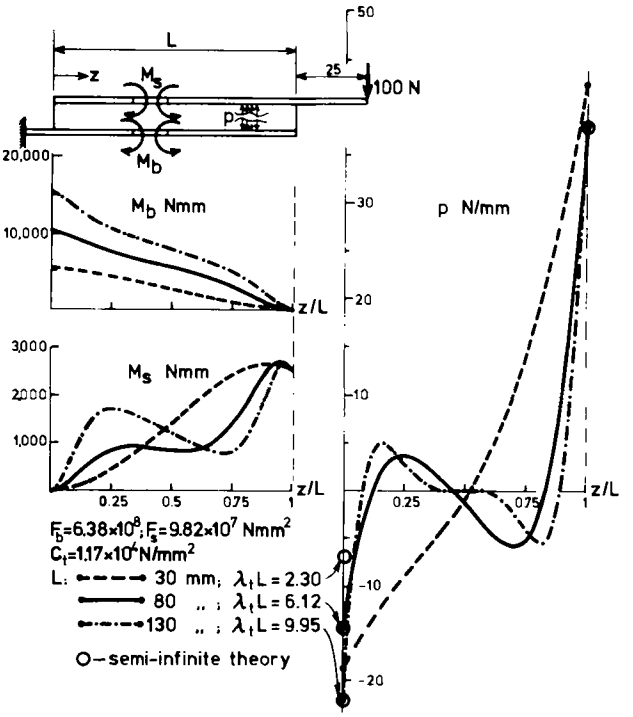

fig. 7.3: Bending moments in the stem and the bone ($M_s(z)$ and $M_b(z)$) and the continuously distributed transverse load p(z) as calculated with the beams-on-elastic-foundation theory for three different stem lengths. Note that, in this case, z/L is put on the horizontal axis. The values for p(0) and p(L) as calculated with the approximative formulas are also indicated. For the very short stem these formulas no longer apply very accurately.

The influences discussed above are confirmed for other stress components as well, when the three-dimensional FEM model is used to analyze the effect of the stem length, as was shown in Huiskes *et al* (1977). As discussed in chapter 5, the stem and bone stresses are quite accurately described in the beams-on-elastic-foundation models, but several stress components

in the cement layer are neglected. These components show the same tendencies as the ones discussed above, as for example is shown in fig. 7.4 as regards the hoop stress (σ_t), the axial stress (σ_z) and the shear stress (τ_{rz}) in transverse loading.

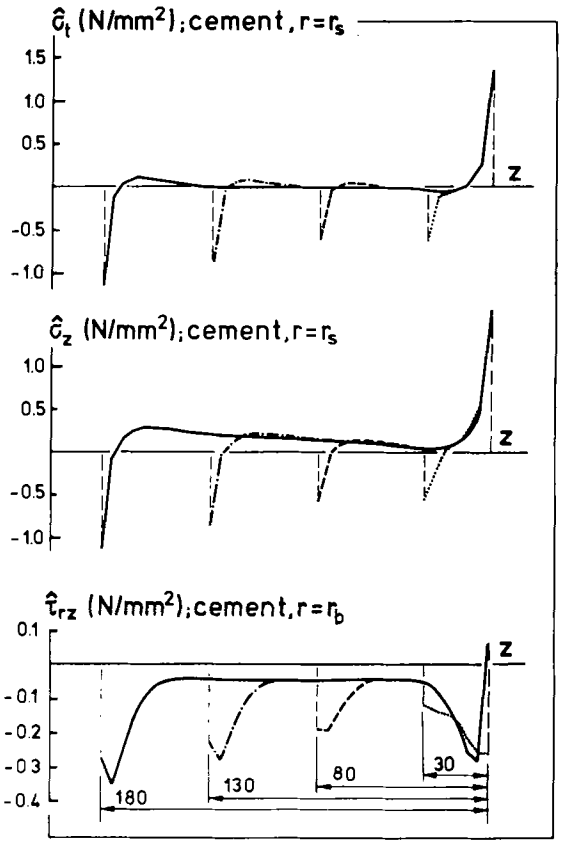

fig. 7.4: Hoop stresses and axial stresses in the cement layer at the stem-cement interface and shear stresses at the cement-bone interface as calculated with the three-dimensional FEM model, on transverse loading, for four stem lengths.

7.3. The structural stiffness of the cement mantle

The factors α_m and β_m are proportional to $\sqrt{C_t}$, α_t and β_t to $\sqrt[4]{C_t}$ and α_n and β_n to $\sqrt{C_a}$. Hence, all important cement and interface stresses will decrease with decreasing C_t and C_a. Also, λ_t and λ_a are influenced by C_t and C_a, respectively. In general it can be said that the load introduction at the proximal and distal sides will be smoother for lower values of C_t and C_a.
Fig. 7.5 shows an example of values for $M_s(z)$, $M_b(z)$ and $p(z)$ on transverse loading as calculated for three values of C_t, using the beams-on-elastic-foundation theory. The decrease in the proximal and distal maximal values of $p(z)$ on decreasing C_t is apparent. The stresses in the stem are only slightly influenced. Owing to the decreasing value of λ_t, with decreasing C_t the middle region is shortened. The same effects are apparent in axial loading. For low C_a, the shear stresses will tend to be smoothened towards a constant value over the length of the

structure. There is only a minor influence on the stem and the bone stresses in this case, too.

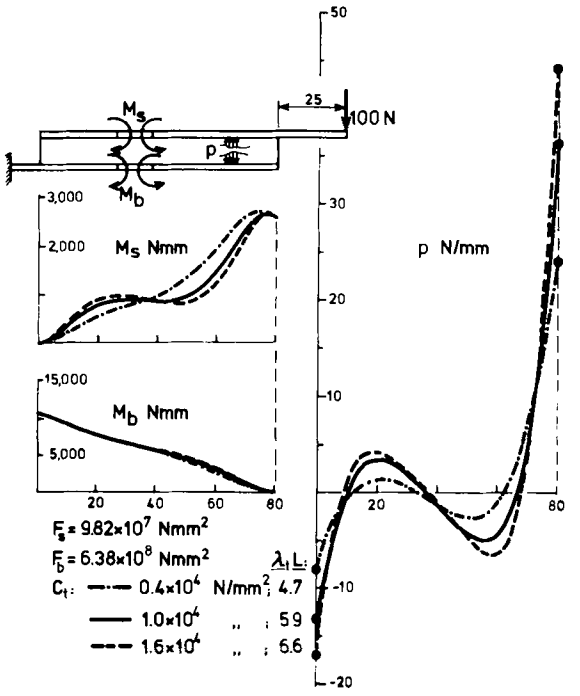

fig. 7.5: $M_s(z)$, $M_b(z)$ and $p(z)$ as calculated with the beams-on-elastic-foundation theory for three different values of C_t, keeping the other parameters (F_s, F_b and L) constant.

C_t and C_a depend on the thickness, the Young's modulus and the Poisson's ratio of the cement layer. The layer thickness depends on the dimensions of the stem and the bone, which will be discussed later. C_t and C_a are directly proportional to E_c. C_t is by approximation proportional to $(1-\nu_c)/(1+\nu_c)(1-2\nu_c)$ (appendix B); for $0.2 \leq \nu_c \leq 0.4$, this factor varies from approximately 1.1 to 2.1. C_a is by approximation proportional to $1/(1+\nu_c)$, which varies from only 0.8 to 0.7 in the above-mentioned range. Hence, overall, a low value of ν_c is advantageous.

These effects were again confirmed for other stress components as well with the three-dimensional FEM model (Huiskes, 1977; Huiskes and Slooff, 1978). Only in one respect did this model give additional information: the value of ν_c has a marked influence on the axial and hoop stresses in the cement mantle, as shown in fig. 7.6.

7.4. The structural stiffness of the stem

The structural stiffness of the stem, expressed in F_s and P_s, depends on its material stiffness (Young's modulus) and its geometrical stiffness (cross-sectional area and second moment of inertia). Higher values of F_s and P_s will reduce λ_t and λ_a, so that the proximal and distal load introduction regions will be extended.

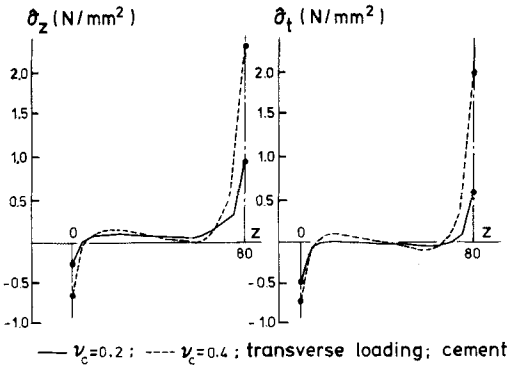

fig. 7.6: Axial and hoop stresses in the cement at the stem-cement interface, on transverse loading, as calculated with the three-dimensional FEM model for two different values of ν_c.

The values of α_m, α_t and α_n will also decrease, causing p(L) and q(L) (proximal side) to decrease; β_m, β_t, β_n, ϵ_m and ϵ_n will increase, as a result of which p(0) and q(0) (distal side), $M_s(z)$ and $N_s(z)$ (middle region) increase. This is illustrated in fig. 7.7 for transverse loading, where $M_s(z)$, $M_b(z)$ and p(z) are shown as calculated for three values of F_s, using the beams-on-elastic-foundation model. Apparently p(L) is more sensitive to F_s than p(0) due to the fact that β_m, for example is approximately proportional to $\sqrt{F_s}$ and α_m to $1/F_s$.

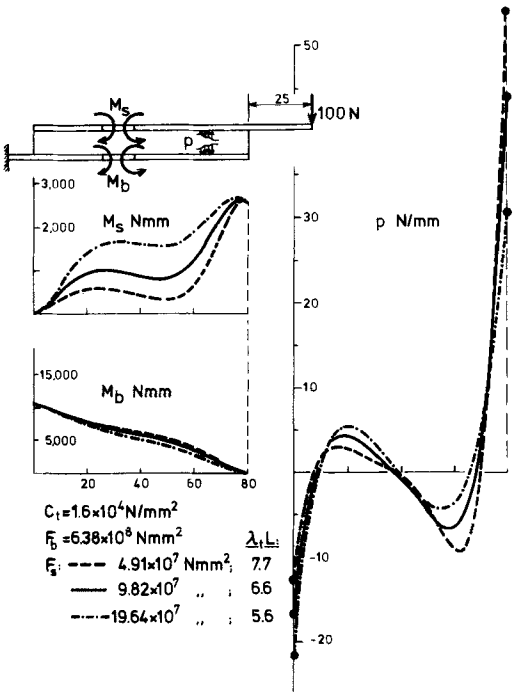

fig. 7.7: $M_s(z)$, $M_b(z)$ and p(z) on transverse loading, as calculated with the beams-on-elastic-foundation theory for three different values of F_s, keeping the other parameters (F_b, C_t and L) constant.

Changing F_s and P_s without affecting other parameters is only possible by changing E_s. In this case the structure will be influenced purely as described above. This was again confirmed for other stress components in the cement on application of the three-dimensional FEM model (Huiskes, 1977; Huiskes and Slooff, 1978).
When the thickness of the stem is changed, apart from the influences on F_s and P_s, two other effects play a role: the thickness of the cement layer changes, hence C_a and C_t are influenced, and the load-transferring area of the stem-cement interface (represented by r_s) changes, which has a local effect on the stresses. At the proximal side the first effect (F_s and P_s) and the last effect (r_s) combine to decrease or increase the stresses, but the second effect (C_t and C_a) works in the opposite direction. At the distal side the first effect (F_s and P_s) and the second effect (C_t and C_a) combine to decrease or increase the stresses, but the third effect (r_s) works in the opposite direction. In the middle region C_t and C_a have little influence on the stem stresses, the other two effects work in opposite directions. Hence, optimal values for the stem thickness in the different regions should be expected to exist. For circular geometry these effects are evaluated in the figs. 7.8 through 7.10 as the influences of the stem radius on the factors α and β. It is evident that on the distal side the stem should, for all stress components, be as thin and flexible as possible. On the proximal side the stem material should be as stiff as possible; for the stem thickness, however, there is an optimum value that in this case (the chosen bone properties) is $r_s \approx 8$ - 9 mm (layer thickness of 1 - 2 mm) on transverse loading, and $r_s \approx 6$ - 8 mm (layer thickness of 2 - 4 mm) on axial loading.

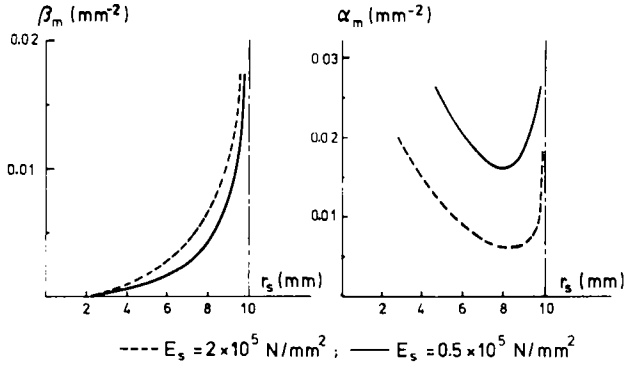

fig. 7.8: The factors α_m and β_m as functions of r_s (circular geometry), for two different values of E_s.

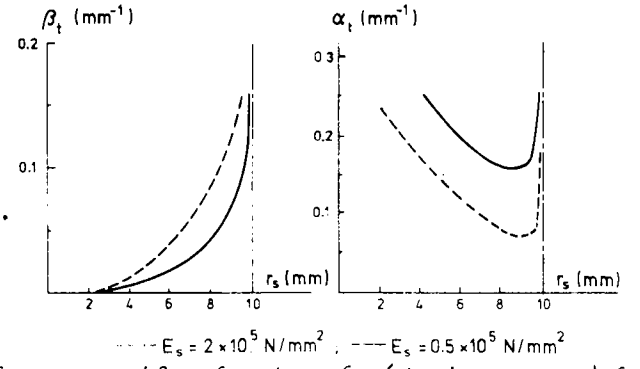

fig. 7.9: The factors α_t and β_t as functions of r_s (circular geometry), for two different values of E_s.

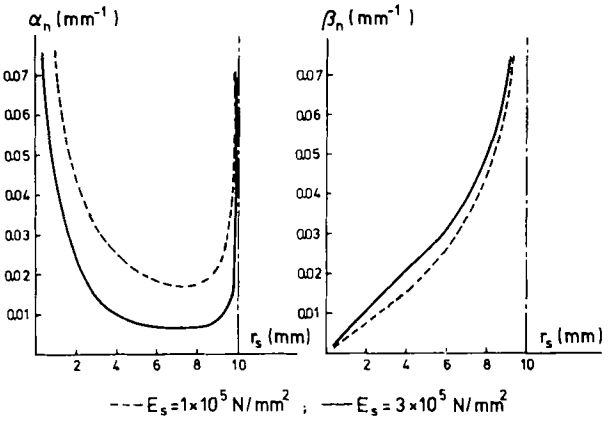

fig. 7.10: The factors α_n and β_n as functions of r_s (circular geometry), for two different values of E_s.

The values of r_s for which the minima in α_m, α_t and α_n occur are independent of E_c, ν_c and the interface conditions. As follows from figs. 7.8 through 7.10, they are not very sensitive for the stem Young's modulus, too. Since the factors $-1/\ln\rho$ and $\rho/(1-\rho)$ (on which C_a and C_t depend) are rather strong for ρ close to 1, the locations of the minima will thus be determined by r_b-r_s (the layer thickness), rather than by the stem thickness itself. Hence, the optimal values for the layer thickness mentioned above can probably be regarded as generally applicable. It should be remarked, however, that in this case the presence of a soft bone layer (spongeous bone) was not taken into account.

In the middle region the stem stresses decrease for a thicker stem on axial loading. On transverse loading the stem stresses will be lower for a thin stem as well as for a very thick stem; for circular geometry, a maximum occurs for $r_s = \sqrt[4]{(16F_b/3\pi E_s)}$. For both the transverse and axial loading cases the stem stresses decrease on decreasing Young's modulus of the stem material. On transverse loading the stem stresses are almost proportional to the modulus, on axial loading the influence is somewhat less pronounced.

The thickness of the stem also affects the coefficients λ_a and λ_t. Here, too, the effects of the changes in the stem stiffness and the cement mantle stiffness work in opposite directions, hence minimal values for λ_a and λ_t exist.
For circular geometry the influences of the stem thickness (r_s) on the values of λ_a and λ_t are shown in fig. 7.11.

In a cross-section of the structure the total bending moment and the total axial force follow from

$$M(z) \approx M_s(z) + M_b(z) \quad \text{and} \quad N(z) \approx N_s(z) + N_b(z)$$

In using these formulas the influence of the structural stiffness of the stem on the bone stresses can directly be evaluated if the effect on the stem stresses is known.

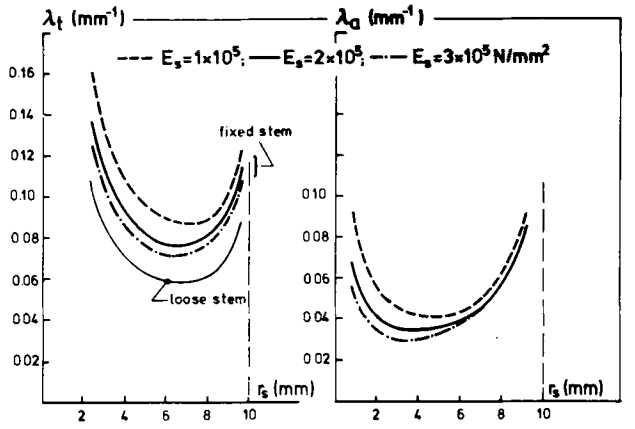

fig. 7.11: The coefficients λ_t and λ_a as functions of r_s (circular geometry) for different values of E_s.

7.5. The structural stiffness of the bone

As regards the mechanical behavior of the structure, the roles of F_b and P_b are equivalent to those of F_s and P_s, but inversed at the proximal and distal sides. When E_b and r_o change, only F_b and P_b are affected. Higher values of F_b and P_b will reduce λ_t and λ_a, respectively, so that the proximal and distal load-introduction regions will be extended. The values of α_m, α_t and α_n will increase, causing p(L) and q(L) (proximal region) to increase; β_m, β_t, β_n, ϵ_m and ϵ_n will decrease, as a result of which p(0) and q(0) (distal region) and $M_s(z)$ and $N_s(z)$ (middle region) decrease.

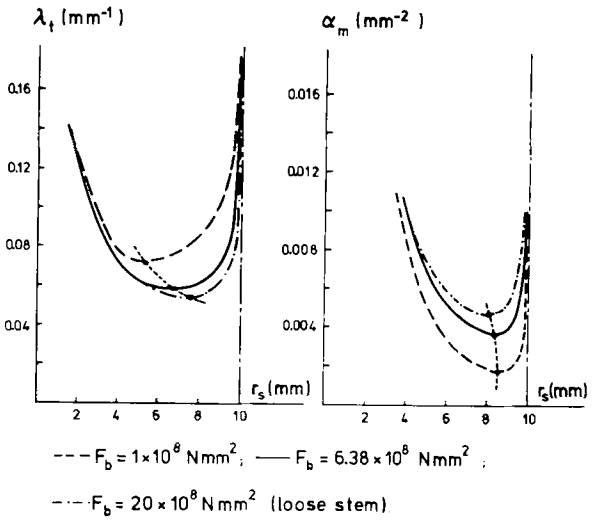

fig. 7.12: The coefficient λ_t and the factor α_m as functions of r_s (circular geometry) for three different values of F_b.

For circular geometry the influences of F_b on $\lambda_t(r_s)$ and $\alpha_m(r_s)$ are shown in fig. 7.12, assuming a constant inner bone radius (r_b) and constant stem and cement materials properties. Apparently the value of r_s for which the minimum in α_m occurs is not very sensitive for F_b also.
If r_b changes then the cement layer thickness also changes. In this case it can be expected, as discussed in paragraph 7.4., that a layer thickness of around 2 mm will still be an optimum where the stresses at the proximal side are concerned.

These tendencies were again confirmed by the results of the three-dimensional FEM model (Huiskes, 1977). Fig. 7.13 shows an example of stem, cement and bone equivalent stresses on transverse and axial loading for two different Young's moduli of the bone

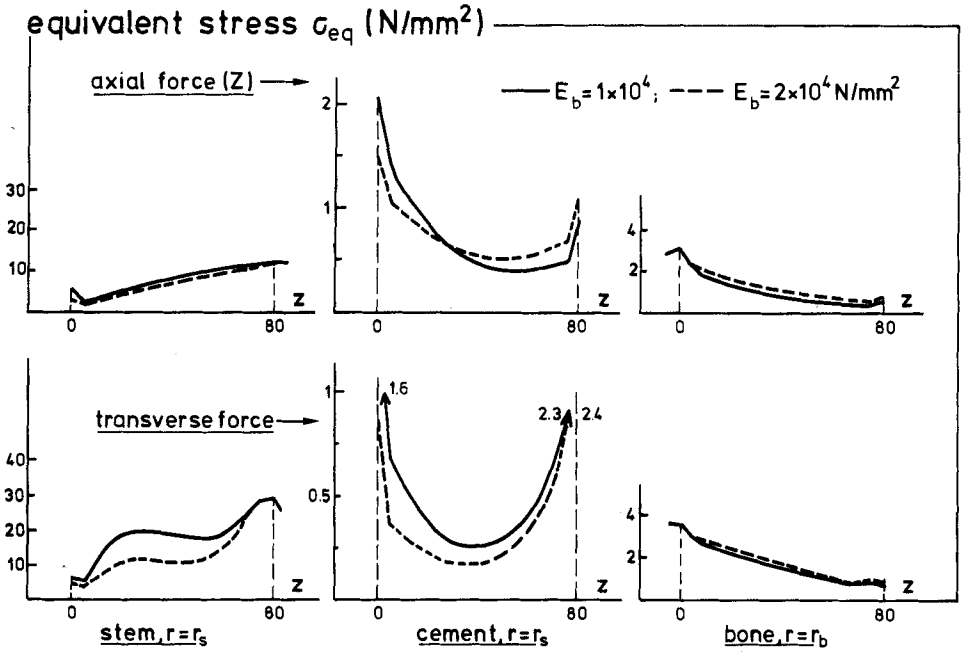

fig. 7.13: Equivalent stresses in stem, bone and cement (at the stem-cement interface) on axial loading and transverse loading as calculated with the three-dimensional FEM model, for two different values of E_b.

CHAPTER EIGHT

GUIDELINES FOR STEM DESIGNS AND IMPLANTATION PROCEDURES

In the previous chapter the influences of the characteristic parameters of the structure on its mechanical behavior were studied. It was shown that the analytical models, described in chapter 5, could conveniently be used for these parametric analyses and that, by using the approximative formulas, practically all influences could be evaluated. The results of the three-dimensional FEM model, that are more detailed especially where the cement layer is concerned, confirmed the tendencies found. Only with respect to the influence of ν_c on axial and hoop stresses did the FEM model give information that could not be provided by the analytical models.
From the concepts developed in the previous chapters some guidelines for stem designs and implantation procedures can be derived, as will be discussed in this chapter.

It was shown, that all cement and interface stresses are reduced by using an intermediate layer of low Young's modulus and Poisson's ratio. It should be borne in mind, however, that a material with a low modulus usually also has low strength properties. Silastics, for instance, have a low modulus but are not very strong and almost incompressible (high Poisson's ratio), which makes them rather unsuitable for use as intermediate material. Obviously, in the case of acrylic cement, its quality should be optimal. From a mechanical point of view the use of an intramedullary plug, cleansing before cement insertion and inserting under pressure (see section I) would therefore be advantageous.

In order to reduce the cement and interface stresses at the distal side, the stem length should be kept restricted. An adequate length is the one for which the proximal and distal sides are approximately independent in their mechanical behavior, a length that is determined by the coefficients λ_a and λ_t. These depend on the structural stiffness of the stem, the bone and the cement layer, that is, on the material and geometrical characteristics of the stem, the bone and the intermediate layer. This implies for instance that a titanium alloy stem will require a different length compared to a cobalt-chromium steel-alloy stem; but also, that patients with tiny or osteoporotic bones require stems of different length compared to patients with heavy or dense bones. No doubt an indication of the bone quality can be obtained from pre-operative roentgenograms. If stems of different sizes were available, the best-fitting stem for a specific patient could be chosen pre-operatively by using the concepts presented here.

On the proximal side the stem should be thick and the material stiff in order to reduce the cement and interface stresses in this region. A cement layer of about 2 mm should be retained, however, and this again implies a more 'custom-fit' approach, measuring the bone dimensions pre-operatively and choosing an implant from different sizes available.
On the distal side the stem should be thin and flexible. The requirements for the proximal and distal sides can only be met by using a tapered stem. The geometry of the taper can be studied by using the FEM beam model, as will be shown in the following example. In this example the choice of materials for the stem, entailing conflicting influences on the proximal region and the distal and middle regions will also be discussed. In order to reduce the stem stresses in the middle region, the stem should be thick and its material flexible.

However, the middle region serves no specific purpose in the load transmission process from implant to bone and should be kept restricted as much as possible. The effect of the taper shape on the stem stresses will also be discussed in the following example.

A specific bone of given properties is assumed (axisymmetric; r_b = 10 mm; r_o = 15 mm; $E_b = 2x10^4 N/mm^2$). For this bone an adequate stem design will be developed, as an example, using the concepts and methods presented previously.
In the proximal region the stem should be as thick as possible, leaving a layer thickness of 2 mm, so that r_s = 8 mm at the proximal side. In the first instance the stem material is taken as Co-Cr steel ($E_s = 2x10^5 N/mm^2$). The Young's modulus of the cement is taken as $E_c = 2x10^3 N/mm^2$, its Poisson's ratio as $\nu_c = 0.33$.
In accordance with the results presented in paragraph 6.2, the stem is assumed to loosen upon tension from the cement layer. The resulting values for the mechanical characteristics of the proximal side are shown in table 8.1.

parameter	unit	value	parameter	unit	value
F_s	Nmm^2	$6.43x10^8$	P_s	N	$4.02x10^7$
F_b	Nmm^2	$6.38x10^8$	P_b	N	$7.85x10^6$
C_t	N/mm^2	$1.79x10^4$	C_a	N/mm^2	$2.12x10^4$
λ_t	mm^{-1}	$6.11x10^{-2}$	λ_a	mm^{-1}	$5.68x10^{-2}$

table 8.1: Values for the characteristic parameters at the proximal side.

The length of the proximal side (L_{pr}) is chosen in such a way that the initial load introduction effects are damped out in this region, using the criterion $\lambda_t L_{pr} \geq \pi/2$ or $\lambda_a L_{pr} \geq \pi/2$ as discussed in paragraph 5.3. From this it follows $L_{pr} \geq 27.7$ mm; we took L_{pr} = 30 mm.
As shown in the previous chapter, the distal end of the stem should be thin and flexible; for the extreme distal stem radius we taken r_s = 1 mm. Between the distal tip and the end of the proximal region a certain tapered shape has to be designed. To determine the length of this part of the stem (L_t), λ_a is used in the first instance, because $\lambda_a < \lambda_t$. As shown in fig. 7.11, λ_a varies approximately between 0.060 and 0.035 mm^{-1}, for $1 \leq r_s \leq 4$ mm, and between 0.035 and 0.057 mm^{-1} for $4 \leq r_s \leq 8$ mm. Taking an approximate average value, it follows (with the criterion $\lambda_a L_t \geq \pi/2$) that $L_t \geq 35$ mm; we take L_t = 40 mm to start with. This taper shape, and two longer ones (60 and 80 mm) are analysed as to their mechanical performance in the given bone, using the FEM beam model.
Fig. 8.1 shows an example of results: stem-cement interface stresses $s_{rs}(z)$ and stem stresses $s_{zs}(z)$ on transverse loading, stem-cement interface shear stresses $t_s(z)$ and stem stresses $s_{zs}(z)$ on axial loading. Apparently the taper length of 40 mm has been a good choice where the length of the distal introduction region is concerned, but on transverse loading this stem tip is still too stiff. For L_t = 60 mm the stem stresses are somewhat higher, but the distal cement stresses are considerably lower. By extending the taper length to 80 mm nothing is gained. Taking L_t = 60 mm, two other stem shapes are investigated, as shown in fig. 8.2.
It is remarkable, considering $s_{rs}(z)$ in fig. 8.2, that such a seemingly slight difference as between shapes 1 and 2 has so much effect in transverse loading. It should be noted, too, that the stresses on the proximal side do not differ significantly (as is also evident in fig. 8.1), because the length of the proximal region was chosen in such a way that both ends of the stem will not influence each other.

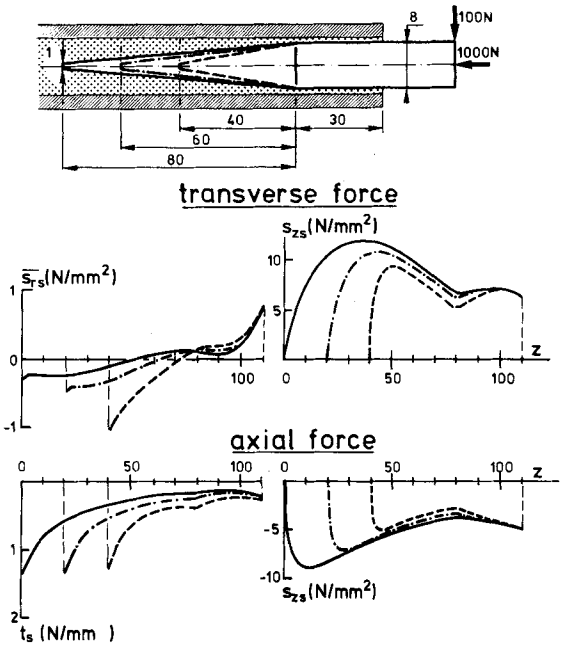

fig. 8.1: Stem stresses and stem-cement interface stresses in axial and transverse loading, as calculated with the FEM beam model for three different stem taper lengths.

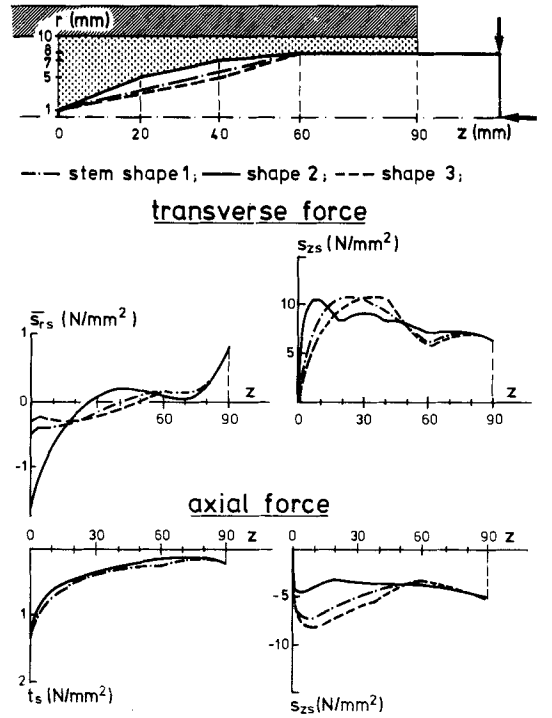

fig. 8.2: Stem stresses and stem-cement interface stresses in axial and transverse loading, as calculated with the FEM beam model for three different stem shapes (1, 2 and 3). Some of the curves (especially s_{zs}) are not smooth, due to the abrupt changes in the stem taper.

Shape 3 is chosen as the best one in this case although there is little difference between 1 and 3. Of course, in reality the abrupt transitions in the taper would have to be somewhat rounded off.
Using this shape, the materials choice is further investigated. The Young's modulus of the stem is taken as $3x10^5$ N/mm^2 (simulating ceramics), $2x10^5$ N/mm^2 (simulating Co-Cr steel) and $1x10^5$ N/mm^2 (simulating titanium), respectively. Some results are shown in fig. 8.3. The important aspects of these results can of course be predicted using the approximative formulas. As is evident when regarding fig. 8.3, the use of ceramics would be advantageous for the proximal cement and interface stresses only, while the use of titanium would be advantageous for all but these stresses (in this case the axial bone stresses are somewhat more natural in addition). Co-Cr steel appears to be a reasonable compromise. However, if the thickness of the proximal titanium stem could be increased by approximately 20%, while retaining a layer thickness of 2 mm, the proximal cement and interface stresses would be approximately equal to or lower than those for the Co-Cr steel stem in the example, as follows from the formulas for F_s and P_s.

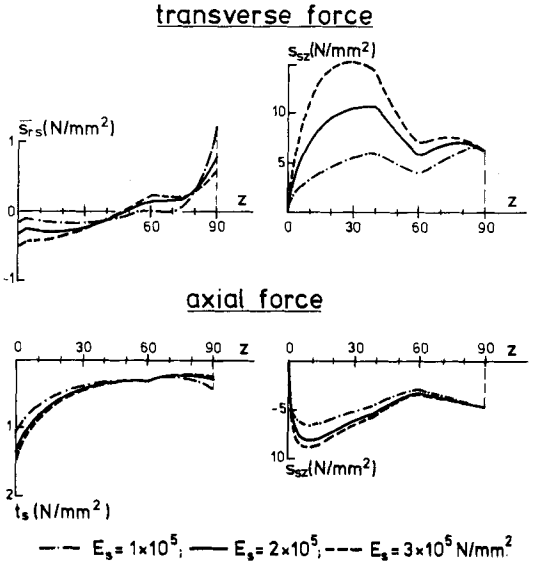

fig. 8.3: Stem stresses and stem-cement interface stresses in axial and transverse loading, as calculated with the FEM beam model for stem shape no. 3 and three different values of Young's modulus of the stem, simulating Co-Cr steel, titanium and ceramics.
(For ceramics $E_s = 3x10^5$ N/mm^2 was taken, in reality this value will even be about 30% higher).

It is thus evident that a stem design should (and can) be adapted to the materials applied. For instance in the literature 'iso-elastic' prostheses are being considered (Morscher *et al*, 1976). The 'apparent' elasticity of this (porous) material is approximately equal to that of bone ($E_s \approx 0.2x10^5$). The use of this material will reduce all important stresses, except in the proximal cement. The cement and interface stresses in this region would be increased by more than 200% in comparison to Co-Cr alloys, which is unacceptable. A solution can be found in the application of a proximal stiffener, a steel tube around the proximal stem, whose length can be established by using the formulas for λ_a and λ_t.

The analyses performed in this example show what can be done to develop an adequate stem design, and to evaluate an existing stem design as regards its mechanical performance in a specific bone.
Other proposals that are more qualitative can be derived from the studies presented. As follows from the stress analyses, the highest stresses in the cement occur close to the stem interface with peak values at the proximal and distal sides. Since the strength of the cement as implanted in the bone is many times less than prefabricated (industrial) PMMA, consideration could be given to the use of plastic-coated stems, thus placing strong material in highly stressed locations. As was shown by Ypma *et al* (1979) a coated stem reduces the chances of cement fracture. For the same reasons the proximal cement layer could be replaced by a (well-fitting) plastic ring to resist the peak stresses here. A schematic representation of these concepts is shown in fig. 8.4. In this example the cement layer is only very thin over the entire fixation length, giving, in addition, less chance of bone necrosis due to thermal damage (see section II). Since the stresses close to the cement-bone interface are not so high, the use of porous (acrylic) cement could be considered, which would even further reduce the temperatures during the polymerization process (hence also the thermal shrinkage stresses) and would possibly ensure better interlocking with the bone, thanks to bone ingrowth. The stem shape in fig. 8.4 has been chosen in accordance with the previously discussed example. The proximal fixation region might be shortened in the course of time due to calcar resorption. To prepare for this effect, this region could be designed somewhat longer.

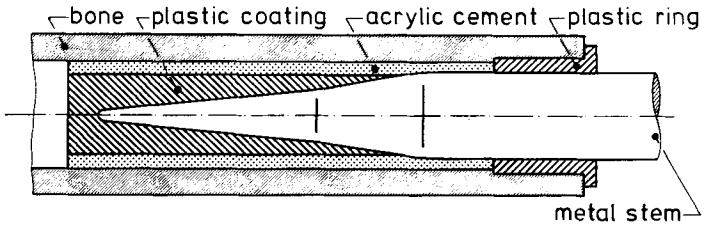

fig. 8.4: A schematic concept for an 'idealized' intramedullary fixation system using plastic coating and a plastic ring in highly stressed regions.

In the examples treated here, only the flexural and compressional stiffness aspects of the stem were discussed. In an actual design these stiffness values have to be translated into cross-sectional geometry. Since the stem on the proximal side should be as stiff as possible, it should be such as to 'fill up' the medullary canal as thoroughly as possible, retaining a cement layer of at least 2 mm at the medial side. On the distal side a flexible stem is needed, but a large load-transferring area is also advantageous. Hence, a cross-section that is small in the lateral-medial direction and somewhat more extended in the anterior-posterior direction would be possible.

CHAPTER NINE

DISCUSSION

The models applied here were intended to describe the intramedullary bone-prosthesis structure in a qualitative sense, to find its characteristic parameters and to evaluate the relations between these parameters and the mechanical behavior.
As has been demonstrated, simplified (especially analytical) models have better options for the development of such general, fundamental concepts than detailed, geometrically refined three-dimensional FEM models. Of course, these refined models are in principle better suited to calculate actual stress values in an absolute sense. However, bone-prosthesis structures have many complicated properties which can as yet hardly be described mathematically and which do not so much affect their mechanical behavior in general but very much affect the local stress distribution, as was shown in chapter 6.
On the other hand, however, simplified models can usually only be developed for such complicated structures when more sophisticated numerical analyses (and experiments) can serve as references. In the analyses presented here, analytical models were developed on the basis that the stem and the bone separately behave by approximation in accordance with beam theory. For other than intramedullary bone-prosthesis structures a suitable (relatively simple) theory might not be so easily found. In that case numerical analyses are all that remain. However, for instance as regards the tibial plateau of the artificial knee joint, too, approximative analytical theories can be applied, as was shown by Haemmerle *et al* (1977).

Owing to the qualitative character of the analyses, no comparison was made between calculated stress values and strength data of the materials and the interfaces. It is difficult, too, to find reliable strength criteria for cement and bone, since so much depends on surgical variables and individual differences. It would be realistic to assume that where the bone is concerned, the stress pattern should be as 'natural' as possible. In this respect the radial transverse stresses and the shear stresses at the cement-bone interface are quite unnatural for the bone and should be kept restricted as much as possible.
The order of magnitude of the maximal stress values found in the cement is such, that cement failure cannot be excluded. This is also true for thermal stresses caused by shrinkage immediately following the polymerization process, as shown in paragraph 6.1. These stresses are maximal in the middle of the cement mass and cracks might thus develop there and not be detected during surgery. Thanks to stress relaxation these 'locked-in' stresses will have no influence on the long-term mechanical behavior of the structure (unless, of course, the damage was already done directly postoperatively).

Using the fundamental concepts developed here, analyses presented in the literature can be evaluated to some extent. As was shown in paragraph 5.5., the intramedullary fixation structure is not very well suited for analyses using two-dimensional models. If no side plates are applied in the model, a sandwich construction is in fact analysed in which unrealistically high shear stresses will occur (McNeice *et al*, 1975, 1976; Andriacchi *et al*, 1975; Kwak *et al*, 1979). Furthermore, slip at the stem-cement (or cement-bone) interface will cause the overall flexural stiffness of such a model to be reduced drastically, resulting in unrealistically high stem and bone stresses.
A two-dimensional FEM model using side plates was presented by Svensson *et al* (1977). They concluded from their analysis that the use of a heavier prosthesis stem may be

beneficial; as we have seen, this is only true for the proximal side, provided a cement layer of adequate thickness is retained. Their remark that stem and cement material properties do not influence the critical stress values can not be correct.
The detailed three-dimensional FEM models of Röhrle *et al* (1977, 1979) and Scholten *et al* (1978) were mainly used for comparative studies on different prostheses designs. They varied the stiffness of the stem material and reached the same conclusions as to the proximal side as were found here.
A more extensive parametric analysis was carried out by Crowninshield *et al* (1979), with their three-dimensional model of an implanted hip endoprosthesis. They varied the Young's moduli of the stem and the cement, the stem length and the stem thickness. Generally speaking, the tendencies of their results agree perfectly with the results presented here. Although theirs is a profound and sophisticated study, the results are rather specific, owing to the empirical character of such numerical analyses. They conclude that measures to be taken in order to minimize the stresses in cement or stem are in conflict. As was shown here, this is not true in general, as can be established if the proximal and distal regions are treated separately. Where it is true, optimal dimensions can usually be calculated. They advise reducing Young's modulus of the cement (which is indeed advantageous for all stress components in the cement and will hardly affect the stem stresses) to increase the Young's modulus of the stem (only on the proximal side, which follows clearly from their results, too), increasing the stem thickness (which is again only advisable for the proximal side and should not be done in general, since an adequate cement layer (at least 2 mm) should be retained on the medial side) and increasing the stem length (which again should not be done in general; as shown here the 'optimal' length depends also on other parameters of the structure and the length should not be increased beyond this 'optimal' value).

Since by using approximative formulas as derived here (together with such simple methods as the FEM beam model), the mechanical behavior of the structure can be adequately described in the general sense, more detailed studies could be conducted by analysing more local phenomena, especially in the cement-bone interface region, using the approximative general results as boundary conditions and also using radiographical and histological data. As discussed in paragraph 6.4., especially taking bone remodeling phenomena into account would be of interest.

REFERENCES

Ahmed, A.M., Pak, W., Miller, J., Burke, D.L. and D'Souza, N. (1977); Thermal stresses in polymethylmethacrylate in bone-PMMA-stem prosthesis fixation systems; thermo-elastic solution assuming instantaneous soldifications; 3rd Annual Meeting of the Soc. for Biomaterials, New Orleans, Louisiana.

Andriacchi, T.P., Galante, J.O., Belytschko, T.B. and Hampton, S. (1975); A stresses analysis of the femoral stem in total hip prostheses; J. Bone Joint Surg. 58-A, No. 5, p. 618.

Askew, M.J., Lewis, J.L., Jaycox, Williams, J.L. and Hori, R.Y. (1978); Interface stresses in a prosthesis-tibia structure with varying bone properties; 24th Annual Meeting Orthopaedic Research Society, Dallas, Tex., February.

Askew, M.J., Lewis, J.L. and Kerr, L.M. (1979); The effect of post geometry, material and location on interface stress levels in tibial components of total knee prostheses; 25th Annual Meeting Orthopedic Research Society, San Francisco, Cal., February.

Banens, J. (1977); Private communications; computer program FEMSYS; Computer Centre Eindhoven University of Technology, The Netherlands.

Barberi, G., Gola, M., Gugliotta, A. and Calderale, P.M. (1978); Flexural coupling of hip-prosthesis stem and femur: a simple method of theoretical analysis; Eng. in Medicine, Vol. 7, No. 3, p. 172.

Bartel, D.L. and Ulsoy, G.A. (1975); The effect of stem length and stem material on stresses in bone-prosthesis systems; 21th Annual Meeting Orthopaedic Research Society, San Francisco, Cal.

Bartel, D.L., Desormeaux, S.G. (1976a); Femoral stem performance; Proceedings Symp. Retrieval and Analysis of Orthopaedic Implants (A. Weinstein, E. Horowitz and A.W. Ruff, eds.); U.S. Dept. of Commerce; Nat. Bureau of Standards Special Publication 472.

Bartel, D.L. and Desormeaux, S.G. (1976b); Stresses in prosthesis stems as a function of cross-sectional shape; 22nd Annual Meeting Orthopaedic Research Society, New Orleans, Louisiana, January.

Bartel, D.L. and Samehyek, E. (1976); The effect of cement modulus and thickness on stresses in bone-prosthesis systems; 22nd Annual Meeting Orthopaedic Research Society, New Orleans, Louisiana.

Brekelmans, W.A.M., Poort, H.W. and Slooff, T.J.J.H. (1972); A new method to analyse the mechanical behaviour of skeletal parts; Acta Orthop. Scand. 43, pp. 301-317.

Brekelmans, W.A.M. and Poort, H.W. (1973); Theoretical and experimental investigation of the stress and strain situation on a femur; Acta Orthop. Bel.; Suppl. I, p. 3-24.

Brockhurst, P.J. (1975); Design of total hip prosthesis, the femoral stem; Centre for Biomedical Eng. Report; Univ. of New South Wales, Australia.

Calderale, P.M., Gola, M.M. and Gugliotta, A. (1977); Calculation of load distribution between bone and prosthesis stem by an analytical method; comparison of several stem types; 6th Int. Conf. of Biomechanics, Copenhagen; published (abstract) in: (1978) "Biomechanics VI B, Int. Series on Biomechanics" (E. Asmussen and K. Jørgensen, eds.); University Park Press, Baltimore, MD.

Campen, v. D.H. (1970); On the stress distribution in an arbitrarily loaded nozzle to flat plate connection; Nucl. Eng. Des. 11, pp. 495-516.

Campen, v. D.H., Croon, H.W. and Lindwer, J. (1978); Influence of cyclic loading on mechanical loosening of hinged knee prostheses; Eng. in Med. Vol. 7, no. 4, p. 235.

Campen, v. D.H., Croon, H.W. and Lindwer, J. (1979); Mechanical loosening of knee-endoprostheses with intermedullary stems; Influence of dynamic loading; 25th Annual Meeting Orthopaedic Research Soc., San Francisco, Cal., February.

Chand, R., Huang, E. and Rim, K. (1976); Stresses in the human knee joint; J. Biomechanics, vol. 9, pp. 417-422.
Chao, E.Y., Wong, H.W., Frain, W.E. and Coventry, M.B. (1977); Stress analysis of the geometric knee under static loading; ASME 77-Bio-6.
Crowninshield, R.D. and Branch, A.J. (1978); The effect of stem cross-sectional shape on the load transmission from total hip prostheses; 24th Annual Meeting Orthopaedic Research Society, Dallas, Tex., February.
Crowninshield, R.D., Brand, R.A. and Johnston, R.C. (1979); An analysis of femoral stem design in total hip arthroplasty; 25th Annual Meeting Orthopaedic Research Society, San Francisco, Cal., February.
Durelli, A.J. (1977); The difficult choice: Evaluation of methods used to determine experimentally displacements, strains and stresses; Appl. Mech. Rev., vol. 30, no. 9, p. 1167.
Evans, F.G. (1973); Mechanical properties of bone; Charles C. Thomas Publ., Springfield, Ill.
Forte, M.R. (1975); Structural analysis consideration in the design of the total hip prosthesis; 21th Annual Meeting Orthopaedic Research Society, San Francisco, Cal., Febr.-March.
Girkmann, K. (1963); Flächentragwerke (6th ed.); Springer-Verlag, Wien, New York.
Gola, M.M. and Gugliotta, A.A. (1979); Analytical estimate of stresses in bone and prosthesis stems; J. Strain Anal., vol. 14, no. 1, p. 29.
Gruen, T.A. and Amstutz, H.C. (1977); Modes of failure of the cement stem-type femoral component; 30th ACEMB, Los Angelos, Cal., p. 87 proceedings.
Haemmerle, J., Bartel, D. and Chao, E.Y. (1977); Mechanical analysis of polycentric tibial track loosening; ASME-publication 77-Bio-7.
Hampton, S.J., Andriacchi, T.P., Galante, J.O. and Belytschko, T.B. (1976); Analytical approach to the study of stresses in the femoral stem of total hip prostheses; paper 32.1, 29th ACEMB, Boston, Mass., November.
Harris, L.J., Chao, R., Bloch, R. and Weingarten, V. (1978); A three-dimensional Finite Element Analysis of the proximal third of the femur; 24th Annual Meeting Orthopaedic Research Society, Dallas, Tex., February.
Hayes, W.C., Swenson, L.W. and Schurman, D.J. (1978); Axisymmetric finite element analysis of the lateral tibial plateau; J. Biomechanics Vol. 11, p. 21-33.
Hayes, W.C. (1978); Theoretical modeling and design of implant systems; Workshop: Mechanical failure of total joint replacement; Atlanta, Georgia, May 31-June 2; The Steering Committee, Am. Ac. of Orthop. Surg., Chicago, Document 916-78.
Heck, v.J. ånd Huiskes, R. (1979); Berekeningen op basis van de elementenmethode en een Fourier-analyse aan een nieuwe gewrichtsprothese uit de Orthopaedie; De Wagner-prothese; Lab. for Exp. Orthop., Dept. Orthopaedics (ORa-79-08), Univ. of Nijmegen, The Netherlands.
Hetényi, M. (1946); Beams on elastic foundation; The Univ. of Michigan Press, Ann Arbor, Mich.
Heugten, v. P.C.M. (1974); Rekstrookmetingen, verricht aan een kadaverfemur in ongeschonden toestand en voorzien van diverse prothesen; Report Dept. Applied Mechanics (W-WE-74-18) Eindhoven Univ. of Technology, The Netherlands.
Heugten, v. P.C.M. (1975); Spanningsanalyse van de schacht van het femur op basis van een balkmodel; Report Dept. Applied Mechanics (W-WE-75-06) Eindhoven Univ. of Technology, The Netherlands.
Huggler, A.H., Jacob, H.A.C. und Schreiber, A. (1978); Biomechanische Analyse der Lockerung von Femurprothesen; Arch. Orthop. Traumat. Surg. 92, p. 261-272.
Huiskes, R. and van Heugten, P.C.M. (1974); A discussion of problem solving methods in biomechanical research; Combined meeting of the Dutch and Danish Orthopaedic Associations; Nijmegen; The Netherlands; published in proceedings (Biermans *et al*, eds.).

Huiskes, R., v. Heugten, P.C.M. and Slooff, T.J.J.H. (1976); Strain-gauge measurements on a loaded femur, intact as well as provided with prostheses; 29th ACEMB, Boston, Mass., November.
Huiskes, R. (1977); Kriteria voor ontwerp en fixatie van orthopaedische implantaten op basis van FEM-berekeningen; Report Lab. for Exp. Orthopaedics, Dept. Orthopaedics (RH 77-10), University of Nijmegen, The Netherlands.
Huiskes, R., Elangovan, P.T., Banens, J.P.A. and Slooff, T.J.J.H. (1977); Finite element computer methods for design and fixation problems of orthopaedic implants; **In:** "Biomechanics VI B, Int. Series on Biomechanics" (E. Asmussen and K. Jørgensen, eds.); Univ. Park Press, Baltimore, M.D.
Huiskes, R. et Slooff, T.J.J.H. (1977); Etude des contraintès à la fixation des articulations artificiéllès; 2ième Congrès de la Soc. de la Biomécanique, Liège, Belgium, sept. 21-23.
Huiskes, R. (1978); Stress analyses of implanted orthopaedic joint prostheses for optimal design and fixation; First Conf. Europ. Soc. of Biomechanics, Brussels, Belgium, May.
Huiskes, R. and Heck, v.J. (1978); Stress analysis and optimization of a new intramedullary fixation system, to be used in finger joint prostheses; Report Lab. for Exp. Orthopaedics, Dept. Orthopaedics (ORa-78-04) Univ. of Nijmegen, The Netherlands.
Huiskes, R. and Slooff, T.J.J.H. (1978); Mechanical properties and stresses in intramedullary prostheses; 24th Annual Meeting Orthopaedic Research Society, Dallas, Tex., February.
Huiskes, R. (1979); Principal parameters in the mechanical performance of intramedullary fixated artificial joints; 2nd Meeting Eur. Soc. of Biomechanics, Strasbourg, France, September.
Huiskes, R., v. Heck, J., Walker, P.S. and Green, D.J. (1979); A three-dimensional stress analysis of a new intramedullary fixation system; 25th Annual Meeting Orthopaedic Research Society, San Francisco, Cal., February.
Huiskes, R. and Schouten, R.Y. (1979); Stiffness characteristics and stress distribution of a slice of bone cement, surrounding an intramedullary fixated orthopaedic implant; Report Lab. for Exp. Orthopaedics, Dept. Orthopaedics (ORa-79-03) Univ. of Nijmegen, The Netherlands.
Huiskes, R. und Slooff, T.J.J.H. (1979a); Experimentelle und rechnerische Spannungsanalysen der Hüftgelenk Verankerung; Pauwels-Symposium, Berlin, Jan.
Huiskes, R. and Slooff, T.J.J.H. (1979b); Geometrical and Mechanical properties of the human femur; 7th Int. Conf. of Biomechanics, Warsaw, Poland, september; To be published in "Biomechanics VII, Int. Series on Biomechanics" (K. Fidelius and A. Morecki, eds.); Univ. Park Press, Baltimore, M.D.
Huiskes, R. and Wijn, de J.R. (1979); Locked-in acrylic cement stresses, caused by thermal shrinkage after fixation of intramedullary joint prostheses; 2nd Meeting Eur. Soc. of Biomechanics, Strasbourg, France, September.
Kempf, I., Jaeger, J.H., Nessius, A., Mochel, D. et Clavert, J.M. (1976); Etude comperative de l'élément fémoral de quelques arthroplasties totales de la hanche; Acta Orthop. Belg. Tome 42, Suppl. I.
Koch, J.C. (1917); The laws of Bone Architecture; Am. J. Anat. vol. 21.
Kwak, B.M., Lim, O.K., Kim, Y.Y. and Rim, K. (1979); An investigation of the effect of cement thickness on an implant by finite element stress analysis; Int. Orthop. (SICOT) 2, pp. 315-319.
Laaper, W. (1973a); Het bepalen van de geometrie van het femur op destructieve wijze; Report Dept. Applied Mechanics (W-WE-73-5) Eindhoven Univ. of Technology, The Netherlands.
Laaper, W. (1973b); Spanningsanalyse van het femur op basis van een balkmodel; Report Dept. Applied Mechanics (W-WE-73-12) Eindhoven Univ. of Technology, The Netherlands.

Lewis, J.L. (1977); Analytical methods in prosthesis design; Proc. Workshop on Internal Joint Replacement, Northwestern Univ. Chicago, pp. 127-134.
McBeath, A.A., Schopler, S.A. and Seireg, A.A. (1979); Circumferential and longitudinal strain in the proximal femur as determined by prosthesis (THR) type and position; 25th Annual Meeting Orthop. Res. Soc., San Francisco, Cal., February.
McNeice, G.M., Eng, P. and Amstutz, H.C. (1975); Finite element studies in hip reconstruction; 5th Int. Conf. of Biomechanics; Jyväskylä, Finland; Published in (1976): "Biomechanics VA, Int. Series on Biomechanics" (P.V. Komi, ed.), Univ. Park Press, Baltimore, M.D.
McNeice, G.M. and Amstutz, H.C. (1976); Stresses in prostheses stems and supporting acrylic, a finite element study of hip replacement; 22nd Annual Meeting Orthopaedic Research Society, New Orleans, Louisiana, January.
McNeice, G.M. and Gruen, T.A. (1976); Mechanical failure of femoral components, radiographic examination of total hip replacement; 22nd Annual Meeting Orthopaedic Research Society, New Orleans, Louisiana, January.
Meyer, H. (1867): Die Architectur der Spongiosa; Archiv. f. Anat. Phys. und Wissensch. Medizin; p. 615.
Minns, R.J., Bremble, G.R. and Campbell, J. (1977); A biomechanical study of internal fixation of the tibial shaft; J. Biomech. vol. 10, pp. 569-579.
Morscher, E., Mathijs, R. and Hence, H.R. (1976); Iso-elastic endoprosthesis – a new concept in artificial joint replacement; In: Advances in artificial hip and knee joint technology (Schaldach and Hohmann, eds.); Springer-Verlag, Berlin, Heidelberg, New York.
Muskhelishvili, N.I. (1963); Some basic problems of the mathematical theory of elasticity; P. Noordhoff, Groningen, The Netherlands.
Oden, J.T. and Bathe, K.J. (1978); A commentary on computational mechanics; Appl. Mech. Rev., vol. 31, no. 8, p. 1053.
Oh, I. and Harris, W.H. (1978); Proximal strain distribution in the loaded femur; J. Bone Joint. Surg. 60-A, No. 1, p. 75.
Olofsson, H. (1975); The stress distribution in the femur; IRCOBI Conf. Birmingham.
Olofsson, H. (1976); Three-dimensional FEM calculation of elastic stress field in human femur; Thesis, Technikum, Inst. of Technology, Uppsala, Univ. Uppsala, Sweden.
Piziali, R.L., Hight, T.K. and Nagel, D.A. (1976); An extended structural analysis of long bones – Application to the human tibia; J. Biomech. 9, no. 11, p. 695.
Rohlmann, A., Bergmann, G. und Kölbel, R. (1978); Aussagewert und Grenzen der Spannungsberechnung mit der Finiten-Element-Methode (FEM) bei orthopädischen Problemen; Submitted for publication Z. Orthop. Chir. u.i. Grenzgebiete.
Rohlmann, A., Kölbel, R. and Bergmann, G. (1977); Practical value of the finite-element method for the stress calculation at the implant-bone surface; 6th Int. Conf. of Biomechanics, Copenhagen; published (abstract) in: (1978) "Biomech. VI B, Int. Series on Biomechanics" (E. Asmussen and K. Jørgensen, eds.); Univ. Park Press Baltimore, M.D.
Rohlmann, A., Kölbel, R. und Bergmann, G. (1979); Uber den Aussagewert der Finiten-Element-Methode bei orthopädische Problemen; Pauwels-Symposium, Berlin, January 19-20, to be published.
Röhrle, H., Scholten, R., Solbach, W., Ritter, G. und Grünert, A. (1977); Der Kraftflusz bei Hüftendoprothesen; Arch. Orthop. Unfall-Chir. 89, 49-60.
Röhrle, H., Scholten, R. und Sollbach, W. (1979); Der Kraftflusz bei neuartigen Hüftendoprothesen; Pauwels-Symposium, Berlin, Febr. 18-19, to be published.
Rybicki, E.F., Simonen, F.A. and Weis, E.B.Jr. (1972); On the mathematical analysis of stress in the human femur; J. Biomechanics, vol. 5, p. 203-215.

Scholten, R. (1975); Über die Berechnung der mechanische Beanspruchung in Knochenstrukturen mittels für den Flugzeugbau entwickelte Rechenverfahren; Med. Orthop. Technik, Heft 6/75, 95. Jahrgang s. 130-138.
Scholten, R., Röhrle, H. und Sollbach, W. (1978); Analysis of stress distribution in natural and artificial hip joints, using the finite-element-method; The South. Afr. Mech. Eng. vol. 28, p. 220.
Schoofs, B. (1979); private communication.
Slooff, T.J.J.H. (1970); De invloed van het acrylcement bij de fixatie van de heupendoprothese; Dissertation, Univ. of Nijmegen, The Netherlands.
Slooff, T.J.J.H. (1971); Spannungsveränderungen im proximalen Femurende bei einzementierten Endoprothesen; Arch. Orthop. Unfall-Chir. 71, s. 281-289.
Stern, J. (1977); Zur Beanspruchung des Knochenzementes bei der Hüftgelenkendoprothese; Arch. Orthop. Unfall.-Chir. 88, pp. 309-312.
Svensson, N.L., Valliapan, S. and Wood, R.D. (1977); Stress analysis of human femur with implanted Charnley prosthesis; J. Biomechanics, vol. 10, pp. 581-588.
Swanson, S.A.V. and Freeman, M.A.R. (1977); The scientific basis of joint replacement; Pitman Med. Publ. Comp.; Tunbridge Wells.
Timoshenko, S.P. and Goodier, J.N. (1970); Theory of elasticity; (3rd ed.); McGraw Hill, Kogahuska, Tokyo.
Toridis, Th.G. (1969); Stress analysis of the femur; J. Biomechanics, vol. 2, pp. 163-174.
Tarr, R.R., Lewis, J.L., Jaycox, D., Sarmiento, A., Schmidt, J. and Latta, L.L. (1979); Effect of materials, stem geometry and collar-calcar contact on stress distribution in the proximal femur with total hip; 25th Annual Meeting Orthopaedic Research Society, San Francisco, Cal., February.
Valliapan, S., Svensson, N.L. and Wood, R.D. (1977); Three-dimensional stress analysis of the human femur; Comput. Biol. Med., vol. 7, pp. 253-264.
Vichnin, H.H. and Batterman, S.C. (1977); Three-dimensional anisotropic stress analysis and failure prediction in a femur with a proximal prosthesis; 30th ACEMB, Los Angelos, Cal., November.
Walker, P.S. (1977); Human joints and their artificial replacement; Charles C. Thomas, Publ. Springfield, Ill.
Wilson, E.L. (1965); Structural analysis of axisymmetric solids; A.I.A.A. no. 3, pp. 2269-2274.
Wolff, J. (1870); Über die Innere Architectur der Knochen und ihre Bedeutung für die Frage vom Knochenwachtstum; Virchow's Arch. f. path. Anat. u. Phys. 50, s. 389.
Wood, R., Valliapan, S. and Svensson, N.L. (1973); Stress analysis of human femur; In: Theory and practice in FEM structural analysis, Tokyo Seminar; (Y. Yamada and R.H. Gallagher, eds.); Univ. of Tokyo Press, Tokyo.
Wood, R.D. (1975); Stress analysis of the femur; Thesis, Univ. of New South Wales, Australia.
Ypma, J., de Wijn, J., Huiskes, R. and Slooff, T. (1979); Strength and ingrowth aspects of porous acrylic bone cement; 11th. Int. Biomaterials Symp.; Clemson Univ. So. Car., April-May.
Zienkiewicz, O.C. (1977); The finite element method; McGraw-Hill, London, 3rd ed.

APPENDICES

APPENDIX A

RESULTS OF THE THREE-DIMENSIONAL FEM CALCULATIONS

The following graphs show the values of the stress 'amplitudes', $\hat{\sigma}_r$, $\hat{\sigma}_t$, $\hat{\sigma}_z$, $\hat{\tau}_{rt}$, $\hat{\tau}_{rz}$, $\hat{\tau}_{tz}$ and the equivalent stress σ_{eq} (maximal value) as functions of z, for $r = r_s$ and $r = r_b$ (lines 1 and 2, 3 and 4 respectively), calculated with the three-dimensional FEM model, for two loading cases (fig. A.1). For the stem only $\hat{\sigma}_z$ has been drawn, since the other stress components have insignificant values in comparison. It should be borne in mind that $\hat{\tau}_{rt}$ and $\hat{\tau}_{tz}$ are zero for the axial loading case and therefore have not been drawn also.

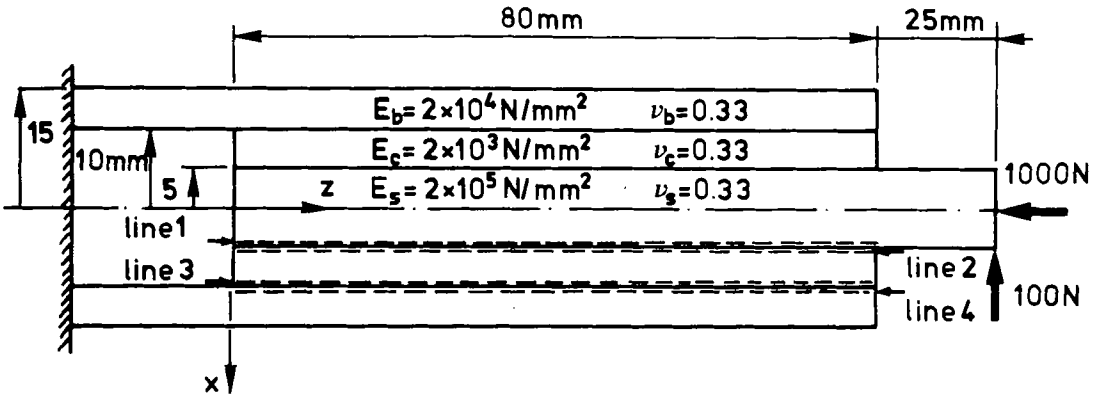

fig. A.1: Characterization of the structure for which the stress 'amplitudes' are given in the following graphs.

Three stress components are continuous across the interface ($\hat{\sigma}_r$, $\hat{\tau}_{rt}$ and $\hat{\tau}_{rz}$), thus equal in both materials. These components are referred to as 'interface stresses' and the values shown are those for the cement (in the calculations the continuity is not always exactly fulfilled; Huiskes, 1977).
The following line codes are used:

..... Axial Force (Z)

+-+-+ Transverse Force (X)

The dots refer to the nodal point values.
Results for the loading case M have not been drawn, since they, in a general sense, give the same kind of information as those for loading case X.

Fig. A.2: stem stresses, line 1 ($r = r_s$); figs. A.3 through A.5: stem-cement interface stresses, line 2 ($r = r_s$); figs. A.6 through A.9: cement stresses, line 2 ($r = r_s$); figs. A.10 through A.13: cement stresses, line 3 ($r = r_b$); figs. A.14 through A.16: cement-bone interface stresses, line 3 ($r = r_b$); figs. A.17 through A.20: bone stresses, line 4 ($r = r_b$).

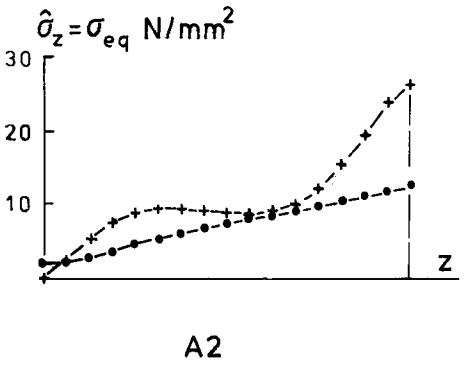
$\hat{\sigma}_z = \sigma_{eq}$ N/mm^2
30
20
10
z

A2

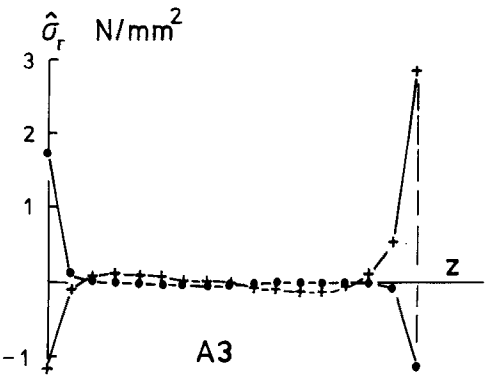
$\hat{\sigma}_r$ N/mm^2
3
2
1
−1
z

A3

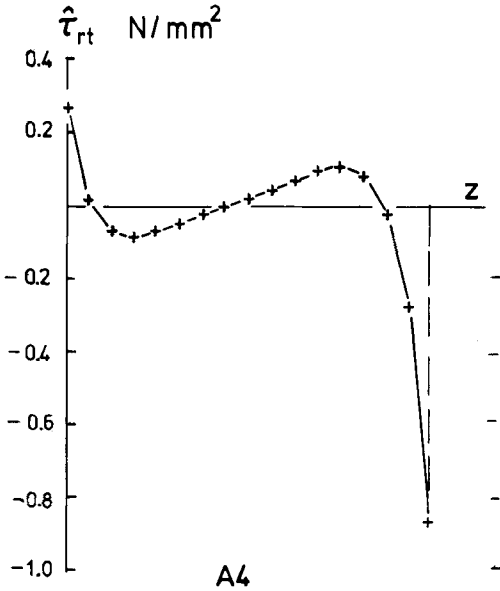
$\hat{\tau}_{rt}$ N/mm^2
0.4
0.2
−0.2
−0.4
−0.6
−0.8
−1.0
z

A4

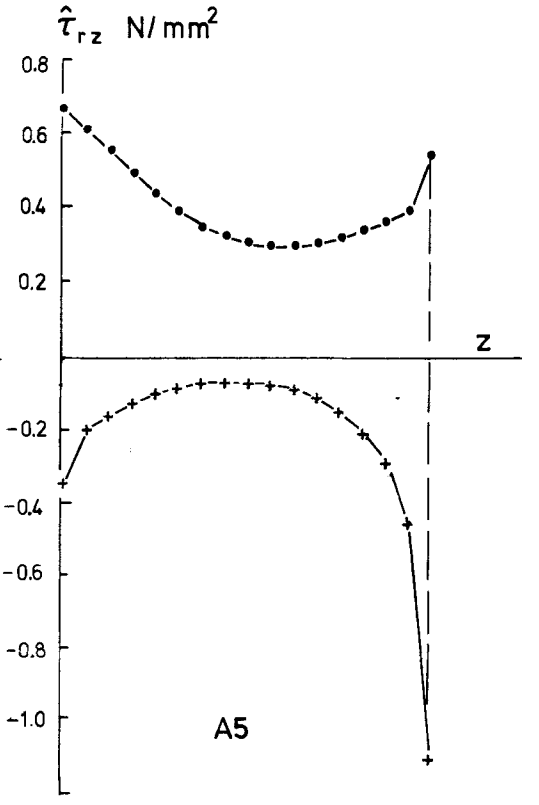
$\hat{\tau}_{rz}$ N/mm^2
0.8
0.6
0.4
0.2
−0.2
−0.4
−0.6
−0.8
−1.0
z

A5

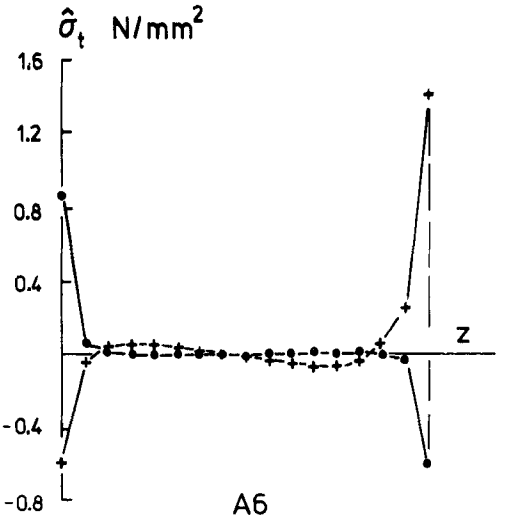
$\hat{\sigma}_t$ N/mm^2
1.6
1.2
0.8
0.4
-0.4
-0.8
z

A6

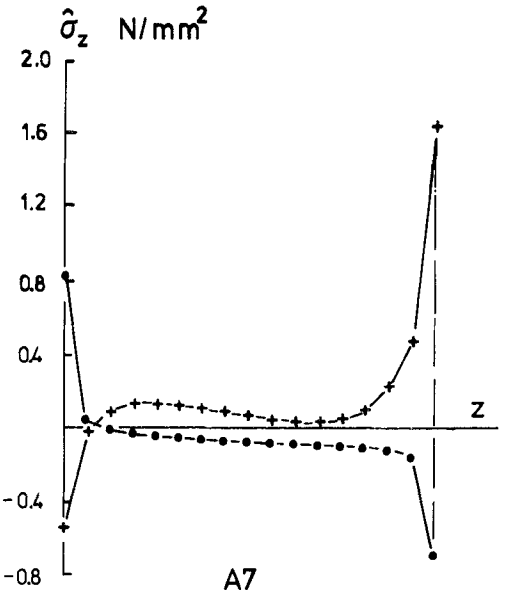
$\hat{\sigma}_z$ N/mm^2
2.0
1.6
1.2
0.8
0.4
-0.4
-0.8
z

A7

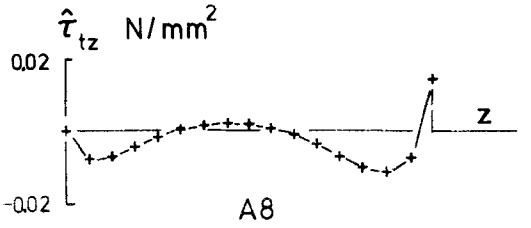
$\hat{\tau}_{tz}$ N/mm^2
0,02
-0,02
z

A8

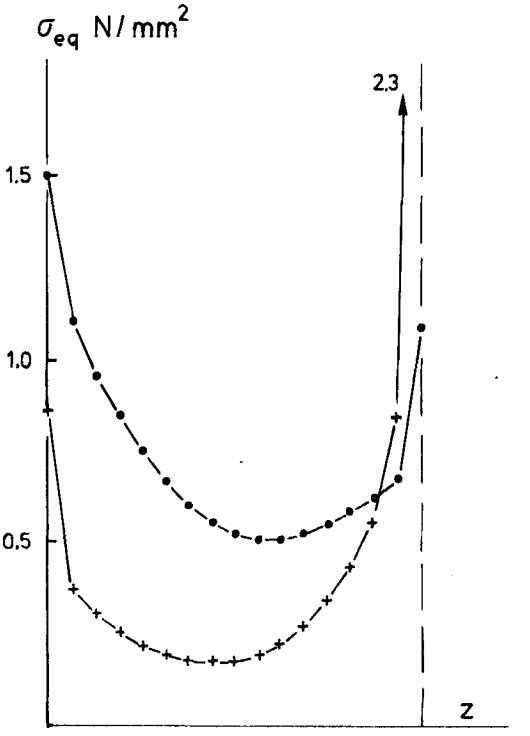
σ_{eq} N/mm^2
2.3
1.5
1.0
0.5
z

A9

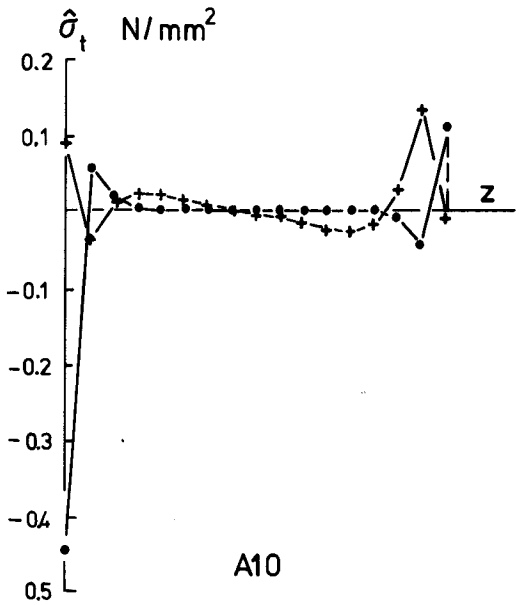

A10

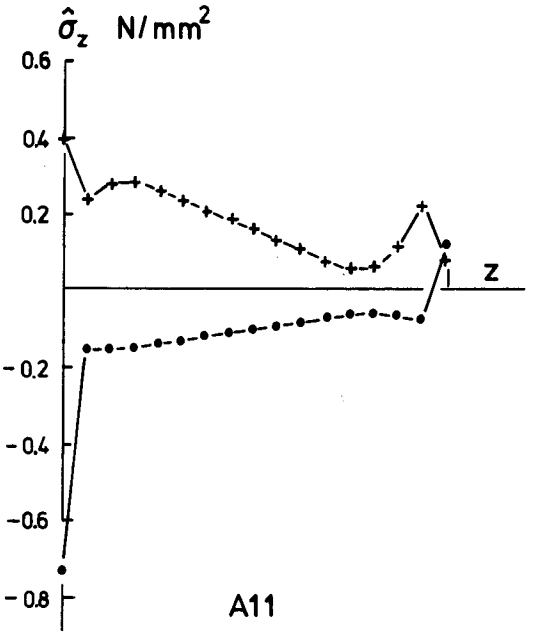

A11

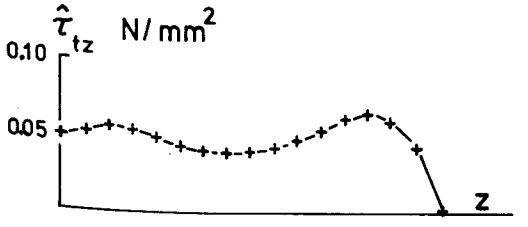

A12

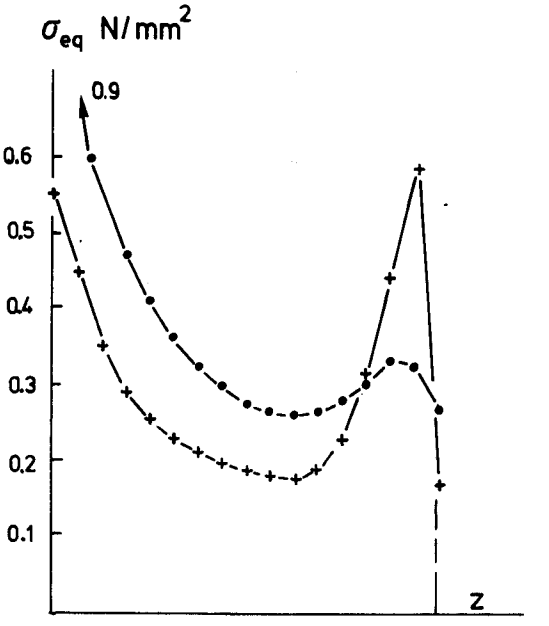

A13

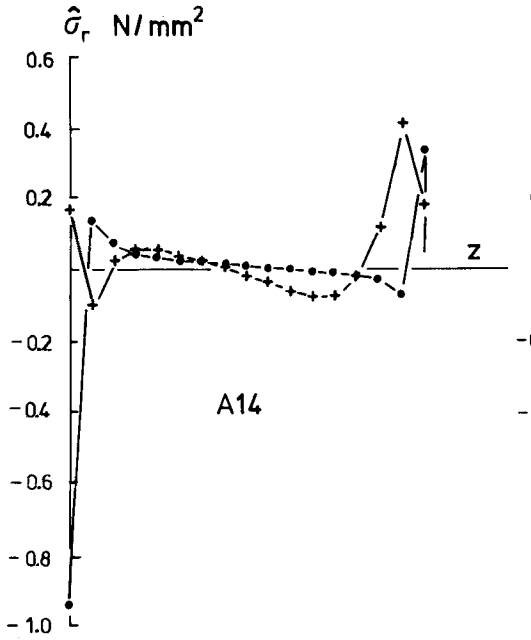
$\hat{\sigma}_r$ N/mm^2
0.6
0.4
0.2
-0.2
-0.4
-0.6
-0.8
-1.0
z

A14

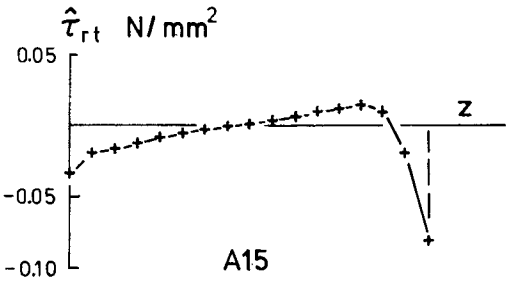
$\hat{\tau}_{rt}$ N/mm^2
0.05
-0.05
-0.10
z

A15

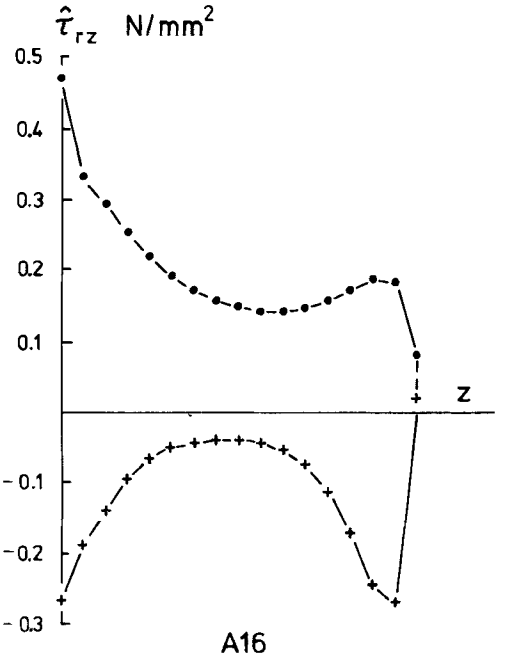
$\hat{\tau}_{rz}$ N/mm^2
0.5
0.4
0.3
0.2
0.1
-0.1
-0.2
-0.3
z

A16

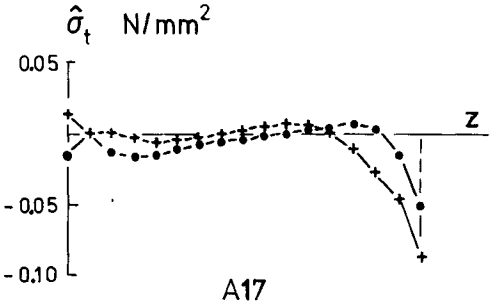

A17

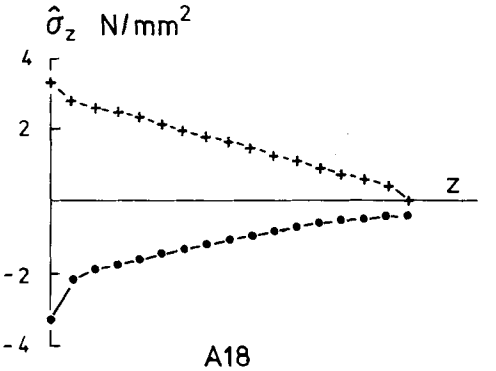

A18

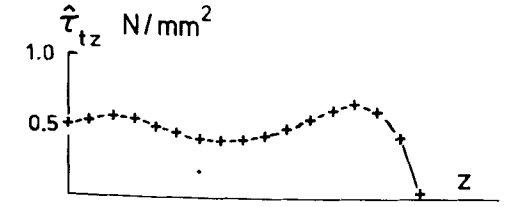

A19

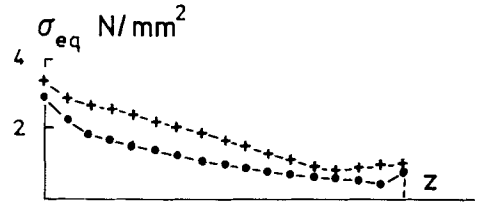

A20

APPENDIX B

THE STRUCTURAL STIFFNESS OF A SLICE OF BONE CEMENT

In the beams-on-elastic-foundation models, the Winkler hypothesis is applied to the acrylic cement layer, which means that the layer is assumed to consist of an infinite number of linear elastic springs, with spring constants C_a (N/mm^2) for axial loading and C_t (N/mm^2) for transverse loading. Approximative formulas for C_a and C_t can be derived using analytical and FEM models. These analyses have been described in Huiskes and Schouten (1979); in this appendix only a summary of the results is given.

Stiffness against axial shear

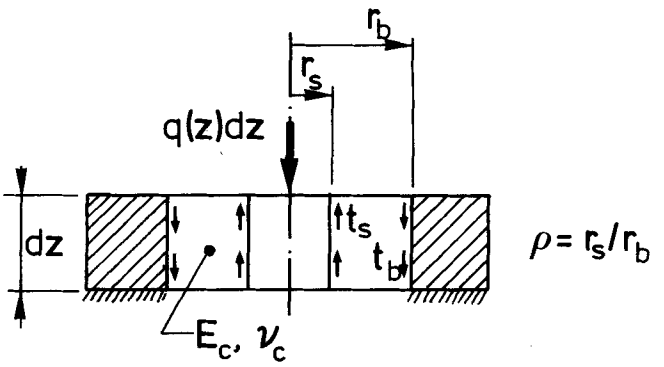

fig. B.1: A slice of the structure in axial loading.

A slice dz of the structure is shown in fig. B.1. The bone and the stem are assumed as rigid. The Winkler hypothesis in this case implies that only shear stress in the axial direction is present in the cement layer. For circular geometry it follows (fig. B.2.a) that

$$C_a \approx - \frac{\pi E_c}{(1+\nu_c)\ln\rho} \quad (\rho = r_s/r_b) \tag{B.1}$$

for rectangular geometry (plane model) (fig. B.2.b) we have

$$C_a \approx \frac{dE_c}{(r_b - r_s)(1+\nu_c)} \tag{B.2}$$

and for arbitrary geometry (fig. B.2.c)

$$C_a \approx \frac{1}{2}\frac{\gamma_s E_c}{\delta_a(1+\nu_c)} \tag{B.3}$$

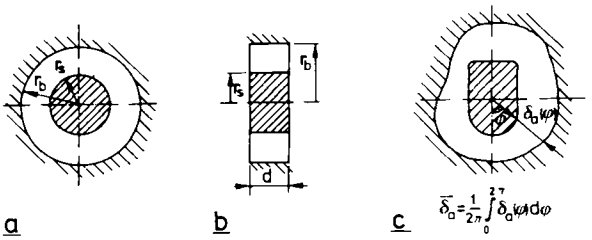

fig. B.2: Different cross-sectional geometries of a cement slice; (a) axisymmetric, (b) rectangular and (c) arbitrary.

where γ_s is the circumference of the stem $\bar{\delta}_a$ the average layer thickness.
For $\rho = 0.5$ ($r_b - r_s = 5$ mm), formulas (B.1) and (B.2) gave good agreements with FEM calculations. For higher ρ the accuracy will be even better; for smaller ρ the accuracy will decrease.
Formula (B.3) is an extrapolation of (B.1) and (B.2) and should only be expected to give reasonable results if the layer is thin and the variation in thickness restricted. When formula (B.3) is used to approximate C_a for circular geometry, for $\rho = 0.5$ an under estimation of about 30% results compared to (B.1); for $\rho = 0.7$, agreement is quite reasonable.

Stiffness against transverse loading

A slice dz of the structure is shown in fig. B.3. The bone and the stem are assumed to be rigid. Plane strain state is assumed in the cement layer (for plane stress state, see Huiskes and Schouten, 1979). The results for different cases are summarized in table B.I.

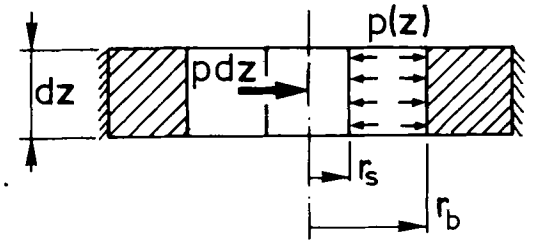

fig. B.3: A slice of the structure in transverse loading.

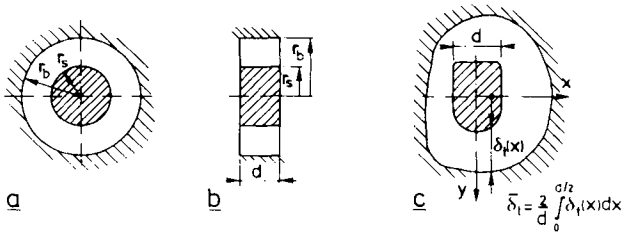

fig. B.4: Different cross-sectional geometries of a cement slice: (a) axisymmetric, (b) rectangular and (c) arbitrary.

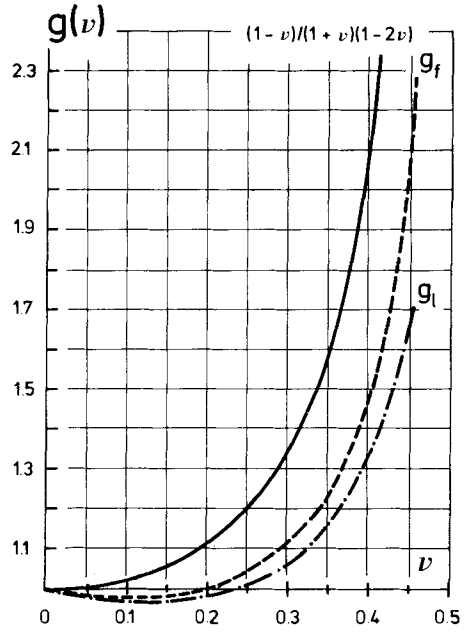

fig. B.5: Three functions of ν_c, used in the expressions for C_t.

	stem-cement interface rigidly connected		stem-cement interface loose and no friction	
circular geometry (1) (fig. B.4.a)	$5.3E_c g_f(\nu_c)\,(0.24 + \frac{\rho}{1-\rho})$	(B.4)	$1.9E_c g_l(\nu_c)\,(0.24 + \frac{\rho}{1-\rho})$	(B.5)
rough approximation	$\frac{4E_c(1-\nu_c)\rho}{(1-\rho)(1+\nu_c)(1-2\nu_c)}$	(B.6)	$\frac{2E_c(1-\nu_c)\rho}{(1-\rho)(1+\nu_c)(1-2\nu_c)}$	(B.7)
rectangular geometry (fig. B.4.b), uni-axial strain assumed	$\frac{2dE_c(1-\nu_c)}{(r_b-r_s)(1+\nu_c)(1-2\nu_c)}$	(B.8)	$\frac{dE_c(1-\nu_c)}{(r_b-r_s)(1+\nu_c)(1-2\nu_c)}$	(B.9)
'arbitrary' cross-section (fig. B.4.c)	$\frac{2.5dE_c(1-\nu_c)}{\delta_t(1+\nu_c)(1-2\nu_c)}$	(B.10)	$\frac{1.25dE_c(1-\nu_c)}{\delta_t(1+\nu_c)(1-2\nu_c)}$	(B.11)

table B.1: Approximative formulas for C_t in different circumstances; (1) for g_f and g_l see fig. B.5.

Formulas (B.8) and (B.9) were derived analytically and apply exactly for the assumption of uniaxial strain. Formulas (B.4), (B.5), (B.6) and (B.7) were derived from analytical considerations combined with FEM calculations. Formulas (B.10) and (B.11) were extrapolated from

(B.8) and (B.9) and will presumably give reasonable results if the stem geometry is not too irregular. If formula (B.10) is used to approximate C_t in circular geometry, the agreement with the FEM results is even better than when formula (B.4) is used; formula (B.10) is, however, somewhat inconvenient, since for circular geometry

$$\delta_t = \frac{1}{2} r_b \left\{ \sqrt{(1-\rho^2)} + \frac{1}{\rho} \arcsin\rho - \frac{\pi}{2}\rho \right\}$$

SECTION FOUR

CONCLUSIONS AND CLOSING REMARKS

The analyses, discussed in the previous sections, provide fundamental data from which guidelines for prosthesis designs, implantation procedures and acrylic cement composition can be derived. Obviously, the aspects treated here are not the only ones that provide guidelines; others, too, affect the system performance and the designs and procedures ultimately chosen will usually be based on compromises between criteria of biological, mechanical, chemical and surgical origin. In this respect the recommendations resulting from the analyses presented here are partial in character and should therefore certainly not be regarded as prescriptions, but merely as guidelines. It is evident, however, that any compromise will have more chances of succes when its various (possibly conflicting) criteria are in themselves firmly based on fundamental data.
Conclusions have been stated at different stages in sections II and III; in the following pages some of them, that may be of interest to orthopedic surgeons, will be discussed in more general terms.

Heat generation and conduction analyses

The heat generation and conduction process in polymerizing acrylic cement and the materials adjacent to it can be described mathematically with quite reasonable accuracy by applying theories of heat conduction. In this way the temperatures as a function of time in a given bone-prosthesis structure during and after polymerization can be predicted by approximation. The parameters that describe the thermal properties of the relevant materials, that have to be used in the calculations, can be estimated on the basis of literature data. In some cases, especially as regards the bone tissue, only a range of probable values can be found.

The cement-bone interface is a region rather than a smooth, well defined area of contact, which has a certain heat-flow resistance. Consequently, a steep temperature drop will occur over a relatively small distance and hence the 'cement-bone-interface temperature' is an undefined quantity, a fact to which the scatter in experimental data as reported in the literature can, at least partly, be ascribed. The thermal conductivity of the interface greatly influences the maximal bone-temperature values and the penetration depth of the heat into the bone. Anything that can be done to reduce the interface conductivity also reduces the chances of bone necrosis, and from this point of view cleansing of the implant bed prior to cement insertion would not be advantageous (contrarily, however, to criteria of mechanical interface strength).

During acetabular-cup fixation, the temperatures occurring in the bone adjacent to the cement are higher than those in the case of intramedullary (metal) stem fixation. The maximal values greatly depend on the amounts of cement used and on the (macro) geometry of the bony implant bed, which should be smooth and concave. When acrylic cement is pressed against trabecular bone, the tips of trabeculae surrounded by cement may reach temperatures up to 70°C, at which instant thermal necrosis is a certainty, in view of the literature data on thermal necrosis threshold levels.
Apart from these trabecular tips, the bone adjacent to the cement may, in general, reach maximal temperatures of, roughly speaking, 50 to 60°C while a bone layer of 1 to 4 mm may be heated to 50°C or beyond, depending on the specific circumstances. In this range, the occurrence of thermal necrosis greatly depends on the time of exposure. For an exposure time of 30 sec., thermal threshold levels for cell necrosis between 50 and 55°C have been reported in the literature.

In view of the probable ranges in the parameter values on the one hand and the ranges in thermal necrosis threshold levels on the other, it can be concluded from the analyses that thermal necrosis in the cortex of the bone during fixation of intramedullary stems is improbable, that the incidence of thermal necrosis in general cannot be excluded and that in specific (predictable) circumstances it will certainly occur.

The heat conduction process and the temperature values are significantly influenced by the dimensions of the bone. Hence, when heat conduction phenomena, or their consequences as regards thermal necrosis (for instance in histological analyses), are studied in smaller animal models, the results cannot simply be translated to human circumstances. In this respect it is found to be rather unlikely that the cortical bone necrosis reported by Feith (1975, see section II) in his rabbit experiments was mainly caused by thermal necrosis. By combining his experimental results with those of the analyses presented here, the hypothesis evolves that the heat of polymerizing has an indirect effect, by influencing the cell-toxic actions of the monomer, rather than a direct necrotic effect on the bone tissue.

In order to reduce the temperatures, several precautions can be taken. Adding 'heat-sinks' as radiopaque fillers ($BaSO_4$ or ZrO_2) to the powder has but little effect. Pre-cooling of the implant and the cement, for instance by 10°C, is also of little effect, while more drastic cooling will probably prejudice the polymerization process. More influence is exerted by the addition of an aqueous gel to the cement mixture (porous cement) and by increasing the powder-to-liquid ratio, although these measures can only be applied in a limited sense, since in this case, too, the cement properties, especially its strength, may suffer. Decreasing the polymerization rate has a moderate influence, but when the auto-acceleration effect is drastically surpressed, the maximal temperatures will be significantly reduced. A quite effective and useful measure is the cooling of the operation region before cement insertion and during the polymerization process. The effectiveness of these measures can easily be evaluated by using the graphs presented in chapter 9 of section II.
The surgeon, furthermore, can effectively reduce the temperatures by limiting the amounts of cement used. In this respect it should be noted that acrylic cement in fact fulfills two different functions: adapting the smooth implant to the irregular implant bed and filling spaces. The latter function could be provided by pre-polymerized materials as well, by applying plastic fillers of different dimensions and shape and plastic-coated implants. In that case only little self-curing acrylic cement would have to be used, thus reducing the bone temperatures and the chances of thermal tissue damage.

Stress analyses

By applying beams-on-elastic-foundation theory to a simplified, general model of intramedullary fixation structures (using results of experimental and three-dimensional Finite Element Method analyses as references), the characteristic mechanical parameters of the structure can be determined and the relations between these parameters and its mechanical performance evaluated. It can be shown that the structure can be divided into a proximal, a distal and a middle region which can be analysed separately. Simple, approximative formulas can be derived for the most important stress values in these regions (in the stem, the bone, the intermediate layer (usually acrylic cement) and at the interfaces).

By applying fundamental, general concepts thus obtained it can be shown that two-dimensional (plane) Finite Element Methods, as reported in the literature, are not very suitable for

detailed and accurate stress analyses of intramedullary fixation structures. Although useful in studying tendencies in a relative sense, provided certain precautions have been taken in the process of modeling, the visual apparent agreement between such a model and, for instance an X-ray of the structure, is often misleading.
The mechanical conditions at the stem-cement contact area, that may slip and cannot transfer tensile stresses, have only a moderate influence on the mechanical performance of the structure in general, but a pronounced effect on the local stress distribution in the intermediate layer (the cement) and at the interfaces. Hence, in detailed stress analyses these phenomena should certainly be taken into account.
Composite beam theory, as often used in the literature, is appropriate for the middle region only, to calculate stresses in the axial direction. Where the cement layer is concerned, however, the stresses in this region are quite insignificant compared to those in the proximal and distal regions.
Based on the same concepts as the beams-on-elastic-foundation model (essentially assuming that both the bone and the stem behave in accordance with linear beam theory and the cement mantle as an elastic layer), a Finite-Element-Methods (FEM) beam model can be developed. This model can take nonhomogeneous properties of the structure into account and may serve as a rapid, inexpensive evaluation method for the mechanical performance of specific stem designs in given bones under different circumstances.

The maximal stem stresses occur, roughly speaking, in the middle region; the maximal cement- and interface stresses at the proximal and distal sides, in both cases at the stem-cement interface (radial and shear stresses). The axial stresses in the bone are lower compared to the 'natural' case; at the proximal side (the calcar region in the case of hip endoprostheses) quite unphysiological radial and shear stresses occur at the cement-bone interface as well as hoop stresses in the bone.
Immediately following the polymerization process, the cooling acrylic cement will shrink around the stem, leaving locked-in stresses in the mantle. These stresses will gradually relax, as can be concluded from relaxation tests, decreasing by about 75% in 7 days. However, during the operation the generated hoop stresses may cause the cement mantle to fracture, as can be concluded from approximative calculations, using data on temperature distributions as evaluated in section II. These stresses are maximal in the middle of the cement mantle, so that tiny cracks may remain undetected.

In using the fundamental concepts provided by the beams-on-elastic-foundation analysis and applying the FEM beam model, guidelines for stem designs and implantation procedures can be developed. These guidelines are derived on the assumption that, although the causes of bone remodeling phenomena are uncertain as yet, a joint replacement will have less chances of failure if the stresses in the stem and the cement, as well as the unphysiological stress components in and on the bone are reduced, or at least smoothened, as much as possible.
From the approximative formulas it follows that on the proximal side the flexural and compressional stiffness of the stem should be as high as possible, which implies a thick stem, but retaining a cement layer of adequate thickness. In the case of the hip endoprosthesis the layer thickness should be around 2 mm. On the distal side the stem should be as flexible as possible, the intermediate layer as thick as possible. Together these requirements point to a tapered stem. The shape of the taper should not be an arbitrary one, since it has a marked influence on the cement and stem stresses. Using the FEM beam model, this shape can be more-or-less optimized.
The length of the stem, too, has an optimal value that depends on the specific stem material properties, its shape, the cement properties and the properties of the bone. An adequate

length can be evaluated also by applying the methods presented here.
A more-or-less optimal mechanical performance of the bone-prosthesis structure depends on an adequate set of structural parameter values. This means that when some of these parameters are given quantities, the others should be adapted to guarantee an adequate stress distribution. On the one hand this implies that, for instance prostheses made of titanium alloys, with lower material stiffness, require different stem designs than those fabricated with cobalt-chromium alloys or ceramics, on the other hand it is evident that patients with small bones require different prostheses than those having heavy bones. It would thus be recommendable if several sizes of a certain prosthesis were available and a choice was made pre-operatively, on the basis of roentgen measurements, taking into account the concepts developed here (simple and rapid evaluation methods as the FEM beam model, too, could be useful in this procedure).
As mentioned previously, the highest cement stress values occur on the proximal and distal sides, close to the stem-cement interface. Since acrylic cement, as present in the bone, is many times weaker than industrial PMMA, it would be advantageous to use pre-polymerized plastic in these regions, for instance by applying plastic-coated stems and plastic rings at the proximal side.

If a specific hip endoprosthesis is placed in valgus then, apart from a possible influence on the joint loading, the cement mantle thickness at the medial, proximal side is increased, so that the unphysiological radial and shear stresses on the cement-bone interface as well as the hoop stresses in the bone at the calcar region are reduced. It is remarkable that Bocco *et al* (1978) (see section I) found a significant reduction in the incidence of calcar resorption after placing the prostheses in valgus position. Especially these remodeling and resorption phenomena, including cement-bone interface remodeling, in relation with stress patterns, present important and challenging research objects in the field of orthopedic biomechanics, calling for detailed local stress analyses, taking radiographically and histologically established tissue changes into account. Since it is practically impossible to develop a model adequately refined to this end in a local sense which at the same time incorporates the whole structure, the concepts and methods developed here provide a good basis for carrying out such analyses in two steps, using the rough overall stress distribution as boundary conditions for a refined model of a detail of the structure.

SUMMARY

It was the object of the studies described in this work to provide general, fundamental concepts on some aspects of human joint replacement and the performance of artificial joints in the body.
The work is divided into four sections of which the first discusses joint replacement and bone-prosthesis structures in general. In section II analyses of the process of heat generation and conduction in self-curing acrylic cement, as used for implant fixation, are presented with the object of establishing the chances of thermal bone-tissue necrosis and evaluating precautions that can be taken to prevent it. Section III is devoted to stress analyses of intramedullary fixation structures under loading, with the object of determining the characteristic mechanical parameters of such structures, evaluating their influences on the mechanical performance and providing guidelines for prosthesis designs and implantation procedures.
In section IV some conclusions and recommendations, as reached on the basis of the analyses, are once more briefly discussed in general terms.

Section I

Chapter 1 outlines some general aspects of artificial joint replacement. The surgical procedure, general requirements for implant designs and the features of commercially available types are briefly discussed. Furthermore, the physiological joint loading, the properties of acrylic bone-cement and bone remodeling phenomena are briefly described. As in the greater part of this work, the data are mainly focussed on the artificial hip-joint.
Chapter 2 gives an overview of a selection from the literature on postoperative complications, especially artificial joint-loosening and fracture.
The objects and methods of the analyses, fully treated in sections II and III, are discussed in chapter 3.
Besides providing data to be used in sections II and III, and outlining the framework for the studies presented, this section may serve as an introduction for those unacquainted with human joint replacement procedures.

Section II

After a short introduction in chapter 1, a review of the literature on previous work as regards temperatures in self-curing acrylic cement and its adjacent materials in bone-prosthesis structures is given in chapter 2. In chapter 3, too, a literature review is presented, this time as regards available data on thermal threshold levels of bone-tissue necrosis.
To evaluate the time-dependent temperatures in the acrylic cement, the implant and the bone during implant fixation, theoretical models are applied, the principles of which are presented in chapter 4. Parameter values that describe the thermal materials properties to

be used in the analyses are estimated on the basis of an extensive literature review, as discussed in chapter 5.
The suitability of the method of analysis and the estimated parameter values are verified by simulating laboratory experiments, published in the literature, and by comparing calculated with measured temperatures, as shown in chapter 6.
In chapter 7 a general model of an intramedullary fixation system is analysed. Time-dependent temperatures in the cement mantle, the prosthesis stem and the cortex of the bone are calculated. In an extensive parametric analysis, the influences of the relevant geometrical, thermal and compositional properties of the system on the temperature values are evaluated. The effects of cement quantities used, implant dimensions and vascular cooling are discussed. Furthermore, the relevancy of using animal models to study thermal damage phenomena in this respect for human circumstances is investigated. By comparing predicted bone-temperature values with thermal damage threshold levels, the chances of bone-tissue necrosis are estimated. On combining results with those of relevant histological studies published in the literature, a hypothesis on the principal causes of the adverse side effects of acrylic cement evolves.
Chapter 8 discusses an analysis of the process of heat generation and conduction during acetabular-cup fixation. Here, too, the occurrence of thermal damage to the bone at different locations is estimated.
In chapter 9 the effectiveness of precautions that can be taken to reduce the temperatures are investigated. Specific recommendations are made and simple graphs are presented for a rapid first-order evaluation of the effect of several temperature reducing measures.

Section III

After a short introduction in chapter 1, a review of the literature on stress analyses of bone-prosthesis structures is presented in chapter 2. It is established that the available data on the mechanical performance of intramedullary fixation structures lack a general, fundamental basis. To provide for this a simplified, general model is analysed using different numerical and analytical methods. This model is introduced in chapter 3. Results of strain-gauge experiments on a cadaveric femur, discussed briefly in chapter 4, serve as references for the analyses. Different methods of analyses are applied and compared in chapter 5. Simple formulas are derived that approximate the most important stresses in the materials of the structure and at the contact regions as a function of the essential structural parameters. A simple computer model is developed that can be used for inexpensive and rapid first-order evaluation of the mechanical performance of specific prosthesis stem designs in given bones. The models used are based on assumptions and simplifications as regards the real structure, and the possible influences of neglected aspects are discussed in chapter 6. Attention is given to the occurrence of thermal locked-in stresses in the cement mantle caused by shrinkage following the polymerization process, the mechanical conditions of the stem-cement and the cement-bone contact regions (interfaces), more arbitrarily shaped stems and bones, the influences of torsional loading on the prosthesis and a few others.
Chapter 7 discusses the influences of the characteristic parameters of the stem, the bone and the intermediate layer on the structural performance on the basis of parametric analyses, using the fundamental concepts derived in chapter 5 combined with the different computer models.
In chapter 8, guidelines for prosthesis designs and implantation procedures, as follow from the analyses, are given. Several recommendations are made and in an example it is shown how, for a specific given bone, an adequate stem design can be developed using the approximative formulas and the rapid-evaluation computer model.